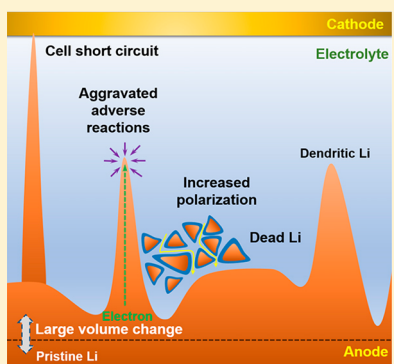


Toward Safe Lithium Metal Anode in Rechargeable Batteries: A Review

 Xin-Bing Cheng¹ Rui Zhang¹ Chen-Zi Zhao¹ and Qiang Zhang^{*1}

Beijing Key Laboratory of Green Chemical Reaction Engineering and Technology, Department of Chemical Engineering, Tsinghua University, Beijing 100084, China

ABSTRACT: The lithium metal battery is strongly considered to be one of the most promising candidates for high-energy-density energy storage devices in our modern and technology-based society. However, uncontrollable lithium dendrite growth induces poor cycling efficiency and severe safety concerns, dragging lithium metal batteries out of practical applications. This review presents a comprehensive overview of the lithium metal anode and its dendritic lithium growth. First, the working principles and technical challenges of a lithium metal anode are underscored. Specific attention is paid to the mechanistic understandings and quantitative models for solid electrolyte interphase (SEI) formation, lithium dendrite nucleation, and growth. On the basis of previous theoretical understanding and analysis, recently proposed strategies to suppress dendrite growth of lithium metal anode and some other metal anodes are reviewed. A section dedicated to the potential of full-cell lithium metal batteries for practical applications is included. A general conclusion and a perspective on the current limitations and recommended future research directions of lithium metal batteries are presented. The review concludes with an attempt at summarizing the theoretical and experimental achievements in lithium metal anodes and endeavors to realize the practical applications of lithium metal batteries.



CONTENTS

| | | | |
|---|-------|--|-------|
| 1. Introduction | 10404 | 5.2.1. Needlelike Li | 10417 |
| 2. Principles of Li Metal Anode with Safe Consideration | 10405 | 5.2.2. Mosslike Li | 10417 |
| 2.1. Intrinsic Property of Li Negative Electrode | 10405 | 5.2.3. Treelike Li | 10417 |
| 2.2. Li Dendrite and Related Issues | 10406 | 5.3. Influencing Factors | 10418 |
| 3. Solid Electrolyte Interphase on Li Metal Anode | 10407 | 5.3.1. Current Density and Charge Capacity | 10418 |
| 3.1. Formation Mechanism | 10407 | 5.3.2. Temperature | 10418 |
| 3.2. Structure and Component Models of SEI | 10407 | 5.3.3. Pressure | 10419 |
| 3.3. Li Ion Diffusion Near SEI Film | 10408 | 6. Theoretical Analysis of Li Dendrite Formation | 10420 |
| 3.3.1. Desolvation before SEI Film | 10408 | 6.1. Ionic Migration | 10420 |
| 3.3.2. Ion Diffusion through SEI Film | 10409 | 6.2. Dendrite Growth | 10421 |
| 3.4. Mechanical Nature of SEI Film | 10409 | 6.3. Surface Diffusion | 10421 |
| 4. Li Dendrite Nucleation | 10410 | 7. Suppressing Li Dendrite Formation for a Safe Li | 10422 |
| 4.1. Initial Nucleation Models | 10410 | Metal Anode | 10422 |
| 4.1.1. Surface Nucleating and Diffusion Model | 10410 | 7.1. Electrolyte Additive | 10422 |
| 4.1.2. Heterogeneous Nucleation Model | 10411 | 7.1.1. SEI Film-Forming Additives | 10423 |
| 4.1.3. Space-Charge Model | 10411 | 7.1.2. Li Ion Plating Additives | 10425 |
| 4.1.4. SEI-Induced Nucleating Model | 10412 | 7.2. Artificial SEI | 10425 |
| 4.2. Nucleation Location of Li Dendrites | 10414 | 7.2.1. Electrochemical Pretreatment | 10425 |
| 4.2.1. Tip-Induced Nucleation | 10414 | 7.2.2. Chemical Pretreatment | 10426 |
| 4.2.2. Bottom-Induced Nucleation | 10414 | 7.2.3. Physical Pretreatment | 10428 |
| 4.2.3. Multidirection Induced Nucleation | 10414 | 7.3. Superconcentrated Electrolyte | 10432 |
| 4.3. Nucleation Time of Li Dendrites | 10414 | 7.4. Nanostructured Electrolyte | 10434 |
| 5. Li Dendrite Growth after Nucleation | 10415 | 7.5. Solid-State Electrolyte | 10435 |
| 5.1. Growth Rate | 10415 | 7.5.1. Inorganic/Polymer Hybrid Electrolyte | 10436 |
| 5.1.1. Electronic Field | 10415 | 7.5.2. Electrolyte/Electrode Interface Modifica- | 10438 |
| 5.1.2. Diffusion Flux | 10416 | tion | |
| 5.2. Growth Patterns | 10416 | 7.6. Structured Anode | 10439 |

Received: February 28, 2017

Published: July 28, 2017

| | |
|--|-------|
| 7.6.1. Lithiophilic Matrix | 10440 |
| 7.6.2. Conductive Matrix | 10441 |
| 7.7. Membrane Modification | 10444 |
| 7.7.1. Dendrite Growth Stage | 10444 |
| 7.7.2. Dendrite Detection and Elimination | 10445 |
| 7.8. Cell Operation | 10446 |
| 7.8.1. Charging/Discharging Rate | 10446 |
| 7.8.2. Intermittent Plating | 10446 |
| 7.8.3. Convection Battery | 10446 |
| 7.9. Methods for Dendrite Inhibition in Other Metal Anodes | 10447 |
| 7.9.1. Na Dendrite | 10447 |
| 7.9.2. Zn Dendrite | 10447 |
| 7.10. Summary of these Strategies | 10448 |
| 8. Full Cell with Safe Li Metal Anode | 10454 |
| 8.1. Li–S Battery | 10454 |
| 8.2. Li–O ₂ Battery | 10455 |
| 8.3. Li–Intercalation Type Cathode Battery | 10457 |
| 9. Conclusion and Outlook | 10457 |
| Author Information | 10458 |
| Corresponding Author | 10458 |
| ORCID | 10458 |
| Notes | 10458 |
| Biographies | 10458 |
| Acknowledgments | 10459 |
| References | 10459 |

1. INTRODUCTION

Advanced energy storage is an intrinsic driving force for modern life. There is a large spectrum of storage technologies with wide variations in terms of energy and power density, service life, efficiency, cost, etc. Batteries have achieved great triumphs in this landscape, as they can be utilized conveniently at low cost.^{1–3} After the first cell invented by Count Volta in the 1800s, several electrochemical batteries have been proposed for commercial markets, including lead–acid, nickel–cadmium, nickel–metal hydride, lithium ion batteries (LIBs), etc.⁴ These electrical energy storage systems, especially LIBs, have revolutionized communications and the transportation style of modern life, enabling the rise of camcorders, mobile phones, laptops, and more recently electric vehicles.^{5,6} The total size of the global battery market accounted for \$54 billion (U.S.) in 2013, with an average growth of 5.0% per year from 1990 to 2013,¹ and the growth rate is estimated to be 30% in recent years. Among various storage technologies, LIBs currently outperform other systems and occupy 63% of worldwide sales with an estimated global market of \$213.5 billion by 2020.⁷

However, despite the impressive growth in sales of LIBs worldwide, the practical energy density of the present commercial batteries improves sluggishly. The practical energy density of commercial batteries has increased only 6-fold in the past 150 years from the first-generation lead–acid batteries ($\sim 40 \text{ Wh kg}^{-1}$) to the present LIBs ($\sim 240 \text{ Wh kg}^{-1}$ and 640 Wh L^{-1}).^{8,9} The growth rates of energy densities of LIBs based on watt-hours per kilogram (Wh kg^{-1}) and watt-hours per liter (Wh L^{-1}) have only been occurring at 7–8% per year.¹⁰ The advance in battery energy density has seriously lagged behind the rate of progress in the computer industry (a doubling of memory capacity each 18 months indicated by Moore's law).⁷ As LIBs are nearly approaching the theoretical value of cathode/anode materials, especially graphite anode, advanced electrode materials are highly demanded for exceptional energy

density to be applied in the emerging cutting-edge electronic devices (Figure 1a).¹¹ With the extra-high capacity (3860 mAh g⁻¹) and the lowest negative electrochemical potential (-3.040 V vs the standard hydrogen electrode), Li metal is regarded as the "Holy Grail" electrode and receives extensive research attention.^{12–14} The Li metal batteries (LMBs), including Li–sulfur (Li–S) batteries, Li–oxygen (Li–O₂) batteries, Li anode vs intercalation type cathode batteries, etc., indicate a huge increase in theoretical energy density relative to the current LIBs (Li–O₂, 3505 Wh kg⁻¹; Li–S, 2600 Wh kg⁻¹).^{15,16} The LMBs are strongly regarded as the next-generation batteries beyond LIBs.^{17,18}

The high-energy-density feature has promoted persistent motivations to realize LMBs into practical applications. In the 1970s, the advantage of LMBs was first demonstrated in digital watches, calculators, and implantable medical devices by Exxon.^{19,20} Until now, Li–I₂ primary batteries are still widely employed in cardiac pacemakers. However, the primary batteries are not rechargeable, resulting in high cost, serious waste, and environmental pollution. The first-generation commercial rechargeable LMBs were developed by Moli Energy in the later 1980s.⁷ These batteries indicated a high energy density of 100–200 Wh kg⁻¹ and 200–300 Wh L⁻¹. The intercalated cathodes, such as TiS₂, VO_x, Li_xMO₂ (where M is Co, Ni, or Mn), and MoS₂ were adopted, which were pioneered by Stanley Whittingham and John Goodenough.¹⁹ Though a positive electrode operated impeccably, LMBs were not viable due to the instability of a Li metal/liquid electrolyte interface induced by the dendrite growth during Li plating/stripping. The short circuit of dendrites leads to thermal runaway and a risk of explosion hazards of LMBs. Safety concerns including battery fires render LMBs to lose the opportunity of the commercial market. Therefore, strategies to inhibit dendrite growth have been strongly considered during the past 40 years.²¹

Since the 1960s, the proposed methods to suppress dendrite growth can be classified into four categories (Figure 1b).^{12,23–26}

1. *LiX alloy* (X = Al, B, Si, Sn, C, etc.). Substituting Li metal with LiX alloy can significantly reduce the dendrite problems, because Li is in its ionic rather than metallic state.²⁷ Unfortunately, the alloy electrodes can only survive limited cycles due to large volume changes during cycling.²⁸ To relieve the volume changes, carbon electrode with 10% volume change during operation was proposed by Murphy et al.²⁹ and Scrosati et al.³⁰ In 1991, Sony Corporation commercialized the C/LiCoO₂ rocking-chair cell, leading to the great success of LIBs in the consumer electronics for the next 25 years, even in today's electronic vehicles.³¹ However, though the carbon electrode partly guarantees safe operation,³² yet large capacity is drastically sacrificed from 3860 to 372 mAh g⁻¹.

2. *Organic electrolyte and Li metal/electrolyte interface modifications*.^{24,33,34} In the 1950s, Li metal was found to be successfully stabilized in some nonaqueous solvents due to the formation of a passivation film on the Li surface.^{35,36} Intensified research activities have been devoted to seeking the proper Li salts, solvent, electrolyte additives, and artificial passivation film. These methods can principally stabilize the electrode/electrolyte interface, leading to the commercialization of a series of primary LMBs in the 1960s and 1970s, and LIBs in the 1990s. However, the function becomes gradually incapable in rechargeable LMBs due to dendrite growth during repeated Li depositing/stripping.

3. *Solid-state electrolytes.* The inorganic, polymer, and their hybrid solid-state electrolytes are expected with a high shear modulus of about twice that of the Li dendrites ($\sim 10^9$ Pa) and thoroughly abandon the use of flammable nonaqueous liquid electrolytes, thus drastically enhancing the safety performance of LMBs. In contrast, the present ionic conductivity of these systems is typically between 10^{-8} and 10^{-5} S cm $^{-1}$ at room temperature and far below that of the nonaqueous liquid electrolyte (10^{-3} S cm $^{-1}$). Batteries based on these systems can only be applied in power-limited devices and high-temperature situations. By introducing a polymeric electrolyte into a liquid system, the first reliable and practical rechargeable hybrid LIBs were developed and commercialized in 1999.³⁷ The hybrid electrolyte based on these solid inorganic/polymer electrolytes also has the potential to be applied in practical LMBs.

4. *Structured anode design.* The recent revolution in nanomaterial and nanotechnology undoubtedly innovates Li dendrite inhibition research by constructing a novel matrix for Li depositing and designing separator/anode integration to modify Li ion depositing behavior. A Coulombic efficiency of 99.8% is achieved with a dendrite-free morphology in 200 cycles in the half-cells. More advanced approaches are required to considerably improve the Coulombic efficiency to 99.9% and lifespan to 1000 cycles to promptly accomplish the practical application of LMBs.

There have been many multidisciplinary scientific ventures in the previous 40 years that brought about several alternative approaches to efficiently and safely utilize Li metal anode, during which primary LMBs and rechargeable LIBs were successfully commercialized. However, rechargeable LMBs should be considered to be in the infancy stage.³⁸ Basic understandings about the intrinsic Li depositing/stripping behavior during cycling are currently very limited and tightly sealed to researchers.³⁹ Most of the research activities are fixed on the cathode side, rather than on the Li metal anode. Take one of the promising LMBs, Li–S batteries as an example: only 3.0% of the published literature focuses on the Li and alternatives (Figure 1c).²² The situations have gradually evolved with more considerations on the anode side (Figure 1d). To realize the practical applications of LMBs, mechanistic insights and strategies are imperatively demanded to intelligently handle the following issues.

1. *Solid electrolyte interphase (SEI).* The electrically insulating and ionically conductive SEI between anode and electrolyte is instantaneously formed by the parasitic reactions of Li metal and electrolyte in the initial cycles. The SEI film can conscientiously protect Li metal with high stability and mechanical strength. Further studies are required to profoundly perceive some essential issues including the following: how this SEI film grows from the Li metal surface to several decades of nanometers thick, what its detailed structure and component are, how solvated Li ions take off solvent molecules and cross the film, and what is its failure mechanism. Though some conclusions are presented by the theoretical calculation and simulations, yet many of them cannot be precisely demonstrated in the laboratory experiments or partly contradict the experimental results.

2. *Li ion transfer and reaction nature.* Unstable Li depositing leads to dendrite growth. Nevertheless, what are the transferring and distribution behaviors for Li ions after they cross the SEI layer? How do Li ions grow into Li dendrites? What are the roles of the dynamic conditions (e.g., current density, ionic concentrations, Li depositing amount) on Li dendrite growth?

How do Li dendrites break the SEI layer? Despite considerable research in the past few decades into rechargeable LMBs and the commercialization of primary LMBs and rechargeable LIBs, the exact working and failure mechanisms for Li metal anode are still puzzles to researchers from the scientific and engineering groups. Apart from the strategies to characterize and suppress dendrite growth,^{40–42} the mechanistic understandings and models are imperatively demanded to completely settle the dendrite problems and finally enable LMBs with an enhanced safety, high efficiency, and long lifespan.

In this review, we first present (in section 2) the working principles and technical challenges of Li metal anode, and then focus on the intrinsic nature of Li metal. Specific attention is paid to the mechanistic understandings and models for SEI formation (section 3), Li dendrite nucleation (section 4), and Li dendrite growth (section 5). Some theoretical calculations and simulation methods are summarized to strengthen the insights into the behavior of Li depositing behavior (section 6). Then, we present the recently proposed strategies to suppress dendrite growth of mainly Li metal anode, but also some other metal anodes (section 7). Additionally, a section dedicated to full-cell LMBs for practical applications is included (section 8). Finally, in section 9 a general conclusion and perspectives on the current limitations and recommended future research directions of LMBs are presented.

2. PRINCIPLES OF LI METAL ANODE WITH SAFE CONSIDERATION

2.1. Intrinsic Property of Li Negative Electrode

Lithium, the lightest member of the alkali metal group, has the smallest atomic radius of all metals. These features provide Li metal with ultrahigh capacity and quick transfer nature. Similar to other alkali metals, Li has high reactivity and reacts slowly in dry air. However, it can be oxidized much more rapidly with a trace amount of water. Therefore, solid Li metal in air is inevitably coated with Li oxide, Li hydroxide (LiOH and LiOH·H₂O), Li carbonate (Li₂CO₃), and Li nitride (Li₃N).⁴³ Elemental Li is not found naturally and, instead, appears only in compounds. The commercialized elemental Li products are isolated electrolytically from Li minerals.

As an anode, Li has the most negative potential of all the currently known electrode materials. This feature endows LMBs with a high discharging voltage and then a high energy density. Meanwhile, the ultralow potential and high reactivity result in the instability of Li metal encountering electrolytes (aqueous and nonaqueous liquid electrolytes, polymer and inorganic electrolytes) in rechargeable batteries.

Different from the insertion–host electrode materials (such as Al, Ge, Sn, Si, and C), Li metal is a conversion-pattern hostless anode (eq 1). At the interface between electrolyte and Li metal, Li ions are electrochemically reduced and deposited onto Li metal. An opposite reaction proceeds during Li stripping. If calculated in a similar manner with the insertion–host electrode materials, the capacity of Li metal anode is infinite due to its hostless nature. It is generally accepted to calculate the specific theoretical capacity (Q_c) of Li metal based on the Li metal, and a very high value of 3.86×10^3 mAh g $^{-1}$ is obtained (eq 2).



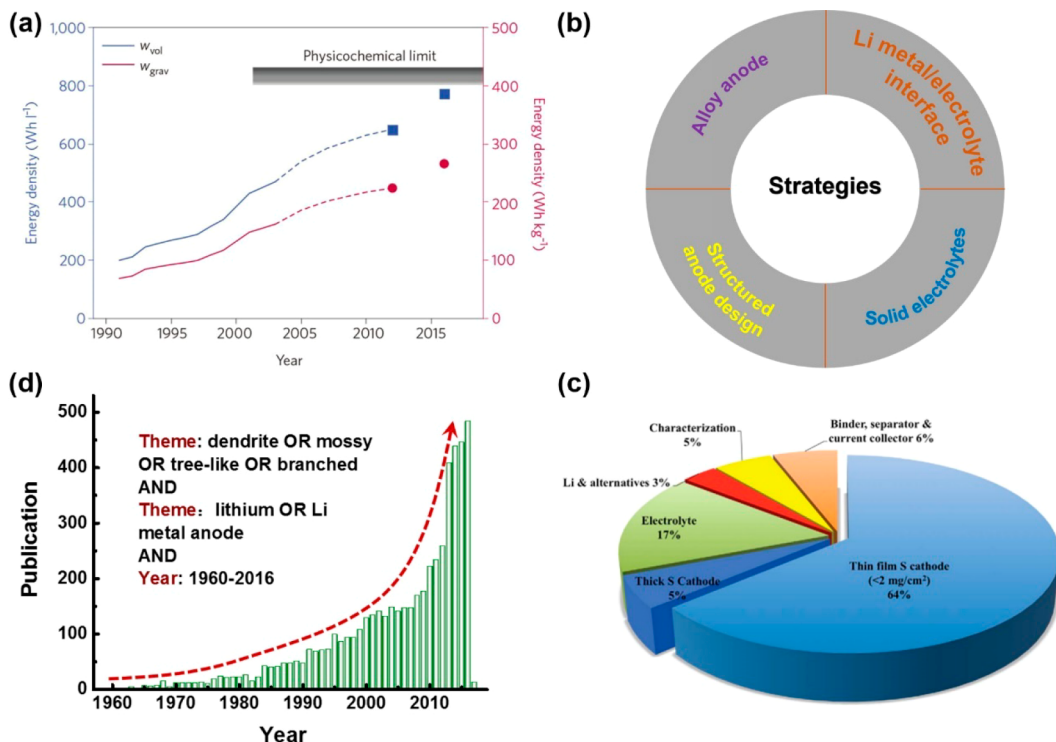


Figure 1. General profiles of Li ion and Li metal batteries. (a) Energy density evolution of lithium ion batteries since 1991. Reproduced with permission from ref 11. Copyright 2016 Nature Publishing Group. (b) Proposed strategies to suppress Li dendrite growth in Li metal batteries. (c) Literature distribution of Li–S batteries. This figure was last updated in June 2014. Reproduced with permission from ref 22. Copyright 2015 WILEY-VCH Verlag GmbH & Co. KGaA, Weinheim. (d) Literature distribution of Li metal batteries from 1960 to 2017 and was last updated in February 2017.

$$Q_c = \frac{\text{charge}}{\text{mass}} = \frac{6.02 \times 10^{23} \text{ atom} \left(1.6 \times 10^{-19} \frac{\text{C}}{\text{atom}} \right) \frac{1 \text{ mAh}}{3.6 \text{ C}}}{1 \text{ mol} \frac{6.94 \text{ g}}{\text{mol}}} = 3.86 \times 10^3 \text{ mAh g}^{-1} \quad (2)$$

2.2. Li Dendrite and Related Issues

The very high chemical and electrochemical reactivity of Li metal results in the corrosion of Li metal by electrolyte and hence low utilization of Li metal anode. The formation of Li dendrites is another critical issue for safe rechargeable batteries.^{44–47} The dendrite growth will give rise to several fatal obstacles (Figure 2):

1. *Cell short circuit.* Li dendrites can seemingly penetrate the separator and reach the cathode, causing the electrical contact and short circuit of a working cell.⁴⁸ The short circuit customarily accompanies cell thermal runaway, even electrolyte

combustion and cell explosion. This is the most mortal obstruction for practical applications of Li metal anode.

2. *Aggravated adverse reactions.* Dendrite growth renders an increased surface area of Li metal and possible parasitic reactions between Li metal and electrolyte. These side reactions consume active Li metal materials and electrolyte irreversibly as well, but do not contribute to the capacity, hence sharply reducing Coulombic efficiency.

3. *Evolution of dead Li from dendrites.* Side reactions between electrolyte and fresh Li dendrites generate large Li dendrites wrapped by the reaction products of SEI films and out of accessibility to current collectors and electrons, converting Li dendrites to electrochemically inert dead Li. This dead Li additionally decreases the Coulombic efficiency.

4. *Increased polarization.* Compared to the uniform and dense dendrite-free Li deposits, Li metal anode with dendrites always has a porous and uneven structure composing numerous dead Li's.^{49,50} These porous Li deposits lead to an increased diffusion pathway and huge resistance of Li ions and electrons, in this way rendering a large polarization and unsatisfactory energy efficiency.

5. *Large volume change.* As a conversion electrode without a matrix to plate/strip Li ions, the volume change during each plating/stripping process for Li metal anode is infinite, far above these intercalated anodes, such as graphite (10%) and silicon (400%). Dendrite growth engenders the volume change issue much harsher due to the porous Li deposits. These porous deposits prompt more volume increase/decrease during Li plating/stripping.

To summarize, Li dendrites not only induce a poor safety issue of LMBs, but also a low Coulombic efficiency and short

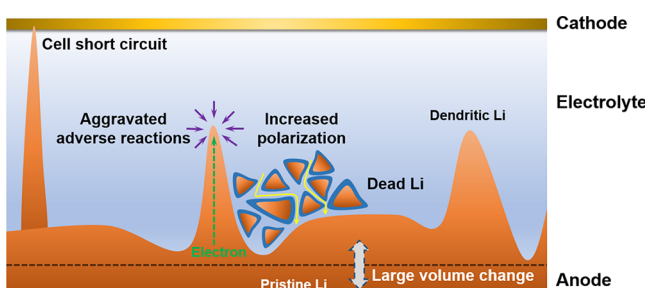


Figure 2. Scheme of dilemma for Li metal anode in rechargeable batteries.

cycling lifespan. Effective regulation of Li depositing behavior and efficient suppression of dendrite growth are the most impending mission on the way to practical applications of LMBs. To eventually reach this goal, a comprehensive understanding of the Li depositing process is critically requested. In sections 3–5, we will describe the state of the art on the surface chemistry of Li deposits and the nucleating and depositing behaviors of Li dendrites to afford the physical/chemical foundation of multidisciplinary routes to suppress dendrite growth.

3. SOLID ELECTROLYTE INTERPHASE ON LI METAL ANODE

Inhomogeneous deposition and dissolution of dendrite/mossy/granular-like Li and holelike structures are believed to be related to inhomogeneous coverage of the SEI film.⁵¹ An ideal SEI for a safe and efficient LMBs ought to have the following features:

- (1) proper thickness, thick enough to completely prevent electron transportation to electrolyte, but not too thick to increase Li ion diffusion resistance
- (2) high ionic conductivity to reduce diffusion resistance of Li ions through this film
- (3) strong mechanical performance to adapt the shocking and nonuniform volume change during repeated Li depositing/stripping
- (4) extraordinary stability in morphology, structure, and chemistry during long-term cycles

However, a practical SEI is not perfect affirmatively. It is critical but mysterious to us. Researchers have put much effort into it over decades and have made remarkable progress. In this section, existing achievements will be reviewed to describe SEI formation, SEI structure, and how Li ions get through it.

3.1. Formation Mechanism

The most negative electrochemical potential of Li contributes much to the very high energy density of LMBs. The large electrochemical activity simultaneously brings about the unique and complicated issue in Li metal anode: the solid electrolyte interphase, whose composition, structure, and mechanical properties have a close relationship with Li ion depositing morphology.⁵² The formed film induced by the reaction of electrolyte and Li was first discovered by Dey in 1970⁵³ and named as SEI by Peled in 1979.³⁶

Goodenough et al.⁵⁴ put forward the relationship between the SEI formation on electrodes and the lowest unoccupied molecular orbital (LUMO)/highest occupied molecular orbital (HOMO) of electrolytes. Suppose that the electrochemical potentials of anode and cathode are μ_A and μ_C , respectively. E_{LUMO} and E_{HOMO} refer to the voltages corresponding to LUMO and HOMO. As illustrated in Figure 3, if $\mu_A > E_{\text{LUMO}}$, electrons on the anode are inclined to transfer to the unoccupied orbital of the electrolyte, inducing the intrinsic reduction reactions of electrolyte. The as-obtained SEI serves as a barrier to avoid further decompositions of organic electrolyte. Similarly, in the case of $\mu_C < E_{\text{HOMO}}$, redox reactions contribute to the generation of SEI between electrolyte and electrode.

Practically, due to the most negative nature of the electrochemical potential of Li, the redox reactions between Li and nonaqueous electrolyte cannot always be avoided. When bare Li is exposed to solution, there are immediate reactions between Li, electrons, and solution species in time constants of milliseconds or less.⁵⁵ SEI growth is initially triggered by

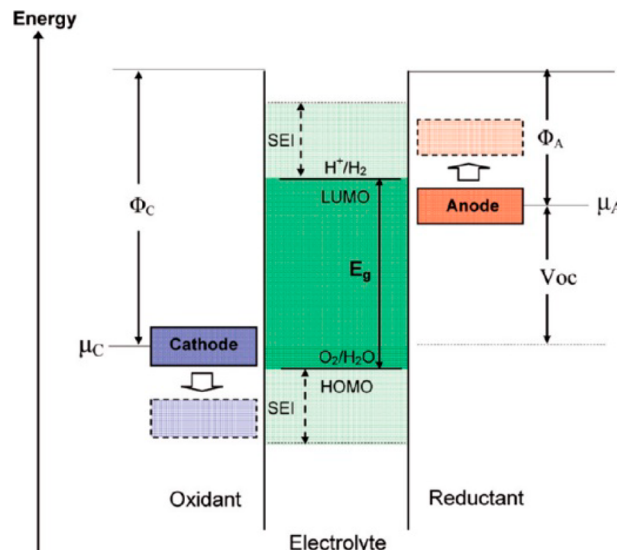


Figure 3. Scheme of SEI formation condition in a liquid electrolyte. Reproduced from ref 54. Copyright 2010 American Chemical Society.

electrons. Endo et al.⁵⁶ investigated the reductive decomposition of electrolytes with electron spin resonance as well as molecular orbital calculation method. Anions in electrolytes are difficult to reduce through the calculations of enthalpy changes between anion positive reduction and free solvent, with $\Delta H_r \approx -1 \text{ kcal mol}^{-1}$. Li⁺ can coordinate with these solvents and help to decrease the reduction enthalpy to $\Delta H_r \approx -10^{-2} \text{ kcal mol}^{-1}$, rendering the process thermodynamically favorable.

SEI grows with the continued electron/electrolyte-participated reactions and stops when lacking one or both of them. SEI growth regulated by solvent diffusion is nominated by Pinson and Bazant,⁵⁷ as well as Ploehn et al.,⁵⁸ whereas the electron conduction mechanism is proposed by Peled.³⁶ When SEI thickness evolves beyond the electron tunneling regime and solvent penetration, radical species (such as EC[·] in ethylene carbonate (EC) electrolyte and F[·] in fluorinated ethylene carbonate (FEC) electrolyte) are responsible for SEI further growth.⁵⁹ After nucleating on the anode, these radicals with extremely high reactivity can readily transfer charge to their surroundings. Nevertheless, SEI film cannot constantly grow due to the huge diffusion resistance of Li ions through this film, which will be discussed in later. There is no final verdict on the maximum SEI thickness yet. The SEI film formed on Li electrode has a practical thickness ranging from a few to several hundreds of nanometers. Its thickness can be roughly estimated by a computational formula based on parallel capacitor assumption (eq 3)

$$T = \frac{\epsilon A}{C\pi(3.6 \times 10^{12})} \quad (3)$$

where ϵ is the dielectric constant, C is capacitance, A is the electrode area, and T is the thickness of SEI. Even so, predicting the thickness of an SEI film precisely in a working cell is very difficult, which strongly depends on the electrolyte components and formation conditions.

3.2. Structure and Component Models of SEI

Due to the highly reactive nature, untreated Li electrode before contacting electrolyte has a pristine surface film including an outer part of Li₂CO₃ and LiOH and an inner part of Li₂O.⁶⁰ After immersion into the electrolyte, a new surface film will

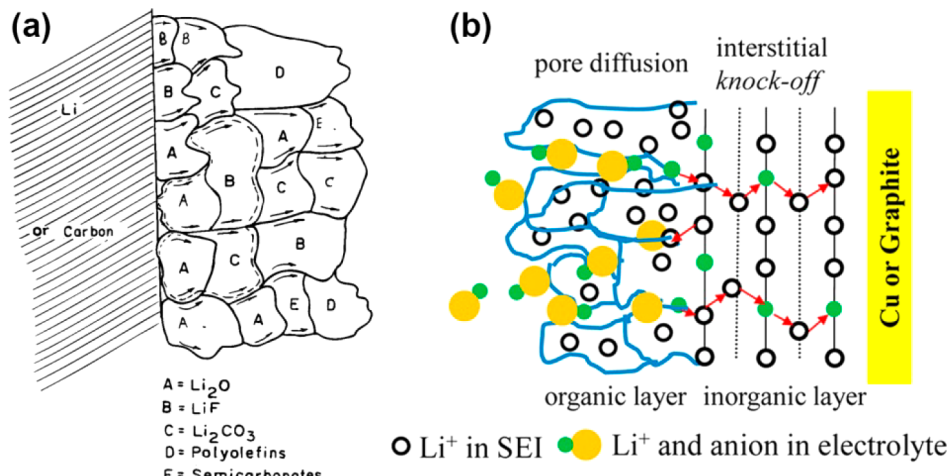


Figure 4. Scheme of SEI structure. (a) Mosaic structure in the top view. Reproduced with permission from ref 61. Copyright 1997 The Electrochemical Society. (b) Dual-layer structure in the cross-section view. Reproduced from ref 62. Copyright 2012 American Chemical Society.

form, named as SEI. The generally accepted description of the SEI structure is the mosaic model,⁶¹ indicating the surface is not homogeneous. Several reductive decompositions proceed on the negatively charged anode surface simultaneously, and a mixture of insoluble multiphase products deposits on the anode. The formed SEI with a mosaic morphology allows the Li ions to migrate through it rapidly (Figure 4a).

The SEI layer in thickness direction is not homogeneous as well, with dual-layer structure and various components (Figure 4b).^{62–65} The layer close to the Li metal surface contains species of low oxidation states such as Li₂O, Li₃N, LiF, LiOH, and Li₂CO₃, labeled as the inorganic layer. The outer part of the surface films is comprised of species with higher oxidation states, such as ROCO₂Li, ROLi, and RCOO₂Li (R is an organic group related to the solvent), labeled as the organic layer. One possible forming mechanism for this dual-layer structure is that organic components begin to coat on the electrode surface after initially nucleating in the liquid electrolyte region, and later transform into inorganic components like Li₂O and LiF.^{66,67} Several components of this film probably do not form directly from the reaction of electrolytes and Li metal, but convert from some intermediate products. Therefore, the clear identification of each SEI composition and distribution is the first step to unraveling the formation mechanism of SEI film.

The specific components of SEI film strongly depend on the electrolyte composition, which principally decides the primary nature of SEI films. In most cases, the organic composites of SEI layers are established by solvent, and inorganic composites are originated from the reactions between the salt and solvents. This principle is appropriate to establish the SEI specificity connected to each electrolyte, while Li₂CO₃ is frequently found in all carbonate electrolytes and some ether electrolytes. Beyond that, LiCl is detected on electrodes in SOCl₂-based (thionyl chloride) electrolytes,⁶⁸ Li₂S₂O₄ in electrolytes containing sulfur dioxide,⁶⁸ (CH₂OCO₂Li)₂ in EC, ROLi-(CH₃OLi) in 1,2-dimethoxyethane (DME), CH₃CH₂OCH₂OLi and HCO₂Li in 1,3-dioxolane (DOL), LiF in LiBF₄/LiPF₆/FEC electrolytes, etc.^{12,24,69–72} It is worth noting that these results are usually obtained from X-ray photoelectron spectroscopy (XPS) and infrared spectroscopy, where specific components are identified by peak fitting based on the experimental data and theoretical calculations. As one original spectrum may result in various peak-fitting results, they

present some biased results in certain cases. Up to now, it is still undoubtedly challenging to clearly describe the complete chemical components of SEI film.

One factor that obstructs the separation of different SEI components is that they work synergically not separately. The mixture of organic/inorganic composites can achieve a competitive equilibrium and coexistence on a working Li metal anode. When the components form a mosaic mixture, their chemical/electrochemical natures unexpectedly change. Leung et al. found that Li₂CO₃ and lithium ethylene dicarbonate (LEDC) were electrochemically stable but thermodynamically unstable near the equilibrium Li⁺/Li potential.⁷³ Li₂CO₃ and LEDC proved to be brittle, decomposing on Li(100) with reaction barriers predicted to be significantly lower than 0.92 eV. Attributed from these reactions, a thin layer of Li₂O emerges locating between Li metal surfaces and the residual Li₂CO₃/LEDC, unless Li₂O is subsequently converted into LiF when active F sources are affordable.

The nature of every possible SEI component can be investigated by theoretical calculation and simulation. Lin et al. estimated the critical thickness that blocks electron tunneling for LiF, Li₃PO₄, and Li₂CO₃ with the order Li₂CO₃ > Li₃PO₄ > LiF, indicating LiF has superior electronic insulation.⁷⁴ Due to the difference in employed methods (generalized gradient approximation (GGA) or HSE06), the critical thickness ranges from 2.0 to 3.0 nm in GGA calculation and from 1.6 to 2.1 nm in HSE06 calculation. The SEI with only several-nanometers thickness is enough effective to protect Li metal from the parasitic reactions between electrolyte and Li metal, if the coating material is a complete crystal without pinholes. Though this conclusion is obtained theoretically, this thickness can shed some light when designing the coating layers for Li metal anode.

3.3. Li Ion Diffusion Near SEI Film

SEI film is an essential path when Li ions get desolvated and reduced in the electrode, where Li ion diffusion seriously affects the morphology of Li deposits. To design a dendrite-free electrode, it is rewarding to investigate Li ion behaviors near SEI film.

3.3.1. Desolvation before SEI Film. Generally, one Li ion is generally solvated with two to six solvent molecules in a

liquid electrolyte. The structure of solvated Li ions heavily depends on the solvent species^{75,76} and Li ion concentrations.^{77,78} Before Li ions obtain electrons and subsequently deposit onto current collectors, the solvated Li ions must shed solvent molecules and migrate through the bulk phase of SEI film afterward.^{24,36} Using density functional theory and a time-of-flight secondary ion mass spectrometer (TOF-SIMS) test, Shi et al. demonstrated a novel two-layer/two-mechanism model: pore diffusion in the outer layer and knock-off diffusion in the inner layer (Figure 4b).⁶² The desolvation process takes place gradually at the pore diffusion stage in the outer layer. Xu et al. successfully differentiated each contribution of the two distinct processes, desolvation of Li ions and the migration of naked Li ions through the interfaces, by masterly selecting the SEI-free electrode material (lithium titanium oxide) (Figure 5).⁷⁹ The stripping of the solvation sheath of Li ions is the rate-

field to model Li⁺ energetics and dynamics within an SEI film, modeled as an amorphous mixture of carbonates with no vacancy or interstitial.⁸¹ Li⁺ moves as soon as it is dissolved in a liquid of polar-ionic species. Therefore, Li ions can transport through the SEI film via porous regions, grain boundaries between each component, or interstitials and vacancies.⁸² All these routes have been advanced in the literature, and some of them are verified by experimental results. The reason for the apparently mutual contradiction is attributed to that such transport behavior is likely unique to each SEI component. Even so, they can consolidate the profound understanding of SEI film.

Considerable experiments are conducted to probe the ionic diffusion in some specific SEI material. Li₂CO₃, Li₂O, LiF, and Li alkylcarbonate are four important inorganic components that build up the dense layer of SEI film.^{33,34,83} The electronic structures of these materials are all insulated with a large forbidden band gap. Li ion diffusion in Li₂CO₃ and Li₂O can be very rapid when Li vacancies are easily available. The energy barriers of Li migration in Li₂CO₃ (ranging from 0.227 to 0.491 eV) and Li₂O (0.152 eV) are comparable, while Li migration in LiF (energy barrier of 0.729 eV) is much slower even when there are Li vacancies in the lattice.⁸⁴ This knowledge can present an instructional approach when designing the electrolyte additives and artificial layers to construct a stable and efficient SEI film. However, due to the complex mosaic and heterogeneous structural nature of formed SEI, the ionic conductivity is not determined by a single substance, but by interfacial defects and topological distributions of these composite phases.⁸⁵

Apart from the pristinely formed SEI film, ionic conductivity (or ion diffusion) is strongly affected by other introduced phases. Al₂O₃ is frequently incorporated into the SEI layer accompanying other components to investigate the role of an extra phase on the SEI conductivity. The introduction of insulating Al₂O₃ nanoparticles into LiI increases the Li vacancy (the diffusive carrier) concentration by orders of magnitude and accordingly the ionic conductivity due to a space-charge layer effect.⁸⁶ However, the introduction of Al₂O₃ nanoparticles into LiF seems contrasting.⁸⁷ Li ion conductivity near the LiF/Al₂O₃ interface decreases because of the depletion of ionic carriers near the interface. Therefore, how SEI components affect the ionic conductivity synergistically or antagonistically remains an open question.⁸⁸

3.4. Mechanical Nature of SEI Film

Li metal anode has infinite volume change during Li depositing/stripping, generating a critically vital effect on the stability of SEI film and Li depositing morphology.⁸⁹ SEI with a superior mechanical property is preferable to stop the amplification of the dendrite growth and achieve a safe and efficient LMB. It turns out that Li dendrites can be partly suppressed if the shear modulus of the SEI film is high enough relative to that of the Li anode ($\sim 10^9$ Pa).⁹⁰ However, the practical SEI film always exhibits a low and heterogeneous shear modulus. When Li dendrite nucleates, SEI film experiences repeated breakdown and reparation.⁹¹ To detect the mechanical performance of SEI film, atomic force microscopy (AFM) has been intensively employed to monitor the interface topography on the anode surface. Liu et al.⁹² and Zhang et al.⁹³ recorded modulus mapping of SEI by in situ AFM and found that SEI film showed a Young's modulus within the range 50–400 MPa due to the composition nature of the SEI

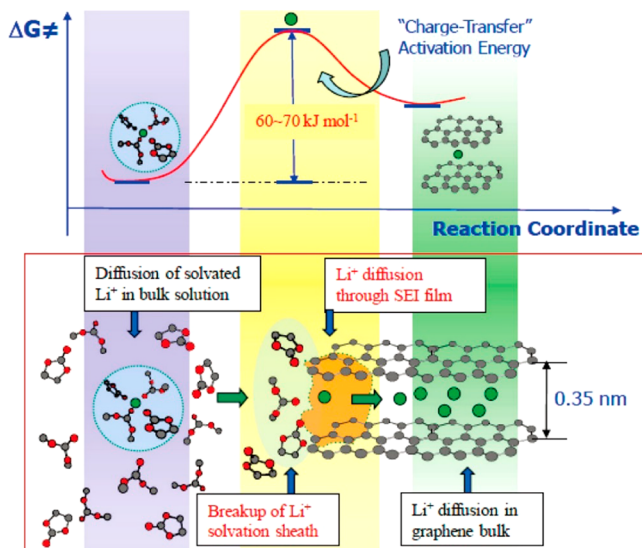


Figure 5. Scheme of energetic coordinates for Li⁺ transfer and desolvation. Reproduced from ref 79. Copyright 2010 American Chemical Society.

determining step with an activation energy of 50 kJ mol⁻¹, while the energy barrier of bare Li ions through SEI film is only 20 kJ mol⁻¹. Therefore, a thinner SEI layer is not the most important concern to obtain a highly conductive SEI film. It is of high significance to design and tailor the interfacial chemistry that can adequately dissociate solvent molecules from the primary solvation sheath of Li ions. However, there is little knowledge of the designing strategy to achieve an SEI with a lower energy barrier to dissociate solvent molecules of solvated Li ions.

3.3.2. Ion Diffusion through SEI Film. With the strong interest in solid-state conductors, Li ion diffusion in SEI film has been extensively investigated. Surface diffusion is an essential mechanism to describe the frequently observed dendrite growth. A large ionic conductivity of SEI film can render a dendrite-free Li depositing morphology. Several models and mechanisms have been proposed to describe the ion diffusion through an SEI film. Peled et al. afforded direct evidence for Li transport via SEI grain boundaries.⁶¹ Newman's group proposed a model to simulate the growth of the SEI and transport of Li ions through this film via vacancies and interstitials, but concluded that grain boundaries are very important.⁸⁰ Borodin et al. established a quantum-based force

(Figure 6a). Li et al. adopted AFM to characterize their artificial Li_3PO_4 film on Li metal anode (Figure 6b).⁹⁴ They found that

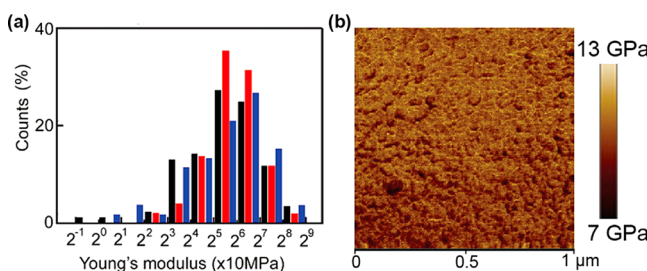


Figure 6. (a) Histogram of Young's modulus distributions in SEI film on Li metal. The black, red, and blue bars represent experimental results from single-layered SEI and the inner and outer layers of dual-layered SEI on Li metal, respectively. Reproduced from ref 93. Copyright 2012 American Chemical Society. (b) Mapping of Young's modulus on Li_3PO_4 artificial SEI film. Reproduced with permission from ref 94. Copyright 2016 WILEY-VCH Verlag GmbH & Co. KGaA, Weinheim.

the artificial film on Li anode indicated a smooth surface and a Young's modulus of 10–11 GPa, which can sufficiently suppress the Li dendrite growth. Much more efforts are requested to be devoted to AFM, especially *in situ* AFM investigation into the mechanical performance of SEI film on Li metal anode.

Other than the AFM characterization, density functional theory (DFT) calculations provide mechanical properties as well, which cannot be achieved by state-of-the-art experimental investigations. LiF/Li and $\text{Li}_2\text{CO}_3/\text{Li}$ interfaces associated with an SEI film on Li metal anode were investigated.⁹⁵ Li_2CO_3 was more mechanically stable covering the Li metal surface than LiF when it served as an SEI component on Li metal anode. $\text{Li}_2\text{CO}_3/\text{Li}$ interfaces were less likely to delaminate than LiF/Li interfaces. Nevertheless, $\text{Li}_2\text{CO}_3/\text{Li}$ interfaces were more likely to result in Li dendrite nucleation and growth than LiF/Li interfaces. This is attributed to that the LiF/Li interface has a larger electron tunneling barrier,⁷⁴ indicating LiF has less electron tunneling probability than Li_2CO_3 . Consequently, the dendrite growth is much more complicated. The continuous

growth of Li dendrites is strongly affected by several interrelated factors, rather than by an isolated one.

4. LI DENDRITE NUCLEATION

4.1. Initial Nucleation Models

Li metal in rechargeable batteries is plated and stripped repeatedly, and the nucleation process occurs in each cycle under various circumstances. During Li deposition, the initial nucleation sites play an important role in the subsequent Li depositing behavior. Several models to illustrate Li depositing behavior in the initial nucleation stages are proposed from both theoretical derivation and experimental observation.

4.1.1. Surface Nucleating and Diffusion Model. Li metal thermodynamically easily grows dendritic morphology, while Mg is preferable for obtaining a dendrite-free morphology on electrode surfaces.^{96–98} Definitely comparing the distinction of Mg and Li in crystal structures can present some instructional approaches to understand the growth of Li dendrites. Due to the stronger Mg–Mg bond strength predicted by DFT calculation, Mg has a higher free energy difference between high-dimensional and low-dimensional phases than Li.⁹⁹ This demonstrated that, relative to Li, Mg deposits are more preferable to form high-dimensional (such as three- (3D) and two-dimensional (2D)) structures rather than one-dimensional (1D) dendritic whiskers (Figure 7a). Through a comparative study of Li, Na, and Mg metal anodes, the surface diffusion on Mg electrode is significantly more rapid than on Li and Na metals, indicating that Mg ions exhibit a tendency to deposit toward the nearby areas rather than on a lumped site to form dendrites.¹⁰⁰ Consequently, these two factors are thermodynamically responsible for Li dendrite growth on Li metal anode: lower surface energy and higher migration energy.

Surface formation energies and diffusion barriers are two important indexes for the tendency of uniform deposition. Multiple categories of materials including layered (LiOH), multivalent (Li_2O , Li_2CO_3), and halide (LiF , LiCl , LiI , LiBr) compounds were calculated (Figure 7b).¹⁰¹ Li_2CO_3 has a high diffusion barrier and low surface energy for Li ions, both of which are undesirable in an SEI film to achieve a dendrite-free

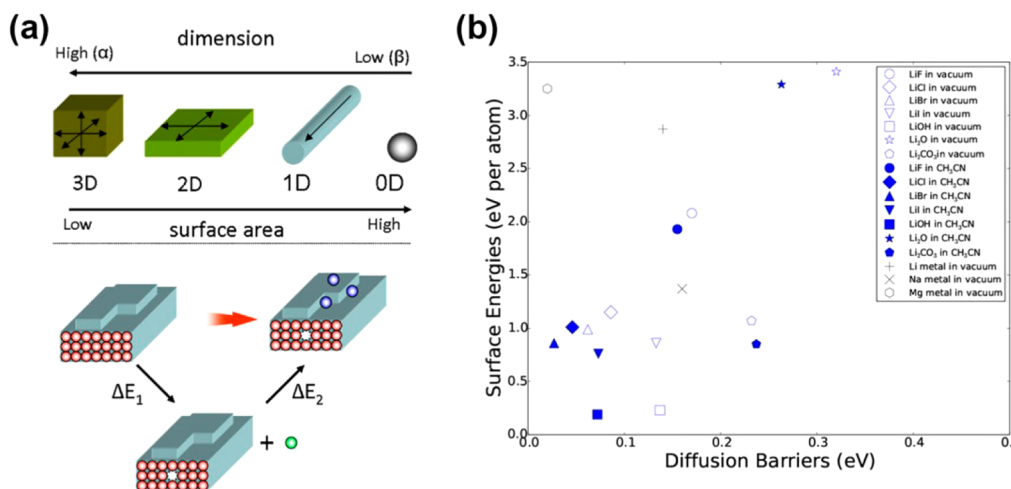


Figure 7. (a) Scheme of high-dimensional phases (α) and low-dimensional phases (β). Reproduced with permission from ref 99. Copyright 2012 Elsevier. (b) Surface energy vs surface diffusion barrier of possible SEI component on Li metal. Reproduced with permission from ref 101. Copyright 2012 arXiv.org.

morphology. Li halides have either equal or higher surface energies; however, they have lower surface diffusion barriers than Li_2CO_3 , which is preferable to render a dendrite-free morphology. Experimental lifespans represented by cell short-circuit times of SEI with these materials are correlated to diffusion barriers. The data indicate a clear linear trend consistent with an Arrhenius-like behavior between the experimental lifespans and diffusion barriers. The diffusion and surface energies can bring some fresh viewpoints to understand the Li electrochemical process and search for an effective solution to suppress Li dendrite growth.

4.1.2. Heterogeneous Nucleation Model. At initial stages of Li ion plating, Li ions obtain electrons and plate on the current collectors. This is regarded as a heterogeneous nucleation behavior. The initial nucleating morphology can generate a crucial role in the final Li depositing patterns. Therefore, comprehensive understanding and delicate control of the heterogeneous nucleation are decidedly worthwhile.

The heterogeneous nucleation process is investigated by Ely et al. both thermodynamically and kinetically through numerical simulations.¹⁰² Five regimes are clearly identified to illustrate the complex heterogeneous nucleation behavior: a nucleation suppression regime, a long incubation time regime, a short incubation time regime, an early growth regime, and a late growth regime (Figure 8). Embryos in the nucleation suppression regime are thermodynamically unstable and hence have a tendency to redissolve into the electrolyte. In the long incubation time regime, thermodynamically favored embryos stay and sequentially grow after some fluctuations

from electric and ionic fields. Exceeding a critical overpotential, a short incubation time regime facilitates narrow size distributions of embryos. Eventually, Li with a size of critical kinetic radius nucleates and grows rapidly with the rise of overpotentials. In the early and subsequently later growth regimes, thermodynamically and kinetically stable nuclei grow to reach the same terminal size. Once the Li nucleus has been stably established, the growth rate remains constant until the final form. Based on these considerations, Li dendrite growth can be dramatically suppressed by (1) smoothening the surface roughness of the Li electrode surface, (2) designing the anode particle size below the thermodynamically stable critical radius, (3) limiting the plating overpotential below the critical value and a cycling capacity that is below the characteristic incubation demand, and (4) promoting the wetting nature of Li electrodeposits.

Cui's group successfully explored the initial heterogeneous nucleating process through direct observation.^{103,104} They first explored the nucleation pattern of Li ions on various metal substrates and unraveled a substrate-dependent growth mode.¹⁰³ The plating/stripping cycling performance of Li metal strongly depends on the substrates.¹⁰⁵ Various substrates (e.g., Pt, Al, Mg, Zn, Ag, and Au, with some solubility in Li; Si, Sn, C, Ni, and Cu with negligible solubility in Li) were selected to probe the nucleating process. When these two categories of substrates (such as Au and Cu) coexisted as current collectors, Li ions tended to deposit on the Au substrates (Figure 9). These results can evidently demonstrate a preferable heterogeneous nucleating model and make it possible to intentionally induce lithium deposition. The role of current density in the initial nucleating process was probed.¹⁰⁴ The nuclei size is inversely proportional to the overpotential, and the number density of nuclei is directly proportional to the cubic power of overpotential (Figure 10). This also confirms that decreasing local current density through scaffolds with high specific surface area results in smoother deposits, which will be introduced in section 7.6.2.

4.1.3. Space-Charge Model. A space-charge theory proposed by Chazalviel is accepted to describe Li dendrite nucleation.¹⁰⁶ During Li ion deposition at high rates in dilute solution, the concentration of anions drops near the electrode surface. Anion depletion in the vicinity of electrode surface creates a very large space charge and electric field near the electrode/electrolyte interfaces, leading to a ramified growth of Li deposits.¹⁰⁷

To consider the nucleation of dendritic Li metal induced by space charge, Chazalviel calculated the distribution of electrostatic potential and ion concentrations in a dilute electrolyte of a thin rectangular symmetrical cell (Figure 11a).¹⁰⁶ Both region I (the quasi-neutral region) and region II (the space-charge region) are defined in a cell (Figure 11b). Region I refers to the bulk electrolyte and occupies the larger part of the cell, in which ion transfer is predominantly governed by diffusion. Region II only accounts for a small area near the electrode surface, in which ion transfer is governed by electric-field migration and the potential becomes markedly smaller than V_0 (the anode potential). There will later remain a space charge $Z_c e C_o$ driving the ramified growth of metallic Li electrodeposits at a high rate in dilute salt solutions. Space charge is frequently observed in the nonaqueous liquid electrolyte. Enhancing the cation conductivity/transference number or immobilizing anions can relieve the space-charge-induced dendritic Li growth.

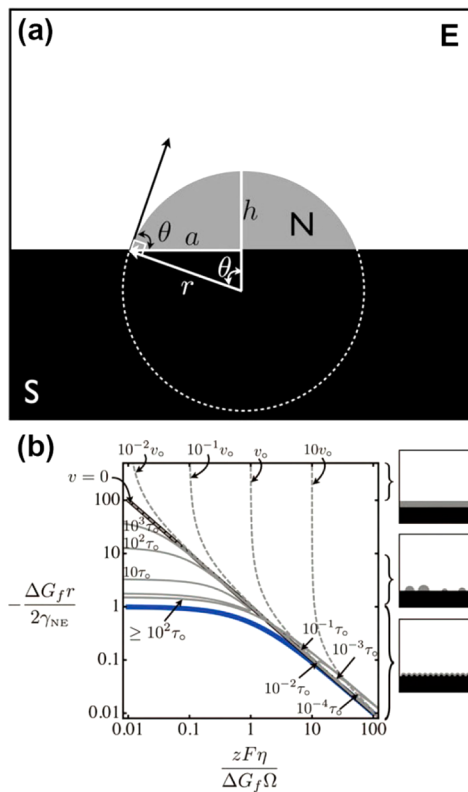


Figure 8. (a) Scheme of a spherical cap-shaped nucleus (N) plated on a flat substrate (S) immersed in an electrolyte (E). (b) Regimes of behavior during the initial stages of nucleation and growth of Li dendrites. Reproduced with permission from ref 102. Copyright 2013 The Electrochemical Society.

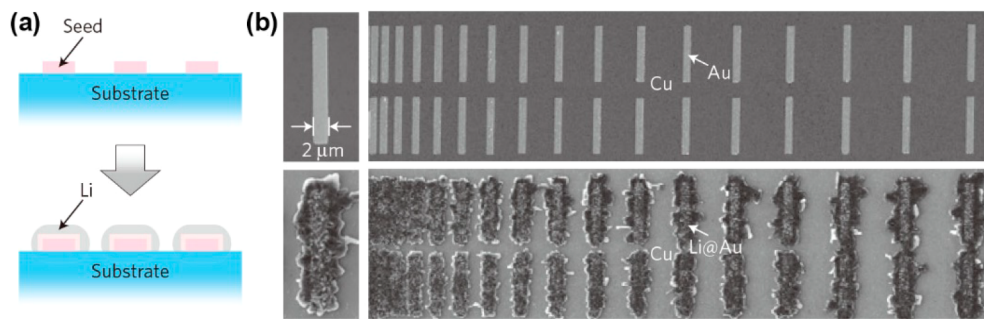


Figure 9. Patterned deposition of Li metal. (a) Scheme of patterned Li deposition. (b) SEM images of an Au strip before (top) and after (bottom) Li deposition at 0.5 mA cm^{-2} and 0.1 mAh cm^{-2} . Li was found to deposit over the Au strip. The size of the Au strip is $2 \mu\text{m}$ by $16 \mu\text{m}$, where no Li metal was directly deposited into the gap. Reproduced with permission from ref 103. Copyright 2016 Nature Publishing Group.

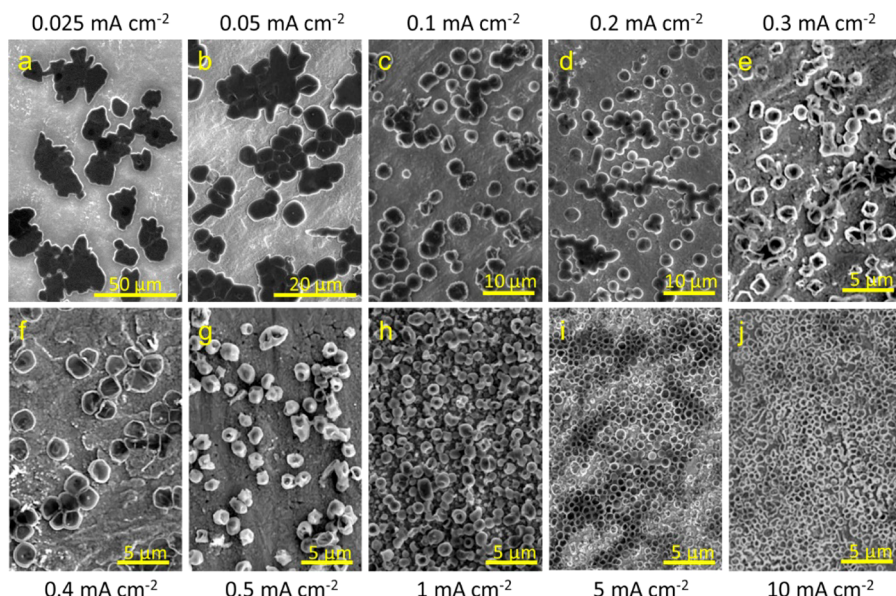


Figure 10. Li nuclei deposited at different current densities. (a–j) SEM images of Li nuclei deposited on Cu for an equivalent amount of total areal capacity of 0.1 mAh cm^{-2} . Reproduced from ref 104. Copyright 2017 American Chemical Society.

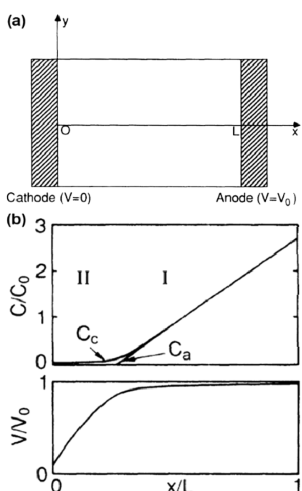


Figure 11. (a) Scheme of a symmetrical cell. (b) Profile of ion concentrations and electrostatic potential obtained from the numerical simulation in the hypothetical case of uniform deposition. Reproduced with permission from ref 106. Copyright 1990 American Physical Society.

4.1.4. SEI-Induced Nucleating Model. Different from Zn/Cu metal electrodes without SEI film in most cases, SEI film plays a very critical role in Li metal electrode, which is not stable and usually cracks as a result of volumetric expansion and stress caused by Li plating/stripping. The cracking at the defects of SEI films causes electrochemical hot spots and triggers filamentary and dendritic Li growth. Except for the pinholes of SEI film leading to dendrite growth, the intrinsic nature of unruptured SEI can as well decisively affect Li depositing behavior.

There are many arguments about the formation sequence of Li deposits and SEI formation. In situ electrochemical transmission electron microscopy (TEM) was utilized to afford a direct visualization of dendrite evolution on working electrodes and SEI formation (Figure 12).¹⁰⁸ The dark front (dashed curve), referring to formation of SEI, traveled prior to Li deposits. The total thickness of condensed SEI and Li deposits is 300–400 nm. SEI formed prior to Li metal nucleation possibly due to the high ion conductivity and electrical conductivity. The deposition process occurs between the SEI layer and the substrate. After SEI formation, Li depositing is triggered, which is induced by the intrinsic polycrystalline nature of SEI film. Similarly, the inhomogeneous deposition on Au electrode is captured in a liquid electrolyte,

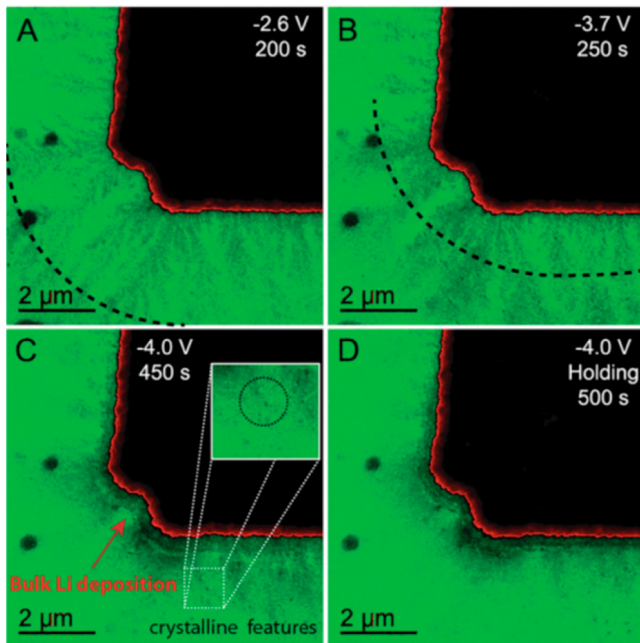


Figure 12. Li dendrite evolution on a working electrode. The wavefront corresponds to amorphization of SEI by Li deposition as is highlighted in (A) and (B). (C) and (D) exhibit Li deposition/SEI layer formation at a constant potential; the inset in (C) highlights formation of crystalline features. Reproduced with permission from ref 108. Copyright 2014 The Royal Society of Chemistry.

where SEI films can be identified easily and Li dendrites emerged after the SEI film formation.¹⁰⁹ During the initial stages of Li deposition, Li reacts with Au substrate to form Li–Au alloy. Bubbles are generated accompanying electrolyte decomposition and SEI formation by sustained decreasing of the negative bias on Au substrate. Simultaneously, Li dendrites appear between the bubbles. Nevertheless, during the whole Li depositing process, SEI growth always accompanies Li deposition. The SEI films are never constant, continuously growing in thickness and newly forming all the time.

Li ion diffusion in the liquid electrolyte is extremely crucial to the depositing morphology, and it is also important for Cu and Zn electrodes without an SEI film. In contrast to the liquid-state diffusion-controlled growth of Cu and Zn dendrites, Li electrode morphology is additionally modified by short-range solid-state diffusion through the amorphous SEI film. The growth and dissolution of dendrites and/or mossy deposits were modulated by ion diffusion through the SEI film at typical operating currents.¹¹⁰ The dendritic growth process is divided into four distinct stages (Figure 13).

Stage I. Spherical Li nuclei emerged on the Li surface and grew along with diameters proportional to the square root of growing time, indicating a limited diffusion of short-range solid-state transport through the SEI film, rather than long-range liquid-state diffusion. The SEI film passivated the Li surface and gradually reduced the Li depositing rate, since Li ions had to diffuse across the thickening SEI film covering the surface.

Stage II. Li dendrites started to grow from the root and pushed the initially formed Li away from the electrode. Herein a rapid increase in the dendritic Li length was observed, while its width remained almost constant. The dramatic upturn in depositing rate between stages I and II exhibited an abrupt transition.

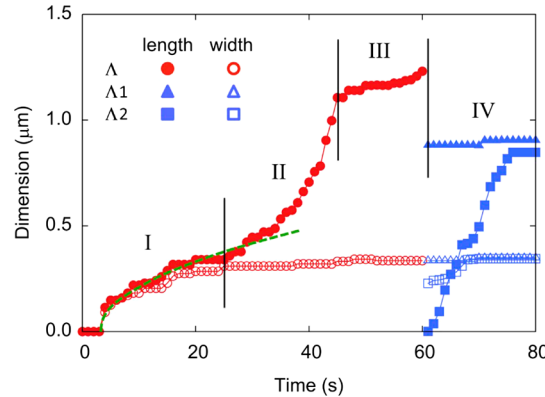


Figure 13. Length and width of Li dendrites in the four growth stages. Λ , Λ_1 , and Λ_2 are three different kinds of dendrites. Λ is the pristine dendrite; Λ_1 and Λ_2 are the derived dendrites from Λ at 60 s. Reproduced with permission from ref 110. Copyright 2017 Elsevier.

Stage III. The growth rate significantly decreased, induced by the newly formed/thickened SEI covering layer on the formed portion of the whisker.

Stage IV. A kink was formed on a Li whisker, dividing it into two segments. While one segment increased its length and width, the length of the other remained constant.

The continual slowing down of the initial surface growth rate is likely attributed to rapid SEI formation, which competed with Li deposition and slowed Li⁺ transport. Li growth cannot be regulated by liquid-state diffusion at this small length and short time scale, but is instead determined by local interfacial kinetics (including solid-state diffusion in the SEI film) (Figure 14).¹¹⁰

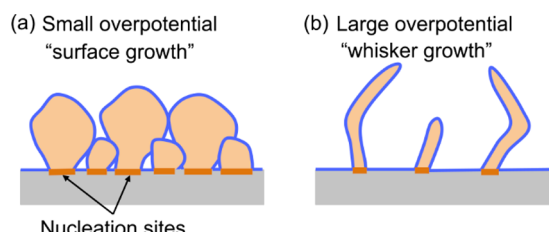


Figure 14. Scheme of root growth of lithium whiskers regulated by a short-range solid-state diffusion through an SEI film. Reproduced with permission from ref 110. Copyright 2017 Elsevier.

At a small overpotential, Li ion diffusion in the solid-state SEI film is relatively rapid and the diameter of Li deposits can grow further, rendering a surface growth pattern with a macroscopically compact morphology. When the polarization increases at high rates, Li ion diffusion in the SEI film is critically slow and becomes the rate-determining step for Li deposition. Li deposits grow in length rather than in diameter, resulting in the dendrite growth. Therefore, the SEI formation is a nanoscale event (notorious side reaction) that competes with metallic Li deposition in consuming the Faradaic current. The formed SEI film can distinctly impact the root vs tip growth patterns of Li dendrites.

The result was confirmed by Pei et al. experimentally.¹⁰⁴ The morphology of Li deposits was characterized in the early stages of nucleation on planar Cu electrodes in liquid organic electrolyte at different current densities. The diameter of Li deposits was very large at a small current density. With the increased current density, many more nucleation sites were

achieved with a reduced diameter, inducing a dendritic growth pattern (Figure 10).

4.2. Nucleation Location of Li Dendrites

The Li nucleation site during deposition is a critically important issue determining the growing direction of dendritic branches. To explore the origins of dendrite growth, direct observation is a visualized and effective strategy. Various viewpoints about the location, including tip-induced nucleation, bottom-induced nucleation, and multidirection induced nucleation, have been proposed to describe the nucleation sites in a working Li metal battery. No final conclusion has been reached yet. In this section, we introduce some theories on Li nucleation locations based on optical and electron microscopes.

4.2.1. Tip-Induced Nucleation. The tip is usually considered to be an active point in deposition. Presuming that the whisker tip is a static hemisphere, Li ion deposition easily occurs on the protrusions due to the enhanced electric and ionic fields near the spherical tips; this has been verified by direct observation.¹¹¹ The tip can determine dendrite initiation, and the growth rate is related to tip radius.¹¹² Relative to the fact that concentration overpotential induces electroplating on flat surface, electrochemical deposition over the tips is mainly controlled by the activation.¹¹³ Once the depositing is activated, dendritic growth continues regardless of the ionic concentration.

The inhomogeneous surface was adopted to explain the unexpected dendrite growth in Li polymer cells.¹¹⁴ The electric charges tend to accumulate over the tips, on which Li ions are more likely to deposit due to the abundant charges. In consideration of the dendrite tip curvature and growth kinetics, the dendrite growth is surface energy controlled in Li/polymer systems (Figure 15).¹¹⁵ Benefiting from a large diffusion

the surface layer, second-phase impurities, dislocations, and grain boundaries in the vicinity of SEI and Li electrodes. Li ions tend to deposit on those active sites, resulting in heterogeneous deposition.

4.2.2. Bottom-Induced Nucleation. Traditionally, Li dendrites are believed to grow from the tip. Nevertheless, a number of observation results intriguingly reveal that the dendrite tips remain unchanged during deposition, which is different from the theoretical calculation results. The subsurface structures underneath dendrites were detected with hard X-ray microtomography in Li–poly(ethylene oxide) copolymer (SEO) cells (Figure 16).¹¹⁷ The volume occupied by the subsurface was larger than that occupied by the tips protruding out in the early stage of Li dendrite formation. The subsurface structure was identified in another polymer electrolyte, poly(ethylene oxide) (PEO), which was attributed to the contaminant acting as nucleation sites such as Li₃N. Tip-induced nucleation is attributed to the enhanced ionic and electronic fields, while Li dendrite nucleation on the bottom is mostly caused by defects of SEI films of Li deposits.

4.2.3. Multidirection Induced Nucleation. The dendrite growth can be detected in many regions of cells with multiple directions except for some specially designed cells. The growth of Li dendrites in Li/polymer cells was tracked by scanning electron microscopy (SEM), indicating that there were both lateral growth and base growth.¹¹⁸ An optical microscope was employed in a dry room to observe Li whiskers.¹¹⁹ The dendrite branches grew from bottom, from tip, and between kinks, among which growth from the bottom was most common. No change was found for the tip shape. The diameter of the whiskers remained the same during growing. The region of whisker growth was not immobile on the electrode and moved from time to time. Steiger et al. in situ monitored Li dendrite growth with an optical microscope and indicated that Li dendrites grew simultaneously at the Li/substrate interface, kinks, or tips.¹²⁰ They argued that the growth was hardly effected by electric fields and concentration gradients at tips, which was not compatible with the prevailing mechanisms for dendritic Li growth. Thus, a new mechanism of insertion at defects was proposed. It is crystalline defect that dominates dendrite growth, including weak points on the SEI, dislocations, grain boundaries, and even contaminants (Figure 17).

4.3. Nucleation Time of Li Dendrites

A rechargeable battery with superb security is a prerequisite for practical applications. A superb lifespan before cell short circuit is one of the foremost indexes for a safe LMB. Dendrites are regarded as a forerunner for cell short circuit and failure. When dendrites form, they have a fair chance to short-circuit the cells and shorten cell life.

In dilute solutions, “Sand’s time” is widely accepted to measure the initiation time of dendrite growth. “Sand’s time” was first proposed in 1901 when Henry J. S. Sand investigated the liberation of hydrogen in a mixture of copper sulfate and sulfuric acid.¹²¹ During Cu deposition, Cu²⁺ concentration goes to zero near the electrode, after which H₂ generates. This concept was borrowed and extended to a more general case. For Li metal anode at high charge rates in binary electrolytes, the cation will be rapidly consumed and its concentration in the vicinity of electrode is expected to drop to zero at a time τ_s . Next, the strong negative electronic field will electroabsorb and electroplate massive Li ions in short periods, resulting in

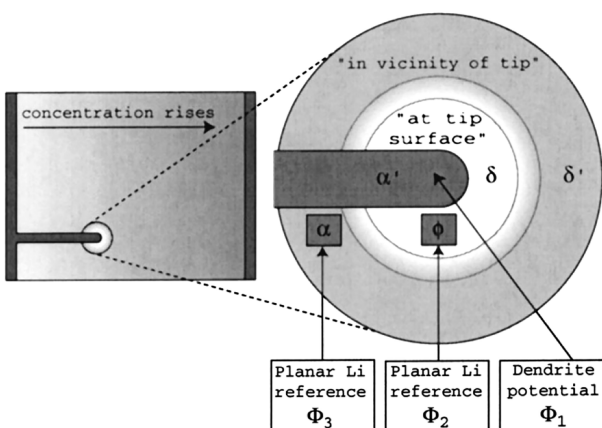


Figure 15. Diagram of a region near the tip of Li dendrites. Reproduced with permission from ref 115. Copyright 2003 The Electrochemical Society.

coefficient and a long interelectrode distance, the duration time before cell shorting is extended, although it is not so applicable in the case of organic electrolyte with a high transference number.

Besides tips, the active patterns for dendrite formations also include dislocations, boundaries, and impurities on the Li metal electrodes. Chen et al. probed the origins of metal growth during homoepitaxial electrodeposition on planar crystal surfaces.¹¹⁶ They argued that many kinds of defects can severe as nucleation sites during electroplating, including pinholes in

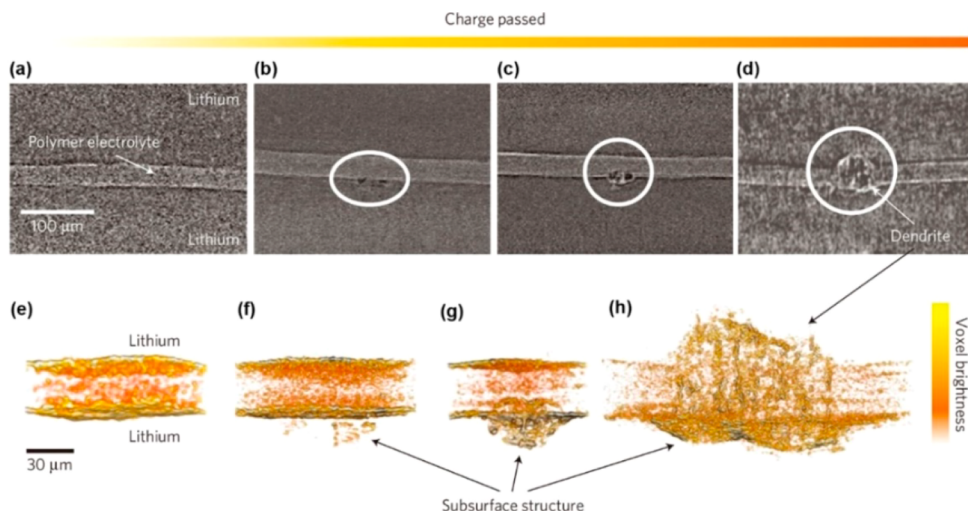


Figure 16. Evolution of Li dendrites. (a)–(d) X-ray tomography slices exhibiting cross sections of symmetric Li cells cycled to various stages. (e)–(h) Magnified, 3D reconstructed volumes of cells shown in the top panel. The amount of charged capacity is (a) and (e) 0 C cm^{-2} , (b) and (f) 9 C cm^{-2} , (c) and (g) 84 C cm^{-2} , and (d) and (h) 296 C cm^{-2} . Reproduced with permission from ref 117. Copyright 2014 Nature Publishing Group.

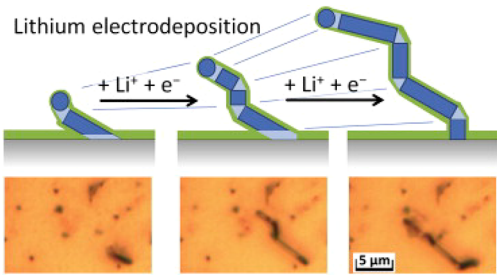


Figure 17. Scheme and optical images describing growth of Li needle as observed in in situ videos recorded under optical microscopy. Reproduced with permission from ref 120. Copyright 2014 Elsevier.

dendrite growth. This behavior is known as Sand's behavior and the time τ_s is called Sand's time (eq 4).¹²²

$$\tau_s = \pi D \left(\frac{C_0 e z_c}{2J} \right)^2 \left(\frac{\mu_a + \mu_c}{\mu_a} \right)^2 \quad (4)$$

where μ_c and μ_a are cationic and anionic mobilities, e is the electronic charge, J is current density, z_c is the cationic charge number, and C_0 is the initial cation (Li salt) concentration. D is the ambipolar diffusion coefficient $D = (\mu_a D_c + \mu_c D_a)/(\mu_a + \mu_c)$, where D_c and D_a are cationic and anionic diffusion coefficients.

The Sand's time model provides a quantitative understanding to describe Li dendrite formation and indicates that the time needed for dendrite growth is proportional to J^{-2} . Usually, Sand's time predicts dendrite formation at a relatively high density, $J > J^* = 2eC_0D(\mu_a + \mu_c)/\mu_a l$, where l is the length between two electrodes.¹²³ The marginal value of J^* indicates a negative correlation with the length between two electrodes, meaning that dendrite growth is easier in the pouch cell and electrolytic bath with larger length between two electrodes than tightly pressed coin cells. In the case of low current density $J < J^*$, the ionic concentration exhibits linear variations and local inhomogeneities seem to play a key role. Similar to these conclusions, some empirical results indicated that the occurrence time of dendrite increases as J^{-2} , while the period for crossing the cell is proportional to J^{-1} .¹¹⁴

Sand's time in varied temperatures was measured to describe the influence of cell resistance to dendrite growth.¹²⁴ It was found that, even though the current density remained constant, dendrites developed more slowly with the rise of temperature. Akolkar proposed a model for dendrite initiation at subambient temperature, where Li dendrite growth was accelerated at low temperature owing to the increased ion diffusion resistance and surface reaction resistance on the electrode surface.¹¹³ This model also predicted a critical temperature for uncontrolled dendrite growth at certain current densities.

5. LI DENDRITE GROWTH AFTER NUCLEATION

After nucleation, Li dendrites continue to grow into large deposits with prolonged length and sometimes augmented diameter. Other than being mastered by the interface feature of Li metal and electrolyte in the nucleation stage, Li dendrite growth is predominantly controlled by the electrolyte and the external applied factors. In this section, the Li dendrite growth process will be carefully described from different angles, including growth rate, growth patterns, and critical factors that influence them.

5.1. Growth Rate

The growth rate of Li dendrites is in essence determined by the Li ion migration direction and rate, which are driven by the electronic field and concentration gradient in electrolytes. These factors are mainly directed by external applied charging conditions (current density, charging time, etc.). Besides, the properties of the SEI layer (electronic and ionic conductivity) and electrolytes (viscosity, ionic mobility, etc.) also play roles in impacting the Li ion migration. Several models have been proposed on Li dendrite growth rate. Most of these models are based on the electric field and Li ion concentration distribution in liquid electrolytes of LMBs. Here, we summarized the essential parameters that directly drive the growth rate of Li dendrites.

5.1.1. Electronic Field. The electronic field is the first driving force in Li dendrite growth. Several models have been proposed to describe the Li dendrite growth based on the electronic field. Chazalviel found that the growth of a ramified metallic electrodeposit like Li dendrites in dilute salt solutions is essentially driven by the space charge that tends to develop

upon anion depletion near the anode.¹⁰⁶ The front of the dendrites has been shown to advance at a velocity $v_a = -\mu_a E_0$, which is just the velocity of the anion mobility, determined by the mobility μ_a and the electric field E_0 in the neutral region of an electrolyte.

However, Chazalviel's model has to be improved because it does not take into account the variations of parameters such as the diffusion parameters associated with ionic concentration. Brissot et al. observed that individual dendrites exhibit different velocities. Nevertheless, these velocities are not very far from the velocity predicted by Chazalviel's model. In particular, they seem to be almost proportional to the current density.¹²⁵ After several polarizations of the cell, dendrites seem to be unable to grow beyond a "barrier" at a given distance from the negative electrode. This distance is about the size attained by dendrites during the first polarizations (Figure 18).

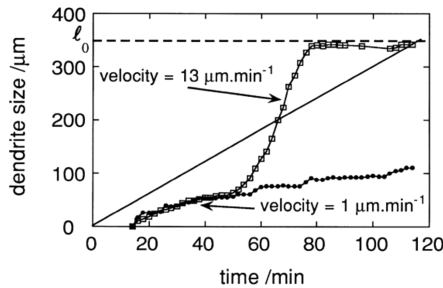


Figure 18. Evolution of size of two typical Li dendrites under 0.7 mA cm^{-2} . The solid straight line exhibits the calculated length predicted by Chazalviel's model for a cationic transport number $t_c = 0.15$. Reproduced with permission from ref 125. Copyright 1998 Elsevier.

The establishment of these models is mainly based on the electric field as the driving force, giving the growth rate and impacting factors of Li dendrites when the plating process is electronic field controlled. However, a practical system is more complicated than that, where many aspects act together.

5.1.2. Diffusion Flux. The electric field plays the main driving force for lithium ion migration only at the beginning stage of the Li plating process, which will then become a diffusion-controlled process afterward. Therefore, an accurate model must take into account both the effect of the electric field and the effect of concentration gradients on the growth of dendrites.

Akolkar developed a mathematical model to describe the dendritic growth process during Li electrodeposition near the Li surface along with electrochemical reactions (deposition) at the flat surface and at the dendrite tip (Figure 19).¹²⁶ This model incorporated transient diffusional transport of Li ions in a diffusion boundary layer. Generally, Li dendrite growth is strongly affected by an applied current density. When a cell is operated well below a limited current density, dendritic growth with a relatively low dendrite growth rate can be also observed. The numerical diffusion-reaction model proposed by Akolkar¹²⁶ estimated a dendrite growth rate of about 0.02 mm s^{-1} at an operating current density of 10 mA cm^{-2} . This result is very comparable with experimentally observed dendrite propagation rates from Nishikawa et al.¹²⁷

The Li dendrite growth rates in propylene carbonate (PC) and dimethyl carbonate (DMC) solvents with different ratios of PC/DMC were measured.¹²⁸ Dendrite growth rates were ranged at a relatively high value from 0.5 to 1.0 μm s^{-1} at a current density of 4.0 mA cm^{-2} . At the initial stage after Li

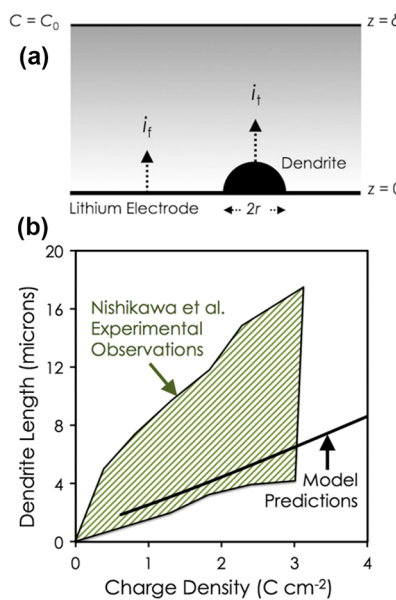


Figure 19. (a) Scheme of Li surface. A hemispherical dendrite "precursor" of radius r is presented on the Li surface. The dendrite tip grows at i_t and the flat electrode surface grows at i_f . (b) Comparison of model prediction with experimental results on Li dendrite propagation at 10 mA cm^{-2} . The cross-hatched region indicates the spread in the experimental observation. Reproduced with permission from ref 126. Copyright 2013 Elsevier.

dendrites were first observed, high PC content resulted in high dendrite growth rate. However, the growth rate in high PC content electrolyte decayed rapidly, while low PC content electrolyte could maintain a high growth rate with little decay during the full observation periods (300 s).

A global motion of the electrolyte toward the negative electrode occurred during the polarization. This is due to the variations of the salt concentration near the electrodes, inducing variations of the volume of the electrolyte in these regions.¹²⁵ Using data for the PEMO/Li bis(trifluoromethanesulfonyl)imide (LiTFSI) system, Newman's group found that dendrites always accelerated across cells, whose growth can considerably be slowed by lowering the current density.¹¹⁵ Cell shorting occurred during typical charges above 75% of i_L . Interelectrode distance was increased to put off cell failure, while the advantages decreased as distance lengthened. Surface forces have little effect on cell failure. Besides, no consistent trend was observed when varying the transport properties in the separator.

5.2. Growth Patterns

The Li dendrites exhibit various kinds of morphologies. Based on the main structures, deposition mechanisms, and different implications on cell performance, the morphologies of Li dendrites can be divided into three main patterns: needlelike, mosslike, and treelike (Figure 20). Needlelike dendrites grow simultaneously in both the length and diameter directions without branches. Such needlelike Li dendrites are the main culprit to cause short circuits in LMBs. Mosslike dendrites are always with smaller diameters, consuming more Li to form an SEI layer due to the high specific surface area, and they easily break off to form dead Li during the Li stripping process. Treelike dendrites, a textbook dendrite pattern, are widely investigated in dendrite simulations, and they can grow in all directions with typical disciplinary branches. Naturally, such

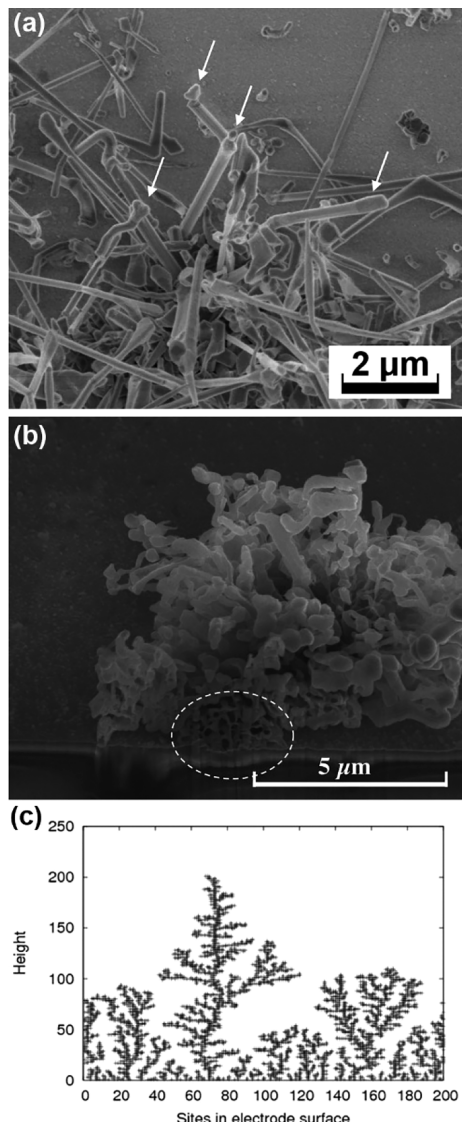


Figure 20. (a) SEM image of Li filaments deposited on W substrate at -100 mV. Reproduced with permission from ref 120. Copyright 2014 Elsevier. (b) SEM image of an FIB cross section of a Li bush grown in LP30 electrolyte on a W substrate. The marked region corresponds to the bush that connects to the W substrate. Reproduced with permission from ref 134. Copyright 2014 Elsevier. (c) Statistical DLA model results of treelike growth of Li dendrites. Reproduced with permission from ref 135. Copyright 2014 Nature Publishing Group.

treelike dendrites will also bring all kinds of hazards including short circuits and Li capacity loss. These three patterns have the same base units of cylindrical Li deposits.¹²⁹ The cylindrical structure is induced by the much higher growth rate at the tip than at the sidewalls.¹³⁰ Confirmed by the crystallinity of Li dendrites, the deposition rate is crystal face dependent with some faces being more active for electrodeposition than other ones.¹³¹ A comprehensive understanding of this crystal face dependent growth of Li deposits will be critically important in suppressing Li dendrite growth.

5.2.1. Needlelike Li. The needlelike pattern is a category of Li dendritic deposits without too many branches and can maintain the features of 1D structure.^{132,133} Needlelike Li deposits are frequently reported in the literature (Figure 20a).¹²⁰ Steiger et al. observed the growth and dissolution of electrodeposited Li filaments.¹²⁰ The observed Li dendrites can

grow from all the locations of previous Li nucleation, such as the tip, the base, and areas between kinks, which may be dominated by insertion at crystalline defects, e.g., kinks or interfaces. These sites for Li dendrite growth are always considered to be induced by defect control, including thin parts of the SEI, grain boundaries or amorphous regions, and chemical inhomogeneities of previous Li deposits.¹³⁰ Compared to other dendrite patterns, needlelike Li deposits always possess the most complete and largest metallic Li crystal. Some of the needlelike dendrites have a length of several decades of micrometers. Such highly crystalline needlelike dendrites with long length and large diameter could easily penetrate the separator, causing cell short circuit and safety concerns.

5.2.2. Mosslike Li. Li needlelike growth is a quasi-1D and linear elongation. At some certain conditions including branching and the multiplication of defects, the 1D needlelike Li can grow into the 3D omnidirectional mosslike (or bushlike) Li. The transition from 1D filaments to 3D moss growth occurs by broadening and branching during filament growth. The growth of moss Li can be described by the raisin bread expansion model (or cosmological model, Figure 20b).¹³⁴ In this model, there is no preferred direction and the distance between each raisin in the bread increases as the bread expands. The growth of the raisin bread has no growth center, but the movement of the parts can be restricted due to its support. In the case of mossy Li growth, the metal substrate fixes the bases of the bushes. Li atoms are inserted into the bush at several points that are scattered over the whole structure. During the mossy Li growth, it is observed that the dendritic tips can grow and get broader in some cases. However, mossy growth does not necessarily occur at the tips. Instead, the mossy growth often happens in growth points distributed throughout the moss. The grain boundaries, e.g., at kinks of needles or in between Li particles, are the relevant growth points where Li is inserted into the intact metallic backbone of the moss.

Mossy growth of metallic battery anodes has to be avoided to minimize interface area and reduce electrolyte decomposition in cells. The growth and dissolution of Li mossy structures is a very dynamic process involving nonlinear, apparent random growth and motion of the tips of the Li filaments, which are not dominated by the direction of the electric field in the bulk electrolyte solution. During dissolution, large parts of the moss can get isolated from the current collectors causing a loss of active material, known as “dead Li” in the literature.^{136,137} This can happen even if the material remains attached to its original position at the substrate, because the electrical contact sites are substituted by insulating SEI layer.

5.2.3. Treelike Li. Treelike Li has been widely investigated in recent years. Treelike dendrites can grow at all directions including length, diameter, and branches. Besides, the branches are always disciplinary with a neat hierarchical structure. They are the most basic type of electrodeposition in modeling and simulations, but are not common like needlelike and mosslike dendrites in experimental LMBs. We considered that, under most experimental conditions, metallic Li dendrites cannot grow in all directions at the proper rates and with stable branch structures, since the plating process is mainly controlled by mass transfer of Li ions in electrolyte. As a result, the dendrites may grow into needlelike (main growth in length and diameter) or mosslike (main growth in length and irregular branches). These treelike Li deposits were observed by experimentally and theoretically (Figure 20c).¹³⁵ The treelike morphology is also frequently observed in other metal electroplating, such as Pb¹³⁸

and Au.¹³⁹ A nonlinear phase-field model, accounting for the Butler–Volmer electrochemical reaction kinetics, was employed to investigate the treelike patterns during an Li ion electrodeposition process.¹⁴⁰ This treelike pattern greatly depends on the applied voltage and the interface morphology.

Except for some differences, these Li plating morphologies and patterns can transform into each other at some specific conditions. There is a space-charge region concentrated near the tips of the growing dendrites.¹⁰⁶ These Li deposits can progressively transform from the “dense-branching” (treelike) morphology to the “diffusion-limited aggregation” (mosslike) morphology due to the change of the electric field and the induced average dendrite spacing. A current–capacity relationship to differentiate the mosslike Li and needlelike Li was discovered.¹⁴¹ The Li depositing pattern change from root-growing mossy Li to tip-growing needle Li at the onset of electrolyte diffusion limitation was visualized (Figure 21). The



Figure 21. Current-dependent Sand's capacity. Reproduced with permission from ref 141. Copyright 2016 The Royal Society of Chemistry.

dense root-growing mossy Li forms on Li metal anode at a low current ($<10 \text{ mA cm}^{-2}$). With increasing depositing capacity (time), needlelike Li emerges. When the current density exceeds 20 mA cm^{-2} , the depositing morphology is a typical needlelike Li. Similar results have also been achieved by Brissot et al.¹²⁵ and Orsini et al.¹⁴² Therefore, these three patterns always coexist in the Li deposits and it is really difficult to clearly distinguish them from each other. Nevertheless, conveniently simplifying Li depositing morphology is critically necessary to efficiently tailor electrode surface morphology and design a safe battery with dendrite-free deposits.

5.3. Influencing Factors

In addition to the essential factors brought by the electrolytes, electrode material, and SEI layer, the growth rate and growth patterns can be also significantly affected by external conditions, such as the charging current density, charging capacity, operating temperature, and inner pressure of the LMB.

5.3.1. Current Density and Charge Capacity. It is generally accepted that a large current density and a long charge duration lead to severe dendrite growth. However, when the Li deposition is charge transfer controlled and the current is relatively small, the deposits can distribute well with an increased current density.¹⁴³ The effect of the amount of charge and current density on the surface morphology of a Li powder electrode was systematically investigated.¹⁴⁴ An empirical formula (eq 5 or simplified as eq 6) and corresponding curve were established to clearly indicate the relationship between Li

dendrite growth and current density/amount of charge (Figure 22).

$$Q = \frac{5.58133}{1 - 1.0286J + 0.4957J^2} \quad (5)$$

$$\{(J - 1)^2 + 1\}Q \approx 11 \quad (6)$$

where J is the current density and Q is the total amount of charge.

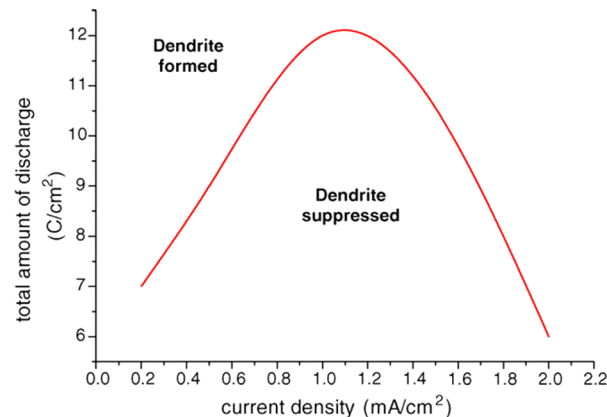


Figure 22. Relationship between the total amount of discharge and current density. Conditions corresponding to the area under the line suppress dendrite growth of Li deposits. Reproduced with permission from ref 144. Copyright 2008 Elsevier.

Based on the prediction results by eqs 5 and 6, with the rise of current density, there is a rise and then fall of the amount of charge needed to guarantee no dendrite formation. Li dendrite growth cannot be fully suppressed when the amount of charge exceeds 12 C cm^{-2} (3.3 mAh cm^{-2}). The tendency to dendrite formation is reduced when the current density is smaller than about 1.0 mA cm^{-2} with an extended depositing time.

A similar conclusion can also be achieved on the destructive role of large current density and long charge time for the 2D Li metal foil electrode, but without an empirical formula.^{145–147} The current density can affect the Li^+ ionic mass transfer rate associated with the electrodeposition, Li^+ bulk concentration, and the state of SEI layer depending on the Li salt to strongly control Li depositing morphology. Nevertheless, higher applied current density does not always promote larger dendrites because larger current density leads to an increase in the number of the electrodeposition sites and thus a dendrite-free morphology. Furthermore, apparent current density is totally different from the local current density value. Both low Li^+ ion concentration and localization of current density induced by a large local current density promote dendrite growth.¹²⁷ The recent concepts later introduced in section 7 demonstrate that, though employing a large apparent current density, low local current density can be achieved. Consequently, Li dendrite growth is suppressed.^{145,148}

5.3.2. Temperature. The viscosity and ion association of electrolyte, as well as surface SEI thickness, are highly dependent on the temperature. Therefore, the diffusion and surface reactions of Li ions are strongly temperature-dependent processes. The cycling performance of a Li metal anode in a vinylene carbonate (VC) containing electrolyte at different temperatures (0, 25, 50 °C) was investigated (Figure 23).¹⁴⁹ Adding FEC into the EC + DMC (1:1) electrolyte results in a

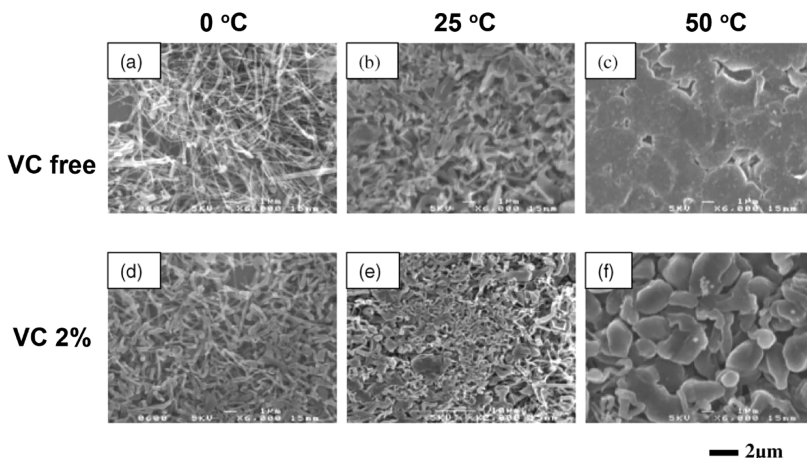


Figure 23. Li deposits on Ni substrate after initial Li plating at (a, d) 0, (b, e) 25, and (c, f) 50 °C in (a–c) 1.0 mol L⁻¹ LiPF₆/EC + DMC (1:1), and (b–f) 1.0 mol L⁻¹ LiPF₆/EC + DMC (1:1) + 2.0 wt % VC using pressurized Li/Ni cell. Reproduced with permission from ref 149. Copyright 2004 Elsevier.

Li dendritic morphology, thicker surface film, and decreased Coulombic efficiency at a low temperature of 0 °C. When the temperature is elevated to 50 °C, the cell containing FEC indicates an excellent cycling performance. The conflicting role of FEC on the cell performance is induced by the extreme temperature sensibility of FEC induced SEI film. They also extended to ethylene carbonate (EC) + tetrahydropyran (THP), dimethoxyethane, dimethyl carbonate (DMC), propylene carbonate (PC), and γ -butyrolactone (GBL) solvents and found the superiority of high temperature (50 °C). AFM was employed to probe the role of the further improved temperature (40, 60, 80 °C).¹⁵⁰ The surface SEI film formed at 40 °C is inhomogeneous, and large masses of dendritic Li deposits appear after prolonged deposition (0.3 C cm⁻²). In contrast, increasing the electrolyte temperature (60 and 80 °C) can lead to a closely packed, uniform surface film consisting of particle-like deposits of 100–200 nm. Even after prolonged deposition and repeated dissolution, no significant morphology change is observed. An enhanced surface diffusion of Li ions at the elevated temperatures contributes much to dendrite-free Li deposits.

To theoretically explore temperature effects on Li ion diffusion and surface film formation, an analytical model was contributed by Akolkar.¹⁵¹ The model adopting a steady-state diffusion–reaction model can predict the dendrite growth rate during Li electrodeposition at subambient temperature to investigate the temperature dependence of the dendritic growth process (Figure 24). The model predicted a critical temperature below which uncontrolled dendrite formation was initiated at a given applied current density (corresponding to a battery charging rate). The in situ method was employed to optically investigate the Li nucleation number, dendrite initiation duration, and growth rate at ambient and subambient temperatures (−10, 5, and 20 °C) in symmetrical Li|Li cells.¹⁵² Compared with cells operated at −10 and 20 °C, the cells failed most rapidly at 5 °C. Dendrite initiation occurs earliest at −10 and 5 °C, while longer initiation times were obtained at 20 °C. The morphology of electrodeposits changed with formation temperature, where low temperature formed mushroom-shaped deposits while Li needles transformed into round balls and particulates at 5 and 20 °C, respectively.

5.3.3. Pressure. When physical pressure is applied to Li electrode in the working cell, Li dendrite deposition can be

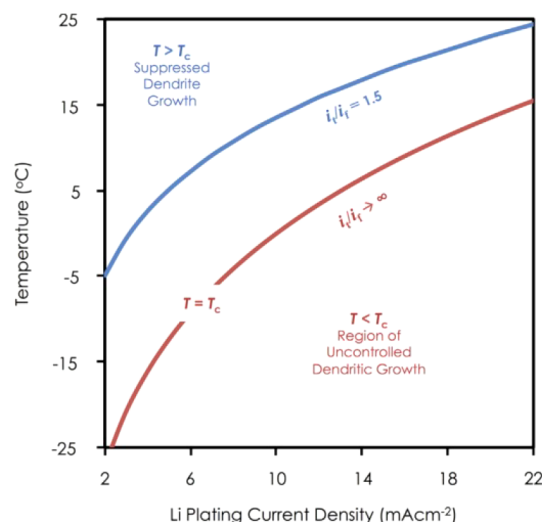


Figure 24. Dependence of Li dendrite growth rate with temperature and Li plating current density. Reproduced with permission from ref 151. Copyright 2014 Elsevier.

partly inhibited. The pressure widely exists in the cell, which can be produced by the cell assembly, membrane and SEI squeezing, and Li depositing. Nevertheless, the critical role of pressure is hard to evidently investigate due to the difficulty in practical operations of pressure modification. Monroe and Newman pioneered the research of theoretically understanding how mechanical forces affect Li dendrite nucleation and growth.¹¹⁵ Based on the prestressed Li electrodes, they assumed that surface tension can hamper the evolution of interfacial roughness. This scenario reached a conclusion that prevention of dendrite growth by mechanical methods can be achieved by adopting electrolytes with a very high shear modulus at least 2 times larger than that of Li metal. The role of pressure on Li depositing was further considered, and a different scenario of relaxed Li metal without any preexisting surface stresses was scrutinized (Figure 25).¹⁵³ During cycling, new Li deposited at the electrode–electrolyte interface. To accommodate this freshly deposited Li, both the Li electrode and electrolyte (either liquid or solid) were pushed backward, giving rise to compressive forces. Likewise, Li deposits also experienced compressive forces from the neighboring electrode

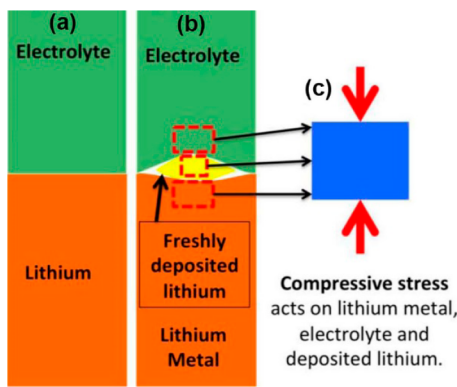


Figure 25. (a) Scheme of initially relaxed Li/electrolyte interface. (b) Li deposition at Li/electrolyte interfaces. (c) Compressive stress acting on Li metal, electrolyte and newly deposited Li. Reproduced with permission from ref 153. Copyright 2017 The Electrochemical Society.

and electrolyte. Therefore, Li metal, electrolyte, and the freshly formed Li deposits all experienced compression. This scenario was quite different from the prestressed one proposed by Monroe and Newman, where Li metal was regarded to be under a preset tension.¹¹⁵

A direct verification of the role of pressure on Li plating was conducted by Hirai et al.¹⁵⁴ They studied the impact of cycling efficiency (E) on stack pressure in LiAsF_6 electrolytes with different solvents, where a figure of merit (FOM), $\text{FOM} = 1/(1 - E)$, was introduced to amplify the difference between efficiencies. The results revealed that approximately all the cycling efficiencies increased with the rising of applied pressure. This influence was more pronounced in 2-methyltetrahydrofuran (2MeTHF) and ethylene carbonate (EC)/2MeTHF electrolytes than in PC and EC/PC electrolytes.

6. THEORETICAL ANALYSIS OF LI DENDRITE FORMATION

Li dendrite nucleation and growth simulation is becoming a critically important method to investigate Li ion diffusion and depositing behavior, since the induction of Li dendrite growth mechanisms by only experiments is particularly difficult. The simulation of Li ion migration in electrolytes has been widely conducted to investigate the Li plating process in the liquid phase. Both coarse-grain models and finite-element methods based on electric field and ion concentration distribution are proposed to simulate the Li ion flow in the electrolyte phase.

But the simulation of electrochemical plating in solid phase (continuously transformed electrode surface) is not easy like the one of Li ion migration. Recently, the phase field model has also been introduced to simulate the Li deposition process, taking into account both liquid and solid phases. Hence, the models and simulations of Li ion migration and the Li plating process have become relatively mature. These models and simulations mainly focus on the ionic migration in electrolyte, surface diffusion on Li metal, and Li plating interface reactions. However, there is still no report on the more accurate simulations taking into account the SEI layer in the Li plating process.

6.1. Ionic Migration

The simulation of ionic migration is the most basic one in the theoretical analysis of lithium dendrite growth. A coarse-grain Monte Carlo (GC-MC) model was proposed by Hoffmann and co-workers to describe the ionic migration; electromigration in time-dependent electric fields and deposition at the anode were able to predict the experimental trends of pulse charging on average dendrite lengths.¹⁵⁵ The runaway growth of electrolytic Li dendrites could be better controlled by increasing the mobility of Li atoms on the solid than by increasing the mobility of Li^+ ions in the electrolyte. Based on these simulations, specific approaches to suppress Li dendrite growth can be obtained, such as enhancing interfacial Li atom diffusion by implanting extrinsic defects (Figure 26).¹⁵⁶

Miller and co-workers introduced a coarse-grained simulation model for the reductive deposition of Li cations in LMB. The heterogeneous and nonequilibrium natures of the electrode-deposition dynamics were accounted for. The coarse-grained simulation model enabled simulation of the long time scales and length scales associated with metal dendrite formation. The effects of applied overpotential and material properties on early stage dendrite formation, as well as the molecular mechanisms that govern this process, were predicted. The dendrite formation propensity increased with the applied electrode overpotential. The time dependence of the applied electrode overpotential can lead to positive, negative, or zero correlation between cation diffusivity in the SEI film and dendrite formation propensity.¹⁵⁷

Most research into Li dendrites concentrates on Li plating/stripping behavior in isotropic electrolytes (i.e., an isotropic diffusion coefficient in electrolytes). However, this is quite different from a real working electrolyte, because properties including the diffusion coefficient are not identical in every

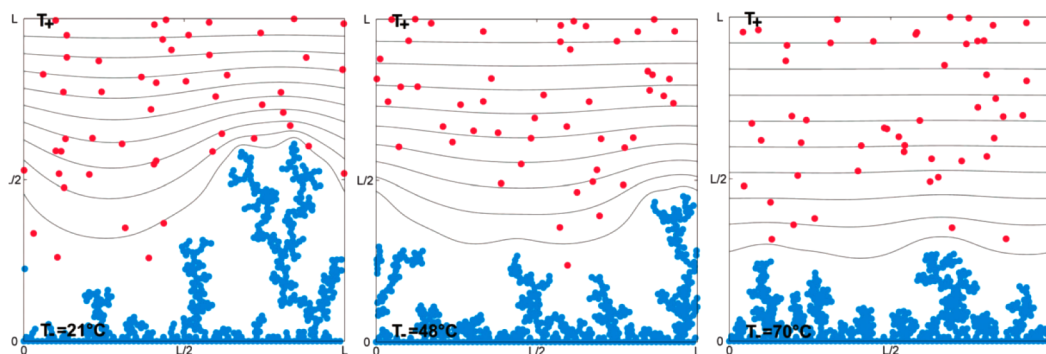


Figure 26. Calculation results of both Li^+ transport and Li thermal relaxation through a CG-MC method. Blue dots: Li in dendrites. Red dots: Li^+ ions in solution. Gray lines are isotherms. From left to middle to right, results at $T_+ = 21, 48,$ and $70\ ^\circ\text{C}$, respectively. Reproduced with permission from ref 156. Copyright 2015 The Royal Society of Chemistry.

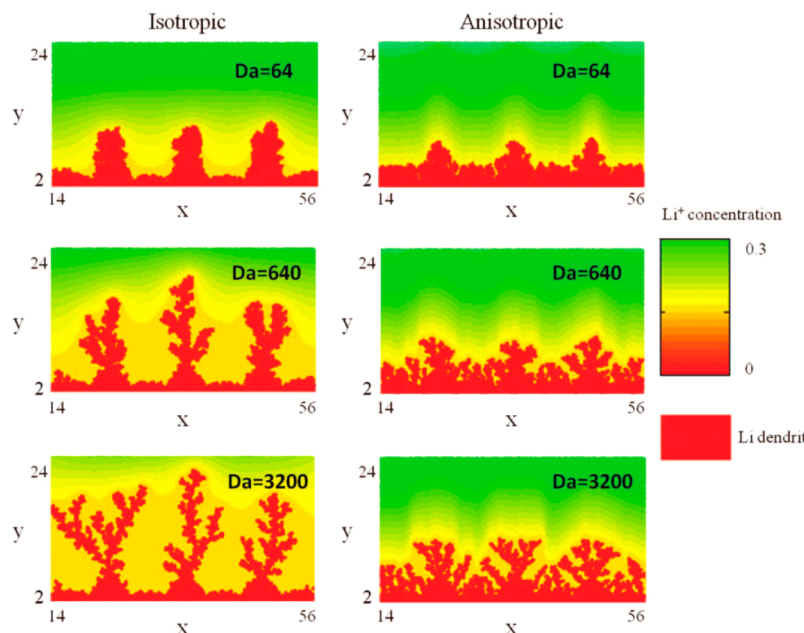


Figure 27. Simulation of Li dendrite growth (time = 3000) resulting in isotropic and anisotropic electrolytes. Isotropic cases: $L = 64$, $D = 1$. Anisotropic cases: $L = 64$, $D_{xx} = 0.01$, $D_{yy} = 1$. Reproduced with permission from ref 158. Copyright 2016 The Electrochemical Society.

position of working cells. A novel smoothed particle hydrodynamics–continuum surface reaction (SPH–CSR) model was proposed to describe the dendrite growth in anisotropic electrolytes.¹⁵⁸ This model adopted a Lagrangian particle-based method rather than previous particle-based anisotropic diffusion models (Figure 27). Several conclusions were reached based on the results from this model: (a) Anisotropic electrolytes can enhance the mass transport near the sites for dendrite nucleation and growth to reduce the replenishment time for Li ions. Consequently, dendrite growth in anisotropic electrolytes is significantly suppressed. (b) The effect of anisotropic mass transport on suppressing Li dendrite growth reaches saturation when the mass transport anisotropy is more than 10^2 . This method demonstrated the effects of anisotropic transport on dendrite growth and morphology, and exhibited the possible advantages of anisotropic electrolytes for dendrite suppression.

6.2. Dendrite Growth

The simulation of dendrite growth itself is challenging due to the continuously transformed electrode surface during Li plating and the electrochemical plating reaction. By extending the asymptotic analysis of the phase-field theory, a reference frame invariant formulation was developed that incorporated experimentally measurable physical parameters, including work of adhesion, interfacial electroplating, and electrolyte–dendrite surface tension.¹⁵⁹ In the absence of diffusion limitations, they demonstrated the importance of the chemistry of the substrate for Li electrodeposition. The small contact angles favored uniform Li layers and high Coulombic efficiencies, while large contact angles and high C-rates promoted Li dendrite detachment, lower charging rate efficiencies, and undesirable side reactions, as a consequence of the electrochemical shielding and field localization (Figure 28).

A novel thermodynamically consistent phase-field model, accounting for the nonlinear reaction kinetics, was proposed to investigate the dendritic patterns during an electrodeposition process (Figure 29).¹⁴⁰ The model has been validated by

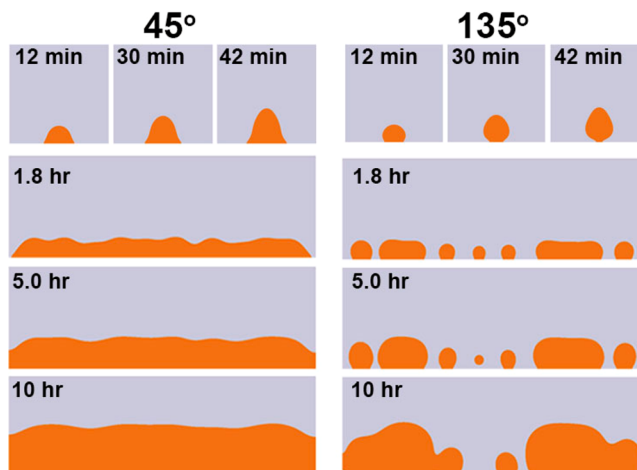


Figure 28. Phase morphology of deposited Li nuclei at different contact angle boundary conditions at 0.04 mA cm^{-2} . Reproduced with permission from ref 159. Copyright 2014 Elsevier.

comparing the equilibrium electrode–electrolyte potential difference with the Nernst equation, taking an example of Li electrodeposition on Li metal. They reproduced the Butler–Volmer nonlinear electrochemical kinetics in a 1D non-equilibrium system. Three different dendritic patterns have been discovered depending on the applied voltage and the interface morphology. A phase diagram was proposed, which was potentially used as the guide to experimentally regulate Li dendrite patterns. Analysis of the dendritic patterns demonstrates that the large applied voltage or the flat protuberance at the interface contributes to the side branches of dendrites, and even promotes an unstable tip splitting.

6.3. Surface Diffusion

Surface diffusion is often simulated by CG-MC methods. The thermal annealing kinetics of Li dendrites was quantified to describe the Li ion diffusion on the anode surface.¹⁶⁰ The Li dendrite was simulated using the CG-MC framework and by

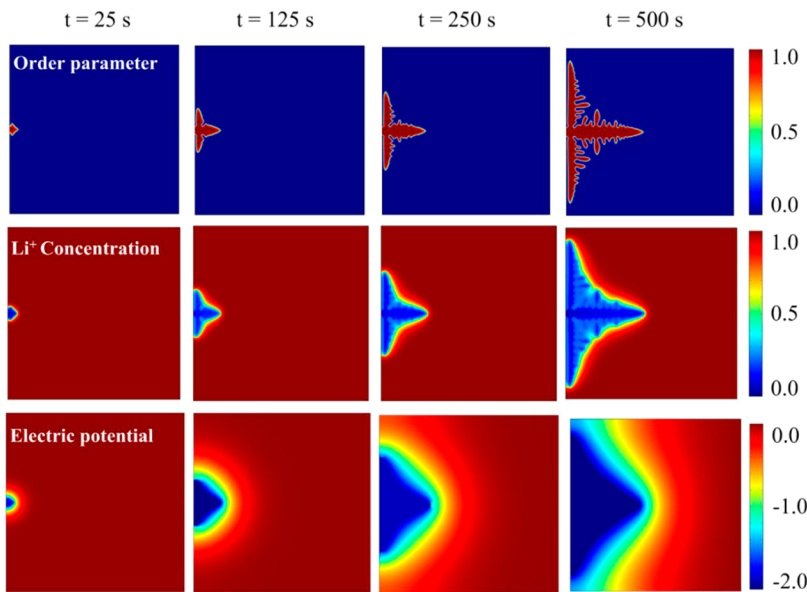


Figure 29. Snapshots of order parameter, Li^+ concentration, and electric potential. Reproduced with permission from ref 140. Copyright 2015 Elsevier.

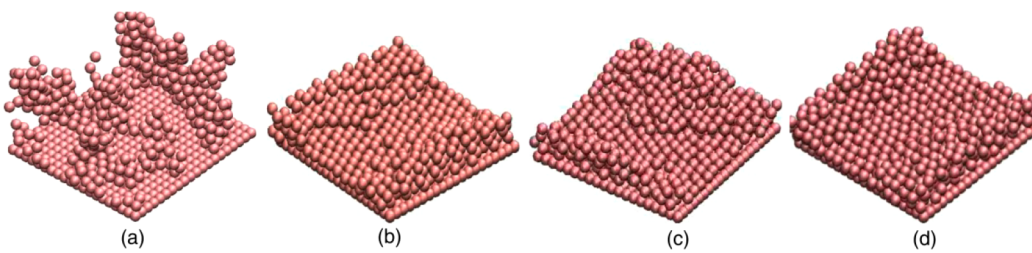


Figure 30. (a) Calculated initial optimized dendrite glass phase through on CG-MC method. Final morphologies after 200 ps NVT simulations at (b) 317, (c) 337, and (d) 357 K. Reproduced with permission from ref 160. Copyright 2015 Elsevier.

training the ReaxFF framework for Li. The effective thermal relaxation energy barrier was therefore predicted. The acquired effective activation energy of 7.1 kcal mol⁻¹ from the experiments matches well with the corresponding value of 6.3 kcal mol⁻¹ from simulations. The surface diffusion of low-coordinated atoms and bulk diffusion are ascribed as the dominant mechanisms for thermal relaxation of Li dendrites. The results have potential to predict the internal structural properties of amorphous dendrites such as the dominant coordination number, porosity, branching characteristics, and material dependency (Figure 30).

In summary, these simulations on Li dendrite growth have successfully presented some of the properties on Li ionic migration in electrolytes and Li atom surface diffusion in the electrode, and have even given simulated Li dendrite patterns with the introduction of the phase-field model. Nevertheless, the simulations on the SEI layer which impact directly the electrochemical plating reactions are still less involved. New models and simulation methods are highly required to describe the Li dendrite growth process in consideration of the formation and impact of the SEI layer. With more accurate models and simulations, it is promising to even precisely predict the Li plating morphology with given electrolyte, electrode, and external charging conditions.

7. SUPPRESSING LI DENDRITE FORMATION FOR A SAFE LI METAL ANODE

Until now, there has been no model that can precisely and completely describe how Li dendrites nucleate, grow, and deteriorate the cycling performance of LMBs. Some models even contradict each other. That is very understandable, due to the difficulty in characterizing the working Li metal anode and high-throughput calculation under the participation of ions and electrons. Nevertheless, a considerable number of methods have been proposed to suppress Li dendrite growth. Some Li metal anodes with dendrite-free morphology have been achieved under specific conditions. Especially with the hot research of high energy density Li–S and Li–O₂ batteries, safe operation of Li metal anode has been greatly valued. By modifying the separator, electrolyte, and anode itself, many solutions have been presented to reveal the secret of the Li metal anode.

7.1. Electrolyte Additive

Dendritic Li growth at all stages is highly influenced by the chemical nature of the electrolyte, including the ester and ether based liquid electrolyte, and the solid-state electrolyte. Liquid electrolyte can severely react with Li metal and lead to a low Coulombic efficiency. The ester based liquid electrolyte has a higher reactivity with Li metal than the ether based electrolyte, which results in serious dendritic Li growth and low Coulombic efficiency. Compared with the liquid electrolyte, solid-state electrolytes are relatively stable against Li metal, though some

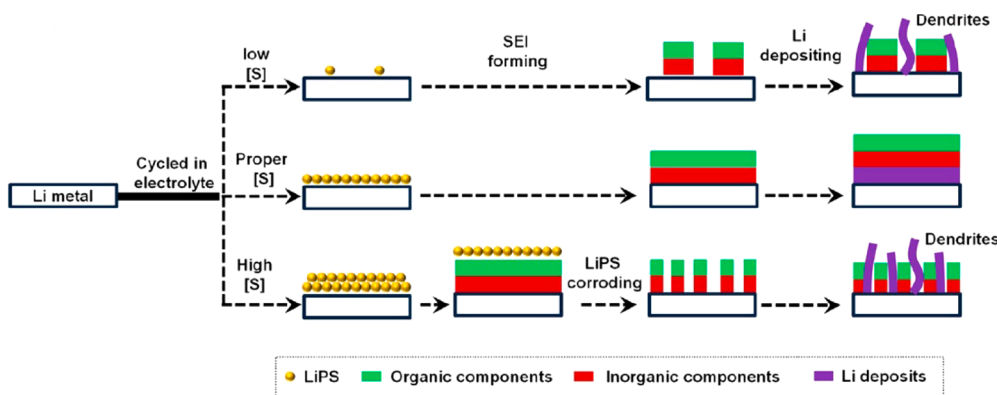


Figure 31. Scheme describing the role of Li polysulfide concentrations on SEI evolutions and Li depositing. Reproduced with permission from ref 195. Copyright 2016 Elsevier.

of them can partly react with Li metal. The reduced reaction between Li metal and a solid-state electrolyte is helpful to improve the Coulombic efficiency, reduce the dead Li, and suppress Li dendrites. Nevertheless, the solid-state electrolyte is not perfect. There are dendrite issues in a cell with a solid-state electrolyte. Deeply analyzing the dendritic Li growing behavior in these electrolytes is significant. In this section, dendritic Li growth and inhabitation in the liquid electrolyte are discussed.

Modifying an electrolyte with additives is one of the most convenient methods to suppress Li dendrite growth. Only small amounts of additives will bring about obvious changes.¹⁶¹ Except for constructing a stable SEI film to suppress dendrite growth, some electrolyte additives can render the composite electrolyte with a flame-retarded nature.^{162–164} Therefore, in the past decades, many research activities from scientific and engineering fields have been concentrating on the rational design of powerful additive species.

7.1.1. SEI Film-Forming Additives. Electrolyte additives are conventionally deemed sacrificial and designed to promote the formation of stable SEI during the initial activation cycles of Li metal anode. The formation of this SEI film can adequately prevent the electrolyte decomposition on Li metal anode in the following cycles.¹⁶⁵ First-principles calculations and microgravimetric measurements theoretically and experimentally indicate the availability of SEI coating to reduce the electrolyte decomposition.¹⁶⁶ SEI film is preferable for a highly efficient LMB, which has played an important role in the commercialization of graphite anode and high-voltage oxide cathode.

As discussed in section 3.1, nearly all the Li salts and nonaqueous organic electrolyte can react with Li metal to form a film on the Li metal due to the most negative nature of the electrochemical potential of Li. An effective electrolyte additive is able to react with Li metal before other electrolyte components to protect the stability of the electrolyte, and the formed film can stably exist in the interface of Li metal/electrolyte in a long-term cycling. Therefore, as a good electrolyte additive for Li metal anode, three primary requirements have to be satisfied:

1. It has a higher HOMO and lower LUMO to ensure the preferential reactions with Li metal, relative to Li salts in the electrolyte.
2. The reaction products (SEI component) can remain stable in chemical and electrochemical environments with an ionically conductive and electronically insulative nature.
3. The formed SEI film holds a dense and continuous structure without pinholes.

Apart from these three primary features, high modulus is also of critical importance to suppress Li dendrite growth in a Li metal anode. However, the *in situ* formed SEI during the activation cycles in the liquid electrolyte can hardly have a high and uniform modulus to suppress Li dendrite growth (see section 3.4). The electrolyte additives with the three primary features can function with other methods (such as structured anode) to suppress Li dendrite growth and achieve a high Coulombic efficiency of Li metal anode.

Various electrolyte additives have been designed, including the ones successfully adopted in commercialized Li ion batteries (including FEC^{167,168} and VC^{167,169,170}) and the other burgeoning ones for Li metal anode (including LiNO₃ and Li polysulfide). FEC is an extensively used film-forming additive in anodes of LIBs (such as graphite anode), because it can preferentially form a stable and dense LiF-rich SEI film and suppress the salt anion decompositions.¹⁶⁷ FEC was tried in the electrolyte systems for Li metal anode, 1.0 M LiTFSI–tetraethylene glycol dimethyl ether (TEGDME) electrolyte,¹⁶⁸ 1.0 M LiPF₆–dimethyl carbonate (DMC),¹⁷¹ and 1.0 M LiPF₆–ethylene carbonate (EC)/diethyl carbonate (DEC),¹⁷² achieving a good performance to suppress Li dendrite growth.¹⁷³ The 5.0 wt % FEC induced efficient SEI rendering a stable cycling when the Li metal anode matched the Li–LiNi_xCo_yMn_zO₂ (NCM, $0 \leq x, y, z < 1$) cathode.¹⁷² However, the protective role of FEC strongly depends on its concentration and high concentration usually results in long cycling life. Therefore, FEC can indeed protect Li metal anode, but it is continuously consumed during long-term cycling due to the instability of the formed SEI against Li metal in the long-term cycles.¹⁷⁴

FEC and VC are the kinds of electrolyte additives which can effectively protect graphite anode and also indicate some effects on the Li metal anode. Some other additives are specially designed for Li metal anode, such as Li[N(SO₂F)₂] (LiFSI),¹⁷⁵ KNO₃,¹⁷⁶ succinic anhydride,¹⁷⁷ Li bis(oxalato)borate (LiBOB),¹⁷⁸ LiODFB,¹⁷⁹ lanthanum nitrate,¹⁸⁰ 2-(triphenylphosphoranylidene) succinic anhydride,¹⁸¹ Py13TFSI ionic liquid,¹⁸² Li[(FSO₂)_nC₄F₉SO₂N]₁₈₃ 1,4-dioxane,¹⁸⁴ bromide ionomers,¹⁸⁵ methyl viologen,¹⁸⁶ poly(ethyl α -cyanoacrylate),¹⁸⁷ AlCl₃,¹⁸⁸ LiNO₃,¹⁶⁹ and even a mixed carbonate–ether electrolyte.¹⁸⁹ Some intermediates induced by the multielectron conversion chemistry can also be adopted as additives to protect Li metal anode. Li polysulfides (LiPS) are regarded as disgusting intermediates of Li–S battery, attributing much to cell capacity decay.^{190–192} Li et al.,¹⁹³ Zhao et al.,¹⁹⁴ and Yan et

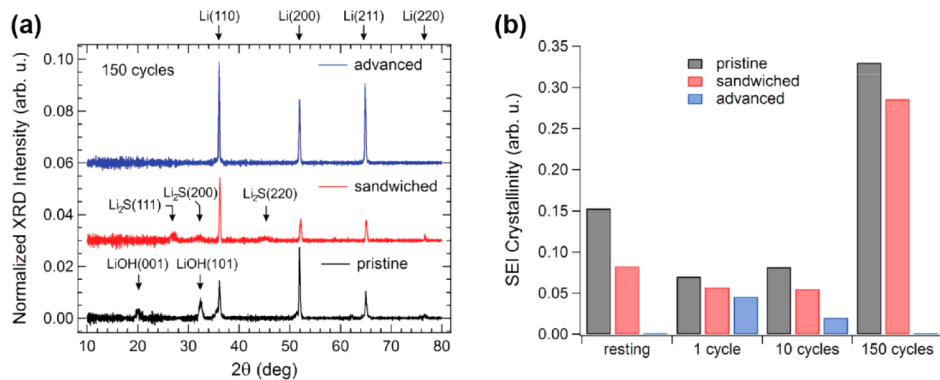


Figure 32. Structural and electrochemical properties of SEI films on Li metal. (a) XRD patterns for Li anodes of pristine, sandwiched, and advanced cells after 150 cycles. (b) Variation of SEI crystallinity on Li metal in different batteries. Reproduced with permission from ref 201. Copyright 2016 WILEY-VCH Verlag GmbH & Co. KGaA, Weinheim.

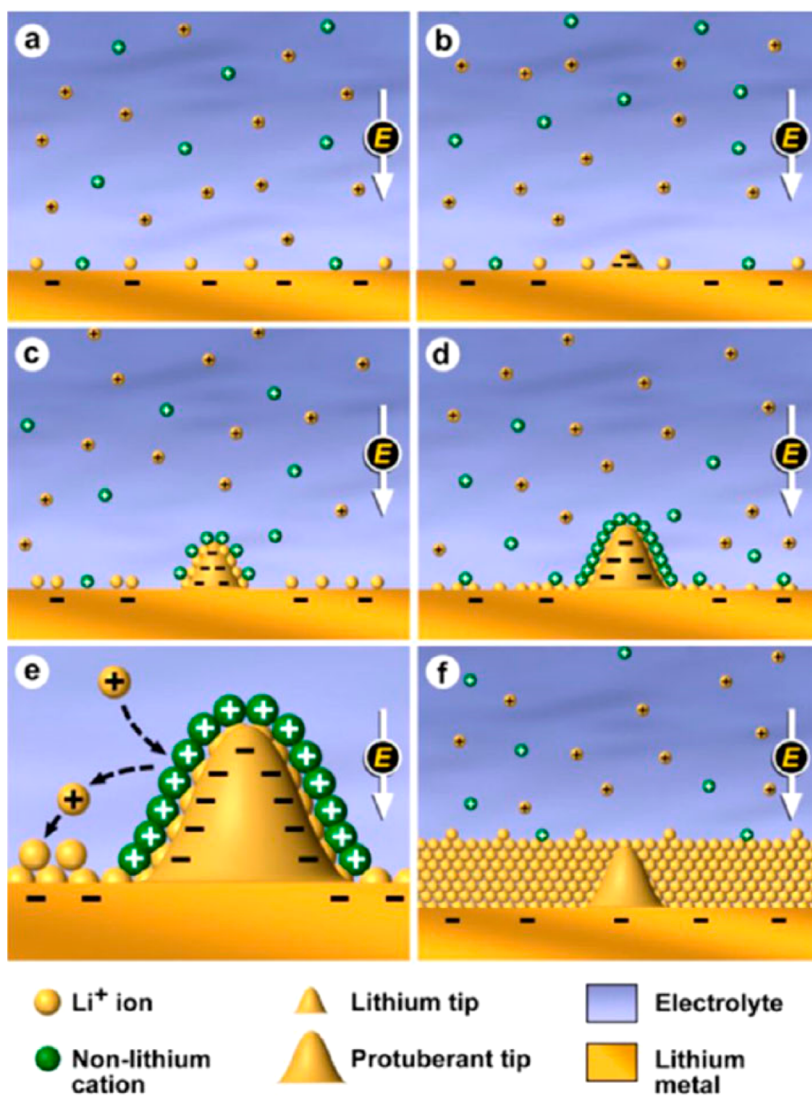


Figure 33. Illustration of Li deposition process based on the self-healing electrical shielding mechanism. Reproduced from ref 204. Copyright 2013 American Chemical Society.

al.¹⁹⁵ demonstrated that the growth of Li dendrites can be significantly suppressed by exploiting the reaction between Li, LiNO_3 , and Li polysulfide. A uniform and stable SEI film is constructed based on the synergistic effect of both LiPS and LiNO_3 in $\text{LiTFSI}-\text{DOL}/\text{DME}$ electrolyte.¹⁹⁶ The protective

role of LiPS on the SEI film relates tightly to its species and concentration (Figure 31). The role of the coaddition of both LiNO_3 and Li polysulfide were adequately confirmed by the in situ liquid-phase electrochemical SEM investigation.¹⁹⁷ Another magic molecule is water (H_2O), which is widely regarded as a

detrimental factor of nonaqueous electrolytes for Li batteries. However, a controlled trace amount of water (H_2O , 25–50 ppm) in LiPF_6 -based electrolytes can act effectively to achieve a dendrite-free Li metal deposition.¹⁹⁸ The controlled content of H_2O can well protect Li metal anode by constructing a uniform and dense LiF-rich SEI.^{199,200}

SEI film can be regarded as an ultrathin solid electrolyte attached to the anode, and the ionic conductivity is one of the most important indices of its performance (see section 3.3.2). Therefore, a certain kind of additive is especially put forward to improve the ionic conductivity of SEI film. A routine SEI film has a multilayer organic and inorganic layer, and the inorganic layer contributes much to the Li ion conductivity. The key to improve the Li ion diffusion flux lies in the inorganic layer. There are two methods to achieve this goal:

1. *Enhancement of ionic conductivity in the inorganic layer.* The crystallinity of SEI film formed between Li metal and electrolyte additives very much affects the ionic conductivity of the SEI film.^{201,202} A low crystallinity can lead to a high ionic conductivity. The crystallinity of SEI film can be reduced by electrolyte additives containing metal ions that have lower reactivity with sulfur than Li (e.g., Cu, Ag, and Au) (Figure 32)²⁰¹ and Li polysulfides that form Li_2S nanocrystals as “nanopins” to stop the growth of other inorganic crystals.^{193–195}

2. *Enrichment of conductive inorganic components in the SEI film.* When the content of the inorganic components rises, the ionic diffusion flux can be improved, and thus an extended Sand’s time and a suppressed dendrite growth (see section 4.3). A 10 mM KPF_6 additive shows an obvious impact on enriching the inorganic components.²⁰³ By analyzing the SEI film, the fraction of insulating PEO components in the KPF_6 -induced SEI is dramatically reduced by nearly half (from 12.1 to 6.6%), while the fraction of less resistive and more Li^+ -conductive components is improved from 36 to 47.9%. Therefore, the added KPF_6 increases the fraction of inorganic salts in the SEI film, making it highly Li ion conductive. This highly conductive SEI film can eliminate the growth of dendrites at 0.5 mA cm^{-2} . However, the growth of Li dendrites can be still observed at 2.5 mA cm^{-2} .

Electrolyte additives are of extreme importance to protect Li metal from the corrosion of electrolyte and improve the cycling Coulombic efficiency. However, the formed SEI film generally cannot stand the Li dendrite due to its low and unevenly distributed modulus. Therefore, high conductivity and compactness are more important, urgent, and feasible than the modulus for a successful SEI film. If an electrolyte additive can form this SEI film with high conductivity and compactness, it can work with some other methods to suppress Li dendrite growth and achieve a good performance of Li metal anode.

7.1.2. Li Ion Plating Additives. Another category of additive is the one that will not react with Li metal and electrolyte during the initial activation cycles and hopes to remain stable in the long-term cycling. These additives mostly do not participate the construction of SEI film, but affect Li ion diffusion and plating behavior. These kinds of additives are less often proposed than the SEI-forming additives. Up to now, only two kinds of additives acting this manner have been discovered: (1) alkali metal ions and (2) halide ions.

1. Ding et al. employed alkali metal ions with specific concentrations as the additives and proposed a shielding mechanism to fundamentally alter dendrite formation (Figure 33).²⁰⁴ These alkali metal ions (such as cesium or rubidium

ions) have a lower effective reduction potential than that of Li ions at low concentrations, rendering them stable during Li plating. After Li plating, a positively charged electrostatic shield around the initial growth tip of Li dendrites was achieved from these additives to force the further deposition of Li ions to adjacent regions of the anode. This strategy can effectively suppress continuous Li dendrite growth and improve the safety performance of Li metal anode.^{205–207} However, the concentration of metal ions needs to be carefully selected to avoid electrochemical reduction. Other alkali metal ions (such as sodium¹³⁰), alkaline earth metal ions²⁰⁸ (such as calcium, strontium, and barium), and *N*-methyl-*N*-butylpiperidinium²⁰⁹ can render a similar effect on dendrite growth.

2. Li halides with a low diffusing energy and high surface energy have exhibited an overwhelming importance in controlling surface diffusion of Li ions during electrodeposition, and thus the dendrite-free Li depositing morphology is achieved.¹⁰¹ The halogenated salt blends are employed in liquid electrolytes to stabilize Li metal anode. The as-obtained cell exhibits stable long-term cycling at room temperature, often with no signs of deposition instabilities over hundreds of cycles of charge and discharge and thousands of operating hours.^{210,211}

These additives are promising for suppressing Li dendrite growth if they can stably exist in long-term cycling. However, there does not exist a methodology to include all the methods of these plating additives. Therefore, it is very hard to sustainably design these plating additives. They are like isolated gems. Successfully discovering them needs much luck if you do not have a clear instructional principle.

7.2. Artificial SEI

The *in situ* formed SEI films are complicated, and limited understanding has been achieved on what are the specific components of the formed SEI and how they influence SEI layer properties and cell performance.³⁹ To avoid an uncontrolled process during SEI forming, a family of methods have been explored to construct a robust layer before cell cycling *ex situ* and artificially. These artificial strategies afford another feasibility to modify SEI films in a working cell.²¹²

7.2.1. Electrochemical Pretreatment. Electrochemical pretreatment is accessible to achieve a real SEI film similar to that formed in a working cell, because the initiators are often the effective additives. The requirements of these initiators are comparable to those of the SEI-forming additives discussed in section 7.1.1. Relative to the *in situ* formed SEI film in the working cells, the advantage of coating layer on Li metal anode obtained by the electrochemical pretreatment is that the electrolyte adopted in the activation stage can be different from that in the cycling stage and hence the selection of electrolyte additives is free from the cycling electrolyte. This can lead to several merits:

1. Any possible electrolyte additive can be chosen, though they are not beneficial for long-term cycling of Li metal anode when they exist in the electrolyte.

2. The concentration of additives can be extrahigh or extralow, despite the requirement of the cycling electrolyte in the viscosity and ionic conductivity.

3. The selection of solvent in the pretreatment is not subjected to requirements of the cathode, such as the oxidative stability of electrolyte in the high-voltage cathode, routinely ether based solvent in the sulfur cathode, routinely carbonate ester based solvent in the oxide cathode, etc.

In a word, the electrochemical pretreatment renders the selection of initiators to not be subject to the requirements of the electrolyte, cathode, and anode in the long term cycling, but only to the initial cycle activation to form a good SEI film on the Li metal anode.

Several initiators have been employed to demonstrate this strategy in Li metal protection, such as the frequently used FEC.²¹³ The formed artificial SEI film can effectively preserve the merits of FEC-induced SEI film to be applied in Li–O₂ batteries. An efficient artificial SEI film was electrochemically preconstructed through the chemical reactions between a strong Lewis acid (aluminum iodide (AlI₃)), Li metal, and aprotic liquid electrolytes.²¹⁴ The as-obtained SEI film was with components of Li–Al alloy, a LiI salt layer, and a stable thin polymer layer on Li metal anode, significantly enhancing the inhibition of Li dendrite growth and the Coulombic efficiency. The artificial SEI film can also be constructed by galvanostatically cycling Li metal only once in a composite electrolyte, including PC and DMC with Li salt of Li bis-(perfluoroethylsulfonyl)imide (Li(C₂F₅SO₂)₂N) and an additive of aluminum, AlI₃.²¹⁵ The pretreated Li electrode exhibited high cycling ability in the subsequent cycles even after it was transferred to an AlI₃-free electrolyte. Some researchers reported that cyclic voltammetry premodulation can drastically improve lithium electrodeposition kinetics by tailoring the top layer of SEI film to facilitate a two-dimensional growth mode.²¹⁶

However, these strategies do not highlight the advantages of the electrochemical pretreatment, because the cycling electrolyte seems the same with the pretreated electrolyte except for the initiators. An implantable SEI film was constructed by a general electroplating route by precycling Li metal in a LiTFSI (1.0 M)–LiNO₃ (5.0 wt %)–Li₂S₅ (0.02 M)–1,3-dioxolane (DOL)/1,2-dimethoxyethane (DME) ternary salt electrolyte (Figure 34).²¹⁷ The implantable SEI can adequately suppress Li dendrite growth by increasing the short circuit time from 3 to 5.5 h. Importantly, the formed implantable SEI film can not

only work well in the original DOL/DEM electrolyte, which is adopted to form the implantable SEI film, but also realize a high cycling performance in the EC/DEC electrolyte.

The electrochemical pretreatment provides a promising method to modify Li metal anode in an electrolyte different from the cycling one. However, the current research does not maximally take advantage of the electrochemical pretreatment and merely considers it as a conventional method to ex situ construct the SEI film. Besides, the electrochemical pretreatment is a little complicated, including pretreatment in cells, disassembly of the cells to obtain the protected anode, assembly, and operation in new cells. How to simplify this process to be facilely applied in practical cells is of vital importance. Nevertheless, this strategy is very ingenious and promising to separate the SEI formation from the cell cycling and is expected to achieve a highly stable and efficient Li metal anode.

7.2.2. Chemical Pretreatment. During the electrochemical pretreatment, the reactions and the corresponding reaction products are very similar to the SEI film formed in section 7.1.1. However, due to the limited understanding on the SEI film, accurately modifying each component by the initiator (or electrolyte additive) is very difficult. Chemical pretreatment presents a possibility to regulate the protective layer according to our requirements. Attributing from the chemical reaction of initiator and Li metal, one or several kinds of components can be introduced onto the Li metal to act as protective film to suppress electrolyte decomposition and dendrite growth.

Gas processing is an effective and convenient method to regulate the surface chemistry of Li metal anode (Figure 35).²¹⁸ According to the results of Koch et al., several conclusions can be reached on the different gas (including N₂, O₂, CO₂, and SO₂) processing Li metal:

1. Depending on the dosed gas, different energetically favored Li surface terminations can be obtained. Whereas F₂ treatment led to the Li(100) surface being energetically favored, N₂, O₂, and CO₂ dissociation resulted in Li(110) being energetically favored. Contrary to the results caused by the former gases, SO₂ treatment rendered the Li(111) surface to be energetically favored.

2. SO₂ was found to be the most powerful gas in constructing a thin and insulating passivation layer. All the other gases lead to metallic layers.

3. Except for N₂, all molecularly dissociated layers resulted in substantial changes in the elastic properties of the slabs, with an overall tendency to elastic stiffness or, equivalently, reduced elastic compliance. Notably, N₂ dissociation into N adatoms was found to yield the most elastically compliant layer, indicating small initial N₂ dosage could be beneficial for increased elasticity of the pristine passivation layer. N₂-pretreated Li metal showed an overwhelming role to protect Li metal by the direct reaction between the Li and N₂ gas at room temperature to form a Li₃N protection layer on the Li surface,^{219,220} which is believed to have unique stability against Li metal.²²¹

Apart from the gas processing, liquid processing on the Li metal is another powerful method to construct a defensive film for Li metal anode. An artificial SEI layer with a uniformly distributed Li₃PO₄ component was innovatively fabricated by Guo and co-workers through an in situ reaction of polyphosphoric acid with metallic Li and its native film (Figure 36).⁹⁴ The Li₃PO₄ layer can not only enhance Li ion transport between the Li metal interface and the electrolyte, but also

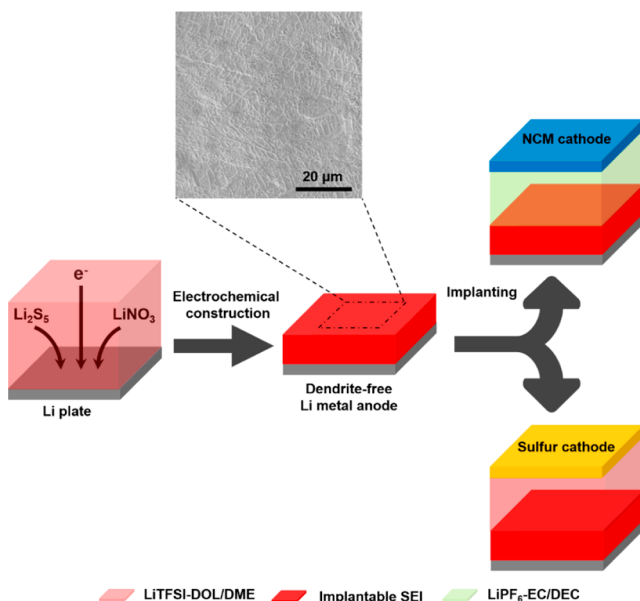


Figure 34. Scheme of implantable SEI on Li metal anode and working in both Li–S and Li metal oxide batteries. Reproduced with permission from ref 217. Copyright 2017 Cell.

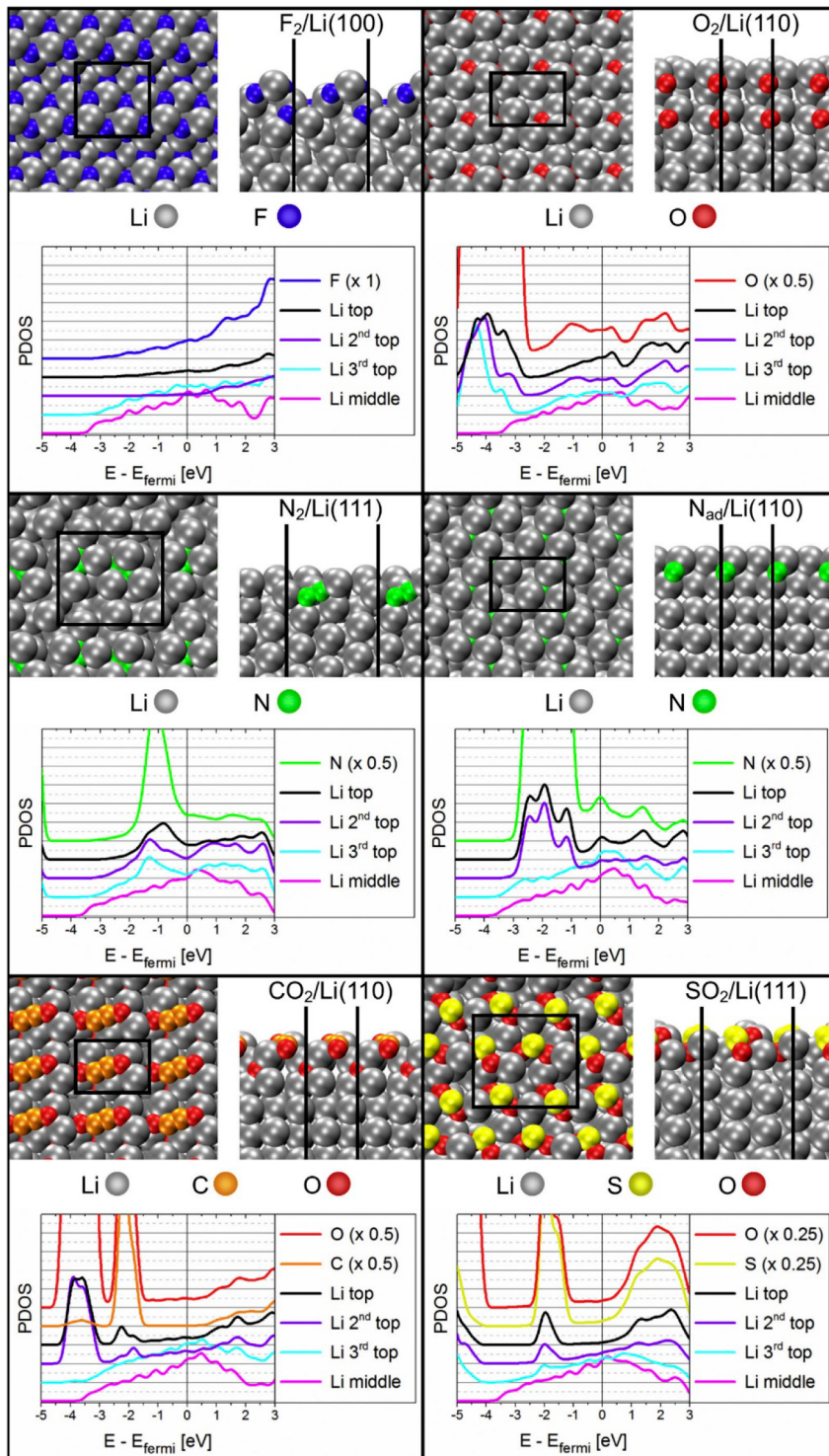


Figure 35. Optimized geometry and layer-resolved atom-projected density of states (PDOS) for the lowest E_{form} systems. Reproduced with permission from ref 218. Copyright 2015 Elsevier.

exhibit a smooth surface and high Young's modulus of 10–11 GPa, which were sufficient to suppress the Li dendrite growth by mechanical resistance. An artificial SEI layer composed of Cu₃N nanoparticles associated together by styrene–butadiene rubber (Cu₃N + SBR) was proposed by Cui and co-workers (Figure 37).²²² The Cu₃N nanoparticles were passivated immediately when in contact with metallic Li to form Li₃N. Compared to pure inorganic phase coatings, composite artificial SEI with both inorganic nanoparticles and a polymeric binder

well maintained structural integrity during Li plating/stripping. Therefore, this composite artificial film simultaneously possessed high mechanical strength (0.81 GPa), good flexibility, and high Li ion conductivity (ionic conductivity of Li₃N is on the order of $\approx 10^{-3}$ – 10^{-4} S cm⁻¹ at room temperature.). When adopted in a Li|Cu cell, the Coulombic efficiency can be improved to above 97.4% at a high current density up to 1.0 mA cm⁻² in the corrosive carbonate electrolyte on Cu current collector. Simply immersing Li metal into the ionic liquid

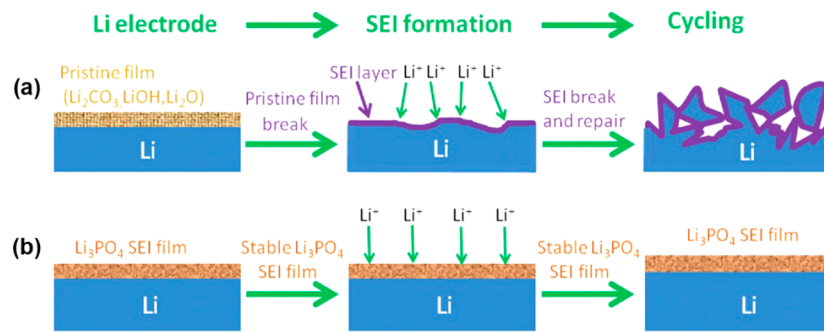


Figure 36. Scheme of Li anode with different SEI films. (a) General Li metal and (b) Li_3PO_4 -modified Li metal anodes during SEI formation and cycling. Reproduced with permission from ref 94. Copyright 2016 WILEY-VCH Verlag GmbH & Co. KGaA, Weinheim.

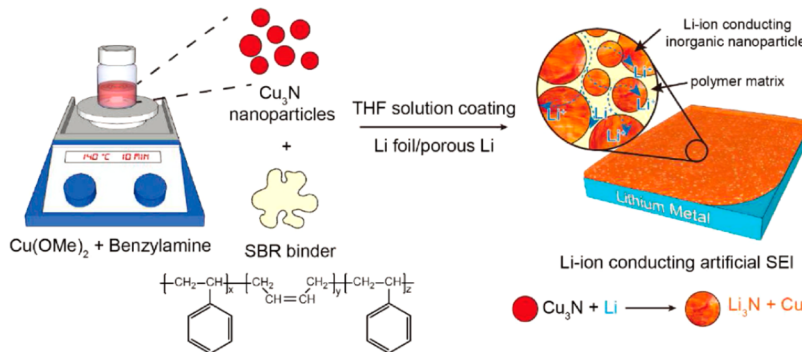


Figure 37. Scheme of Cu_3N + SBR composite artificial SEI formation on Li metal. Reproduced with permission from ref 222. Copyright 2017 WILEY-VCH Verlag GmbH & Co. KGaA, Weinheim.

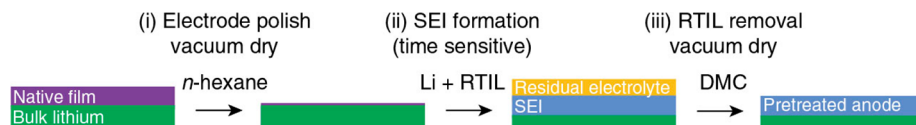


Figure 38. Scheme of SEI fabrication on Li metal anode via chemical pretreatment with ionic liquid electrolyte. Reproduced with permission from ref 223. Copyright 2016 Nature Publishing Group.

electrolyte for a period of time before cell assembly can easily achieve a protecting role of Li metal surface (Figure 38).²²³ This method constructed a durable and Li^+ -permeable SEI film, achieving 1000 safe cycles of $\text{Li}|\text{LiFePO}_4$ batteries with a Coulombic efficiency of 99.5%.

Relative to the SEI film additive and electrochemical pretreatment, the chemical pretreatment can targetedly regulate the SEI components due to our expectations.²²⁴ However, subject to the current chemistry development, this method can merely introduce several components into this film, while the real SEI formed in electrochemical conditions is actually complicated. There is no hard evidence to demonstrate which has better performance between fewer components induced by the chemical reactions and more components induced by the electrochemical reactions. Even so, the chemical pretreatment is an efficient route to deliberately regulate the SEI film and, with the development of chemistry techniques, it will become more powerful.

7.2.3. Physical Pretreatment. Similar to chemical pretreatment, physical treatment is also a method to targetedly regulate the protective layer of Li metal anode. Physical coating is a facile and cost-effective method to deposit the protective layer onto Li metal anode, which is conveniently applied in practical LMBs. Due to its simplicity, various methods have been proposed and nearly all the coating materials can indicate

suppression of Li dendrite growth under some certain conditions. The current physical coating methods include spin-coating, atomic layer deposition, magnetron sputtering, flash evaporation, doctor-blade coating, etc. The deposited materials can be divided into two items: inorganic materials (including Al_2O_3 , carbon, and other contributing inorganic materials in the SEI) and organic polymer to simulate the role of a real SEI film. The uniformity of the deposited layer and its role in the dendrite inhibition depend much on the deposited material and the chosen methods. Relative to the electrochemical and chemical pretreatments, the key of the physical method much depends on the process engineering to achieve a dense and thin coating layer.

Al_2O_3 is frequently used to construct the protective layer for Li metal anode.^{225,226} Several methods have been put forward to construct this Al_2O_3 layer, such as spin-coating²²⁶ and atomic layer deposition (ALD).²²⁷ The porous Al_2O_3 protective layer obtained by a facile spin-coating method can not only act as a stable and dense interlayer to suppress the side reactions between Li and electrolyte, but can also avoid the formation of serious cracks on the protected Li anode to suppress Li dendrite growth.²²⁶ The ALD method can achieve an ultrathin 14 nm thick ALD Al_2O_3 layer to effectively prevent Li metal from corrosion of electrolyte.²²⁸ The thickness of the ALD Al_2O_3 layer can be even reduced to ~ 2 nm, which can still

prevent dendrite formation upon cycling at a current density of 1.0 mA cm^{-2} .²²⁹ Al_2O_3 can also function with other components to form a composite protective layer. An $\text{Al}_2\text{O}_3/\text{poly(vinylidene fluoride-co-hexafluoropropylene)}$ (PVdF-HFP) composite layer can efficiently protect Li metal anode, and it achieved a superior cycling when the protected Li metal anode was employed in $\text{Li}-\text{O}_2$ batteries (Figure 39).²³⁰

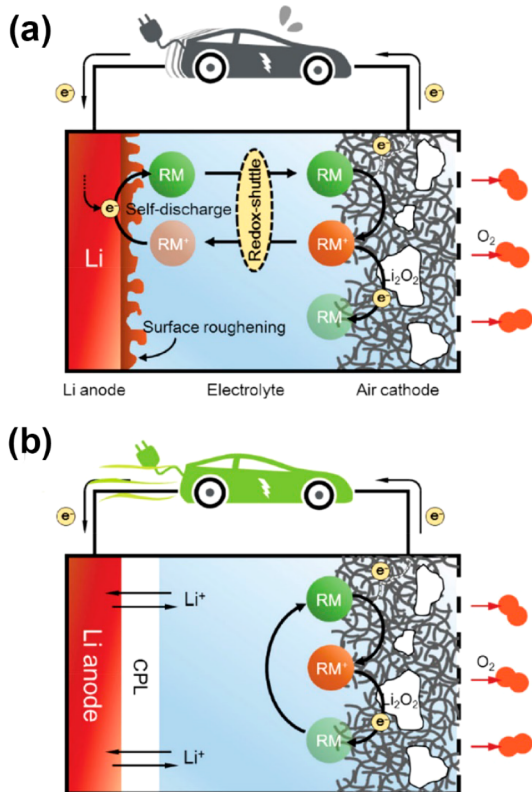


Figure 39. Scheme of (a) self-discharge of the redox mediator in a $\text{Li}-\text{O}_2$ battery and (b) CPL-coated Li electrode, which retards the reaction between the redox mediator and Li metal electrode. Reproduced with permission from ref 230. Copyright 2016 WILEY-VCH Verlag GmbH & Co. KGaA, Weinheim.

Carbon is also one of the frequently adopted inorganic materials used to protect Li metal anode.²³² Tu's group magnetron-sputtered amorphous carbon coatings on metallic Li with a thickness ranging from 50 to 110 nm.²³³ Flash-

evaporation strategy was adopted to deposit an electrochemically stable monolayer of interconnected amorphous hollow carbon nanospheres on the Li metal anode as the artificial SEI film (Figure 40).²³¹ This thin amorphous carbon layer did not increase the Li ion diffusion resistance, but had a Young's modulus of $\sim 200 \text{ GPa}$ to suppress Li dendrites. The carbon layer has a proper adhesion strength with the current collector. When Li ions were plated/stripped on a current collector, the carbon layer moved up and down to eliminate the volume change during cycling. This strategy achieved a high cycling Coulombic efficiency of $\sim 99\%$ with a dendrite-free morphology for more than 150 cycles at $1.0 \text{ mA cm}^{-2}/1.0 \text{ mAh cm}^{-2}$.

Other protective inorganic components in the in situ formed SEI film are adopted as well to deposit on the Li metal anode. LiF is a critically important component in the SEI film. When LiF was deposited onto the Li metal surface by magnetron-sputtering deposition, the electrodes exhibited a remarkable ability to promote smooth Li deposition during charging at a high current density of 1 mA cm^{-2} .²³⁴ Li_3PO_4 has been tried to be deposited as a thin film on Li metal foils by magnetron sputtering.²³⁵ The amorphous Li_3PO_4 thin films have thicknesses of 0–200 nm, and have an almost insulated property with a low electronic conductivity of $1.4 \times 10^{-10} \text{ S cm}^{-1}$ and a small ionic conductivity of $2.8 \times 10^{-8} \text{ S cm}^{-1}$. The conformal coating layer Li_3PO_4 can successfully suppress Li dendrite growth and extend its lifespan.

Another category of the coated material is organic polymers.²³⁶ Due to their high flexibility, they are strongly expected to remit a volume change during Li plating and stripping.²³⁷ A soft and multilayered film on a Li metal anode was constructed, adopting a layer-by-layer (LBL) self-assembly technique,²³⁸ which is usually employed to form a protective layer. The positively charged polymer poly(allylamine hydrochloride) (PAH) contains $-\text{NH}_3^+$ functionalities. When used as a first layer, PAH allowed for the assembly of the multilayer due to its charged $(-\text{NH}_3^+)$ functionality (Figure 41). A high Coulombic efficiency of 95% was on average achieved in 50 cycles when 14 layers of PDAD/PEDOT:PSS, PPy/PE-DOT:PSS, or PDAD/Nafion were coated on the Cu substrate by a pH-sensitive PAH layer.

Nafion is an important binder and positively charged polymer. The positively charged nature can build rapid Li ion channels in the cells.²³⁹ The feature of a single Li ion channel renders Nafion-modified separator as an ion-selective separator in working Li–S batteries, in which the shuttle of polysulfides is

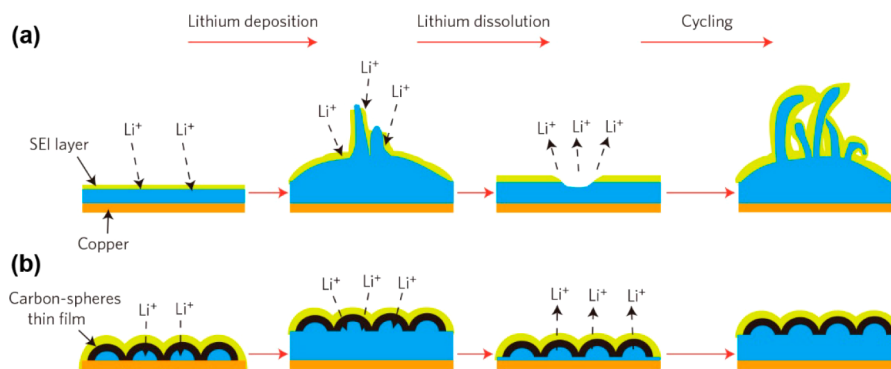


Figure 40. Scheme of different Li anode structures. (a) Thin film of SEI film forms on the surface of deposited Li (blue). (b) Modifying the Cu substrate with a hollow carbon nanosphere layer as a 3D scaffold for SEI layer stabilization. The volumetric change of Li deposits is accommodated by a flexible hollow-carbon-nanosphere coating. Reproduced with permission from ref 231. Copyright 2014 Nature Publishing Group.

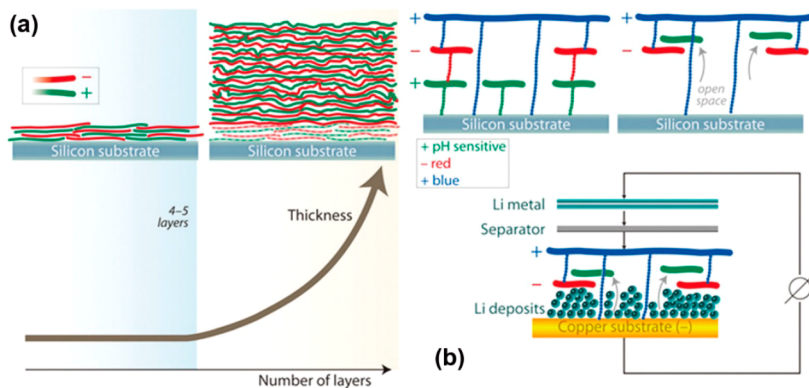


Figure 41. (a) Scheme depicting layer-by-layer deposition of oppositely charged polymers. (b) To accommodate the nondendritic deposition of Li, “open spaces” are cleared by modifying the ionic character of a pH-sensitive polymer. Reproduced with permission from ref 238. Copyright 2016 The Royal Society of Chemistry.

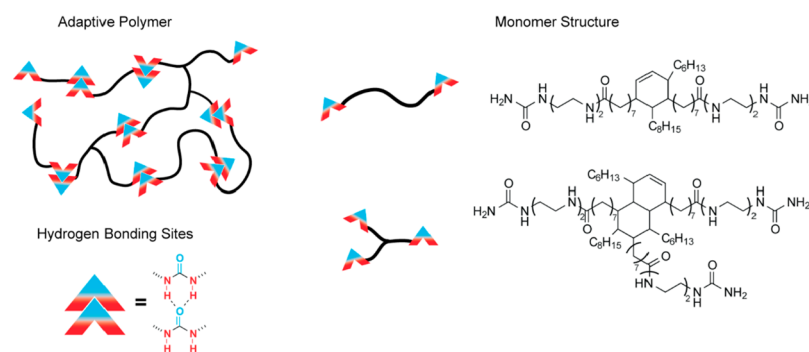


Figure 42. Chemical structure of the polymer. Black lines are the fatty acid backbone, and the red–blue boxes are the urea hydrogen bonding sites. The right-hand side exhibits the molecular structure of the diacid and triacid backbones. Reproduced from ref 244. Copyright 2016 American Chemical Society.

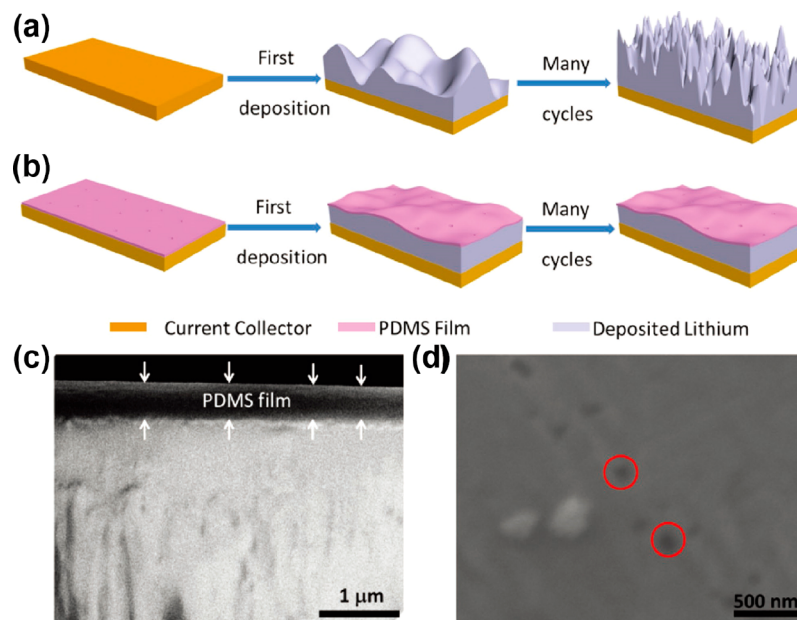


Figure 43. Scheme of Li deposition in a working cell. (a) Li deposition on a bare Cu foil, mossy Li, and Li dendrites appear after many cycles. (b) Li deposition on a Cu foil coated with a PDMS film with suppressed dendrite growth. (c) Cross-section SEM image of the PDMS film and (d) top-view SEM image of PDMS film after HF acid treatment (red circles, nanopores). Reproduced with permission from ref 245. Copyright 2017 WILEY-VCH Verlag GmbH & Co. KGaA, Weinheim.

retarded and the cycling life of the cell is significantly enhanced.^{240,241} This feature is likewise favored for a dendrite-free Li depositing on the Li metal anode surface.

Nafion is positively charged, and can absorb Li ions on its surface to prevent Li⁺ depletion at the interface during Li plating. In addition, the bulk resistance of the LMB is

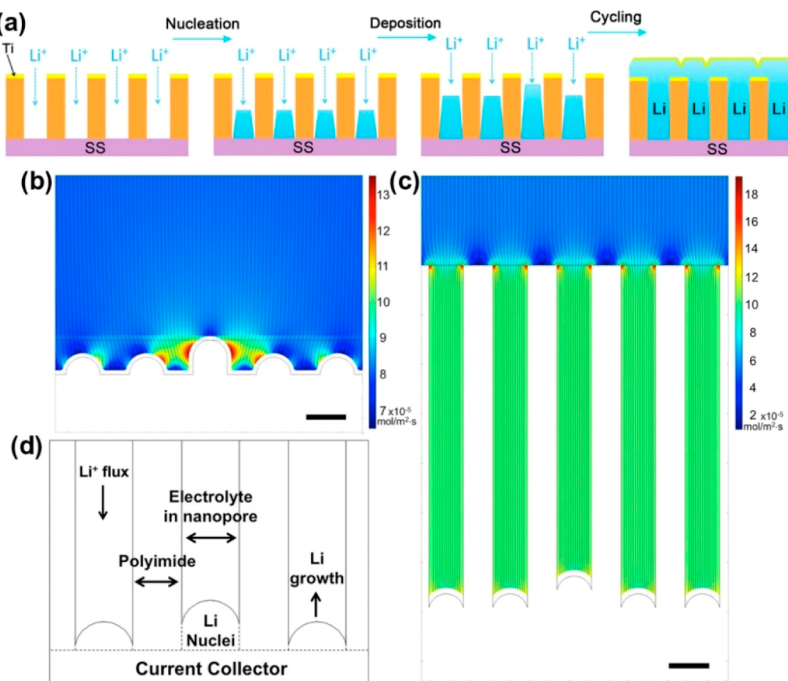


Figure 44. (a) Modified stainless steel electrode coated with a nanochannel layer. (b) Simulation for the bare electrode. (c) In the case of the electrode with the nanochannel coating, Li^+ flux is evenly distributed within the pores. (d) Cell geometry for the simulation. The scale bars in this figure are 400 nm. Reproduced from ref 247. Copyright 2016 American Chemical Society.

minimized by reducing the thickness of the Nafion layer down to a few micrometers. When Nafion is coated onto the Li metal anode, the symmetric Li/Li cell is stably operated at a high current density of 10 mA cm^{-2} for more than 2000 h.²⁴² The Li/LiCoO₂ prototype cell with the layer exhibited extraordinary cycling stability for more than 350 cycles. Nafion can further act with poly(vinylidene difluoride) (PVDF) on the Li metal anode to suppress Li dendrite growth.²⁴³ The Nafion/PVDF-coated Li anode exhibits substantially enhanced rate performance and cyclability as well as improved Coulombic efficiency for Li–S prototype batteries with a high-S-content cathode.

Apart from the positively charged polymer (such as Nafion), other polymers have been tried to protect Li metal anode, such as a soft polymer coating ($4 \mu\text{m}$) on the electrode (Figure 42).²⁴⁴ The polymer was highly viscoelastic, which afforded a pinhole-free coating on the Li surface during repeated charging and discharging, inhibiting dendrite formation by avoiding the creation of “hot spots” where the Li^+ flux was dramatically increased. At a high current density of 5.0 mA cm^{-2} , a flat and dense Li metal layer was achieved. A stable cycling Coulombic efficiency of $\sim 97\%$ was preserved for more than 180 cycles at a current density of 1 mA cm^{-2} . This adaptive polymer is an important buffer for the high volume change of Li metal anode.²⁴⁶

Nevertheless, the routine polymer is not a good conductor for Li ions. A polymer with well-developed channels for Li ions is much desired. A modified poly(dimethylsiloxane) (PDMS) film with nanopores was fabricated by a facile spin-coating strategy (Figure 43).²⁴⁵ HF acid treatment was adopted to intentionally create nanopores as the pathways of Li^+ transport in the PDMS film. The sizes of these pores can be regulated by tuning the etching duration. A superior PDMS film was achieved with a thickness of 500 nm and pore sizes of 40–100 nm are obtained, allowing efficient transportation of Li ions. Meanwhile, the PDMS film was chemically and mechanically

stable when matching Li metal to suppress Li dendrite nucleation and growth. Therefore, the PDMS protective film renders a stable cycling for 200 cycles with a high Coulombic efficiency of 94.5% in a routine carbonate electrolyte under a current density of 0.5 mA cm^{-2} . Relative to disordered nanopores obtained from the chemical etching, well-organized channels on the Li metal anode surface are beneficial for a dendrite-free Li plating. A polyimide layer with vertical nanoscale channels of high aspect ratio on Li metal anode was established (Figure 44).²⁴⁷ This film rendered Li ions to homogeneously distribute on the anode through nanoscaled confinement, leading to a uniform Li nucleation and growth. Furthermore, the highly conductive nature of these polymers can be still achieved when they are functionalized with some inorganic materials. For example, when the routine PMMA interfacial layer was substituted by the SiO₂@PMMA core–shell nanosphere layer, the ionic flux through this film was effectively increased while still maintaining the dendrite-inhibiting ability.²⁴⁸

The physical coating layer is a facile and effective method to protect Li metal. This layer can be regarded as one kind of solid electrolyte. Its thickness and conductivity are very important in practical cells. In routine tests, this physical coating layer is usually conducted in the liquid electrolyte, achieving a good rate performance. This indicates a novel pattern by employing the liquid/solid hybrid electrolyte to realize a safe and efficient Li metal anode.

In summary, these three pretreatments on Li metal suppress Li dendrite growth from different perspectives. Each one of them has its peculiarity and application scenario (Table 1). It is very difficult to indicate which one is the best. Integrating them into a functional SEI means much, not physical mixing, but theoretical cooperation.

Table 1. Comparison of the Three Artificial Methods: Electrochemical Pretreatment, Chemical Pretreatment, and Physical Pretreatment^a

| | electrochemical pretreatment | chemical pretreatment | physical pretreatment |
|------------------------|------------------------------|-----------------------|-----------------------|
| complexity | +++ | ++ | + |
| modulus | + | ++ | +++ |
| thickness | + | ++ | +++ |
| ionic conductivity | +++ | ++ | + |
| component quantity | +++ | ++ | + |
| similarity to real SEI | +++ | ++ | ++ |

^aMore “+” means higher data.

7.3. Superconcentrated Electrolyte

It is generally acknowledged that ~ 1 M is the most accepted concentration for Li salt in the electrolyte to achieve a trade-off among ionic conductivity, viscosity, and cost.^{33,34} With strong considerations of the high-energy-density Li–S and Li–O₂ batteries employing Li metal anode, a new salt concentration should be explored to safely use Li metal anode. Recently, superconcentrated (or highly concentrated) electrolyte has received extensive attention and this indicates an enormous potential for safe Li metal anodes in rechargeable batteries (Figure 45).²⁴⁹

Superconcentrated electrolyte often refers to an electrolyte system with a concentration of over 3 M. This electrolyte shows ionic liquidlike bulk properties and reduced free solvent molecules due to the increased fixed solvent by Li salts.^{250,251} In 2008, Jeong et al. first employed superconcentrated electrolyte with Li metal anode and demonstrated the reversibility of Li ion plating/stripping in highly concentrated PC electrolytes.²⁵² The poor cycling stability of the Li electrodes in the routine concentration solutions was considerably enhanced by increasing the electrolyte concentration. TEM images of Li deposits revealed that a highly concentrated electrolyte rendered a thinner SEI than that formed in a routine concentration solution (35 nm in 1.28 mol kg⁻¹ electrolyte vs 20 nm in 3.27 mol kg⁻¹ electrolyte) (Figure 46). The highly solvated Li ions characterized by Raman spectroscopy contributed much to the thinner SEI film. Hence a superior Li dendrite suppression performance was achieved. Hu's group proposed a general concept for solvent-in-salt electrolyte and systematically investigated the role of the LiTFSI concentrations on the performance of Li metal protection and Li–S

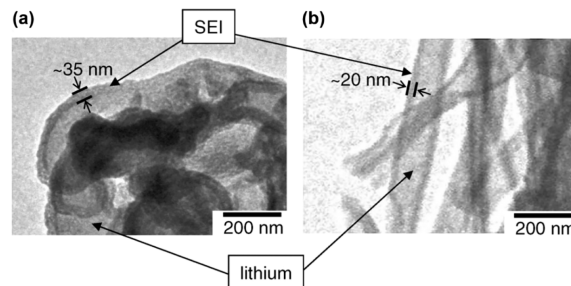


Figure 46. TEM images of nickel substrates obtained after 30th cycle in (a) 1.28 mol kg⁻¹ Li(N(SO₂C₂F₅)₂)/PC and (b) 3.27 mol kg⁻¹ Li(N(SO₂C₂F₅)₂)/PC, indicating the SEI is very thin. Reproduced with permission from ref 252. Copyright 2008 Elsevier.

batteries (Figure 47).²⁵³ A 7.0 M LiTFSI electrolyte indicates the best cycling performance, while unfortunately it has a large

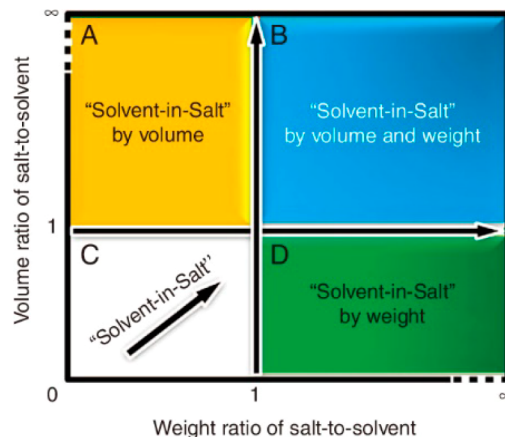


Figure 47. Phase diagram of nonaqueous liquid electrolytes with weight and volume ratios of salt to solvent. Reproduced with permission from ref 253. Copyright 2013 Nature Publishing Group.

polarization. To further address this issue, Li bis-(fluorosulfonyl)amide (LiFSI) salt emerged. Fast electrode kinetics was recently achieved for superconcentrated LiFSI salt electrolyte. For example, 4.5 M LiFSI in acrylonitrile (AN) indicates an ionic conductivity of 10⁻² S cm⁻¹ (at 30 °C).²⁵⁴ The superior conductivity is almost comparable to those of the state-of-the-art commercial 1 M electrolytes, which is always regarded as impossible for its high viscosity (23.8 mPa at 30 °C). Compared to LiTFSI with a less complete reduction and

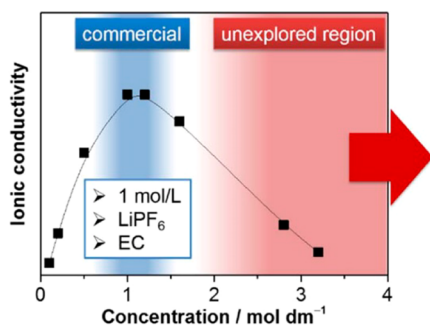


Figure 45. Relationship of ionic conductivity and Li salt concentration in an aprotic solvent mixture. Highly concentrated electrolytes with decreased ionic conductivities and unusual functionalities beneficial for Li metal batteries. Reproduced with permission from ref 249. Copyright 2015 The Electrochemical Society.

Various unusual functionalities

- High reductive stability
- High oxidative stability
- Al anti-corrosion
- High thermal stability
- Low volatility
- High carrier density
- Fast electrode reaction
- Low polysulfide dissolution, etc.



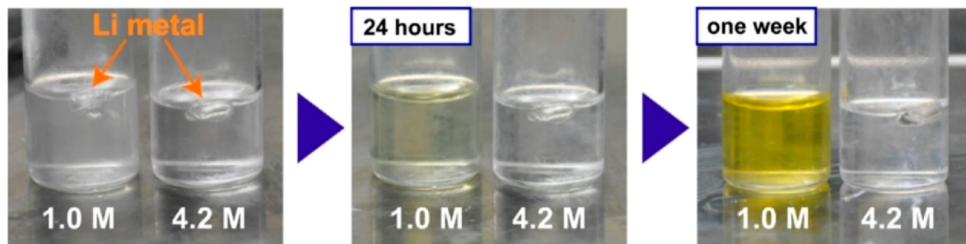


Figure 48. Reactivity of Li metal foil and LiTFSA/AN solutions at 1.0 and 4.2 mol L^{-1} . Reproduced from ref 254. Copyright 2014 American Chemical Society.

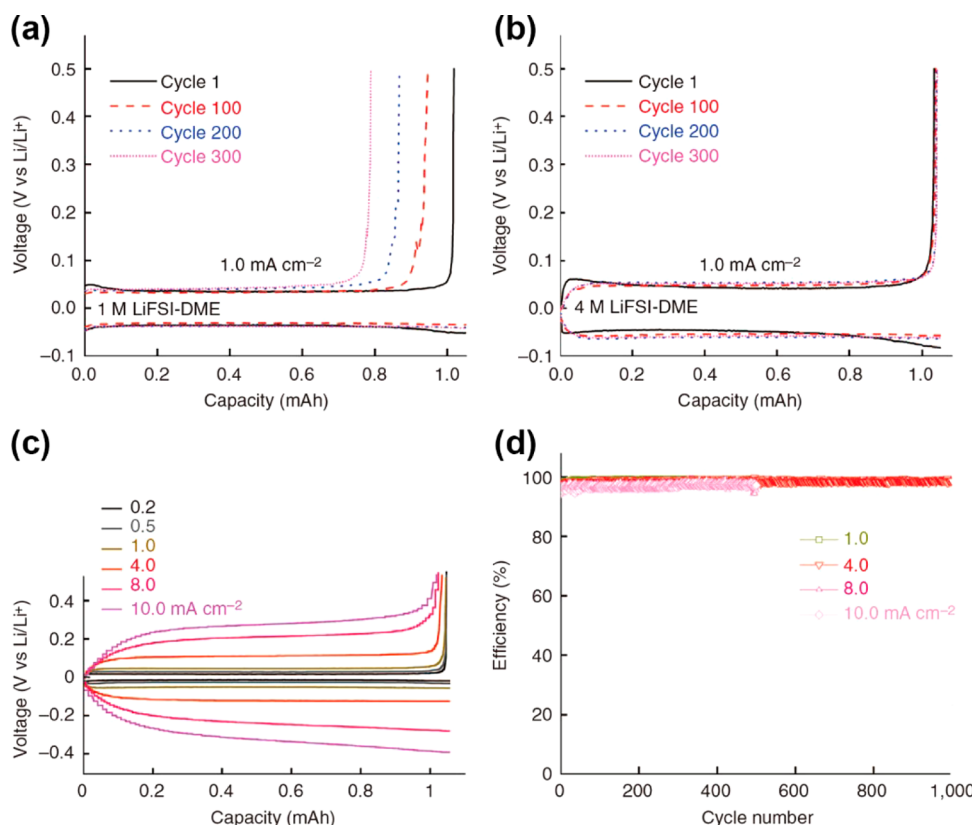


Figure 49. Electrochemical performance of Li metal plating/stripping on a Cu working electrode. (a) Voltage profiles for a cell cycled in 1.0 M LiFSI–DME electrolyte. (b) Voltage profiles for a cell cycled in 4.0 M LiFSI–DME electrolyte. (c) Polarization of Li plating/stripping for 4.0 M LiFSI–DME electrolyte. (d) Coulombic efficiency of Li deposition/stripping in 4.0 M LiFSI–DME. Reproduced with permission from ref 78. Copyright 2015 Nature Publishing Group.

easy charge transfer from the anode, LiFSI exhibits a more complete decomposition forming LiF as one of the main SEI products.²⁵⁵ Therefore, this electrolyte can remain stable when matching Li metal anode (Figure 48).²⁵⁴

Zhang's group matched 4.0 M LiFSI in DME electrolyte with Li metal anode.⁷⁸ The increased solvent coordination and enhanced availability of Li ions in the electrolyte led to superior performance in the Li metal anode. Quantitative ^6Li solid-state magic angle spinning (MAS) nuclear magnetic resonance (NMR) experiments found that the SEI formed in the 4.0 M LiFSI–DME electrolyte was denser than that in the routine electrolytes. The dead Li in the 4.0 M LiFSI–DME electrolyte had a large possibility to be reduced onto active Li metal.²⁵⁶ With 4 M LiFSI in DME solvents, a Li|Li cell can be stably operated at 10 mA cm^{-2} for more than 6000 cycles. When this electrolyte was adopted in Li|Cu half-cells, very high Coulombic efficiencies were achieved: 99.1% for >1000 cycles at 0.2 mA cm^{-2} , 98.5% for >1000 cycles at 1.0 mA cm^{-2} , 98.4% for >1000

cycles at 4.0 mA cm^{-2} , and 97% for >500 cycles at 10.0 mA cm^{-2} (Figure 49). This was very high data for Li efficiency evaluated by the ratio of stripping and plating capacities in the Li|Cu cells. They also employed this electrolyte system to anode-free Li metal anode²⁵⁷ and Li–oxygen batteries.²⁵⁸

The superconcentrated electrolyte can be extended to other systems. A 3.2 mol kg^{-1} LiFSI in ionic liquids (ILs)²⁵⁹ and 4.0 M LiNO₃ in DMSO²⁶⁰ can also suppress Li dendrite growth. The superconcentrated electrolyte affords the possibility of aqueous electrolyte in Li batteries as well. Suo et al. dissolved 21 M LiTFSA in water as the electrolyte.²⁶¹ The superconcentrated electrolyte expanded the narrow electrochemical stability window (1.23 V) of H₂O to 3.0 V . A full LIB of 2.3 V was first constructed by such a superconcentrated aqueous electrolyte and achieved a nearly 100% Coulombic efficiency for 1000 cycles at high (4.5 C) discharge and charge rates.

The highly concentrated electrolyte indicates great potential to suppress Li dendrite growth and achieve a high Coulombic

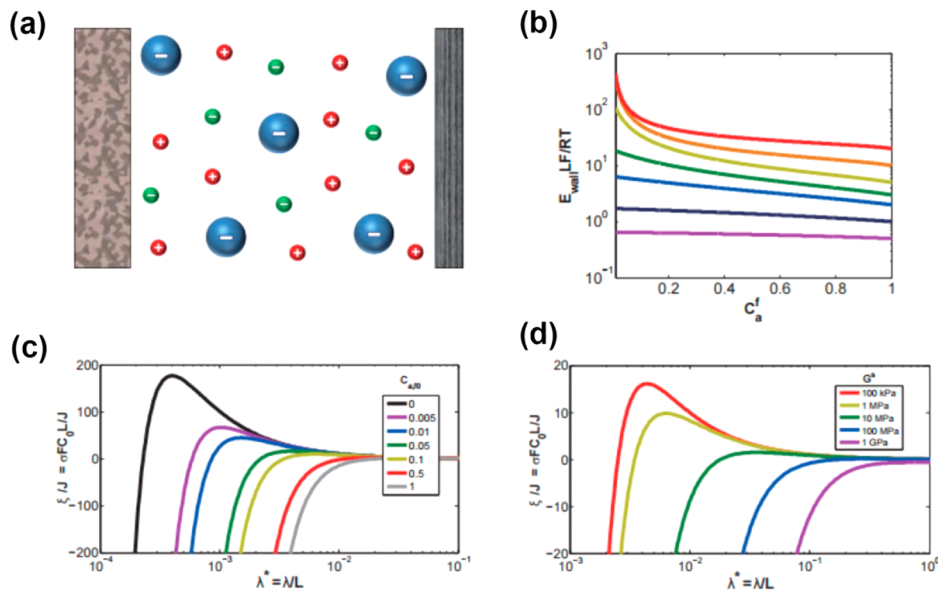


Figure 50. (a) Illustration of electrolyte with immobilized anions. (b) Electric field at the metal electrode against a fraction of fixed anions from down to up as 0.5, 1, 2, 3, 5, 10, 20 (violet to red, respectively). (c) Growth rate vs wavelength of perturbations with different fractions of immobilized anions. (d) Growth rate vs wavelength of perturbations with different separator moduli. Reproduced from ref 262. Copyright 2015 American Chemical Society.

efficiency. Though it is still conducted in the liquid system, the concentrated electrolyte has some features similar to those of the solid-state electrolyte. It can be regarded as an intermediate state between the liquid electrolyte and solid-state electrolyte, which holds the high ionic conductivity of the liquid electrolyte and the high modulus of the solid-state electrolyte to suppress Li dendrite growth. The only drawback of this electrolyte is the high price of the electrolyte salts with high concentrations. This can be partly conquered when the production techniques of electrolyte salts can be improved accompanied by the mass application of this electrolyte in Li metal anode. The next scientific research can be fixed on the regulation of the salt and solvent to further improve the ionic conductivity, suppress Li dendrite growth, and hence achieve a Coulombic efficiency of 99.9% in 1000 cycles.

7.4. Nanostructured Electrolyte

The space-charge model in section 4.1.3 indicates a space-charge region induced by anion depletion, which can produce a large electric field at the metal surface. The as-obtained electrical field drives electroconvection and causes rapid dendrite growth. Consequently, it can be reasonably inferred that dendritic Li growth is inhibited by prolonging the development of the space-charge region by preventing the anion depletion during Li plating.

Recently, Archer and co-workers proposed a novel nanostructured electrolyte with immobilized anions to suppress Li dendrite growth by preventing the formation of a large electric field caused by space charge (Figure 50).²⁶² As indicated by Sand's time model (section 4.3), When the anions are immobilized ($\mu_a = 0$), Sand's time (τ_s) tends to be infinite, indicating a dendrite-free and safe Li metal anode. In a practical system, more immobilized anions result in a safer Li metal anode.^{263,264} The electrode surface is more uniform at higher fractions of immobilized anions. Immobilizing even a small fraction (10%) of anions can significantly improve the uniformity relative to routine liquid electrolytes.

Lu et al. obtained an organic–inorganic hybrid nanostructured electrolyte by densely functionalizing silica nanoparticles with the ionic liquid 1-methyl-3-propylimidazolium bis(trifluoromethanesulfone)imide and conventional PC/LiTFSI liquid electrolyte ($\text{SiO}_2\text{-IL-TFSI-Li}$) (Figure 51).²⁶⁵ The

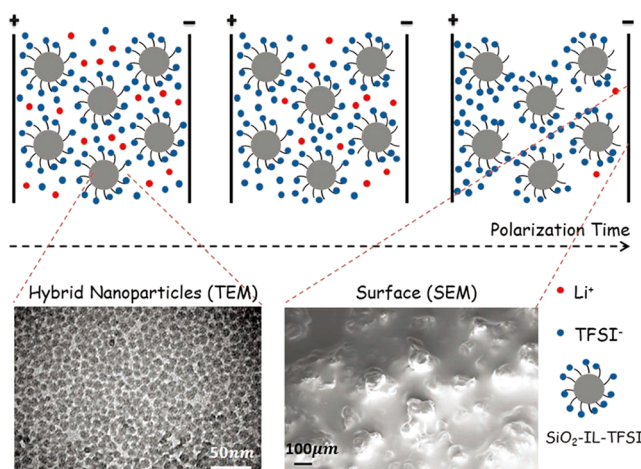


Figure 51. Scheme of transient response of $\text{SiO}_2\text{-IL-TFSI/PC}$ electrolyte during polarization of $\text{Li}|\text{SiO}_2\text{-IL-TFSI/PC}|\text{Li}$ cell. Bottom left: TEM image of pure hybrid nanoparticles. The figure exhibits the stunted, mushroomlike morphology of the Li dendrites. Bottom right: SEM image of the Li metal in a $\text{Li}|\text{SiO}_2\text{-IL-TFSI/PC}|\text{Li}$ cell with $\phi = 0.23$ after short circuit. Reproduced with permission from ref 265. Copyright 2012 WILEY-VCH Verlag GmbH & Co. KGaA, Weinheim.

brushlike structure of the ionic liquid molecules linked to the particles is deemed to promote dispersion of silica nanoparticles. The nanoparticles can serve as reservoirs and constraints for anions to prevent them from migrating, thus avoiding development of a space charge. These systems delivered exceptional electrochemical and interfacial stability when matching Li metal anode, and improved thermal stability

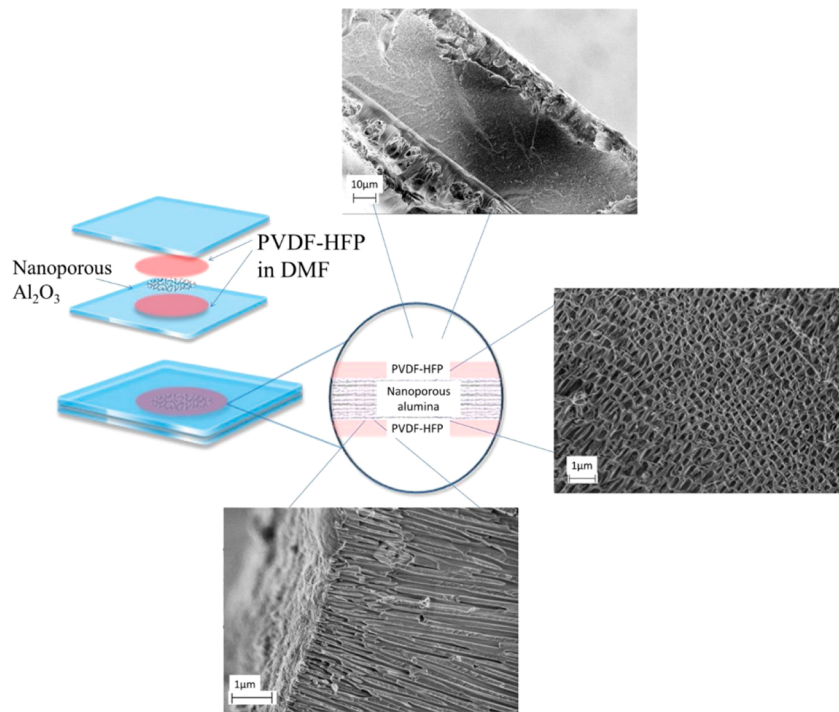


Figure 52. (left side) Scheme of structure and preparation method of PVDF–HFP/Al₂O₃ separator. SEM images of the composite separator: top, cross section of the composite; right, cross section of the internal alumina layer; bottom, boundary between alumina and polymer. Reproduced with permission from ref 271. Copyright 2014 WILEY-VCH Verlag GmbH & Co. KGaA, Weinheim.

over a pure PC-based electrolyte. Such hybrid electrolytes significantly retarded Li dendrite growth and displayed a cell-short-circuit period as much as 1 order of magnitude larger than the pure PC electrolyte. Similar principles are extended to other materials, such as nanoporous lithiated perfluorinated polymer electrolyte,²⁶⁶ SiO₂–SO₃BF₃Li in tetraglyme,²⁶⁷ nanocomposites and gel–polymer electrolytes,²⁶⁸ ionic liquid connected PMMA nanoparticles,²⁶⁹ and SiO₂ hollow nanosphere based composite solid electrolyte,²⁷⁰ which are exceptionally efficient in suppressing Li dendrite growth in LMBs.

Another kind of nanostructured composite electrolyte retaining a laminate and trilayer structure was released (Figure 52).²⁷¹ In this trilayer structure, a liquid electrolyte was injected into the pores of a nanometer-sized-pore Al₂O₃ ceramic monolith, which is infibulated by a polymer with microporous pores, such as poly(vinylidene fluoride-*co*-hexafluoropropylene) (PVDF–HFP). This vertical structuring configuration realized a rapid Li ion diffusion from the bulk electrolyte to anode surface, hence preventing the formation of space charge and a large electric field, which was critically important to suppress Li dendrite growth. Besides, the performance of this nanostructured electrolyte much depended on the diameter of the AAO pores.²⁷² The electrochemical results anticipated a transition from stable to unstable deposition when the mean pore diameter of deposit nucleates exceeded a critical value $\lambda \approx 200$ nm. This effect was related to the charge intensity in pores with different sizes. When pore sizes of a membrane with charged walls are distributed at a nanometer length scale, electroosmotic flow becomes pronounced and dramatically retards diffusion of ions, hence regulating the ionic current when an electric field is applied and modifying the Li ion diffusion and depositing behavior.^{273,274}

Similar to the superconcentrated electrolyte, the nanostructured electrolyte can also be regarded as the intermediate

state of the liquid and solid-state electrolytes. Relative to the superconcentrated electrolyte usually as a liquid, the nanostructured electrolyte is complicatedly fabricated and can be a liquid or solid state. Further research can focus on optimizing the fabricating routes to obtain a cost-effective nanostructured electrolyte. The research of the nanostructured electrolyte has just started and it is hopefully to be applied into Li metal anode.

7.5. Solid-State Electrolyte

The routine liquid electrolyte is widely employed in current rechargeable batteries. However, these liquid electrolytes indicate several safety issues including leakage, poor chemical stability, and flammability. The employment of solid inorganic/polymer electrolyte can totally or partly relieve these safety issues.^{11,275–278} More importantly, these electrolytes with a high modulus can efficiently suppress Li dendrite growth.^{12,279} Replacing liquid electrolytes with solid-state electrolytes has been strongly considered to avoid the safety hazard, especially in large-scale applications.^{280–282}

The most researched solid inorganic electrolytes include Li phosphorus nitride (LiPON),²⁸³ Li₃N,^{284,285} Li₇La₃Zr₂O₁₂ (LLZO, La sites: Ca, Sr, Ba, K, etc.; Zr sites: Ta, Nb, etc.),^{286,287} Li_{3-x}La_{(2/3)-x}TiO₃ (LLTO, La sites: Al, Mg, Fe, Ta, etc.; Ti sites: Pr, Nb, Sr, etc.),²⁸⁸ Li_{1+x}Al_xGe_{2-x}(PO₄)₃ (LAGP, Al sites: Y, Ga, Cr, In, Fe, Se, La, etc.; Ge sites: Ta, Zr, Ti, Ge, Sn, Si, Fe, V, Hf, etc.),²⁸⁹ Li₁₄Zn(GeO₄)₄ (Ge sites: Si, S, P; Zn sites: Zr, Cr, Sn),²⁹⁰ xLi₂O–(1 – x)SiO₂ (or xLi₂O–(1 – x)B₂O₃),²⁹¹ Li₁₀GeP₂S₁₂ (Ge sites: Sn, Pb, Si; P sites: Si, Al),^{292,293} and xLi₂S–(1 – x)P₂S₅ (or xLi₂S–(1 – x)Al₂S₃, xLi₂S–(1 – x)SiS₂).^{294–296} The gel electrolyte is mostly based on poly(ethylene oxide) (PEO), poly(propylene oxide) (PPO), poly(ethylene glycol) (PEG), poly(methyl methacrylate) (PMMA), poly(acrylonitrile) (PAN), or poly(vinylidene fluoride hexafluoropropylene) (PVdF–HFP).^{25,297,298} The current ionic conductivity of solid-state electrolyte is still

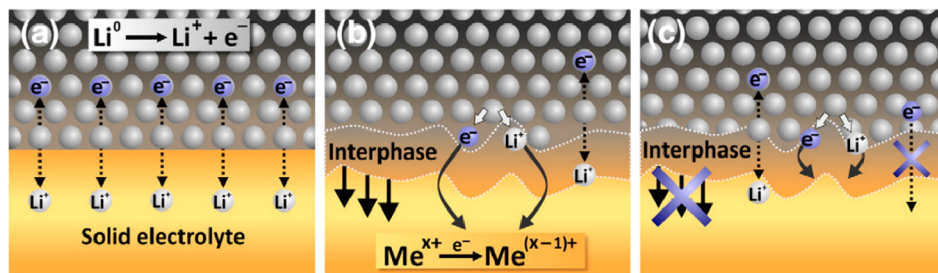


Figure 53. Scheme of interfaces between Li metal and solid lithium ion conductor. (a) Nonreactive and thermodynamically stable interface. (b) Reactive and mixed conducting interphase. (c) Reactive and metastable solid-electrolyte interphase. Reproduced with permission from ref 301. Copyright 2015 Elsevier.

much lower than that of liquid electrolyte.²⁹⁹ Even so, there is much hope to further improve it,³⁰⁰ for crystalline solid sulfide electrolyte has indicated a very high ionic conductivity at room temperature (around $10^{-2} \text{ S cm}^{-1}$).²⁹²

Though various solid inorganic electrolytes have been proposed, there are two main obstacles before their practical application in the Li metal anode, except for the foremost ionic conductivity:

1. Several of the solid inorganic electrolytes are not stable against Li (Figure 53),³⁰¹ such as the solid sulfide electrolyte. Though it has a really high conductivity, the solid sulfide electrolyte cannot remain stable when contacting Li metal anode. When investigating the detailed information on the chemical reactions at the Li/Li₁₀GeP₂S₁₂ (LGPS) interface, an interphase composed of Li₃P, Li₂S, and Li–Ge alloy was discovered.³⁰² Ceder's group developed a computational methodology to examine the thermodynamics of formation of resistive interfacial phases between solid-state electrolyte and electrodes (Figure 54).³⁰³ To stabilize the interface between the solid-state electrolytes and Li metal anode, increasing Li₂S exposure on the solid sulfide electrolyte surface can afford a protective buffer layer to relieve the reactions to some extent.³⁰⁴

2. Poor stability in air is the other main obstacle. Several solid-state electrolytes are not stable in the atmospheric environment and can react with water and carbon dioxide. Taking the promising Li₇La₃Zr₂O₁₂-based Li-rich garnets as an example,³⁰⁵ it can react to form a Li ion insulating Li₂CO₃ layer on the surface of the garnet particles, bringing a large interfacial resistance for Li ion transfer. In situ introducing LiF to garnet Li_{6.5}La₃Zr_{1.5}Ta_{0.5}O₁₂ (LLZTO) during its synthesizing process can increase the stability of the garnet electrolyte against moist air.

Similar to solid inorganic electrolyte, the solid polymer electrolytes are confronted with several dilemmas,^{306–308} including low ionic conductivity and poor stability against Li metal, though much progress has been achieved. To realize the practical application of the solid-state electrolyte in the Li metal anode, there is still a long way to go. In sections 7.5.1 and 7.5.2, we will concentrate on the methods to fabricate solid inorganic and polymer electrolytes and reduce the interfacial impedances to further improve the ionic conductivity of the solid-state electrolyte.

7.5.1. Inorganic/Polymer Hybrid Electrolyte. It is hard for individual inorganic or polymer electrolytes to satisfy the practical applications yet, due to flaws such as low ionic conductivity, high interface resistance, low mechanical modulus, high price, etc. Many superior nonliquid electrolytes are constructed by synergetically integrating two or three kinds

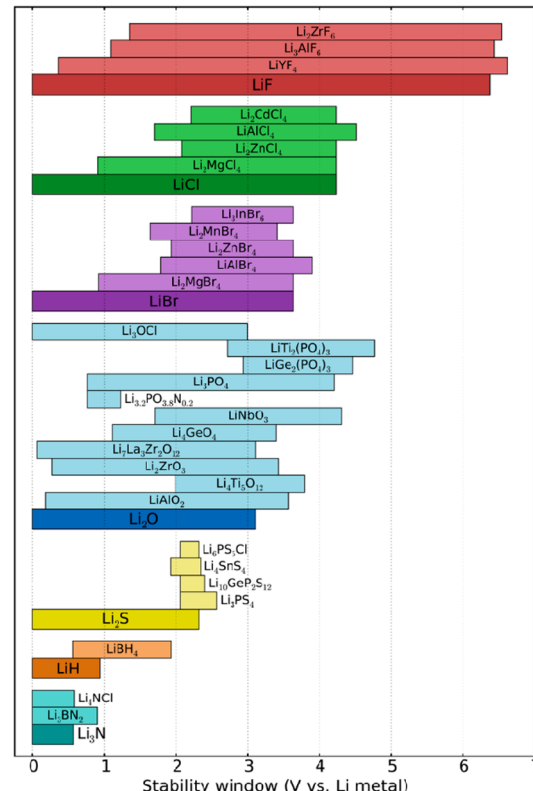


Figure 54. Electrochemical stability ranges of various electrolyte materials. The high-voltage stability is primarily determined by anions. Reproduced from ref 303. Copyright 2016 American Chemical Society.

of them to achieve an acceptable performance between ionic conductivity, structural stability, and anode surface contact.^{276,309–311} Therefore, inorganic/polymer hybrid electrolyte will also hopefully realize the demand of the solid-state electrolyte for LMBs. In the following section, we focus on the solid inorganic/polymer hybrid electrolyte to improve the bulk conductivity of this solid-state electrolyte. Electrode/electrolyte interface modification has also received extra attention in this review to further enhance Li ion flux through the solid-state electrolyte.

The conventional compositing strategy is to dope polymer with Li salt or other insulting oxides, such as SiO₂,^{276,312,313} while the conjunction of nanoscale Li-ion-conducting particles and polymer provides a promising solution to produce powerful solid-state electrolytes with high ionic conductivity.³¹⁴ Composite solid inorganic/polymer electrolyte with ceramic

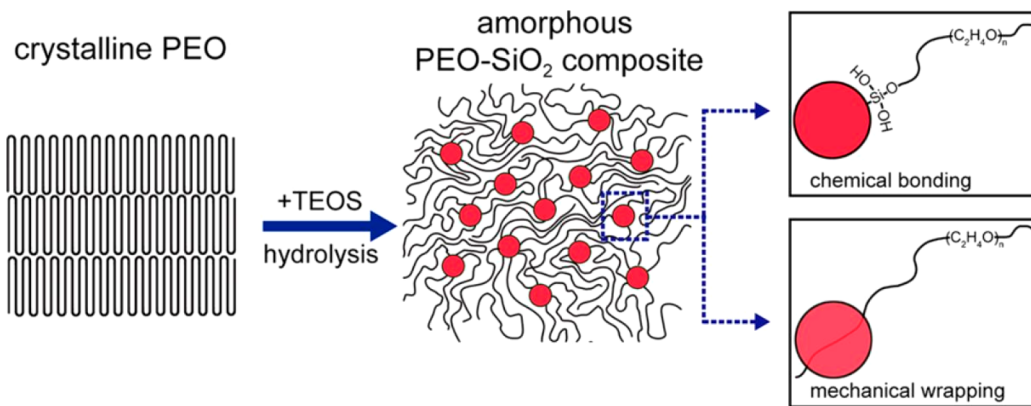


Figure 55. Scheme of in situ hydrolysis and interaction mechanisms among PEO chains and MUSiO₂. Reproduced from ref 316. Copyright 2016 American Chemical Society.

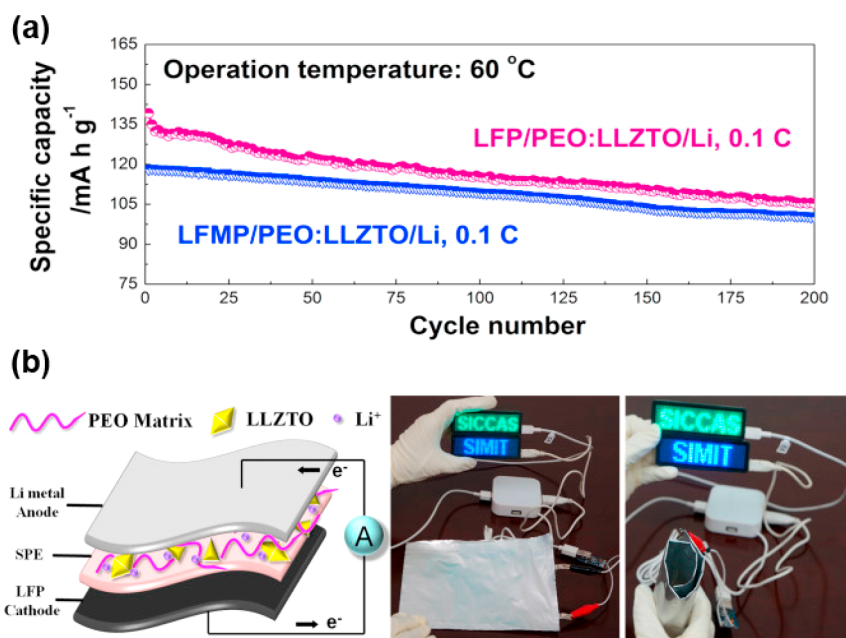


Figure 56. (a) Cycling performance of solid inorganic/polymer hybrid electrolyte at 0.1 C and 60 °C. (b) Scheme of flexible pouch cells with and cells to power LEDs with the “SIMIT” and “SICCAS” signals. Reproduced with permission from ref 314. Copyright 2016 Elsevier.

fillers has strongly been considered for LMBs due to the enhancement in ionic conductivity.

The compositing purpose is to achieve a good mechanical flexibility and high ionic conductivity. The mechanical flexibility is much contributed by the polymer electrolyte. Hence, the fraction of the polymer electrolyte in the composite electrolyte cannot be too low.³¹⁵ The ionic conductivity, the most important issue of the composite electrolyte, much depends on the compositing manner of the inorganic and polymer electrolyte, such as the following:

1. *Synthesizing model, including in situ synthesis and mechanical mixing.* The mechanical mixing method is really convenient and cost-saving, which is mostly adopted to obtain the composite electrolyte. However, the composite electrolyte obtained by this method often has a poor distribution of the inorganic and polymer electrolytes, leading to the aggregation into large particles, which is adverse for the ionic conductivity. In situ synthesis of ceramic filler particles (such as SiO₂) incorporated into polymer electrolyte (such as PEO) can render the good distribution of the two agents (Figure 55).³¹⁶ Much stronger

chemical/mechanical interactions were generated between PEO chains and monodispersed 12-nm-diameter SiO₂ nanospheres via in situ hydrolysis, therefore greatly suppressing the crystallization of PEO and notably facilitating polymer segmental motion for ionic transmission. All of these factors synergistically rendered a high ionic conductivity (4.4×10^{-5} S cm⁻¹ at 30 °C, 1.2×10^{-3} S cm⁻¹ at 60 °C).

2. *Particle sizes of the adopted inorganic electrolytes.* For the solid inorganic electrolyte, nanocrystallization always results in high ionic conductivity, due to the increased diffusion routes for Li ions.^{317,318} In the composite electrolyte, polymer electrolyte is like the binder to interlink the inorganic electrolyte as an integrity with high mechanical flexibility. The nanosized solid inorganic electrolyte has large contact area with the polymer electrolyte, which is believed to be critically important for the ionic conductivity.³¹⁴ The small size of the inorganic electrolyte filler is beneficial for the strong mechanical flexibility as well. The nanosized filler can exhibit an apparent conductivity of more than 10^{-4} S cm⁻¹ at 30 °C, nearly 2 orders of magnitude larger than those with the microscale inorganic

filler. The solid-state hybrid electrolyte can deliver a high cell energy density of 345 Wh kg⁻¹ (662 Wh L⁻¹) for LiFePO₄/Li batteries (Figure 56).

3. Dimensionality (*D*) of the inorganic fillers. Conventionally, the inorganic filler adopted is zero-dimensional (0D) particles. Recently, 1D fiber is also proposed as a filler in the polymer electrolyte. Compared to ceramic particles, ceramic nanowire fillers render more contact area between the inorganic and polymer electrolytes, improve the mechanical performance, and facilitate the formation of such ionic conduction networks in the polymer-based solid electrolyte to enhance its ionic conductivity by 3 orders of magnitude.^{319,320} A garnet-type Li_{6.4}La₃Zr₂Al_{0.2}O₁₂ (LLZO) nanofiber was generated by the electrospinning method. Incorporating the nanofiber fillers into PEO matrix formed a 3D ceramic/polymer network (Figure 57).³²¹ The 3D networks including randomly distributed and

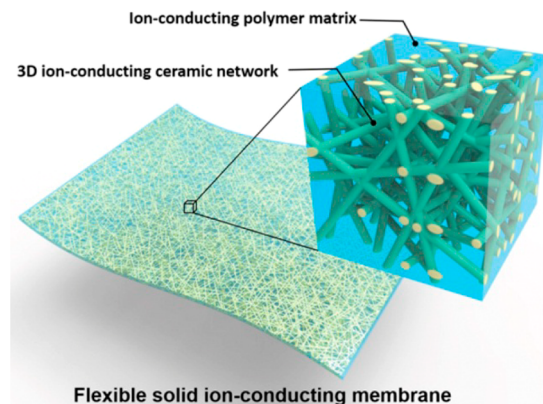


Figure 57. Scheme of hybrid solid-state composite electrolyte. Reproduced with permission from ref 321. Copyright 2016 National Academy of Sciences of the United States of America.

interconnected nanofibers in the polymer matrix led to a continuous Li ion conducting framework. Further investigations indicated, relative to the random ceramic nanowires, the aligned nanowires realized a higher ionic conductivity.³²²

The combination of ceramics and polymer electrolytes offers a new strategy to create excellent electrolytes with both high ionic conductivity and good mechanical properties. After obtaining a good hybrid electrolyte, it is of scientific significance to identify the ionically conductive channels in a composite electrolyte, which is helpful when designing the compositing manner of the hybrid electrolyte. The prevailing view is that the amorphous phase facilitates ion transport. Some research results claimed that ion conduction within composite electrolytes mainly occurs at the ceramic–polymer interface,^{323,324} while others do not accept it.^{324,325} By combining selective isotope labeling and high-resolution solid-state Li NMR, Li ion pathways within LLZO/PEO composite electrolytes were tracked by monitoring the replacement of ⁷Li in the composite electrolyte by ⁶Li from the ⁶Li metal electrodes during battery cycling, presenting the first experimental evidence to show that Li ions favor the pathway through the LLZO ceramic phase instead of the PEO–LLZO interface or PEO (Figure 58).^{324,325}

Compositing is a facile strategy to achieve a 1 + 1 > 2 consequence when the individual role is not satisfactory. The inorganic/polymer hybrid electrolyte is expected to be an electrolyte with a high ionic conductivity and mechanical flexibility. However, the compositing process should be

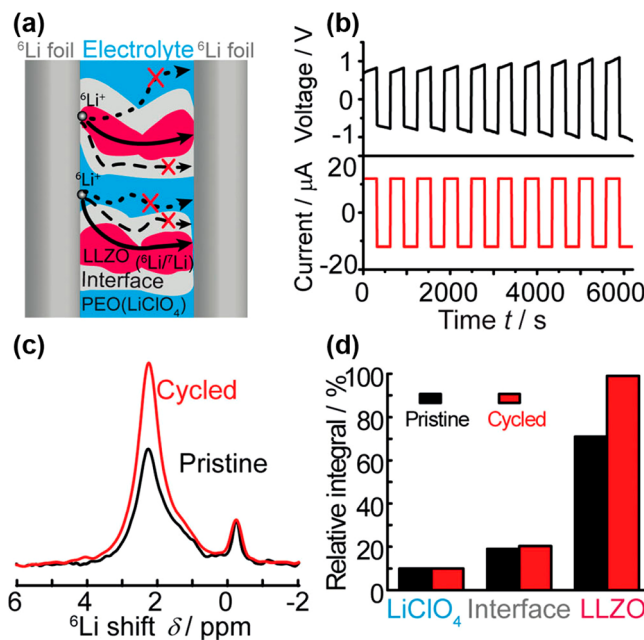


Figure 58. (a) Illustration of possible Li⁺ transport pathways. (b) Electrochemical profile of symmetric lithium battery. (c) ⁶Li NMR spectra of LLZO–PEO (LiClO₄) composite electrolytes. (d) Quantitative analysis of ⁶Li amount in LiClO₄ interface, and LLZO of LLZO–PEO (LiClO₄). Reproduced with permission from ref 325. Copyright 2016 WILEY-VCH Verlag GmbH & Co. KGaA, Weinheim.

elaborately conducted to avoid rendering the composite electrolyte poorer than any one of them. More compositing manners are required to be clearly investigated. For example, more *in situ* synthesizing routes and highly dimensional fillers (including 2D sheet fillers) are needed. The conducting channels in the composite electrolyte are required to be clearly probed, which is certainly important to designing the composite electrolyte.

7.5.2. Electrolyte/Electrode Interface Modification. Except for the effort to improve the ionic conductivity of the solid-state electrolyte, reducing the resistance between the solid-state electrolyte and electrode is of extreme critical importance.^{326,327} Interfacial resistance is increasingly becoming the bottleneck in many solid-state electrolyte systems.^{328,329} If the conductivity of a solid-state electrolyte is 0.1 mS cm⁻¹ and the thickness of the solid-state electrolyte is no more than 16.7 μm, the major voltage drop from the cathode to the anode is mainly derived from the poor interfacial impedance between the solid-state electrolyte and the electrodes.³³⁰

With the booming development of nanoscience, the electrode materials usually have nanosized particles, while the solid-state electrolytes are usually of microsizes.³³¹ Intimate contact between nanosized active materials and micrometer-sized electrolytes will be a great challenge, which is also the main source for the interfacial resistances and instability. Designing a transition layer, which can tightly contact Li metal and the solid-state electrolyte, is helpful to reducing the interfacial impedance.^{332,333}

Hu's group proposed several strategies to decrease the interfacial resistance by coating lithiophilic materials, including Al₂O₃,^{228,334} amorphous Si,³³⁵ and ZnO,³³⁶ through an atomic-layer-deposition method (Figure 59). These coating materials render a tight contact between the solid-state electrolyte and Li electrode, and a sharp reduce in the resistance from several

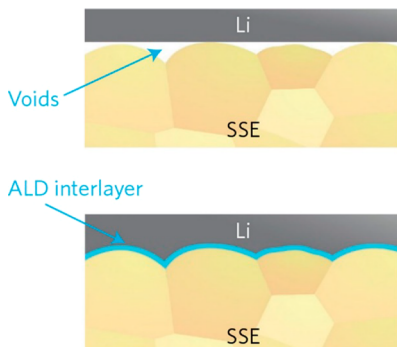


Figure 59. Wetting behavior of garnet surface with molten Li. Reproduced with permission from ref 334. Copyright 2017 Nature Publishing Group.

thousands to a few tens $\Omega \text{ cm}^{-2}$. Especially for the Al_2O_3 layer, when they modified this interfacial layer, a significant decrease of interfacial impedance, from 1710 to 1 $\Omega \text{ cm}^{-2}$, was observed at room temperature, effectively negating the Li metal/garnet interfacial impedance.³³⁴ The largely reduced impedance is induced by the lithiated alumina interface, enabling wetting of metallic Li in contact with the garnet electrolyte surface and the allowed effective Li^+ transport between the Li metal anode and garnet electrolyte. Li–metal (such as Li–Al) alloy can also act in a similar role.³³⁷ Another strategy to construct this intermediate layer is derived from the in situ reaction between the electrolyte and Li metal. For example, solid inorganic electrolyte $\text{LiZr}_2(\text{PO}_4)_3$ with a rhombohedral structure at room temperature can react with a metallic Li anode to form a Li^+ -conducting passivation layer containing Li_3P and Li_8ZrO_6 ,³³⁸ which is wet by the Li anode and also wets the $\text{LiZr}_2(\text{PO}_4)_3$ electrolyte to afford a small Li^+ transfer resistance across the interface.

The coating layer can not only enhance the contact between the solid-state electrolyte and Li metal, but also suppress Li dendrite growth. Habitually, solid-state electrolyte is believed to be able to stop the penetration of Li dendrites from reaching the cathode, while it cannot completely suppress the nucleation and growth of Li dendrites. The several micrometer and nanometer pinholes can be the preferential sites for Li dendrite nucleation and growth. Ishiguro et al. in their Nb- and Ta-substituted LLZO^{339,340} and Sudo et al. in their Al-substituted LLZO³⁴¹ observed the large dendrite growth when operating the cells at a relatively low current density of 0.5 mA cm^{-2} . Li

dendrite formation conceivably stemmed from the inhomogeneous contact between the solid-state electrolyte and Li electrodes (Figure 60).³⁴² By flattening the electrolyte surface and using thin Au buffer layers to reinforce the contact between solid-state electrolyte and Li electrodes, the interface resistance can be dramatically reduced and satisfactorily eliminate cell short circuit caused by dendrite growth at a current density of 0.5 mA cm^{-2} . Similarly, introducing Li_3PO_4 additive into garnet-type $\text{Li}_{6.5}\text{La}_3\text{Zr}_{1.5}\text{Ta}_{0.5}\text{O}_{12}$ can improve the interfacial compatibility and suppress dendritic Li growth during long-term Li plating/stripping.³⁴³

Introducing the third phase is the currently most adopted method to regulate the interfacial impedance.³⁴⁴ Two methods have been proposed, including the ex situ coating material on the solid-state electrolyte and the in situ reaction production from the solid-state electrolyte and Li metal. Motivated by the successful operation of the physically coated analogous-solid-state electrolyte in the liquid electrolyte (section 7.2.3), adding some liquid electrolyte onto the solid-state electrolyte may be useful to reduce the interfacial impedance between the solid-state electrolyte and Li metal.

In summary, the solid-state electrolyte is expected to handle the leakage, poor chemical stability, and flammability of the liquid electrolyte. When put into practical application, the solid-state electrolyte will generate an unprecedented effect on battery energy storage systems including Li metal batteries. The most important flaw is the low room-temperature conductivity, usually 10^{-8} – 10^{-5} S cm^{-1} . When the room temperature ionic conductivity reaches 10^{-4} – 10^{-3} S cm^{-1} , it is hopefully applied practically. Different from other anode materials, Li metal anode is really reactive. The research of solid-state electrolyte for Li metal anode requires caring about and taking advantage of this feature. The next research spots of solid-state electrolyte for Li metal anode can concentrate on discovering more proper solid-state electrolytes for Li metal, further enhancing the interfacial contact, and improving the ionic conductivity.

7.6. Structured Anode

The Li battery has successfully realized its commercialization by intercalating Li ions into a graphite matrix to solve the volume expansion during Li ion intercalation and deintercalation.^{345,346} The volume change issue is more severe for LMBs. As a “hostless” electrode, Li metal anode has a virtually infinite relative-volume change during Li plating/stripping, resulting in the poor mechanical stability of the SEI layer, low Coulombic

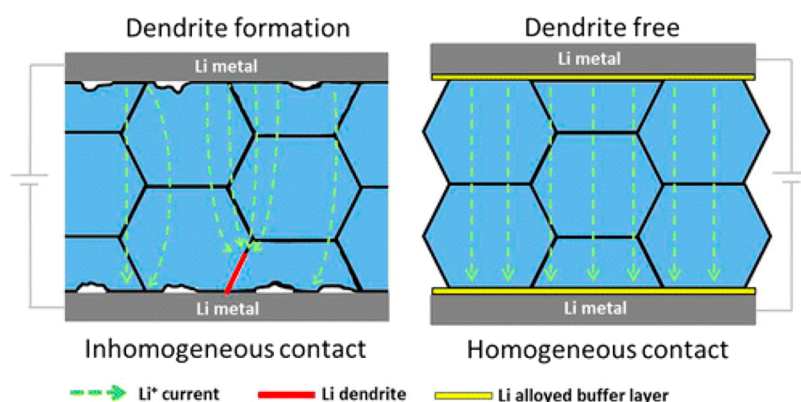


Figure 60. Schematic of $\text{Li-La}_3\text{Zr}_2\text{O}_{12}$ interface modification with alloy buffer layer to prevent Li dendrite formation. Reproduced from ref 342. Copyright 2016 American Chemical Society.

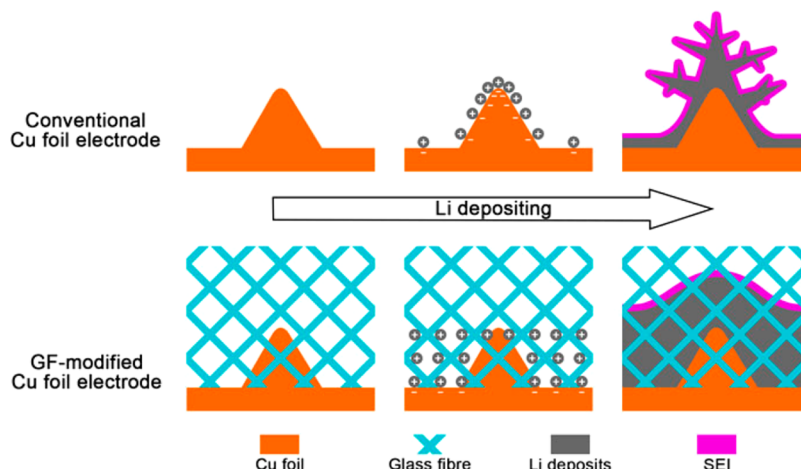


Figure 61. Scheme of Li deposition under the protection of polar fiber membrane. The routine 2D Cu foil electrode always has an uneven surface. The glass fiber (GF) cloth has large quantities of polar functional groups that attract the spatial charges above Li metal. The concentrated Li ions by the protuberances on the Cu foil electrode are evenly plated, therefore retarding the formation of Li dendrites on a working Li anode. Reproduced with permission from ref 352. Copyright 2016 WILEY-VCH Verlag GmbH & Co. KGaA, Weinheim.

efficiency, and poor lifespan of LMBs. Therefore, a proper matrix for Li plating and stripping is pressingly demanded to realize the practical applications of LMBs. An efficiently designed matrix can not only significantly mitigate the volume change at the electrode level during repeated cycling, but also regulate Li ion plating/stripping behavior to suppress Li dendrite growth.¹⁴⁸

7.6.1. Lithiophilic Matrix. Dendrite growth is mainly induced by inhomogeneous distribution of Li ions and current density on a current collector. If Li ions can be distributed uniformly on the anode surface, Li dendrite issue can be critically suppressed. Lithiophilic oxidized polyacrylonitrile nanofiber was adopted to guide Li ion deposition and form uniform Li metal deposits.³⁴⁷ This nanofiber can lead to stable cycling of metallic Li anode with an average Coulombic efficiency of 97.4% in 120 cycles at 3 mA cm^{-2} and 1 mAh cm^{-2} . N-doped PAN, N-doped graphene, and metal–organic framework (MOF) materials can also enable the stable operation of lithium plating/stripping by chemical interactions.^{348–351} Placing glass fibers (GFs) with many polar functional groups on the anode surface can facilely and evenly distribute Li ions (Figure 61).³⁵² The polar functional groups of GFs rendered a binding energy between glass fiber and Li of 1.0 eV higher than that of Cu foil and Li atom. The higher binding energy can adsorb considerable Li ions to compensate the electrostatic interactions between Li ions and protuberances of Cu foil or the previously grown Li dendrites. This strategy can avoid the accumulation of Li ions and thus suppress Li dendrite growth. Under current densities of 0.5, 1.0, 2.0, 5.0, and 10.0 mA cm^{-2} , cells with GF layers presented enhanced Coulombic efficiencies of 98, 97, 96, 93, and 91% for 90, 70, 65, 50, and 40 cycles, respectively. The polar Kimwipe paper rendered a dendrite-free Li plating morphology as well.³⁵³

The nonconductive polar surface of Li plating matrix can not only suppress Li dendrite growth, but also shed an emerging strategy to fabricate Li metal composite anode to be applied in Li–S and Li–O₂ full batteries. Nevertheless, it is really complicated to fabricate Li metal composite anode, because these matrixes either are nonlithiophilic or are not able to survive at a high temperature to melt Li metal solid.³⁵⁴ Cui's group pioneered fabrication of a composite Li metal anode by a

melting strategy.^{355–357} Liu et al. employed polyimide as a thermal-stable matrix with lithiophilic ZnO coating layer (Figure 62a).³⁵⁵ ZnO particles can serve as a lithiophilic scaffold.³⁵⁸ This composite anode can realize minimum volume change and effective dendrite suppression at a high current density of 5 mA cm^{-2} in both carbonate and ether electrolyte. To further improve the conductivity of the composite anode, Liang et al.³⁵⁶ employed conductive carbonized polyacrylonitrile fiber as the matrix with a lithiophilic Si coating layer (Figure 62b). However, this trilaminar composite anode is a little complex, and requires a tedious materials processing. To simplify the fabricating methods for the composite anode, Lin et al. proposed a simple yet subtle “spark” strategy to obtain uniform nanogaps (Figure 62c).³⁵⁷ The lithiophilic graphene oxide (GO) is used as a porous matrix for Li metal. When the GO film partially contacts with molten Li, a spark reaction is triggered until the whole film is filled by molten Li. After the spark reaction, molten Li enters the GO matrix and the nonconductive GO is converted to porous and conductive reduced graphene oxide (rGO). This Li–rGO anode can indicate a dendrite-free morphology during Li plating and a high rate performance of 60 mAh g^{-1} at 10 C when matching lithium cobalt oxide (LCO) cathode. Metallic Ni foam can be employed as a matrix to accommodate molten Li, probably because of some alloying reactions.³⁵⁹ Further, a one-step method has been proposed to obtain a matrix and its surface protective layer by reacting overstoichiometry of Li with SiO to form a $\text{Li}_x\text{Si}-\text{Li}_2\text{O}$ matrix.³⁶⁰ This composite anode can not only enable relatively constant electrode-level volume, but also protect the embedded Li from direct exposure to the electrolyte.

The lithiophilic matrix presents a possibility to redistribute Li ions on the anode surface by a chemical binding interaction to achieve a dendrite-free morphology and pioneers fabrication of the composite Li metal anode by a melting method. This composite Li metal anode can match a non-Li cathode, such as high capacity sulfur and oxygen cathodes, and has potential to be applied into a full cell. Selection of proper lithiophilic matrix species and ratio in the composite anode is further required to boost its practical application.

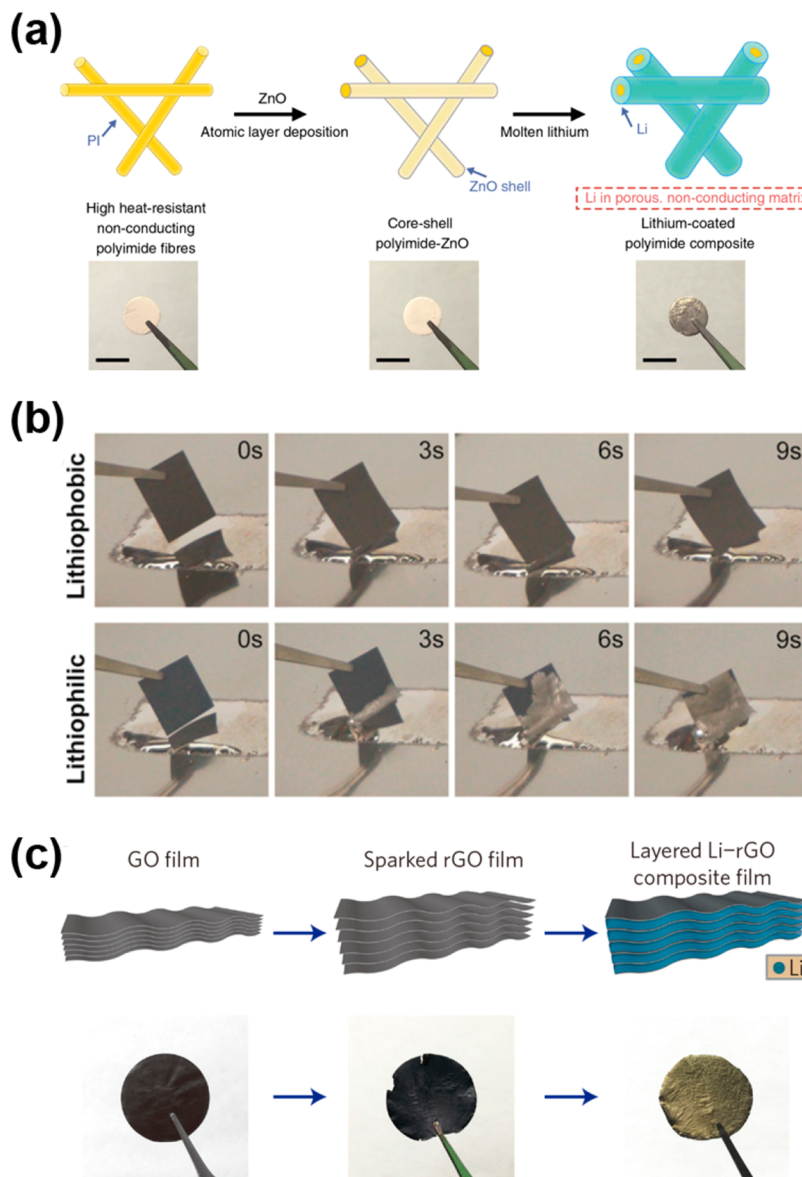


Figure 62. (a) Scheme of composite Li-PI metal anode. Electrospun PI was coated with “lithiophilic” ZnO. Li coated onto a porous, nonconducting polymeric matrix. The scale bar is 1 cm. Reproduced with permission from ref 355. Copyright 2016 Nature Publishing Group. (b) Time-lapse images of Li melt infusion for lithiophilic and lithiophobic materials. Reproduced with permission from ref 356. Copyright 2016 National Academy of Sciences of the United States of America. (c) Fabrication of a layered Li-rGO composite film. Reproduced with permission from ref 357. Copyright 2016 Nature Publishing Group.

7.6.2. Conductive Matrix. Compared with a nonconductive matrix, a composite anode with a conductive matrix exhibits many advantages, such as high electrical conductivity of the composite anode and unique surface chemistry to inhibit dead Li and recycle dead Li.³⁶¹ The strategy by a conductive matrix to suppress Li dendrite growth is motivated by Li powder anode.³⁶² Relative to 2D Li foil, Li powder has a large surface area and then effectively suppresses Li dendrite growth.^{363,364}

The microneedle surface treatment technique is an economical and efficient technique to cover a wide range of Li surface areas with a simple rolling process (Figure 63).³⁶⁵ The current density distribution over the Li metal was drastically regulated by changing pyramid hole dimensions and a type of pyramid hole pattern dimension (height = 50 μm, width = 50 μm, ridge length = 40 μm) exhibited the lowest

current density at its top.³⁶⁶ As preferential sites for controllable Li plating were generated by the rolling process, the as-obtained surface structure can conveniently suppress high-surface-area Li dendrite formation during the Li deposition process. This technique indicated an improved rate capability and cycling stability, as well as a reduced interfacial resistance, which enhanced the rate capability by 20% at 7.0 °C and increased the cycling stability by 200% after 150 cycles of LiFePO₄ cathode relative to the untreated bare Li metal electrode. Micro/nanoarchitected porous silicon (Si) and ZnO electrodes were demonstrated to be equally effective in guiding the deposition of Li metal and validated the importance of the rational design of porous electrode to guide Li deposition in a working cell.³⁶⁷

Nevertheless, the microneedle surface treatment technique holds two problems:

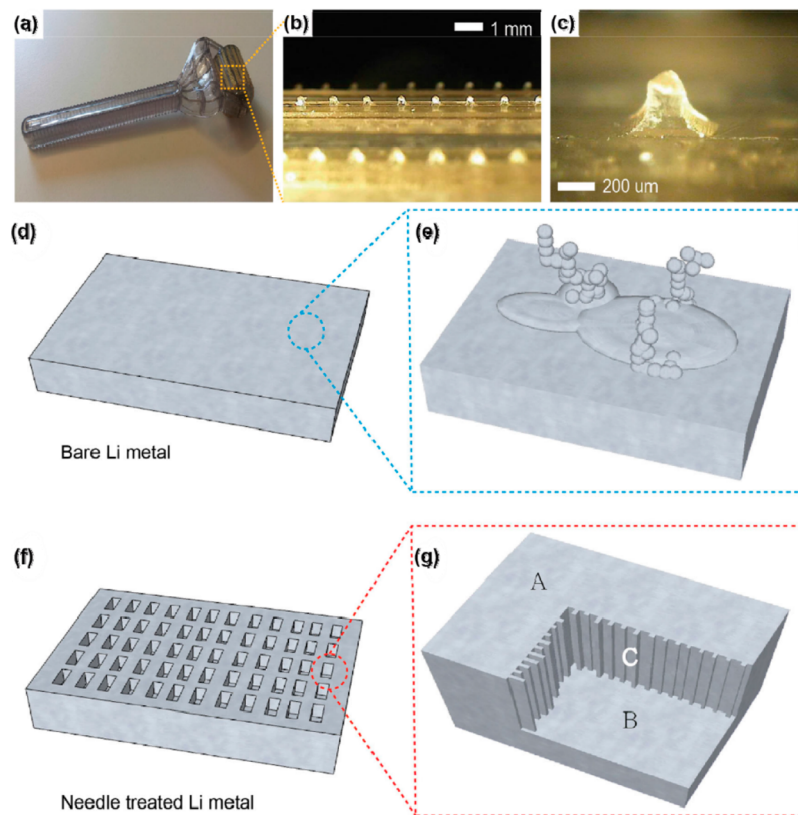


Figure 63. Microneedle surface treatment for Li metal. (a) Digital image of microneedle roller. (b) Roller head and (c) microneedle. (d, e) Bare Li metal and (f, g) microneedle treated Li metal. Reproduced with permission from ref 365. Copyright 2015 WILEY-VCH Verlag GmbH & Co. KGaA, Weinheim.

1. The lithiation capacity is very limited. When the deposited Li exceeds the amounts accommodated in the holes, Li deposits will grow out to be a dendrite.

2. Without a preset inert matrix, Li powder electrode and the Li plate electrode with microneedle surface treatment cannot be well preserved during a long cycling test. After several cycles, Li powders and microneedle Li convert into 2D Li foil and lose the feature to retard Li dendrite growth.

Consequently, it is of considerable importance to design an inert and stable matrix in the metallic Li anode. There are three main reasons responsible for the significant role of the conductive matrix on Li metal anode:

1. Compared with the 2D Cu foil current collector, the 3D conductive matrix can improve the surface area and then reduce the local current density of the anode, thus suppressing Li dendrite growth (see Sand's time model in section 4.3). A high-surface-area graphene framework well proved this concept (Figure 64).¹⁴⁵ This graphene framework possessed a very large specific surface area of $1666 \text{ m}^2 \text{ g}^{-1}$, a pore volume of $1.65 \text{ cm}^3 \text{ g}^{-1}$, and an electrical conductivity of 435 S cm^{-1} , affording the feasibility to largely reduce the local current density to effectively regulate Li depositing morphology. This anode framework can not only suppress Li dendrite growth, but also exhibit a high Coulombic efficiency of 93% at 0.5 mA cm^{-2} when matching the LiTFSI–LiFSI dual-salt electrolyte.

2. The 3D conductive matrix with high surface area has a high electric field intensity, which can absorb Li ions to deposit on the conductive matrix, rather than on the previously formed Li dendrite tip. Therefore, the continuous growth of Li dendrites is retarded. The Li_7B_6 framework was adopted to demonstrate this assumption.¹⁴⁶ The Li_7B_6 nanostructured

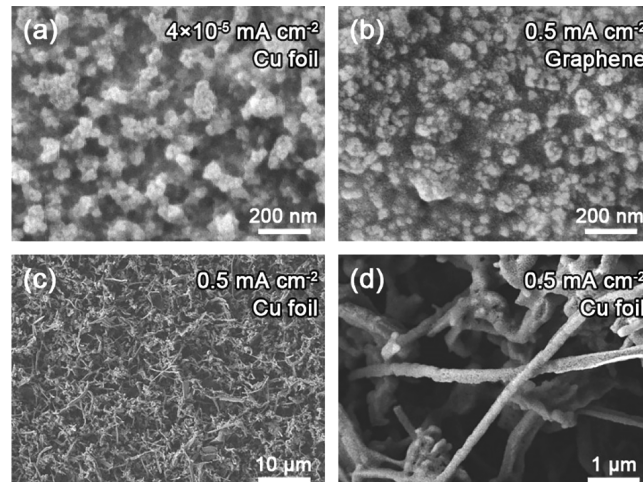


Figure 64. High surface area current collector renders small local current density for uniform deposition of Li metal. (a) Li deposits on Cu foil-based anode at $4 \times 10^{-5} \text{ mA cm}^{-2}$. (b) Li deposits on graphene-based anode at 0.5 mA cm^{-2} . (c, d) Li dendrites on Cu foil at 0.5 mA cm^{-2} . Reproduced with permission from ref 145. Copyright 2016 WILEY-VCH Verlag GmbH & Co. KGaA, Weinheim.

anode rendered a dendrite-retarded morphology at a high current density of 10 mA cm^{-2} , while the routine Li plate anode has severe dendrite formation (Figure 65). When employed in Li–S batteries, this nanostructured anode delivered an unprecedented cycling life extended to 2000 cycles, a high Coulombic efficiency of 91–92% (without LiNO_3 additives), and a low cyclic capacity degradation of 0.032% per cycle.

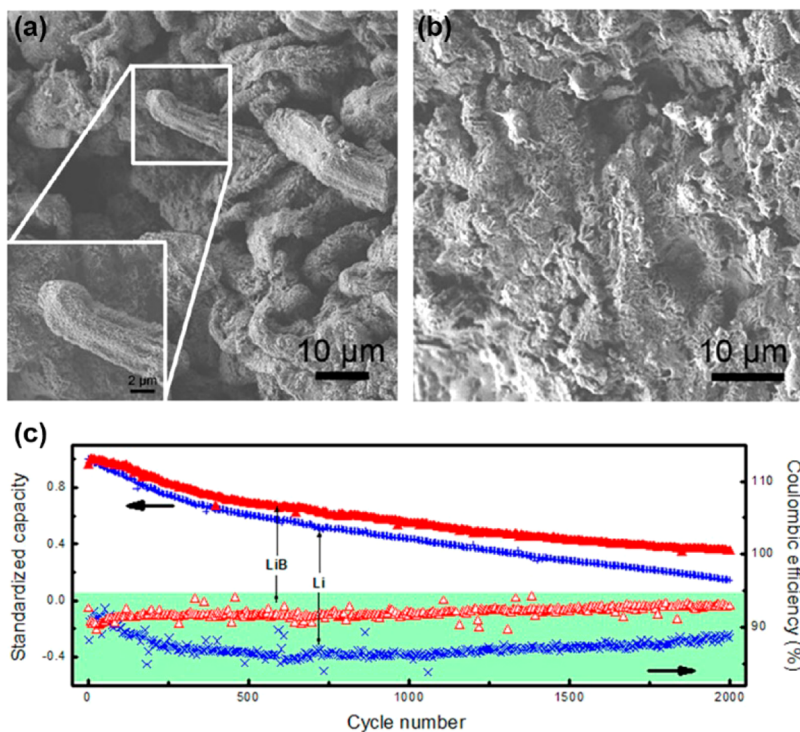


Figure 65. Morphologies of (a) plate Li metal and (b) nanostructured Li–B electrodes after charging at 10 mA cm^{-2} for 40 h. (c) Long-term cycling performance at 1675 mA g^{-1} . Reproduced with permission from ref 146. Copyright 2014 WILEY-VCH Verlag GmbH & Co. KGaA, Weinheim.

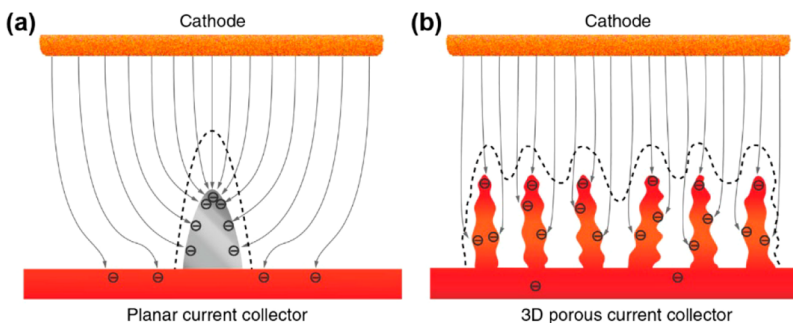


Figure 66. Illustration of electrochemical deposition of Li metal on (a) a planar current collector and (b) 3D current collector. The dashed lines illustrate the possible position where Li is deposited. Reproduced with permission from ref 368. Copyright 2015 Nature Publishing Group.

3. In the submicrometer conductive skeleton, the electric field is roughly uniform and the charges are homogeneously dispersed, eventually forming a relatively even Li surface. Not all the conductive matrixes are beneficial for Li plating. Guo and co-workers discovered that 3D Cu foam with a median pore diameter (by volume) of $170 \mu\text{m}$ cannot suppress Li dendrite similar to 2D Cu foil.³⁶⁸ Three-dimensional Cu current collector with a median pore diameter (by volume) of $2.1 \mu\text{m}$ can effectively accommodate Li deposits in the 3D pores without uncontrollable Li dendrites (Figure 66). With the efficient inhibition of Li dendrite growth, Li metal anode in the 3D current collector can cycle for 600 h without any short circuits and exhibit a very low voltage hysteresis and charge transfer resistance. In the Li/LiCu cells, this Li metal electrode with 3D current collector achieved a high areal capacity and showed a good plating/stripping efficiency of 98.5% at 0.5 mA cm^{-2} .

Afterward, several structured Li metal anodes are developed, such as Li_7B_6 framework with different Li contents,^{146,369} carbon nanotubes (CNTs),^{370–373} graphene ma-

trix,^{145,361,374–377} a seamless graphene–CNT hybrid electrode,³⁷⁸ carbon nanofibers,^{379–381} porous carbon film,³⁸² spherical carbon granules,³⁸³ 3D graphene@Ni scaffold,³⁸⁴ 3D Cu current collector,^{385–387} Cu nanowires,¹⁴⁷ and fibrous metal felt.³⁸⁸ Designing Li metal electrodes possessing alert architecture with appropriate micro/nanopores is a promising strategy to well regulate the deposition of the Li metal and suppress Li dendrite growth. These efficiently structured anode matrixes have great potential to serve as the next-generation Li metal anode.

Various conductive matrixes have been proposed. However, complete investigations into the specific roles of different electrical conductivities, pore structures, and surface areas are less involved. Besides, except for the complex electroplating method to obtain a composite Li anode with the conductive matrix, there is no method to fabricate the composite Li anode to match a non-Li cathode. Further optimizing the matrix and developing a facile method to fabricate the composite Li metal anode is of essential significance.

In summary, the matrix is of vital importance for Li metal anode, not only because of its role to suppress Li dendrite growth, but also to relieve the large volume change during Li plating and stripping. It can even be concluded that no matrix, no Li metal anode. These matrixes can cooperate with the solid-state electrolyte to realize a dendrite-free and highly conductive Li metal anode. When the matrixes are applied to the liquid electrolyte, electrolyte additives are required to form a stable SEI film to protect the deposited Li from the corrosion of liquid electrolyte. Nevertheless, it should be noted that the ratio of the matrix in the composite Li metal anode should be properly controlled to ensure the high practical mass and volume energy density of the composite anode. The matrixes are very potentially able to achieve a safe and efficient Li metal anode after some optimizing and matching other strategies, such as liquid electrolyte additives.

7.7. Membrane Modification

Routine membranes in LIBs act as a layer to separate the cathode and anode from electronic contact and short circuit. High ionic and heat conductivity, good mechanical flexibility, and heat stability are the primary requirements as a membrane.³⁸⁹ For a Li metal battery, the membrane is a very important part. As the membrane affects much on the Li ion diffusion in the bulk electrolyte and the final Li dendrite growth to the cathode, it has stronger roles in the dendrite growth and the postgrowth detecting stages, rather than the initial nucleation stages.³⁹⁰

7.7.1. Dendrite Growth Stage. The conventional polymer membrane is designed to physically separate the cathode and anode with a high ionic conductivity and thermal stability,^{391,392} but without a role to suppress Li dendrite growth. Several designing principles are required for a remarkable membrane in LMB to suppress Li dendrite nucleation, growth, and final cell short circuit.

1. *Reduced pore size.* When the pore size of the composite membrane is smaller than that of Li dendrites, it can eliminate “weak links” where the dendrites pierce the membranes. A composite membrane from Kevlar-derived aramid nanofibers through layer-by-layer assembling of PEO³⁹³ and a nonporous, elastomeric solid-electrolyte separator³⁹⁴ have solidly demonstrated this idea. Relative to the routine polyolefin separators, the separator was more effective at blocking dendrite growth at large current density (10 mA cm^{-2}) and accommodated the large volume change during Li plating/stripping.

2. *Improved mechanical performance.* Similar to solid-state electrolyte (section 7.5), the separator can stop the dendrite growth when its modulus exceeds that of Li dendrites.³⁹⁵ An ultrastrong poly(*p*-phenylene benzobisoxazole) nanofiber was exfoliated from Zylon microfibers to assemble into a nanoporous membrane with an ultimate strength of 525 MPa and Young’s modulus of 20 GPa (Figure 67).³⁹⁶ This stiff separator can lead to plastic and elastic deformation of Li at the negative electrode to flatten the electrode considerably.³⁹⁷ Nitrogen and sulfur codoped graphene nanosheets on the membrane can also suppress Li dendrite growth by enhancing interfacial interaction between the separator and Li metal, induced by electrostatic attraction that released the surface tension of Li metal.³⁹⁸

3. *Thermally conductive nature.* Thermal runaway is an important aspect of battery failure. A thermally conductive separator can evenly distribute heat in the battery and avoid heat accumulation. The thermally conductive separators can be achieved by an inorganic–organic hybrid polymer and boron

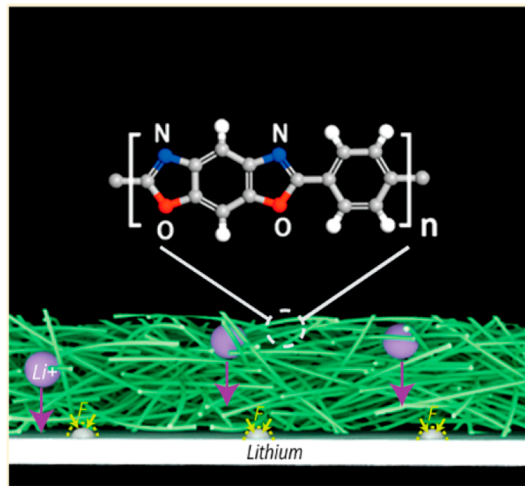


Figure 67. Diagram of PBO. PBO consists of three ring moieties: benzene (B), oxazole (O), and phenylene (P) groups. Reproduced from ref 396. Copyright 2016 American Chemical Society.

nitride nanosheet coating on separators.^{399–401} The obtained hybrid composite separators exhibited small thermal shrinkage and homogeneous thermal atmosphere to realize thermal stability and suppress Li dendrite growth. A ceramic (SiO_2)-grafted polyethylene (PE) separator displayed a strong dimensional thermostability, as the shrinkage ratio was only 20% even at an elevated temperature of 180°C , which is very important to realizing a safe battery in thermal runaway condition (Figure 68).⁴⁰²

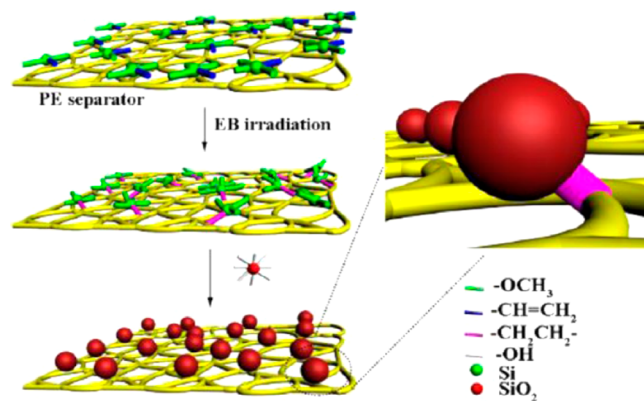


Figure 68. Mechanism for ceramic-grafted PE separator preparation through a facile irradiation grafting of VTMS and silication. Reproduced from ref 402. Copyright 2015 American Chemical Society.

4. *Improved Li diffusion behavior.* High ionic conductivity of the separator can rapidly transfer Li ions between the cathode and anode to reduce the Li ion depletion on the anode surface, which is helpful to stopping Li dendrite growth. A composite by a simple layer-by-layer self-assembly of ZrO_2/POSS multilayer was fabricated on a PE separator (Figure 69).⁴⁰³ The ZrO_2/POSS multilayer can weaken the solvation effect of Li ions, significantly enhancing ionic conductivity and Li^+ transference number, as well as the Li/electrolyte interfacial stability. The ionic conductivity and Li^+ transference number through the PE separator can also be altered by the polyelectrolyte coating on the separator (including PEI-PSS-PLLgPEG),⁴⁰⁴ lithium salt

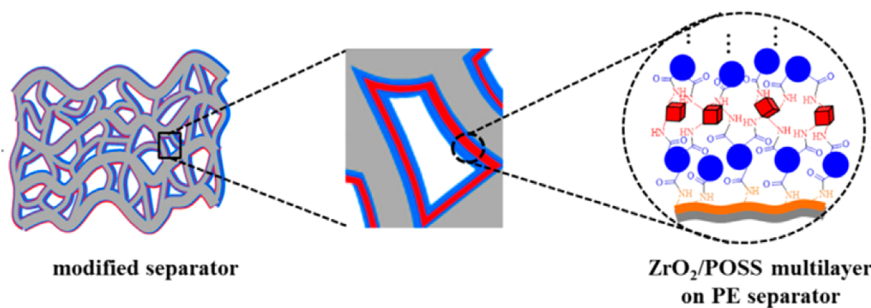


Figure 69. Cross-sectional diagram of PE separator before and after self-assembly for Li metal batteries. Reproduced with permission from ref 403. Copyright 2016 Elsevier.

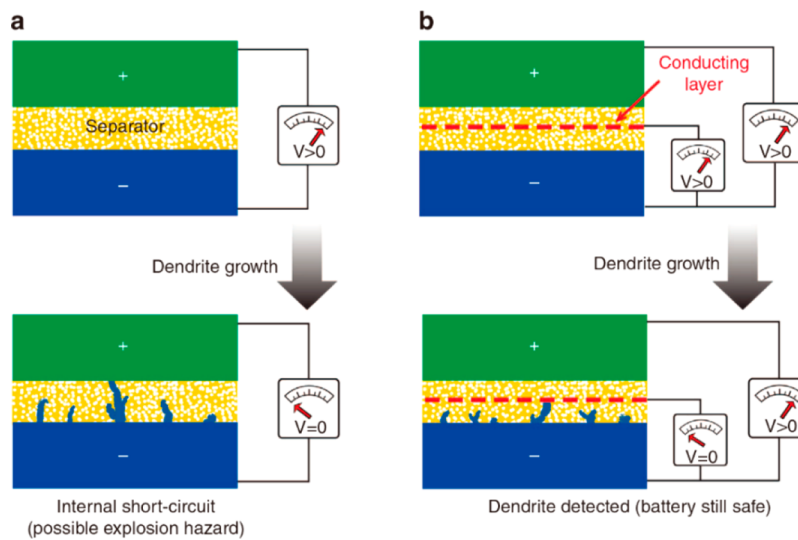


Figure 70. Scheme of smart battery design and fabrication. (a) In a routine Li battery, Li dendrites are only detected with a voltage of zero after completely penetrating the separator. (b) A Li battery with a composite separator can detect Li dendrites when they penetrate the separator. Reproduced with permission from ref 408. Copyright 2014 Nature Publishing Group.

inclusion into the separator,⁴⁰⁵ a porous cellulose-based membrane,⁴⁰⁶ and 3D porous ZSM-5 coated membrane.⁴⁰⁷

7.7.2. Dendrite Detection and Elimination. After Li dendrites form, the membrane becomes the final protective barrier, because if Li dendrites are expected to electronically connect the cathode and anode, and short circuit the cell, they must permeate through the membrane. In this stage, dendrites can be detected and partly eliminated to avoid the final thermal runaway and fire/explosion disaster.

1. *Li dendrite detection.* It is very hard to detect the growth of Li dendrite before the final cell short circuit. Before cell short circuit, Li dendrites have to reach the membrane first, and the membrane can act as an alert to discover the growth of Li dendrites. Based on this role, a functional membrane with a sensing terminal within the dual-layer separator was designed to detect Li dendrites crossing the separator (Figure 70).⁴⁰⁸ The electronic insulating separator evolved to a polymer–metal–polymer triple layer configuration. With the electrochemical potential difference, the voltage between the sandwiched metal and the anode can be identified. During battery operation, once dendrites emerged and grew until they finally reached the sandwiched metal layer before penetrating through the whole separator, a sharp voltage drop could be recorded, indicating the dendrite growth in the cells. On detecting this information, the battery can be stopped to avoid the cell short circuit, thermal runaway, possible fire, and even explosion. An all-

integrated PI/Cu/PI bifunctional separator for dendrite detection can also function as an early alarm of Li penetration.⁴⁰⁹

2. *Dendrite elimination.* Apart from being able to detect Li dendrites, the sandwiched separator layer can incorporate the Li metal reactive materials to eliminate Li dendrites to improve the safety performance. A layer of silica nanoparticles sandwiched by two layers of commercial polyolefin separators was proposed to enhance the safety performance of Li metal anode.⁴¹⁰ When Li dendrites grow and penetrate the separator, they contact the silica nanoparticles in the sandwiched layer. The silica nanoparticles react with Li through a solid-state conversion reaction, thus efficiently etching away dangerous Li dendrites and retarding their further growth (Figure 71). Therefore, Li dendrites are retarded and thereby the life of a battery is extended.

As a layer to separate the cathode and anode, the membrane can regulate Li dendrite nucleation and growth by modifying its surface chemistry and pore structure. Innovatively designing the membrane component and structure can detect and eliminate the dendrites in the postgrowth stage. Besides, when designing the membrane, the features of other modifications, including solid-state electrolyte and surface coating of Li metal can be incorporated to achieve a superstructure. Efficiently integrating these features will be of great significance for a LMB.

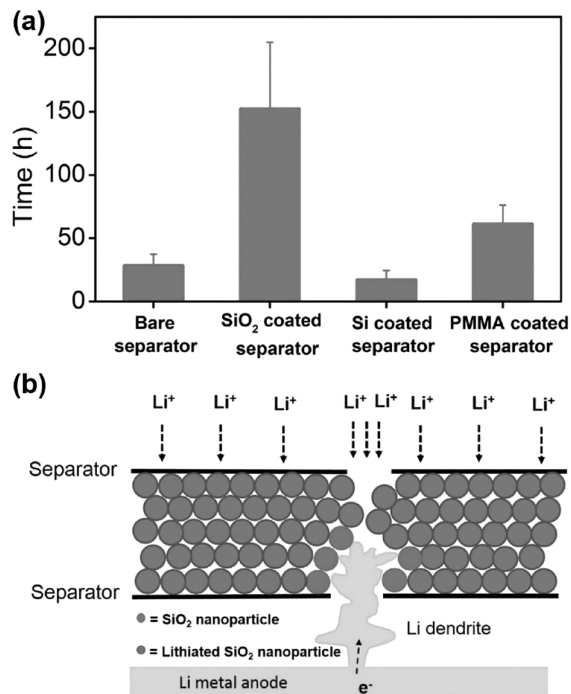


Figure 71. (a) Average battery lifetime of trilayer separator. (b) Scheme exhibiting the mechanism for the very long cycling life with a silica nanoparticle sandwiched separator. Reproduced with permission from ref 222. Copyright 2017 WILEY-VCH Verlag GmbH & Co. KGaA, Weinheim.

7.8. Cell Operation

Beyond the electrolyte, electrode, and membrane modification to suppress Li dendrite growth, cell operation patterns also critically determine Li ion depositing behavior. In the following section, some strategies to suppress Li dendrite growth based on cell operation patterns will be reviewed.

7.8.1. Charging/Discharging Rate. The charging/discharging rate can alert the electrode current density and the current density can heavily affect Li ion plating/stripping dynamics, as indicated in section 5.3.1. Hence, the Li dendrite nucleation and growth and the cell cycling performance critically depend on the charging/discharging rate. Li/LiNi_{0.8}Co_{0.15}Al_{0.05}O₂ (NCA) cells were discovered to indicate a superior cycling performance at a small charging (Li plating) rate (0.2 C).⁵⁰ This was understandable, because small Li plating current led to uniform Li deposits and superior cycling performance. When the charging current density was increased (≥ 0.5 C), the cycling performance was badly deteriorated induced by Li dendrite growth and the related dead Li (Figure 72), because large current density always led to severe Li dendrite growth. However, the relation between the discharging rate (Li stripping) and the cycling performance is contrary to that. Li|NCM cells achieved a better cycling performance at a large discharging rate (1–4 C) than that at a small discharging rate (1/10 and 1/3 C).⁴¹¹ A transient high-concentration electrolyte layer on the anode surface formed during high rate discharging was responsible for this unnatural phenomenon. The highly concentrated Li⁺ ions are immediately solvated by the available solvent molecules and render the formation of a flexible and stable SEI film to suppress Li dendrite growth and therefore enable a superior long-term operation of LMBs.

7.8.2. Intermittent Plating. Intermittent plating strategy includes pulse plating and reverse pulse plating without long-

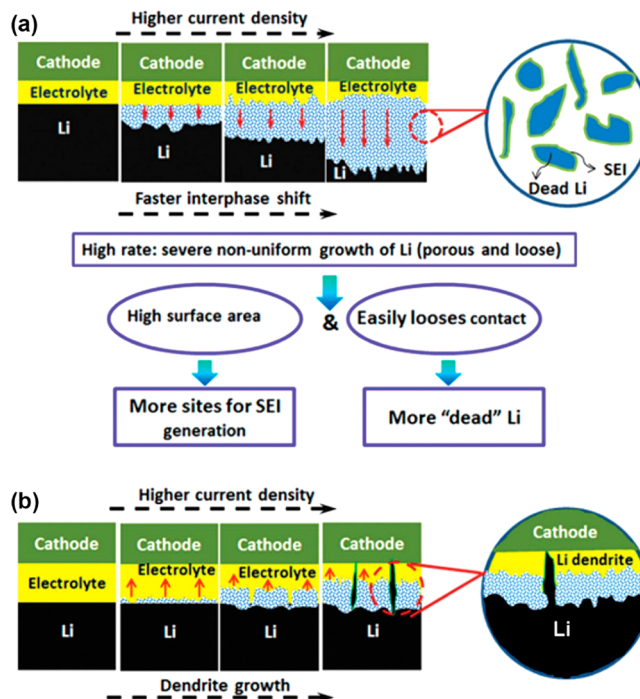


Figure 72. (a) Scheme of the failure mechanism. (b) Routine understanding of the dendrite-related failure mechanism for Li batteries. Reproduced with permission from ref 50. Copyright 2015 WILEY-VCH Verlag GmbH & Co. KGaA, Weinheim.

time Li ion plating to inhibit dendrites continuously growing large. Relative to direct current electrodeposition, pulse plating waveforms with short and widely spaced pulses can significantly improve Li deposition morphology and cycling efficiency.⁴¹² By pulse charging the cell with 1 ms plating and 3 ms rest periods, the average dendrite length can be shortened by ~2.5 times relative to those growing under continuous charging.¹⁵⁵ This conclusion is also confirmed by Monte Carlo simulations.

7.8.3. Convection Battery. Convection strongly affects the nucleation and growth of dendritic Li.⁴¹³ The convection can be caused by electrolyte viscosities,⁴¹⁴ gravity, and electric field.⁴¹⁵ Dornbusch et al. found that stabilized cycling of metallic Li negative electrodes without dendrite failure was possible in a convection battery.⁴⁸ The electrolyte flew through Li electrode first, where Li ions were consumed, prior to entering the separator. Consumption of Li ions prior to entering the separator region resulted in a lowered concentration and reduced electrochemical potential in the separator. Besides, convective flow reduced concentration gradients to lower concentration overpotentials, under which condition dendrite formation was not thermodynamically favored.

The regulations in cell operation present some possibilities to suppress Li dendrite growth. However, these strategies are not universal. For example, the slow changing rate can protect Li metal, but it cannot be accepted in most practical applications, because it extends the charging time much. This issue is also applicable for the intermittent plating method. Some peculiar scenario with enough charging time may be applicable. A convection battery can be applied in the situation without strict requirements on the volumetric energy density. Though these strategies cannot be applied in all situations, the concepts from them may be instructional when designing other methods.

7.9. Methods for Dendrite Inhibition in Other Metal Anodes

The dendrite issue is not exclusive to the Li battery. Other metal batteries, such as Na and Zn metal batteries, have the dilemma of dendrite growth induced safety concern and low cycling stability as well. Compared with the research on the dendrite issue in Li battery, dendrites in other metal batteries have been explored very little. Nevertheless, some effective strategies have been proposed, which can shed some fresh light on the dendrite inhibition in Li metal anode.

7.9.1. Na Dendrite. Room-temperature rechargeable Na metal batteries, including Na–S and Na–O₂ batteries,^{416–418} have attracted much attention due to their high-energy-density (theoretical capacity for Na metal 1166 mA h g⁻¹) and the abundance of sodium resources compared to Li.^{419,420} Similar to Li metal anode, Na deposits also easily grow into a dendritic pattern, hence resulting in safety concern and low efficiency.^{420–422} Differently, Na metal is more active, resulting in a severe adverse reaction with the electrolyte, hence a low Coulombic efficiency. Na ions have a larger ion radius than Li. The large ion radius requires a high conductivity. Therefore, ionic conductivity is a critically important index when designing the methods. All these render Na metal batteries to be more complex.

Though the Na ion battery has achieved much progress,^{423–425} the Na metal battery is less involved. Some strategies to suppress Na dendrite growth similar to that of Li dendrite are proposed, such as the following:

1. *Electrolyte modification.* A simple sodium hexafluorophosphate in glyme electrolyte at room temperature was reported.⁴²⁶ This electrolyte formed a uniform SEI film including sodium oxide and sodium fluoride. This SEI film was highly impermeable to electrolyte solvents and conducive to nondendritic growth. A high Coulombic efficiency of 99.9% was obtained over 300 cycles at a current density of 0.5 mA cm⁻². A 5.3 M Na salt was dissolved in the electrolyte and induced a polygonal growth of dendrite-free Na electrodeposition.⁴²⁷

2. *Solid-state electrolyte.* Polymer/oxide/ionic liquid solid electrolyte⁴²⁸ and nonflammable and highly Na⁺-conductive NaAlCl₄·2SO₂ inorganic electrolyte⁴²⁹ were tried to be applied in the Na metal anode. However, it is still challenging to achieve a high ionic conductivity.⁴³⁰ When the ionic conductivity of Na ion solid-state electrolyte can be comparable with that of liquid electrolyte (1–6 mS cm⁻¹ at room temperature), it will greatly promote the fabrication of safe solid-state Na metal batteries.⁴³¹

3. *Nanocarbon matrix.* Conductive carbon layer,⁴³² carbonized wood,⁴³³ and rGO matrix⁴³⁴ were adopted to regulate the current distribution on the anode surface to suppress Na dendrite growth.

4. *Membrane modification.* A Nafion–Na⁺ membrane selectively blocked the diffusion of anions through the batteries.⁴²⁰ When the sodium ion selective polymer membrane acted as a part of a composite glass-fiber separator to prevent dendrite penetration physically, a significantly enhanced cyclability of Na–O₂ batteries was obtained. The dendrite-blocking role can also be achieved by a similar method with the use of a polymer–Sb₂O₃ separator.

Compared to room temperature metal batteries, the dendrite issues are not as important in the high temperature metal batteries with molten anodes.^{435,436} Realization of a room-temperature battery with a liquid alkali-metal anode may

eliminate dendrite growth. K–Na alloys with a eutectic temperature below room temperature were tried to work as a room temperature liquid metal anode.⁴³⁷ When the liquid metal anode matched MnFe(CN)₆ cathode, it formed a dendrite-free battery (Figure 73). At 25 °C, the liquid electrode extended



Figure 73. Scheme of solid-metal anodes into liquid-alloy anode to suppress dendrite formation. Reproduced with permission from ref 437. Copyright 2016 WILEY-VCH Verlag GmbH & Co. KGaA, Weinheim.

from 9.2 to 58.2 wt % Na. This liquid zone could deliver a high specific capacity of 629 mA h g⁻¹ for a Na metal battery and 579 mA h g⁻¹ for a K metal battery.

Research of Na metal battery is in the startup stage, and its development even falls behind that of Li metal battery. As alkali metals, the Na and Li metals have several similarities and differences. Mutual learning will be favorable for their advances.

7.9.2. Zn Dendrite. As with Li metal batteries, primary Zn metal batteries have been used in numerous applications, while the rechargeable Zn battery technology has the troubles caused by dendrite growth.⁴³⁸ Since the 1960s, numerous strategies have been proposed to characterize and suppress Zn dendritic growth during electrodeposition.⁴³⁹ In the present Zn–oxygen battery research, the battery is often operated by removing spent Zn and resupplying a fresh Zn anode. This avoids the issues of poor Zn electrode reversibility and unstable bifunctional air electrodes.⁴⁴⁰ However, this cannot be widely adopted in practical applications due to the high costs of setting up a network of Zn recharging and supplying stations. Only by completely handling the problems of Zn metal batteries can they be in practical applications.

Different from the highly active Li and Na metals, Zn metal is relatively stable in the electrolyte (aqueous and nonaqueous electrolytes). Hence, the low Coulombic efficiency is not caused by the electrolyte and electrode. The performance of a Zn electrode is limited by four major phenomena that occur during operation in a Zn–air battery: (i) dendrite growth, (ii) shape change, (iii) passivation and internal resistance, and (iv) hydrogen evolution. Here, we only focused on the Zn dendrite issue and the strategies to suppress them. The strategies can be summarized as follows:

1. *Electrolyte modifications.* The early attempts to control Zn electrodepositing morphology mostly concentrated on optimization of the applied potential or current waveform.^{442–444} Later, researchers found that the use of parts per million levels of additives in the plating electrolyte, such as organic additives,⁴⁴⁵ tartaric acid,⁴⁴⁶ and lead chloride,⁴⁴⁷ can achieve

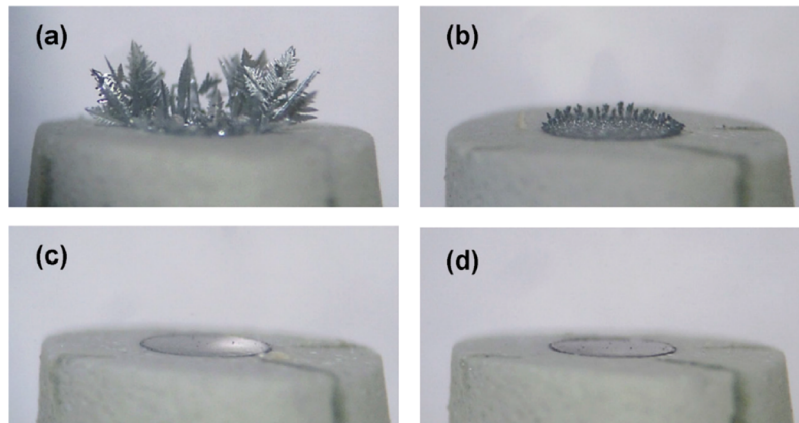


Figure 74. In situ optical microscopy of a Zn wire electrode after potentiostatic Zn electrodeposition at -1.57 V (vs Hg/HgO) for 30 min. Electrolyte contains 0.1 M ZnO–4.0 M KOH and (a) 0, (b) 10, (c) 50, and (d) 100 ppm PEI. Reproduced with permission from ref 441. Copyright 2015 Elsevier.

a superior dendrite inhibition morphology during Zn electroplating. Banik et al. adopted branched polyethylenimine (PEI, MW = 800 g mol⁻¹) as an effective electrolyte additive.⁴⁴¹ PEI additives effectively suppressed dendrite formation during Zn electrodeposition, while they did not accelerate parasitic processes (such as hydrogen coevolution) and obtained a high Faradaic efficiency of 95% (93% for non-PEI electrolyte) (Figure 74). The functional mechanism can be explained by the activation-controlled dendrite tip propagation model proposed.⁴⁴⁸ The PEI additives adsorb on the Zn surface to lower the kinetic parameters (including the exchange current density associated with Zn electrodeposition) and thus retard deposition at an activation-controlled dendrite tip. A similar result can also be obtained in PEG-200 additive⁴⁴⁹ and nickel triflate additive in ionic liquid electrolyte.⁴⁵⁰

2. Structured anode. Similar to Li anode, high surface area or 3D electrode structure was also employed to reduce the current density to suppress the dendrite growth. Hyperdendritic nanoporous Zn foam anode was prepared by electrodeposition methods.⁴⁵¹ Nanoparticles formed on secondary dendrites in a 3D network with a particle size distribution of 54.1–96.0 nm (Figure 75). Compared to the conventional Zn in alkaline

electrolyte, the nanoporous Zn foam led to a large surface area, highly oriented crystals, and quick kinetics. The Zn anode material delivered a Coulombic efficiency of ~88% at full depth of discharge (DOD) at various current densities, indicating a superior rate capability. The rechargeable Zn⁰/Zn²⁺ indicated significant capacity retention over 100 cycles at a 40% DOD to ensure that the dendritic core structure was maintained. Similarly, Cu foam⁴⁵² and porous aperiodic Zn architecture⁴⁵³ was designed to render Zn plating.

However, there are two flaws in this high-specific-area Zn electrode: the volumetric capacity density achieved in this case is several times lower than the theoretical value of Zn electrodes. This is probably attributed to the difficulties in achieving uniform and dense metal electrodeposits throughout the entire surface of metal foams. Another disadvantage of adopting the high-surface-area Zn electrode is the largely enhanced hydrogen evolution rate due to the increased exposed surface area. This results in enhanced self-discharge and deteriorates cell Coulombic efficiency.

A backside-plating configuration was creatively proposed to enable long-term cycling of Zn metal batteries without shorting.⁴⁵⁴ According to the proposal, Zn ions in the aqueous electrolyte travel over the edge and deposit on the open back surface of Cu foil. Consequently, even if Zn dendrites nucleate and grow, they grow away from the counter electrode and will not short the cell. The high ionic conductivity of 6 M aqueous KOH (0.6 S cm⁻¹) affords sufficient ion conduction to maintain reasonable power rates even if Zn ions have to travel over the edge.

Zn metal has a large difference from Li metal. Though some similar methods have been proposed to suppress dendrite growth, such as the electrolyte modification and structured anode, yet the design principles are different. The developments of the strategies for Zn and Li dendrites are nearly independent. Therefore, the strategies for Zn dendrite growth have much referential significance to Li dendrites.

7.10. Summary of these Strategies

In summary, various methods have been proposed to suppress Li dendrite growth, including electrolyte additives, Li anode coating (artificial SEI), superconcentrated, nanostructured, and solid-state electrolytes, anode and membrane modification, and cell operation regulation. Much progress has been achieved in the following.

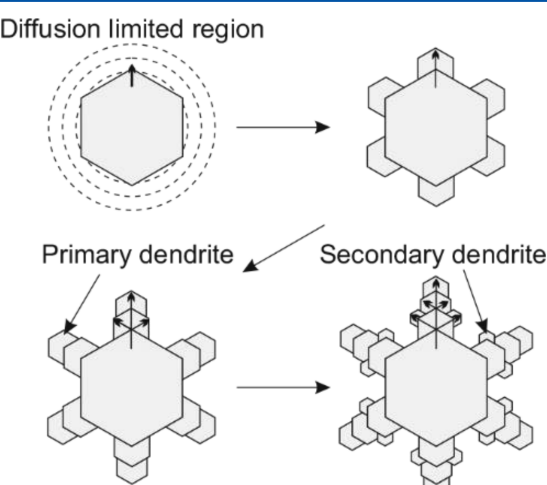


Figure 75. Scheme of Zn dendrite formation based on a diffusion-limited aggregation model. Reproduced with permission from ref 451. Copyright 2015 Nature Publishing Group.

Table 2. Short-Circuiting Time of Li Metal Anode in the Method of Galvanostatic Polarization^a

| current/short-circuiting time (mA cm ⁻² /h) | modifications | ref | current/short-circuiting time (mA cm ⁻² /h) | modifications | ref |
|---|---|-----|---|--|-----|
| 0.01/420 | SiO ₂ -IL-TFSI-Li composite electrolyte | 265 | 0.3/3.1 | LiTFSI-PEO at 90 °C | 114 |
| 0.016/318 | SiO ₂ -IL-TFSI-Li composite electrolyte | 265 | 0.3/145 | PEO ₁₈ LiTFSI-1.44PP13TFSI at 60 °C | 457 |
| 0.02/450 | LiTFSI-PEO at 90 °C | 114 | 0.4/180 | cross-linked polyethylene/PEO electrolytes | 320 |
| 0.025/400 | LiTFSI-PEO at 90 °C | 114 | 0.5/84 | PEO ₁₈ LiTFSI-nano-SiO ₂ and PP13TFSI at 60 °C | 455 |
| 0.029/80 | SiO ₂ -SO ₃ BF ₃ Li nanostructured electrolyte | 267 | 0.5/42 | LiTFSI-PEO with acid-modified SiO ₂ at 60 °C | 456 |
| 0.03/175 | LiTFSI-PEO at 90 °C | 114 | 0.5/75 | PEO ₁₈ LiTFSI-1.44PP13TFSI at 60 °C | 457 |
| 0.034/160 | SiO ₂ -IL-TFSI-Li composite electrolyte | 265 | 0.5/73 | 3D Cu matrix with a pore size of 2.1 μm | 368 |
| 0.04/170 | LiTFSI-PEO at 90 °C | 114 | 0.5/70 | nanostructured graphene matrix | 361 |
| 0.05/65 | LiTFSI-PEO at 90 °C | 114 | 0.625/80 | cross-linked polyethylene/PEO electrolytes | 320 |
| 0.06/70 | SiO ₂ -IL-TFSI-Li composite electrolyte | 265 | 1.0/37 | PEO ₁₈ LiTFSI-nano-SiO ₂ and PP13TFSI at 60 °C | 455 |
| 0.08/25 | LiTFSI-PEO at 90 °C | 114 | 1.0/35 | PEO ₁₈ LiTFSI-1.44PP13TFSI at 60 °C | 457 |
| 0.1/575 | All ₃ electrochemical pretreatment of Li anode | 214 | 1.0/20 | LiTFSI-PEO with acid-modified SiO ₂ at 60 °C | 456 |
| 0.1/672 | PEO ₁₈ LiTFSI-nano-SiO ₂ and PP13TFSI at 60 °C | 455 | 1.0/200 | All ₃ electrochemical pretreatment of Li anode | 214 |
| 0.1/400 | LiTFSI-PEO with acid-modified SiO ₂ at 60 °C | 456 | 1.0/60 | cross-linked polyethylene/PEO electrolytes | 320 |
| 0.1/594 | PEO ₁₈ LiTFSI-1.44PP13TFSI at 60 °C | 457 | 2.0/120 | All ₃ electrochemical pretreatment of Li anode | 214 |
| 0.15/17 | LiTFSI-PEO at 90 °C | 114 | 3.2/23 | All ₃ electrochemical pretreatment of Li anode | 214 |
| 0.25/168 | PEO ₁₈ LiTFSI-nano-SiO ₂ and PP13TFSI at 60 °C | 455 | | | |
| 0.25/114 | LiTFSI-PEO with acid-modified SiO ₂ at 60 °C | 456 | | | |
| 0.25/135 | PEO ₁₈ LiTFSI-1.44PP13TFSI at 60 °C | 457 | | | |
| 0.26/430 | cross-linked polyethylene/PEO electrolytes | 320 | | | |

^aThe galvanostatic polarization method is that Li is continuously stripped from one electrode and plated on the other until the cell short-circuits.

1. *Dendrite suppression.* The routine Li metal anode easily grows large dendrites of several-micrometers length and diameter even at a low current density of 0.1–0.5 mA cm⁻². Dendrites can be effectively suppressed in many modified systems, even at an ultrahigh current density of 10 mA cm⁻².

2. *Coulombic efficiency.* The Coulombic efficiency of Li|Cu half-cell in a routine Li metal anode is usually 50–80%. The advanced Li metal anode with a certain strategy can indicate a Coulombic efficiency of >95%, even 99.9%.

3. *Cycling lifespan.* The routine Li metal anode cannot cycle exceeding 50 cycles. The advanced Li metal anode can stably cycle over 500 cycles in a Li|Cu half-cell. With some excess Li in the anode, Li_x intercalation type cathode and Li–S battery can render a cycling life exceeding 5000 cycles.

4. *Rate performance.* With the ability to suppress Li dendrite growth at a high current density, the Li metal anode can cycle at a high current density from 1–10 mA cm⁻² and 10 mA cm⁻² can even render a stable 300 cycle in the Li|Cu half-cell. In the full cell, the batteries can even stably cycle at 20 C.

To quantitatively evaluate these modifications to Li metal anode, short-circuit time and Coulombic efficiency are usually used. Short-circuit time induced by the dendrite growth is adopted to evaluate the safety performance. The enhanced short-circuit times by the above-mentioned strategies are summarized in Tables 2 and 3. As shown in Tables 2 and 3, two cell patterns are used to evaluate the safety performance. One is the galvanostatic polarization method, where Li is continuously stripped from one electrode and plated on the other until the cell short-circuits. The other is galvanostatic

cycling method, where the current periodically changes the direction and renders a continuous Li plating and stripping, to simulate the processes of a real cell.

1. *Galvanostatic polarization* (Table 2). When a Li metal anode is operated in the galvanostatic polarization method, it is much more easily short-circuited than in the galvanostatic cycling method. The currently highest current density used in this model is 3.2 mA cm⁻² by the All₃ electrochemical pretreatment of Li anode. As this method is rarely adopted by researchers, the samples to be analyzed are really small. However, this method should receive much more attention, as it can present much information on Li plating behavior without the interference of the Li stripping process.

2. *Galvanostatic cycling* (Table 3). This method is extensively used to evaluate the long-term stability and voltage polarization of a Li metal anode, which is nearly an essential one for publications. The currently highest current density used in this model is 10 mA cm⁻² by the few-micrometers-thick Nafion protective layer on Li metal anode with the short-circuit time of 2000 h. Due to the differences in the electrolyte component and purity, the cell assembly parameter, the proficiency of researchers, and modifications to the Li metal anode, the short-circuit times differ much, even at the same current density (Figure 76). Nevertheless, the summary can present a direct comparison among these strategies.

Another indicator to evaluate a practical Li metal anode is the Coulombic efficiency, obtained by the ratio of Li stripping and plating capacity. The current LMBs have much excess Li metal, usually 100 times too much, which conceals the low efficiency

Table 3. Short-Circuit Time of Li Metal Anode in the Model of Galvanostatic Cycling LiLi Cells^a

| current/plating time of each cycle (mA cm ⁻² /min) | short-circuiting time (h) | modifications | ref |
|--|------------------------------|--|-----|
| 0.05/ <i>b</i> | 100 | SBA-15 + ionic liquid + LiTFSI + PVdF-HFP quasi-SSEs | 458 |
| 0.065/535 | 1960 | lithiated polymer electrolyte membrane | 266 |
| 0.1/4.8 | 33 | Al layer on the garnet electrolyte | 337 |
| 0.1/16.2 | 54 | TiO ₂ -based ionogel electrolyte | 459 |
| 0.1/180 | 60 | Li ₃ PO ₄ -added garnet-type SSE | 343 |
| 0.1/ <i>b</i> | 100 | SBA-15 + ionic liquid + LiTFSI + PVdF-HFP quasi-SSEs | 458 |
| 0.1/15 | 2500 | <i>N</i> -propyl- <i>N</i> -methylpyrrolidinium bis(fluorosulfonyl)imide ionic liquid containing different lithium salts | 223 |
| 0.175/240 | 181 | LiTFSI dissolved in polystyrene- <i>b</i> -PEO block copolymers | 460 |
| 0.18/ <i>b</i> | 2100 | 30% LiF in PC | 210 |
| 0.2/5.1 | 41 | Al layer on the garnet SSE | 337 |
| 0.2/180 | 400 | solid polymer electrolyte with Li powder anode | 461 |
| 0.2/30 | 100 | polymeric ionic liquid gel electrolyte | 462 |
| 0.2/30 | 700 | 3D garnet nanofiber-PEO composite electrolyte | 321 |
| 0.2/ <i>b</i> | 300 | ionic liquid decorated mesoporous silica nanoparticles | 463 |
| 0.2/180 | 500 | cross-linked nanoparticle polymer SSE | 268 |
| 0.2/150 | 600 | 3D Cu current collector with a median pore size of 2.1 mm | 368 |
| 0.2/300 | 1000 | 3D Cu current collector derived from a Cu-Zn alloy | 385 |
| 0.25/ <i>b</i> | 800 | covalently connected carbon nanostructures as Li matrix | 370 |
| 0.3/ <i>b</i> | 2600 | inorganic polyhedral oligomeric silsesquioxane and poly(ethylene glycol) polymer | 464 |
| 0.38/180 | 1800 | 30% LiF in PC | 210 |
| 0.38/180 | 700 | ultrastrong polyoxazole nanofiber membranes | 396 |
| 0.4/180 | 1290 | 30% LiBr in PC | 211 |
| 0.5/120 | 940 | AlCl ₃ electrolyte additive | 188 |
| 0.5/120 | 852 | carbonized wood conductive Li matrix | 354 |
| 0.5/120 | 1280 | 3D copper mesh as Li matrix | 387 |
| 0.5/60 | 400 | HIO ₃ chemical pretreatment | 224 |
| 0.5/180 | 600 | a-CN _x coated Li electrodes | 232 |
| 0.5/120 | 1250 | 3D copper mesh as Li matrix | 387 |
| 0.5/120 | 852 | carbonized wood conductive Li matrix | 354 |
| 0.5/ <i>b</i> | 350 | 30% LiF in PC | 210 |
| 0.5/60 | 432 | 10 m KPF ₆ additive | 203 |
| 0.5/180 | 636 | graphitic carbon nitride filler in LiTFSI-DGM polymer | 465 |
| 0.5/30 | 1000 | 3D garnet nanofiber-PEO composite electrolyte | 321 |
| 0.5/ <i>b</i> | 1200 | inorganic polyhedral oligomeric silsesquioxane and poly(ethylene glycol) polymer | 464 |
| 0.5/180 | 300 | SiO ₂ -based composite polymer electrolyte in situ polymerizing tripropylene glycol diacrylate monomer | 270 |
| 0.5/60 | 900 | magnetron sputtering morphous Li ₃ PO ₄ protective layer | 235 |
| 0.5/120 | 940 | AlCl ₃ additive | 188 |
| 0.5/360 | 900 | 3D bisphenol A/poly(ethylene glycol) diglycidyl ether/diaminopoly(propylene oxide)/poly(vinylidene fluoride- <i>co</i> -hexafluoropropylene) GPE | 308 |
| 0.53/10 | 80 | micropatterned Li metal | 366 |
| 0.75/600 | 2000 | few-micrometers-thick Nafon protective layer | 242 |
| 1.0/2.5 | 145 | N-doped graphene matrix | 350 |
| 1.0/60 | 200 | Li _x Si-Li ₂ O matrix | 360 |
| 1.0/60 | 330 | carbonized wood conductive Li matrix | 354 |
| 1.0/60 | 540 | graphitized spherical C granules as Li matrix | 383 |
| 1.0/60 | 100 | Al ₂ O ₃ -CNT matrix | 372 |
| 1.0/ <i>b</i> | 200 | 3D nickel foam Li host | 359 |
| 1.0/60 | 600 | 3D copper mesh Li host | 387 |
| 1.0/60 | 100 | HIO ₃ chemical pretreatment | 224 |
| 1.0/60 | 330 | carbonized wood matrix | 354 |
| 1.0/ <i>b</i> | 430 | inorganic polyhedral oligomeric silsesquioxane and poly(ethylene glycol) polymer | 464 |
| 1.0/15 | 629 | ultrathin (~2 nm) Al ₂ O ₃ protective layers using atomic layer deposition | 229 |
| 1.0/180 | 140 | cross-linked nanoparticle polymer electrolyte | 268 |
| 1.0/60 | 1560 | 20 nm pore size Al ₂ O ₃ membranes infiltrated with 1.0 M LiTFSI DOL:DME | 272 |
| 1.0/240 | 1750 | LiF in EC:DMC electrolyte | 466 |
| 1.0/60 | 138 | concentrated LiTFSI-3DMSO | 467 |
| 1.0/60 | 195 | ZnO-coated polyimide matrix | 355 |
| 1.0/60 | 220 | graphene matrix | 357 |
| 1.0/60 | 500 | onionlike, graphitized spherical carbon matrix | 383 |
| 1.0/120 | 560 | freestanding copper nanowire current collector | 147 |

Table 3. continued

| current/plating time of each cycle (mA cm ⁻² /min) | short-circuiting time (h) | modifications | ref |
|--|------------------------------|--|-----|
| 1.0/9.6 | 160 | glass fiber layer | 352 |
| 1.1/60 | 220 | Nafion and PVDF dual protective layer | 243 |
| 1.5/60 | 1560 | 20 nm pore size Al ₂ O ₃ membranes infiltrated with 1 M LiTFSI DOL:DME | 272 |
| 2.0/30 | 100 | graphitized spherical C granules | 383 |
| 2.0/30 | 120 | 3D copper mesh | 387 |
| 2.0/180 | 662 | graphitic carbon nitride filler in LiTFSI–DGM polymer | 465 |
| 2.0/15 | 250 | N-propyl-N-methylpyrrolidinium bis(fluorosulfonyl)imide ionic liquid containing different lithium salts | 223 |
| 2.0/120 | 600 | LiF in EC:DMC | 466 |
| 2.0/180 | 1000 | Kimwipe paper protective layer | 353 |
| 2.0/30 | 100 | onionlike, graphitized spherical carbon matrix | 383 |
| 2.0/b | 260 | 3D bisphenol A/poly(ethylene glycol) diglycidyl ether/diaminopoly(propylene oxide)/poly(vinylidene fluoride- <i>co</i> -hexafluoropropylene) polymer electrolyte | 308 |
| 2.125/b | 155 | Al ₂ O ₃ additives | 225 |
| 2.5/b | 260 | 3D bisphenol A/poly(ethylene glycol) diglycidyl ether/diaminopoly(propylene oxide)/poly(vinylidene fluoride- <i>co</i> -hexafluoropropylene) polymer electrolyte | 308 |
| 3.0/20 | 150 | carbonized wood conductive Li matrix | 354 |
| 3.0/20 | 60 | Al ₂ O ₃ –CNT matrix | 372 |
| 3.0/b | 70 | 3D nickel foam host | 359 |
| 3.0/20 | 150 | carbonized wood matrix | 354 |
| 3.0/240 | 800 | DME + PEO + SiO ₂ + LiTFSI composite electrolyte | 135 |
| 3.0/b | 700 | PEO–LLZTO (~40 nm) composite electrolyte | 314 |
| 3.0/60 | 1560 | 20 nm pore size Al ₂ O ₃ membranes infiltrated with 1.0 M LiTFSI DOL:DME | 272 |
| 3.0/20 | 85 | Si-coated carbon fiber matrix | 356 |
| 3.0/20 | 67 | ZnO-coated polyimide matrix | 355 |
| 3.0/20 | 69 | graphene matrix | 357 |
| 3.0/60 | 300 | polyacrylonitrile submicrometer fiber array layer | 468 |
| 4.0/15 | 30 | graphitized spherical C granules | 383 |
| 4.0/60 | 130 | LiF in EC:DMC | 466 |
| 4.0/15 | 30 | onionlike, graphitized spherical carbon matrix | 383 |
| 5.0/144 | 650 | cyclic voltammetry premodulation | 216 |
| 5.0/12 | 40 | Li _x Si–Li ₂ O matrix | 360 |
| 5.0/b | 40 | 3D nickel foam host | 359 |
| 5.0/144 | 650 | CV premodulation | 216 |
| 5.0/180 | 1000 | Kimwipe paper protective layer | 353 |
| 5.0/12 | 39 | ZnO-coated polyimide matrix | 355 |
| 5.0/60 | 155 | LiNO ₃ + Li ₂ S ₅ additives | 469 |
| 10.0/6 | 20 | Li _x Si–Li ₂ O matrix | 360 |
| 10.0/60 | 200 | fibrous metal felt as Li matrix | 388 |
| 10.0/90 | 120 | LiTFSI–LiTFSI dual salt electrolyte | 175 |
| 10.0/240 | 2000 | few-micrometers-thick Nafon protective layer | 242 |
| 10.0/180 | 400 | Kimwipe paper protective layer | 353 |
| 10.0/3 | 600 | 4.0 M LiTFSI–DME | 78 |
| 10.0/3 | 180 | nanostructured graphene matrix | 361 |

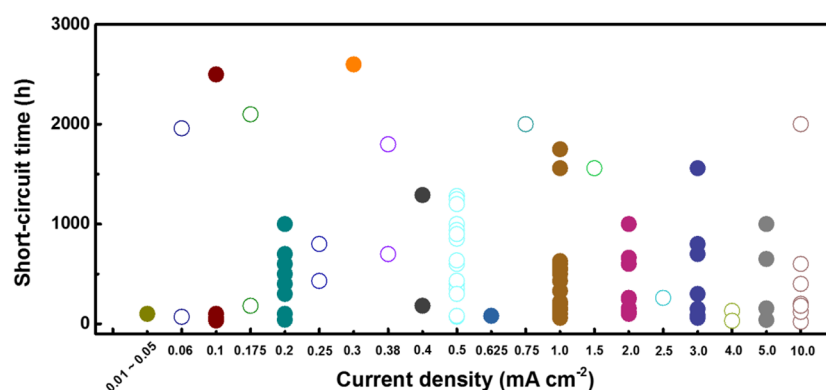
^aSSE: solid-state electrolyte. ^bThe data is not provided in the literature.

Figure 76. Short-circuit time based on galvanostatic cycling Li/Li cells. The data are from Table 3.

Table 4. Coulombic Efficiency (CE) of Li Metal Anode

| current (mA cm ⁻²) | CE/lifespan ^a (%/cycles) | modifications | ref |
|--------------------------------|-------------------------------------|---|-----|
| 0.1 | 98/100 | FEC additives | 172 |
| 0.25 | 98.5/300 | artificial SEI of Cu ₃ N nanoparticles and styrene butadiene rubber | 222 |
| 0.25 | 99/150 | interconnected hollow carbon nanospheres | 231 |
| 0.25 | 92/120 | LiF additives | 466 |
| 0.25 | 97/100 | cross-linked hairy nanoparticle electrolyte | 268 |
| 0.25 | 94/100 | thermally conductive separator coated with boron nitride nanosheets | 400 |
| 0.25 | 99/120 | LiFSI–LiTFSI dual-salt electrolyte | 175 |
| 0.354 | 95/100 | coated Li powder electrodes | 363 |
| 0.5 | 87/50 | interfacial layer of SiO ₂ @PMMA core–shell nanosphere | 248 |
| 0.5 | 98/300 | carbon shell and Au nanoparticles | 103 |
| 0.5 | 98.5/150 | interconnected hollow carbon nanosphere | 231 |
| 0.5 | 97/50 | 2D atomic crystal layer (<i>h</i> -BN and graphene) | 470 |
| 0.5 | 95/100 | FEC additives | 172 |
| 0.5 | 95/100 | Li ₂ S ₅ -based ternary salt electrolyte | 194 |
| 0.5 | 98/90 | 3D glass fiber cloths | 352 |
| 0.5 | 93/50 | unstacked graphene structured anode | 145 |
| 0.5 | 97/100 | SEI-coated graphene structured anode | 361 |
| 0.5 | 99/150 | AlCl ₃ additive | 188 |
| 0.5 | 98/475 | spherical carbon granules with 3D conducting skeletons | 383 |
| 0.5 | 99.1/360 | hybrid ionic liquid electrolyte | 182 |
| 0.5 | 97/50 | 3D Cu current collector | 368 |
| 0.5 | 96/150 | 3D porous Cu/Li metal composite anode | 387 |
| 0.5 | 99/90 | LiF coating | 234 |
| 0.5 | 95/300 | nanostructured hybrid electrolytes (Al ₂ O ₃) | 272 |
| 0.5 | 90/120 | LiF additives | 466 |
| 0.5 | 97/180 | concentrated Li[(FSO ₂) ₂ (n-C ₄ F ₉ SO ₂)N]-based electrolyte | 183 |
| 0.5 | 98.7/200 | concentrated dual-salt electrolytes | 471 |
| 0.5 | 98/350 | polyacrylonitrile as N-doped binder network | 349 |
| 0.5 | 97/150 | Li ₂ O–Cu nanoclusters as porous structured anode | 386 |
| 0.5 | 97/250 | dealloying 3D porous current collector | 385 |
| 0.5 | 92/100 | thermally conductive separator coated with boron nitride nanosheets | 400 |
| 0.885 | 93/100 | coated lithium powder electrodes | 363 |
| 1.0 | 90/50 | interfacial layer of SiO ₂ @PMMA core–shell nanosphere | 248 |
| 1.0 | 97.4/100 | artificial SEI of Cu ₃ N nanoparticles and styrene butadiene rubber | 222 |
| 1.0 | 97.6/240 | polyimide-coating layer with vertical nanoscale channels | 247 |
| 1.0 | 97.7/80 | adaptive polymer coating | 244 |
| 1.0 | 97.9/120 | 3D oxidized polyacrylonitrile nanofiber network | 347 |
| 1.0 | 97.5/150 | interconnected hollow carbon nanosphere | 231 |
| 1.0 | 96/50 | 2D atomic crystal layer (<i>h</i> -BN and graphene) | 470 |
| 1.0 | 98/200 | N-doped graphene structured anode | 350 |
| 1.0 | 95/233 | SEI from polysulfides | 195 |
| 1.0 | 94/75 | Li ₂ S ₅ -based ternary-salt electrolyte | 194 |
| 1.0 | 97/67 | 3D glass fiber cloths | 352 |
| 1.0 | 93/50 | SEI-coated graphene structured anode | 361 |
| 1.0 | 98.5/600 | spherical carbon granules with 3D conducting skeletons | 383 |
| 1.0 | 98.5/1000 | concentrated LiFSI electrolyte | 78 |
| 1.0 | 97.7/200 | concentrated dual-salt electrolytes | 471 |
| 1.0 | 95/200 | polyacrylonitrile as N-doped binder network | 349 |
| 1.0 | 94/90 | Li ₂ O–Cu nanoclusters as porous structured anode | 386 |
| 1.0 | 98.6/200 | Cu nanowire network current collector | 147 |
| 1.0 | 97/140 | dealloying 3D porous current collector | 385 |
| 1.0 | 88/100 | thermally conductive separator coated with boron-nitride nanosheets | 400 |
| 2.0 | 92.9/150 | polyimide-coating layer with vertical nanoscale channels | 247 |
| 2.0 | 99.1/400 | lithium polysulfide and lithium nitrate additives | 193 |
| 2.0 | 97/50 | 2D atomic crystal layer (<i>h</i> -BN and graphene) | 470 |
| 2.0 | 96/100 | N-doped graphene structured anode | 350 |
| 2.0 | 92/36 | Li ₂ S ₅ -based ternary-salt electrolyte | 194 |
| 2.0 | 96/63 | 3D glass fiber cloths | 352 |
| 2.0 | 92/50 | unstacked graphene structured anode | 145 |
| 2.0 | 93/50 | SEI-coated graphene structured anode | 361 |
| 2.0 | 89/90 | Li ₂ O–Cu nanoclusters as porous structured anode | 386 |

Table 4. continued

| current (mA cm^{-2}) | CE/lifespan ^a (%/cycles) | modifications | ref |
|---------------------------------|-------------------------------------|---|-----|
| 2.0 | 97.6/50 | Cu nanowire network current collector | 147 |
| 2.0 | 94/100 | spatially heterogeneous carbon-fiber papers current collector | 380 |
| 3.0 | 88.6/140 | polyimide-coating layer with vertical nanoscale channels | 247 |
| 3.0 | 97.4/120 | 3D oxidized polyacrylonitrile nanofiber network | 347 |
| 4.0 | 98.4/1000 | concentrated LiFSI electrolyte | 78 |
| 5.0 | 93/48 | 3D glass fiber cloths | 352 |
| 5.0 | 97.1/50 | Cu nanowire network current collector | 147 |
| 8.0 | 98/500 | concentrated LiFSI electrolyte | 78 |
| 10.0 | 91/40 | 3D glass fiber cloths | 352 |
| 10.0 | 97/500 | concentrated LiFSI electrolyte | 78 |

^aLifespan is a cycle number which can maintain the Coulombic efficiency.

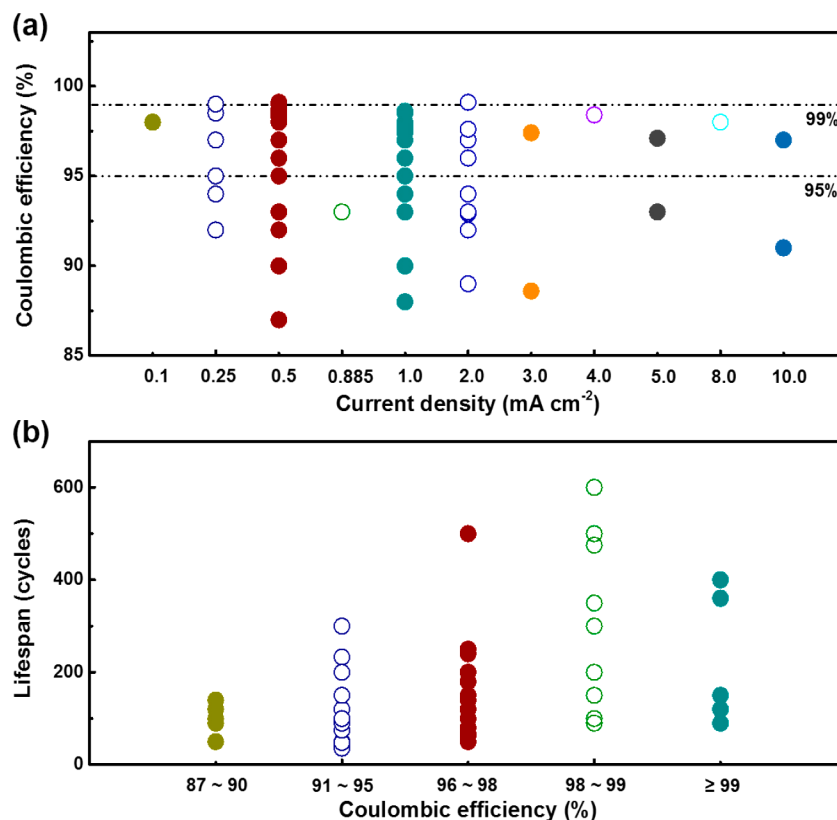


Figure 77. (a) Coulombic efficiency and (b) lifespan of Li metal anode. The data are from Table 4.

of Li metal anode. If 80% residue of the initial Li is defined as the cycling life of a Li metal anode, the lifespan of a Li metal anode with a Coulombic efficiency of 85, 90, 95, 98, 99, 99.9, and 99.99% is 1.4, 2.1, 4.4, 11, 22, 45, 223, and 2231 cycles. Therefore, for a practical Li metal anode, its Coulombic efficiency must be higher than 99.9%. However, the currently highest Coulombic efficiencies at 0.5, 1.0, 2.0, 3.0, 5.0, and 10.0 mA cm^{-2} are 99.1, 98.6, 99.1, 97.4, 97.1, and 97% for 360, 200, 400, 120, 50, and 500 cycles (Table 4, Figure 77). Therefore, there is still a long way to go to realize the practical application of LMBs.

These strategies to protect Li metal anode have their own features and application scenario (Table 5). Each one of them seems weak in the practical applications when facing the tough and indomitable Li metal anode. Mutual combination and integration will be strong to battle with Li metal anode. For example, when the nanostructured anode matches the solid-state electrolyte, dendrite growth can be totally suppressed.

Compared with the nanostructured, highly concentrated, and solid-state electrolytes, nanostructured Li metal anode has more advantages to suppress dendrite growth in the nucleation stage. If these electrolytes (or other coating layer) can reduce the side reactions of Li metal, the composite anode hopefully realizes a high Coulombic efficiency with a dendrite-free Li depositing morphology. Besides, the anode matrix can be designed to tightly contact the solid-state electrolyte to reduce the interfacial impedance. Safe and high rate Li metal batteries can be obtained. Another example is the combination of the liquid and solid-state electrolytes. The interface on the Li metal anode is of critical importance in both the liquid and solid Li metal batteries. The stable interface can be built by the chemical, electrochemical, and physical methods. The knowledge and experience of liquid electrolyte are much more than those of solid-state electrolyte. It is very smart for the solid-state electrolyte to draw lessons from the liquid electrolyte. The strategies to form an efficient layer in the liquid electrolyte can

Table 5. Comparison of Proposed Methods To Suppress Li Dendrite Growth

| | advantage | disadvantage |
|-------------------------------|---|--|
| electrolyte additive | (a) facile operation | (a) poor mechanical strength to suppress dendrite growth |
| | (b) forming a thin and highly conductive SEI | (b) poor long-term stability during cycling |
| superconcentrated electrolyte | high Coulombic efficiency and cycling stability | (a) high price (b) limited rate performance |
| nanostructured electrolyte | (a) suppressing dendrite growth | complicated fabricating process |
| | (b) high ionic conductivity | |
| solid-state electrolyte | (a) without electrolyte leak | low ionic conductivity |
| | (b) suppressing dendrite growth | |
| structured anode | suppressing Li dendrite growth | low Coulombic efficiency |
| membrane modification | (a) stopping dendrites to the cathode | less effect on the dendrite nucleation and growth |
| | (b) detecting the dendrite growth | |

be imitated by the solid-state electrolyte. Additionally, the liquid electrolyte itself can be employed to in situ form a transition layer between Li metal and solid-state electrolyte to render a rapid Li ion diffusion.

There are many other integrations of these strategies. Only one of the strategies definitely cannot realize the practical applications of Li metal battery. Elaborately designing the Li metal anode by integrating these strategies is critically important.

8. FULL CELL WITH SAFE LI METAL ANODE

With the extensive research into LMBs, many strategies have been proposed to suppress Li dendrite growth. Though there are few commercialized rechargeable LMBs, some proof-of-concept LMBs have been constructed in the research field, indicating potentially practical applications. Among various LMBs, Li–S battery with sulfur as the cathode,^{472–476} Li–O₂ battery with O₂ as the cathode,^{6,477} and Li–intercalation type cathode battery^{21,478} are three potential full cells to be applied in the commercial market. In this section, by suppressing dendrite growth, progresses of Li metal based full cells are summarized.

8.1. Li–S Battery

Li–S batteries are strongly recognized as promising candidates for next-generation battery energy storage systems due to their overwhelming energy density (2600 Wh kg⁻¹).^{479,480} Besides, the natural abundance and environmental benignity of elemental sulfur help Li–S batteries gain more advantages.⁴⁸¹ Therefore, Li–S batteries have been receiving global attention in the past few years.^{482,483}

During the charge–discharge processes of Li–S batteries, Li polysulfide (LiPS) intermediates generate, dissolve into the electrolyte, and shuttle to the anode,^{190,484,485} which makes it much more complicated to achieve Li dendrite inhibition in the existence of LiPS intermediates,⁴⁸⁶ especially under the high loading sulfur cathode.^{487–491} It is widely believed that polysulfides are able to penetrate the passivation layer and

corrode the fresh Li metal underlining the surface layer, leading to capacity loss.^{195,492,493} Consequently, preventing Li polysulfide shuttle is not only essential to improving the cathode capacity, but also to obtaining a stable SEI and dendrite-free anode performance in a working Li–S cell.^{494,495} Extensive methods have been put forward, including cathode confinement and adsorption, electrolyte modification, and membrane design.^{472,474,475,496–499} However, it should be noted that these strategies seemed more focused on inhibiting LiPS shuttle and improving the utilization of the S cathodes, but were not directly suppressing dendrite growth in Li metal anodes.^{500–502} The performance of Li–S batteries strongly depends on the anode protection. The methods and progresses to suppress Li dendrite growth in the Li–S batteries are summarized as follows:

1. *Electrolyte additives.* Among various methods to suppress Li dendrite growth and side reactions of Li metal anode in Li–S batteries, LiNO₃ is a superstar.^{498,503} The strong oxidation of LiNO₃ leads to its reactions with electrolyte components and Li metal in the initial cycles, rendering a homogeneous SEI film with organic species (such as ROLi and ROCO₂Li) and inorganic species (such as LiN_xO_y from the reduction of LiNO₃ by Li metal and Li₂SO_y from the oxidation of sulfur).^{503,504} This surface film can effectively suppress Li dendrite growth and protect Li metal from the corrosion by organic electrolyte and LiPS. Recently, Amine's group discovered the irrelevance of redox shuttle suppression to the Li_xNO_y layer.⁵⁰⁵ LiNO₃ is found to have progressive reduction on Li anode.⁵⁰⁶ All these results triggered new thinking on the role of Li–S batteries.⁵⁰⁷ Nevertheless, LiNO₃ electrolyte additives indeed have achieved great success in coin cells with a low sulfur loading of <2 mg cm⁻².⁵⁰⁸ However, when the sulfur loading is increased in the coin/pouch cell, the functional role of LiNO₃ will decay due to its gradual consumption.^{501,509} Therefore, in the commercial Li–S batteries, LiNO₃ is a compromised additive and other electrolyte modification and electrode design are needed to stabilize Li metal anode.

2. *Anode coating.* Except for the electrolyte additives, anode protection by surface coating is another effective strategy.^{510,511} Wen's team has proposed several agents to protect Li metal anode, such as PEDOT-*co*-PEG coating layer through dipping coating,⁵¹² Li₃N layer through in situ reaction between Li and N₂,²¹⁹ (CH₃)₃SiCl layer by exposing Li foils to tetrahydrofuran (THF) solvent, oxygen atmosphere, and trimethylsilyl chloride ((CH₃)₃SiCl) liquid in sequence,⁵¹³ and a bifunctional protective film by dipping coating on Li in 0.10 M (CH₃)₃SnSn(CH₃)₃/THF–5.0 mol % naphthalene solution.⁵¹⁴ Lin et al. achieved efficient LiF surface passivation on 3D layered Li–reduced graphene oxide (Li–rGO) electrode by the gas reactions between Li metal and commercial Freon R134a.⁵¹⁵ The LiF protected Li–rGO electrode can render Li–S cells with a significantly improved safety, cyclability, Coulombic efficiency, and excellent rate capability (~800 mAh g⁻¹ at 2 C).

Solid-state electrolyte is also an important protection for the anode of Li–S batteries.^{516,517} Tao et al. assembled a solid-state Li–S battery and realized a high discharge capacity of >900 mAh g⁻¹ at the human body temperature of 37 °C based on LLZO@C@S cathode|LLZO and PEO composite electrolyte|Li metal anode.⁵¹⁸

3. *Nanocarbon in the anode.* A creative Li–S battery using electrically connected graphite and Li metal as a hybrid anode is designed to suppress Li dendrite growth and control

undesirable surface reactions on Li (Figure 78).⁵¹⁹ Lithiated graphite in front of Li metal functions as an artificial, self-

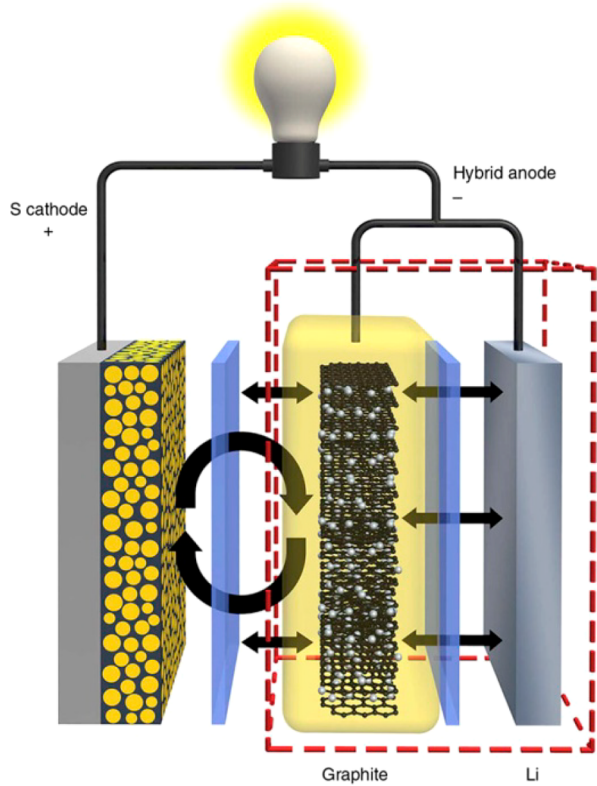


Figure 78. Schematic of the hybrid anode design to regulate the surface reactions on Li–S batteries. Reproduced with permission from ref 519. Copyright 2014 Nature Publishing Group.

regulated SEI film. This functional SEI can effectively suppress Li dendrite growth and actively minimize the deleterious side reactions between Li metal, LiPS, and electrolyte, rendering a significant performance improvement. Li–S batteries incorporating this hybrid anode indicates a discharge capacity of $>800 \text{ mAh g}^{-1}$ for 400 cycles at a high rate of 1737 mA g^{-1} , with only 11% capacity fade and a Coulombic efficiency of $>99\%$. Porous carbon paper and CNT films were also adopted as the interlayer to stabilize the Li metal anode of Li–S batteries.⁵²⁰

Li metals with incorporated conductive matrixes have been investigated as the anode of Li–S batteries. Li metal was electroplated into carbon nanotube/ultrathin graphite foam (CNT/UGF) matrix as the composite anode of Li–S batteries.³⁷⁰ A Li–S cell assembled with the S/CNT–UGF cathode (47 wt % sulfur content, areal loading density of 2.6 mg cm^{-2}) and the Li/CNT–UGF anode (20 wt % Li content) delivers a high-rate capacity of 860 mAh g^{-1} at 12°C , corresponding to a remarkable specific power of 8680 W kg^{-1} with a specific energy of 720 Wh kg^{-1} with respect to the mass of the cathode.

Compared with coin cells, the dendrite issue is more prominent in pouch cells. To realize the practical application of Li–S batteries, attention should be more concentrated on dendrite suppression in pouch cells rather than only on polysulfide shuttle inhibition in coin cells (Figure 79).⁵²¹ Several publications have shifted their attention to pouch cells,^{522–524} and the pouch cells can power electronic devices (Figure 80).¹⁵ However, these pouch cells usually have either low capacity/energy density ($<350 \text{ Wh kg}^{-1}$) or poor lifespan (100 cycles). More research is needed to suppress Li dendrites in pouch cells and realize the application of Li–S batteries.⁵²⁵

8.2. Li–O₂ Battery

Li–O₂ batteries have captured worldwide attention as a revolutionary technology in the electrical energy storage field

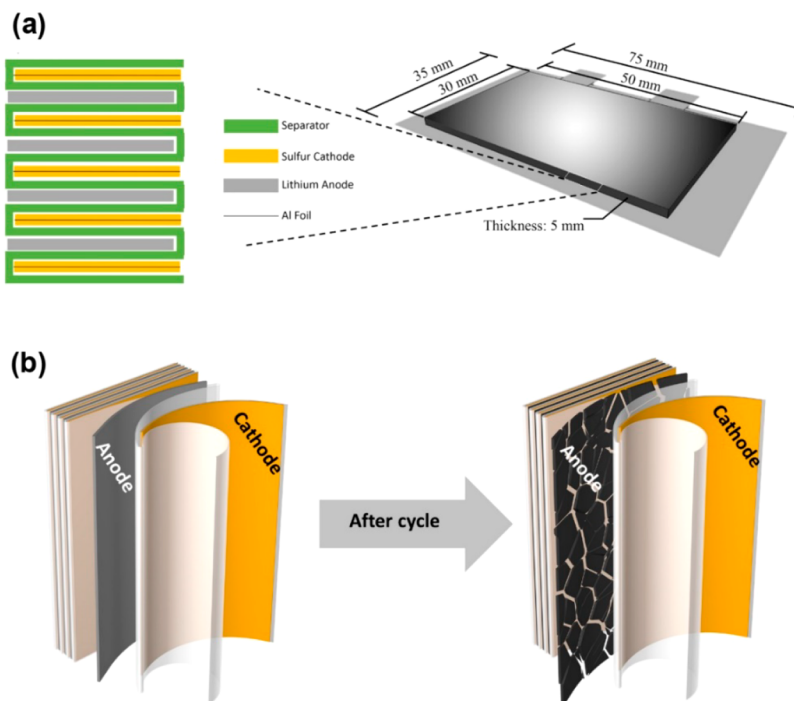


Figure 79. Li–S pouch cells. (a) Schematic diagram of a Li–S pouch cell, its internal structure, and size parameters. (b) Li metal anode evolution during cycles. Reproduced with permission from ref 521. Copyright 2017 Elsevier.

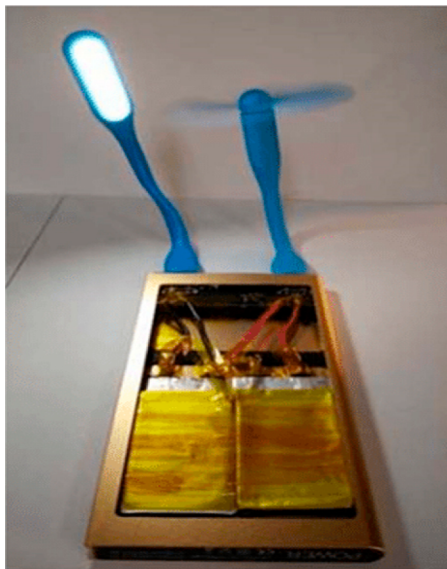


Figure 80. Digital picture of two rechargeable Li–S pouch cells in series connection to power a lamp and a minifan. Reproduced with permission from ref 15. Copyright 2017 Elsevier.

due to their ultrahigh theoretical energy density of 3505 Wh kg⁻¹,^{526,527} far exceeding that of routine LIBs. Therefore, Li–O₂ batteries are strongly regarded as a promising candidate for next-generation energy storage devices.^{528,529}

Similar to LiPS intermediates, O₂ crossover from the cathode of Li–O₂ batteries onto Li metal anode can result in a gradual degradation of Li metal surface, thus electrolyte decomposition during charging, and the formation of LiOH and Li₂CO₃.^{6,530} Some methods are put forward to block the O₂ crossover.^{531–533} Apart from the cathode issue, Li depletion induced by dendrite growth and the formation of a passivation film severely hinders the employment of Li metal in the rechargeable Li–O₂ batteries.⁵³⁴ Several strategies have been proposed to protect Li metal in Li–O₂ batteries,⁴⁸⁸ except for the versatile solid-state electrolytes.^{535–537}

1. *Electrolyte Modification.*^{8,538} An electrolyte with the solvent of *N,N*-dimethylacetamide (DMA) and salt of LiNO₃ was adopted to stabilize the SEI and protect Li metal.⁵³⁹ Li–O₂ batteries including this electrolyte rendered a stable cycle for more than 2000 h (>80 cycles) at a current density of 0.1 mA cm⁻² and good capacity retention. The highly concentrated electrolyte (LiTFSI–DME) was also incorporated into the Li–O₂ batteries.²⁵⁸ These cells with highly concentrated electrolyte exhibited much less reaction residue on the charged air-electrode surface and much less corrosion of the Li metal anode. For the conventional electrolyte (1.0 M), the discharge capacity is maintained at 1000 mAh g⁻¹ at the second cycle, within the given voltage range (2.0–4.5 V), and finally decreased to below 100 mAh g⁻¹ after 29 cycles, respectively. In contrast, the Li–O₂ cells with 3.0 M electrolyte are able to maintain very stable discharge capacity at 1000 mAh g⁻¹ for 55 cycles.

2. *Anode surface coating.* Protecting Li metal with surface coating is a facile and effective method, such as the artificial SEI layer.^{230,540,541} Li–O₂ batteries with Li metal anode protected by an FEC induced artificial film render a superior cycling stability of more than 100 cycles with a fixed capacity of 1000 mAh·g⁻¹ at a current density of 300 mA g⁻¹.²¹³ Solid-state-electrolyte coating layer is another method to protect Li

metal,⁵⁴² such as the bilayer LiPON/Al substituted lithium lanthanum titanate (A-LLTO) solid-state-electrolyte protective layer (Figure 81).⁵⁴³ The aprotic Li–air full cell adopting the

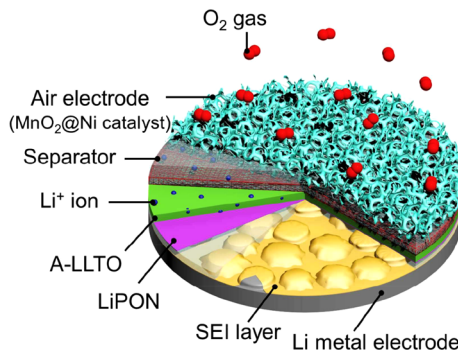


Figure 81. Scheme of bilayer solid electrolyte based on Al₂O₃-substituted LLTO protected Li metal anode in a Li–air battery. Reproduced with permission from ref 543. Copyright 2016 The Royal Society of Chemistry.

LiPON/A-LLTO exhibited superior electrochemical performance when operated even in an air atmosphere. A long lifespan of 128 cycles was achieved in oxygen atmospheres and 20 cycles in air atmospheres under a limited capacity mode of 1000 mAh g⁻¹. The obtained superb Li–air cell performance adopting the LiPON/A-LLTO was due to the effective suppression of the Li dendrite growth and electrolyte decomposition contributed by the LiPON/A-LLTO solid-state electrolyte.

A high-capacity pouch-type Li–O₂ battery was fabricated by modifying the separator and optimizing the electrolyte (Figure 82).⁵⁴⁴ These pouch cells demonstrated a specific capacity of 2711 mAh g⁻¹ based on carbon weight and energy density of 344 Wh kg⁻¹ based on the complete battery weight including the package.

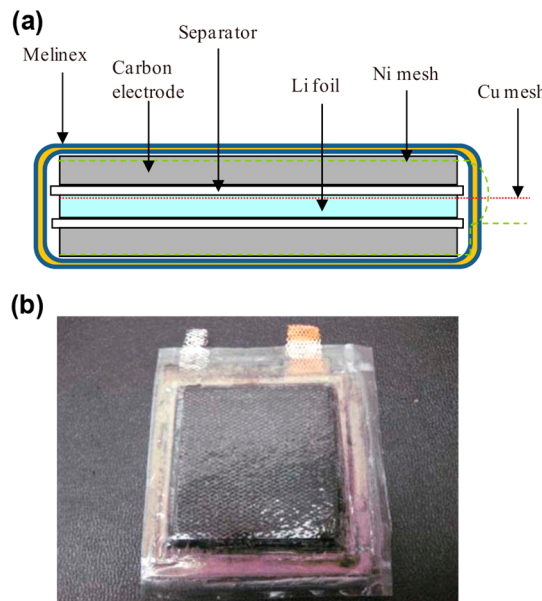


Figure 82. Configuration of Li–O₂ pouch cells. (a) Scheme and (b) digital photo of a Li–O₂ pouch battery. Reproduced with permission from ref 544. Copyright 2010 The Electrochemical Society.

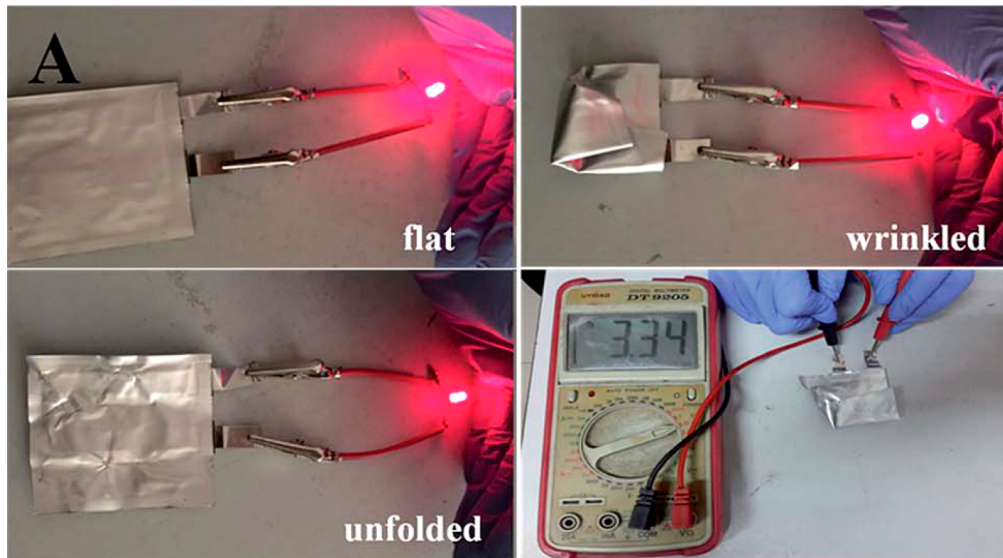


Figure 83. Digital photos indicating a red LED lamp (~ 2.0 V) connected to the LiFePO₄|Li pouch cells. Reproduced with permission from ref 550. Copyright 2016 The Royal Society of Chemistry.

8.3. Li–Intercalation Type Cathode Battery

Intercalation type cathodes, including LiFePO₄, LiCoO₂, NCA, NCM, etc., have a relatively stable structure and a stable cycling performance when matching a graphite anode.^{545–548} If the dendrite issues and the low Coulombic efficiency of Li metal anode can be effectively managed, the Li–intercalation type cathode battery has more possibility to be in the market than the Li–S and Li–O₂ batteries with unstable cathodes. When the graphite is substituted by the high capacity Li metal, the theoretical energy density of the traditional LIB can be further boosted by 20%.

Due to the stability in long-term cycling, the intercalation type cathodes, especially LiFePO₄ and LiCoO₂, are often adopted as the counter electrode to test the long-term stability of Li metal anode in a full cell, while certain transition-metal ions dissolved from the cathode (manganese in particular) of the layered nickel-rich oxide cathode can cause a dendritic lithium deposition.⁵⁴⁹ Several methods have been demonstrated to be effective in the Li–intercalation type cathode full cells, including electrolyte additives,^{172,178} solid-state electrolyte,^{315,318,328,550} surface coating,^{223,254} a rapid discharge rate,⁴¹¹ etc. Some of them are applied to the pouch cells (Figure 83).⁵⁵⁰ Because the strategies discussed in section 7 are mostly appropriate to these intercalation type cathodes, the strategies to protect Li metal in the Li–intercalation type cathode batteries are not present.

In summary, these three Li metal based full batteries are all next-generation batteries with a high energy density relative to the current LIBs with graphite anode. As an intercalation cathode, the intercalation type cathodes have more possibility to be practically applied than the conversion cathodes (sulfur and oxygen cathodes), because there still exist many problems that require handling for the sulfur and oxygen cathodes. However, the sulfur and oxygen cathodes indicate much higher capacity than the intercalation type cathode. Therefore, these three kinds of cathode have their own features (Table 6). Inevitably, realizing the practical application of Li metal anode can generate radical changes to electronic energy storage, either the Li–intercalation type cathode, Li–S, or Li–oxygen batteries.

Table 6. Comparison of Three Li Metal Based Full Cells

| | Li–intercalation type cathode battery | Li–S battery | Li–O ₂ battery |
|---|---------------------------------------|--------------|---------------------------|
| theoretical energy density (Wh kg ⁻¹) | <1200 | 2600 | 3505 |
| maturity of cathode in mechanism and technology | high | medium | low |
| duration to be practically applied after handling Li metal issues | immediately | short time | long time |

9. CONCLUSION AND OUTLOOK

Li metal has been considered as a “Holy Grail” anode for rechargeable batteries. It is strongly revisited in the golden age of energy storage, especially rechargeable batteries. In the past 40 years, quantitative models on Li dendrite nucleation (including surface nucleation and diffusion, heterogeneous nucleation, space charge, SEI, Sand’s time) and growth (electronic field and diffusion flux) models have been put forward to understand the mechanism of Li ion nucleating and dendrite growth. Based on the theoretical understanding of Li ion nucleation and growth, tremendous progress in effective methods to suppress Li dendrite growth has been explored. This indicated a remarkable role in stabilizing Li metal anode, such as electrolyte modification (electrolyte additive selection, nanostructured electrolyte, highly concentrated electrolyte, solid inorganic/polymer electrolyte), Li surface protective layer, anode matrix design, etc. How to optimize these strategies and integrate them into a practical cell seems pregnant for the highly efficient and safe Li metal anode.

Nevertheless, there are many open spaces to be explored from both the theoretical and experimental investigations. For instance, the current proposed models are limited to several specific conditions. Each model fixes on a specific step of Li plating and can only be demonstrated by extremely designed experiments. It is absolutely crucial to develop a more general mechanism, which can describe the whole process for Li dendrite growth. A deep understanding of the Li plating behavior will be of great assistance to suppress Li dendrite growth. Furthermore, the current research on Li metal anode is

mostly conducted in coin cells at a low areal current density. However, for a practical advanced Li anode, tests conducted in pouch cells are more preferred after the proof of concept in a coin cell, because there is a great gap in the distribution of current density between coin and pouch cells.

Therefore, though many breakthroughs have been attained, this field of the high-energy-density LMB is still challenging, but fascinating. Many issues need to be deeply considered:

1. Nonaqueous organic electrolyte is the most adopted system for the Li metal anode, which results in the unstable interface of Li metal and electrolyte. The fundamental understanding of the SEI formation mechanism, structure, component, and regulation is still inadequate. The insights into the exact role of SEI, the accurate process of Li ions crossing SEI, and controllable modification of SEI should be strongly considered.

2. Solid-state electrolytes are considered attractive to handle several safety issues of nonaqueous electrolytes, including leakage, poor chemical stability, and flammability. However, their low ionic conductivity and instability against Li metal, and poor interface between these electrolytes and Li metal, render a long way from their practical application in LMB.

3. For a high-energy-density LMB, tens of micrometers of Li is needed to plate and strip from the anode. The infinite volume change induces a disaster for long-term LMBs. Graphite anode has successfully reduced the volume change to 10% and realized the commercialization of LIBs. Thus, a matrix is critically needed in a practical Li metal anode. Moreover, the structured matrix can contribute to suppressing Li dendrite growth and improving the Coulombic efficiency.

4. The criteria to evaluate Li metal anode are still lacking, such as the tested cell pattern (coin, pouch, or cylinder), current density ($>1\text{--}3 \text{ mA cm}^{-2}$), etc. Li dendrite growth critically depends on the applied cell pattern and current density.

5. Nondendritic growth has been achieved in several systems. Nevertheless, a high Coulombic efficiency of $>99.9\%$ after 1000 cycles at a relatively high current density has not been obtained. If a cell cycles with a 100% DOD in the anode and a Coulombic efficiency of 99.9%, it can only maintain 36.8% of the initial Li and 63.2% of Li is corroded after 1000 cycles. Therefore, enhancement in the Coulombic efficiency is of vital importance for a practical LMB.

6. To clearly reveal the Li ion plating behavior, more smartly designed *in situ* or *operando* techniques are urgently needed to track the process in a working cell. Due to the high reactivity of Li and interfacial features of Li deposition/stripping, *ex situ* characterizations sometimes might destroy its original properties and provide some misleading results. Observing the real Li ion plating/stripping behavior in a working cell will definitely help in understanding the mechanism of dendrite nucleation and growth. The *operando* characterization of working Li metal anodes in pouch cells or winding type cells is highly recommended.

7. Li metal full cells, including Li–S batteries, Li–O₂ batteries, and Li metal vs intercalation type cathode, propose quite different requirements for Li metal anode. The areal capacity and thickness of Li metal in various LMBs are quite different, because 1- μm -thick Li equals 0.2 mAh capacity. The formed SEI is also highly dependent on the chosen electrolytes and cathodes. Therefore, different Li metals are requested to be designed to satisfy the various LMBs.

8. If an energy density of Li–S full cells is set as 400 Wh kg⁻¹, the thickness of Li metal is estimated as 25–50 μm (5–10 mAh cm⁻²). However, the commercial thin Li foil is 100–130 μm in most cases. How to obtain a thin Li foil with SEI protective layer and Li plating matrix is an important project in the engineering aspect.

9. The design of lug and current collector in a pouch or cylinder cell with high energy density is little considered. Though seeming small, the lug and current collector strongly act on the current and heat distribution of the cells.

10. How to effectively protect Li metal during production, packaging, cell assembly, and storage in a whole life is very critical as well. The emerging technology to fabricate Li metal anode with a dendrite-free feature in a roll-to-roll way is under consideration.

We are in a golden age of rechargeable batteries. It is the best of times. Science advances rapidly, which presents many techniques to investigate Li metal anode and facilitates the practical application of LMBs. It is also the worst of times. Various collateral systems are stepping forward along with Li metal anode, and the possible application scenarios are constantly changing. Li metal anode lost a chance to be in practical application with the competing graphite anode in the 1990s. Consequently, more scientific explorations on the precise understanding of Li plating/stripping behavior and strategies to suppress Li dendrite growth are highly required from the electrochemistry, chemistry, nanomaterials, physics, as well as engineering communities. Through the further investigation into the science and engineering of Li metal anode, rechargeable LMBs are quite promising to be practically applied.

AUTHOR INFORMATION

Corresponding Author

*E-mail: zhang-qiang@mails.tsinghua.edu.cn.

ORCID

Xin-Bing Cheng: 0000-0001-7567-1210

Rui Zhang: 0000-0003-3740-8352

Chen-Zi Zhao: 0000-0002-1794-3086

Qiang Zhang: 0000-0002-3929-1541

Notes

The authors declare no competing financial interest.

Biographies

Xin-Bing Cheng received his B.Eng. degree from Tianjin University in 2012 and Ph.D. degree from Tsinghua University in 2017 under the guidance of Prof. Qiang Zhang. In 2016, He was a visiting scholar in the team of Prof. Yury Gogotsi at Drexel University. He has been awarded Outstanding Academic Rising Stars Award of Tsinghua University and Postdoctoral Innovation Talent Plan of China. Now, he is a research assistant at Tsinghua University. His current research interests mainly focus on energy storage materials and devices, including nanocarbon materials, Li–S batteries, and dendrite suppression of Li metal anodes.

Rui Zhang obtained his B.S. degree from the Department of Chemical Engineering at Tsinghua University in 2015. He is currently a Ph.D. student of chemical engineering at Tsinghua University. His research interests focus on lithium-based energy storage materials, especially Li metal anodes.

Chen-Zi Zhao obtained her B.Sc. from the School of Materials Science and Engineering at Tsinghua University (2015). She is now a Ph.D. candidate in the Department of Chemical Engineering, Tsinghua University. Her main areas of research address energy-storage materials, including electrolytes and lithium metal anodes.

Qiang Zhang received his bachelor and Ph.D. degrees from Tsinghua University in 2004 and 2009, respectively. After a stay at Case Western Reserve University, USA, and the Fritz Haber Institute of the Max Planck Society, Germany, he was appointed an associate professor at Tsinghua University in 2011. His interests focus on energy materials, including Li–S batteries, Li metal anodes, 3D graphene, and electrocatalysts. He has been awarded NSF for Outstanding Young Scholars, Young Top-Notch Talent from China, and Newton Advanced Fellowship from the Royal Society, U.K.

ACKNOWLEDGMENTS

This work was supported by the National Key Research and Development Program (Nos. 2016YFA0202500, 2016YFA0200102, and 2015CB932500), Natural Scientific Foundation of China (Nos. 21422604, 21676160, and 21276141), and Tsinghua University Initiative Scientific Research Program. We thank Jia-Qi Huang, Hong-Jie Peng, Chong Yan, Xue-Qiang Zhang, Xiang Chen, Xiao-Ru Chen, Ge Zhang, Ze-Wen Zhang, Ying-Zhi Sun, Xin Shen, Rui Xu, and Jin Xie for helpful discussions.

REFERENCES

- (1) Palacin, M. R.; de Guibert, A. Why Do Batteries Fail? *Science* **2016**, *351*, 1253292.
- (2) Goodenough, J. B. Energy Storage Materials: A Perspective. *Energy Storage Mater.* **2015**, *1*, 158–161.
- (3) Choi, J. W.; Aurbach, D. Promise and Reality of Post-Lithium-Ion Batteries with High Energy Densities. *Nat. Rev. Mater.* **2016**, *1*, 16013.
- (4) Dunn, B.; Kamath, H.; Tarascon, J.-M. Electrical Energy Storage for the Grid: A Battery of Choices. *Science* **2011**, *334*, 928–935.
- (5) Evarts, E. C. To the Limits of Lithium. *Nature* **2015**, *526*, S93–S95.
- (6) Grande, L.; Paillard, E.; Hassoun, J.; Park, J.-B.; Lee, Y.-J.; Sun, Y.-K.; Passerini, S.; Scrosati, B. The Lithium/Air Battery: Still an Emerging System or a Practical Reality? *Adv. Mater.* **2015**, *27*, 784–800.
- (7) Tarascon, J. M.; Armand, M. Issues and Challenges Facing Rechargeable Lithium Batteries. *Nature* **2001**, *414*, 359–367.
- (8) He, P.; Zhang, T.; Jiang, J.; Zhou, H. Lithium–Air Batteries with Hybrid Electrolytes. *J. Phys. Chem. Lett.* **2016**, *7*, 1267–1280.
- (9) Dahn, J.; Ehrlich, G. M. In *Linden's Handbook of Batteries*, 4th ed.; Reddy, T. B., Linden, D., Eds.; McGraw Hill Professional, Access Engineering: New York, 2011.
- (10) Luntz, A. C.; Voss, J.; Reuter, K. Interfacial Challenges in Solid-State Li ion Batteries. *J. Phys. Chem. Lett.* **2015**, *6*, 4599–4604.
- (11) Janek, J.; Zeier, W. G. A Solid Future for Battery Development. *Nat. Energy* **2016**, *1*, 16141.
- (12) Xu, W.; Wang, J.; Ding, F.; Chen, X.; Nasybulin, E.; Zhang, Y.; Zhang, J.-G. Lithium Metal Anodes for Rechargeable Batteries. *Energy Environ. Sci.* **2014**, *7*, 513–537.
- (13) Sun, Y.; Liu, N.; Cui, Y. Promises and Challenges of Nanomaterials for Lithium-based Rechargeable Batteries. *Nat. Energy* **2016**, *1*, 16071.
- (14) Cheng, X.-B.; Zhang, Q. Dendrite-Free Lithium Metal Anodes: Stable Solid Electrolyte Interphases for High-Efficiency Batteries. *J. Mater. Chem. A* **2015**, *3*, 7207–7209.
- (15) Zhai, P.-Y.; Peng, H.-J.; Cheng, X.-B.; Zhu, L.; Huang, J.-Q.; Zhu, W.; Zhang, Q. Scaled-up Fabrication of Porous-Graphene-Modified Separators for High-Capacity Lithium–Sulfur Batteries. *Energy Storage Mater.* **2017**, *7*, 56–63.
- (16) Peng, H.-J.; Wang, D.-W.; Huang, J.-Q.; Cheng, X.-B.; Yuan, Z.; Wei, F.; Zhang, Q. Janus Separator of Polypropylene-Supported Cellular Graphene Framework for Sulfur Cathodes with High Utilization in Lithium–Sulfur Batteries. *Adv. Sci.* **2016**, *3*, 1500268.
- (17) Lin, D.; Liu, Y.; Cui, Y. Reviving the Lithium Metal Anode for High-Energy Batteries. *Nat. Nanotechnol.* **2017**, *12*, 194–206.
- (18) Guo, Y.; Li, H.; Zhai, T. Reviving Lithium-Metal Anodes for Next-Generation High-Energy Batteries. *Adv. Mater.* **2017**, *29*, 1700007.
- (19) Satter, R. Effects of Light-Dark Cycles. *Science* **1976**, *192*, 1226–1226.
- (20) Whittingham, M. S. U.S. Patent US 4009052 A, 1977.
- (21) Zhang, J.-G.; Xu, W.; Henderson, W. A. *Lithium Metal Anodes and Rechargeable Lithium Metal Batteries*; Springer: 2016, and references therein.
- (22) Xiao, J. Understanding the Lithium Sulfur Battery System at Relevant Scales. *Adv. Energy Mater.* **2015**, *5*, 1501102.
- (23) Tikekar, M. D.; Choudhury, S.; Tu, Z.; Archer, L. A. Design Principles for Electrolytes and Interfaces for Stable Lithium-Metal Batteries. *Nat. Energy* **2016**, *1*, 16114.
- (24) Cheng, X.-B.; Zhang, R.; Zhao, C.-Z.; Wei, F.; Zhang, J.-G.; Zhang, Q. A Review of Solid Electrolyte Interphases on Lithium Metal Anode. *Adv. Sci.* **2016**, *3*, 1500213.
- (25) Zhang, K.; Lee, G.-H.; Park, M.; Li, W.; Kang, Y.-M. Recent Developments of the Lithium Metal Anode for Rechargeable Non-Aqueous Batteries. *Adv. Energy Mater.* **2016**, *6*, 1600811.
- (26) Wang, D.; Zhang, W.; Zheng, W.; Cui, X.; Rojo, T.; Zhang, Q. Towards High-Safe Lithium Metal Anodes: Suppressing Lithium Dendrites via Tuning Surface Energy. *Adv. Sci.* **2017**, *4*, 1600168.
- (27) Rehnlund, D.; Lindgren, F.; Bohme, S.; Nordh, T.; Zou, Y.; Pettersson, J.; Bexell, U.; Boman, M.; Edstrom, K.; Nyholm, L. Lithium Trapping in Alloy Forming Electrodes and Current Collectors for Lithium Based Batteries. *Energy Environ. Sci.* **2017**, *10*, 1350–1357.
- (28) Rao, B. M. L.; Francis, R. W.; Christopher, H. A. Lithium-Aluminum Electrode. *J. Electrochem. Soc.* **1977**, *124*, 1490–1492.
- (29) Murphy, D. W.; Di Salvo, F. J.; Carides, J. N.; Waszczak, J. V. Topochemical Reactions of Rutile Related Structures with Lithium. *Mater. Res. Bull.* **1978**, *13*, 1395–1402.
- (30) Lazzari, M.; Scrosati, B. A Cyclable Lithium Organic Electrolyte Cell Based on Two Intercalation Electrodes. *J. Electrochem. Soc.* **1980**, *127*, 773–774.
- (31) Nagaura, T.; Tozawa, K. Lithium Ion Rechargeable Battery. *Prog. Batteries Solar Cells* **1990**, *9*, 209.
- (32) Liu, Q.; Du, C.; Shen, B.; Zuo, P.; Cheng, X.; Ma, Y.; Yin, G.; Gao, Y. Understanding Undesirable Anode Lithium Plating Issues in Lithium-Ion Batteries. *RSC Adv.* **2016**, *6*, 88683–88700.
- (33) Xu, K. Nonaqueous Liquid Electrolytes for Lithium-Based Rechargeable Batteries. *Chem. Rev.* **2004**, *104*, 4303–4418.
- (34) Xu, K. Electrolytes and Interphases in Li-Ion Batteries and Beyond. *Chem. Rev.* **2014**, *114*, 11503–11618.
- (35) Jasinski, R.; Burrows, B.; Malachesky, P. *High Energy Batteries. Final Report*; Tyco Labs, Inc.: Waltham, MA, USA, 1967.
- (36) Peled, E. The Electrochemical Behavior of Alkali and Alkaline Earth Metals in Nonaqueous Battery Systems—the Solid Electrolyte Interphase Model. *J. Electrochem. Soc.* **1979**, *126*, 2047–2051.
- (37) Tarascon, J. M.; Gozdz, A. S.; Schmutz, C.; Shokoohi, F.; Warren, P. C. Performance of Bellcore's Plastic Rechargeable Li-Ion Batteries. *Solid State Ionics* **1996**, *86*–88, 49–54.
- (38) Lang, J.; Qi, L.; Luo, Y.; Wu, H. High Performance Lithium Metal Anode: Progress and Prospects. *Energy Storage Mater.* **2017**, *7*, 115–129.
- (39) Gauthier, M.; Carney, T. J.; Grimaud, A.; Giordano, L.; Pour, N.; Chang, H.-H.; Fenning, D. P.; Lux, S. F.; Paschos, O.; Bauer, C.; et al. Electrode–Electrolyte Interface in Li-ion Batteries: Current Understanding and New Insights. *J. Phys. Chem. Lett.* **2015**, *6*, 4653–4672.
- (40) Sacci, R. L.; Black, J. M.; Balke, N.; Dudney, N. J.; More, K. L.; Unocic, R. R. Nanoscale Imaging of Fundamental Li Battery Chemistry: Solid-Electrolyte Interphase Formation and Preferential

- Growth of Lithium Metal Nanoclusters. *Nano Lett.* **2015**, *15*, 2011–2018.
- (41) Wandt, J.; Marino, C.; Gasteiger, H. A.; Jakes, P.; Eichel, R.-A.; Granwehr, J. Operando Electron Paramagnetic Resonance Spectroscopy - Formation of Mossy Lithium on Lithium Anodes During Charge-Discharge Cycling. *Energy Environ. Sci.* **2015**, *8*, 1358–1367.
- (42) Bieker, G.; Winter, M.; Bieker, P. Electrochemical In Situ Investigations of SEI and Dendrite Formation on the Lithium Metal Anode. *Phys. Chem. Chem. Phys.* **2015**, *17*, 8670–8679.
- (43) Jeppson, D. W.; Ballif, J. L.; Yuan, W. W.; Chou, B. E. *Lithium Literature Review: Lithium's Properties and Interactions*; Hanford Engineering Development Laboratory: Richland, WA, USA, 1978.
- (44) Chandrashekhar, S.; Trease, N. M.; Chang, H. J.; Du, L.-S.; Grey, C. P.; Jerschow, A. ${}^7\text{Li}$ MRI of Li Batteries Reveals Location of Microstructural Lithium. *Nat. Mater.* **2012**, *11*, 311–315.
- (45) Bhattacharyya, R.; Key, B.; Chen, H.; Best, A. S.; Hollenkamp, A. F.; Grey, C. P. In situ NMR Observation of the Formation of Metallic Lithium Microstructures in Lithium Batteries. *Nat. Mater.* **2010**, *9*, 504–510.
- (46) Wood, K. N.; Kazyak, E.; Chadwick, A. F.; Chen, K.-H.; Zhang, J.-G.; Thornton, K.; Dasgupta, N. P. Dendrites and Pits: Untangling the Complex Behavior of Lithium Metal Anodes through Operando Video Microscopy. *ACS Cent. Sci.* **2016**, *2*, 790–801.
- (47) Aurbach, D.; Zinigrad, E.; Teller, H.; Dan, P. Factors Which Limit the Cycle Life of Rechargeable Lithium (Metal) Batteries. *J. Electrochem. Soc.* **2000**, *147*, 1274–1279.
- (48) Dornbusch, D. A.; Hilton, R.; Lohman, S. D.; Suppes, G. J. Experimental Validation of the Elimination of Dendrite Short-Circuit Failure in Secondary Lithium-Metal Convection Cell Batteries. *J. Electrochem. Soc.* **2015**, *162*, A262–A268.
- (49) López, C. M.; Vaughney, J. T.; Dees, D. W. Morphological Transitions on Lithium Metal Anodes. *J. Electrochem. Soc.* **2009**, *156*, A726–A729.
- (50) Lu, D.; Shao, Y.; Lozano, T.; Bennett, W. D.; Graff, G. L.; Polzin, B.; Zhang, J.; Engelhard, M. H.; Saenz, N. T.; Henderson, W. A.; et al. Failure Mechanism for Fast-Charged Lithium Metal Batteries with Liquid Electrolytes. *Adv. Energy Mater.* **2015**, *5*, 1400993.
- (51) Li, W.; Zheng, H.; Chu, G.; Luo, F.; Zheng, J.; Xiao, D.; Li, X.; Gu, L.; Li, H.; Wei, X.; et al. Effect of Electrochemical Dissolution and Deposition Order on Lithium Dendrite Formation: A Top View Investigation. *Faraday Discuss.* **2014**, *176*, 109–124.
- (52) Chang, H. J.; Ilott, A. J.; Trease, N. M.; Mohammadi, M.; Jerschow, A.; Grey, C. P. Correlating Microstructural Lithium Metal Growth with Electrolyte Salt Depletion in Lithium Batteries Using ${}^7\text{Li}$ MRI. *J. Am. Chem. Soc.* **2015**, *137*, 15209–15216.
- (53) Dey, A. Film Formation on Lithium Anode in Propylene Carbonate. *J. Electrochem. Soc.* **1970**, *117*, C248.
- (54) Goodenough, J. B.; Kim, Y. Challenges for Rechargeable Li Batteries. *Chem. Mater.* **2010**, *22*, 587–603.
- (55) Aurbach, D.; Talyosef, Y.; Markovsky, B.; Markevich, E.; Zinigrad, E.; Asraf, L.; Gnanaraj, J. S.; Kim, H.-J. Design of Electrolyte Solutions for Li and Li-ion Batteries: A Review. *Electrochim. Acta* **2004**, *50*, 247–254.
- (56) Endo, E.; Ata, M.; Tanaka, K.; Sekai, K. Electron Spin Resonance Study of the Electrochemical Reduction of Electrolyte Solutions for Lithium Secondary Batteries. *J. Electrochem. Soc.* **1998**, *145*, 3757–3764.
- (57) Pinson, M. B.; Bazant, M. Z. Theory of SEI Formation in Rechargeable Batteries: Capacity Fade, Accelerated Aging and Lifetime Prediction. *J. Electrochem. Soc.* **2013**, *160*, A243–A250.
- (58) Ploehn, H. J.; Ramadas, P.; White, R. E. Solvent Diffusion Model for Aging of Lithium-Ion Battery Cells. *J. Electrochem. Soc.* **2004**, *151*, A456–A462.
- (59) Soto, F. A.; Ma, Y.; Martinez de la Hoz, J. M.; Seminario, J. M.; Balbuena, P. B. Formation and Growth Mechanisms of Solid-Electrolyte Interphase Layers in Rechargeable Batteries. *Chem. Mater.* **2015**, *27*, 7990–8000.
- (60) Hong, S.-T.; Kim, J.-S.; Lim, S.-J.; Yoon, W. Y. Surface Characterization of Emulsified Lithium Powder Electrode. *Electrochim. Acta* **2004**, *50*, 535–539.
- (61) Peled, E.; Golodnitsky, D.; Ardel, G. Advanced Model for Solid Electrolyte Interphase Electrodes in Liquid and Polymer Electrolytes. *J. Electrochem. Soc.* **1997**, *144*, L208–L210.
- (62) Shi, S.; Lu, P.; Liu, Z.; Qi, Y.; Hector, L. G.; Li, H.; Harris, S. J. Direct Calculation of Li-ion Transport in the Solid Electrolyte Interphase. *J. Am. Chem. Soc.* **2012**, *134*, 15476–15487.
- (63) Kim, S.-P.; Duin, A. C. T. v.; Shenoy, V. B. Effect of Electrolytes on the Structure and Evolution of the Solid Electrolyte Interphase (SEI) in Li-ion Batteries: A Molecular Dynamics Study. *J. Power Sources* **2011**, *196*, 8590–8597.
- (64) Aurbach, D.; Zinigrad, E.; Cohen, Y.; Teller, H. A Short Review of Failure Mechanisms of Lithium Metal and Lithiated Graphite Anodes in Liquid Electrolyte Solutions. *Solid State Ionics* **2002**, *148*, 405–416.
- (65) Aurbach, D.; Gamolsky, K.; Markovsky, B.; Gofer, Y.; Schmidt, M.; Heider, U. On the Use of Vinylene Carbonate (VC) as an Additive to Electrolyte Solutions for Li-ion Batteries. *Electrochim. Acta* **2002**, *47*, 1423–1439.
- (66) Ushirogata, K.; Sodeyama, K.; Futera, Z.; Tateyama, Y.; Okuno, Y. Near-Shore Aggregation Mechanism of Electrolyte Decomposition Products to Explain Solid Electrolyte Interphase Formation. *J. Electrochem. Soc.* **2015**, *162*, A2670–A2678.
- (67) Leifer, N.; Smart, M.; Prakash, G.; Gonzalez, L.; Sanchez, L.; Smith, K.; Bhalla, P.; Grey, C.; Greenbaum, S. ${}^{13}\text{C}$ Solid State NMR Suggests Unusual Breakdown Products in SEI Formation on Lithium Ion Electrodes. *J. Electrochem. Soc.* **2011**, *158*, A471–A480.
- (68) Peled, E.; Gabano, J. *Lithium Batteries*; Academic Press: London, 1983.
- (69) Aurbach, D.; Zaban, A.; Gofer, Y.; Ely, Y. E.; Weissman, I.; Chusid, O.; Abramson, O. Recent Studies of the Lithium-Liquid Electrolyte Interface Electrochemical, Morphological and Spectral Studies of a Few Important Systems. *J. Power Sources* **1995**, *54*, 76–84.
- (70) Aurbach, D.; Gottlieb, H. The Electrochemical Behavior of Selected Polar Aprotic Systems. *Electrochim. Acta* **1989**, *34*, 141–156.
- (71) Aurbach, D.; Markovsky, B.; Schechter, A.; Ein-Eli, Y.; Cohen, H. A Comparative Study of Synthetic Graphite and Li Electrodes in Electrolyte Solutions Based on Ethylene Carbonate-Dimethyl Carbonate Mixtures. *J. Electrochem. Soc.* **1996**, *143*, 3809–3820.
- (72) Schechter, A.; Aurbach, D.; Cohen, H. X-Ray Photoelectron Spectroscopy Study of Surface Films Formed on Li Electrodes Freshly Prepared in Alkyl Carbonate Solutions. *Langmuir* **1999**, *15*, 3334–3342.
- (73) Leung, K.; Soto, F.; Hankins, K.; Balbuena, P. B.; Harrison, K. L. Stability of Solid Electrolyte Interphase Components on Lithium Metal and Reactive Anode Material Surfaces. *J. Phys. Chem. C* **2016**, *120*, 6302–6313.
- (74) Lin, Y.-X.; Liu, Z.; Leung, K.; Chen, L.-Q.; Lu, P.; Qi, Y. Connecting the Irreversible Capacity Loss in Li-Ion Batteries with the Electronic Insulating Properties of Solid Electrolyte Interphase (SEI) Components. *J. Power Sources* **2016**, *309*, 221–230.
- (75) Zheng, D.; Qu, D.; Yang, X.-Q.; Lee, H.-S.; Qu, D. Preferential Solvation of Lithium Cations and Impacts on Oxygen Reduction in Lithium–Air Batteries. *ACS Appl. Mater. Interfaces* **2015**, *7*, 19923–19929.
- (76) Uchida, S.; Ishikawa, M. Lithium Bis(Fluorosulfonyl)Imide Based Low Ethylene Carbonate Content Electrolyte with Unusual Solvation State. *J. Power Sources* **2017**, *359*, 480–486.
- (77) Wan, C.; Hu, M. Y.; Borodin, O.; Qian, J.; Qin, Z.; Zhang, J.-G.; Hu, J. Z. Natural Abundance ${}^{17}\text{O}$, ${}^6\text{Li}$ NMR and Molecular Modeling Studies of the Solvation Structures of Lithium Bis(Fluorosulfonyl)-Imide/1,2-Dimethoxyethane Liquid Electrolytes. *J. Power Sources* **2016**, *307*, 231–243.
- (78) Qian, J.; Henderson, W. A.; Xu, W.; Bhattacharya, P.; Engelhard, M.; Borodin, O.; Zhang, J.-G. High Rate and Stable Cycling of Lithium Metal Anode. *Nat. Commun.* **2015**, *6*, 6362.

- (79) Xu, K.; von Cresce, A.; Lee, U. Differentiating Contributions to “Ion Transfer” Barrier from Interphasial Resistance and Li⁺ Desolvation at Electrolyte/Graphite Interface. *Langmuir* **2010**, *26*, 11538–11543.
- (80) Christensen, J.; Newman, J. A Mathematical Model for the Lithium-ion Negative Electrode Solid Electrolyte Interphase. *J. Electrochem. Soc.* **2004**, *151*, A1977–A1988.
- (81) Borodin, O.; Smith, G. D.; Fan, P. Molecular Dynamics Simulations of Lithium Alkyl Carbonates. *J. Phys. Chem. B* **2006**, *110*, 22773–22779.
- (82) Single, F.; Horstmann, B.; Latz, A. Revealing SEI Morphology: In-depth Analysis of a Modeling Approach. *J. Electrochem. Soc.* **2017**, *164*, E3132–E3145.
- (83) Markevich, E.; Fridman, K.; Sharabi, R.; Elazari, R.; Salitra, G.; Gottlieb, H. E.; Gershinsky, G.; Garsuch, A.; Semrau, G.; Schmidt, M. A.; et al. Amorphous Columnar Silicon Anodes for Advanced High Voltage Lithium Ion Full Cells: Dominant Factors Governing Cycling Performance. *J. Electrochem. Soc.* **2013**, *160*, A1824–A1833.
- (84) Chen, Y. C.; Ouyang, C. Y.; Song, L. J.; Sun, Z. L. Electrical and Lithium Ion Dynamics in Three Main Components of Solid Electrolyte Interphase from Density Functional Theory Study. *J. Phys. Chem. C* **2011**, *115*, 7044–7049.
- (85) Bunde, A.; Dieterich, W.; Roman, E. Dispersed Ionic Conductors and Percolation Theory. *Phys. Rev. Lett.* **1985**, *55*, 5–8.
- (86) Liang, C. C. Conduction Characteristics of the Lithium Iodide-Aluminum Oxide Solid Electrolytes. *J. Electrochem. Soc.* **1973**, *120*, 1289–1292.
- (87) Li, C.; Maier, J. Ionic Space Charge Effects in Lithium Fluoride Thin Films. *Solid State Ionics* **2012**, *225*, 408–411.
- (88) Zhang, Q.; Pan, J.; Lu, P.; Liu, Z.; Verbrugge, M. W.; Sheldon, B. W.; Cheng, Y.-T.; Qi, Y.; Xiao, X. Synergetic Effects of Inorganic Components in Solid Electrolyte Interphase on High Cycle Efficiency of Lithium Ion Batteries. *Nano Lett.* **2016**, *16*, 2011–2016.
- (89) He, Y.; Hu, H. Analysis of Lithium Ion Concentration and Stress in the Solid Electrolyte Interphase on the Graphite Anode. *Phys. Chem. Chem. Phys.* **2015**, *17*, 23565–23572.
- (90) Monroe, C.; Newman, J. The Impact of Elastic Deformation on Deposition Kinetics at Lithium/Polymer Interfaces. *J. Electrochem. Soc.* **2005**, *152*, A396–A404.
- (91) Cohen, Y. S.; Cohen, Y.; Aurbach, D. Micromorphological Studies of Lithium Electrodes in Alkyl Carbonate Solutions Using *in situ* Atomic Force Microscopy. *J. Phys. Chem. B* **2000**, *104*, 12282–12291.
- (92) Liu, X.-R.; Deng, X.; Liu, R.-R.; Yan, H.-J.; Guo, Y.-G.; Wang, D.; Wan, L.-J. Single Nanowire Electrode Electrochemistry of Silicon Anode by *in situ* Atomic Force Microscopy: Solid Electrolyte Interphase Growth and Mechanical Properties. *ACS Appl. Mater. Interfaces* **2014**, *6*, 20317–20323.
- (93) Zhang, J.; Wang, R.; Yang, X.; Lu, W.; Wu, X.; Wang, X.; Li, H.; Chen, L. Direct Observation of Inhomogeneous Solid Electrolyte Interphase on MnO Anode with Atomic Force Microscopy and Spectroscopy. *Nano Lett.* **2012**, *12*, 2153–2157.
- (94) Li, N.-W.; Yin, Y.-X.; Yang, C.-P.; Guo, Y.-G. An Artificial Solid Electrolyte Interphase Layer for Stable Lithium Metal Anodes. *Adv. Mater.* **2016**, *28*, 1853–1858.
- (95) Liu, Z.; Qi, Y.; Lin, Y. X.; Chen, L.; Lu, P.; Chen, L. Q. Interfacial Study on Solid Electrolyte Interphase at Li Metal Anode: Implication for Li Dendrite Growth. *J. Electrochem. Soc.* **2016**, *163*, A592–A598.
- (96) Gregory, T. D.; Hoffman, R. J.; Winterton, R. C. Nonaqueous Electrochemistry of Magnesium: Applications to Energy Storage. *J. Electrochem. Soc.* **1990**, *137*, 775–780.
- (97) Guo, Y.; Yang, J.; NuLi, Y.; Wang, J. Study of Electronic Effect of Grignard Reagents on Their Electrochemical Behavior. *Electrochim. Commun.* **2010**, *12*, 1671–1673.
- (98) Matsui, M. Study on Electrochemically Deposited Mg Metal. *J. Power Sources* **2011**, *196*, 7048–7055.
- (99) Ling, C.; Banerjee, D.; Matsui, M. Study of the Electrochemical Deposition of Mg in the Atomic Level: Why It Prefers the Non-Dendritic Morphology. *Electrochim. Acta* **2012**, *76*, 270–274.
- (100) Jäckle, M.; Groß, A. Microscopic Properties of Lithium, Sodium, and Magnesium Battery Anode Materials Related to Possible Dendrite Growth. *J. Chem. Phys.* **2014**, *141*, 174710.
- (101) Ozhabes, Y.; Gunceler, D.; Arias, T. A. Stability and Surface Diffusion at Lithium-Electrolyte Interphases with Connections to Dendrite Suppression. 2015, arXiv:1504.05799 [cond-mat.mtrl-sci]. arXiv.org e-Print archive. <https://arxiv.org/abs/1504.05799>.
- (102) Ely, D. R.; García, R. E. Heterogeneous Nucleation and Growth of Lithium Electrodeposits on Negative Electrodes. *J. Electrochem. Soc.* **2013**, *160*, A662–A668.
- (103) Yan, K.; Lu, Z.; Lee, H.-W.; Xiong, F.; Hsu, P.-C.; Li, Y.; Zhao, J.; Chu, S.; Cui, Y. Selective Deposition and Stable Encapsulation of Lithium through Heterogeneous Seeded Growth. *Nat. Energy* **2016**, *1*, 16010.
- (104) Pei, A.; Zheng, G.; Shi, F.; Li, Y.; Cui, Y. Nanoscale Nucleation and Growth of Electrodeposited Lithium Metal. *Nano Lett.* **2017**, *17*, 1132–1139.
- (105) Xu, Q.; Yang, Y.; Shao, H. Substrate Effects on Li⁺ Electrodeposition in Li Secondary Batteries with a Competitive Kinetics Model. *Phys. Chem. Chem. Phys.* **2015**, *17*, 20398–20406.
- (106) Chazalviel, J. N. Electrochemical Aspects of the Generation of Ramified Metallic Electrodeposits. *Phys. Rev. A: At., Mol., Opt. Phys.* **1990**, *42*, 7355–7367.
- (107) Fleury, V.; Chazalviel, J. N.; Rosso, M.; Sapoval, B. The Role of the Anions in the Growth Speed of Fractal Electrodeposits. *J. Electroanal. Chem. Interfacial Electrochem.* **1990**, *290*, 249–255.
- (108) Sacci, R. L.; Dudney, N. J.; More, K. L.; Parent, L. R.; Arslan, I.; Browning, N. D.; Unocic, R. R. Direct Visualization of Initial SEI Morphology and Growth Kinetics During Lithium Deposition by *in situ* Electrochemical Transmission Electron Microscopy. *Chem. Commun.* **2014**, *50*, 2104–2107.
- (109) Zeng, Z.; Liang, W.-L.; Liao, H.-G.; Xin, H. L.; Chu, Y.-H.; Zheng, H. Visualization of Electrode–Electrolyte Interfaces in LiPF₆/EC/DEC Electrolyte for Lithium Ion Batteries via *in situ* TEM. *Nano Lett.* **2014**, *14*, 1745–1750.
- (110) Kushima, A.; So, K. P.; Su, C.; Bai, P.; Kuriyama, N.; Maebashi, T.; Fujiwara, Y.; Bazant, M. Z.; Li, J. Liquid Cell Transmission Electron Microscopy Observation of Lithium Metal Growth and Dissolution: Root Growth, Dead Lithium and Lithium Flotsams. *Nano Energy* **2017**, *32*, 271–279.
- (111) Barton, J. L.; Bockris, J. O. M. The Electrolytic Growth of Dendrites from Ionic Solutions. *Proc. R. Soc. London, Ser. A* **1962**, *268*, 485–505.
- (112) Gireaud, L.; Grugeon, S.; Laruelle, S.; Yrieix, B.; Tarascon, J. M. Lithium Metal Stripping/Plating Mechanisms Studies: A Metallurgical Approach. *Electrochim. Commun.* **2006**, *8*, 1639–1649.
- (113) Akolkar, R. Modeling Dendrite Growth During Lithium Electrodeposition at sub-ambient Temperature. *J. Power Sources* **2014**, *246*, 84–89.
- (114) Rosso, M.; Gobron, T.; Brissot, C.; Chazalviel, J. N.; Lascaud, S. Onset of Dendritic Growth in Lithium/Polymer Cells. *J. Power Sources* **2001**, *97–98*, 804–806.
- (115) Monroe, C.; Newman, J. Dendrite Growth in Lithium/Polymer Systems: A Propagation Model for Liquid Electrolytes under Galvanostatic Conditions. *J. Electrochem. Soc.* **2003**, *150*, A1377–A1384.
- (116) Chen, Q.; Geng, K.; Sieradzki, K. Prospects for Dendrite-Free Cycling of Li Metal Batteries. *J. Electrochem. Soc.* **2015**, *162*, A2004–A2007.
- (117) Harry, K. J.; Hallinan, D. T.; Parkinson, D. Y.; MacDowell, A. A.; Balsara, N. P. Detection of Subsurface Structures Underneath Dendrites Formed on Cycled Lithium Metal Electrodes. *Nat. Mater.* **2014**, *13*, 69–73.
- (118) Dollé, M.; Sannier, L.; Beaudoin, B.; Trentin, M.; Tarascon, J.-M. Live Scanning Electron Microscope Observations of Dendritic

- Growth in Lithium/Polymer Cells. *Electrochim. Solid-State Lett.* **2002**, *5*, A286–A289.
- (119) Yamaki, J.-i.; Tobishima, S.-i.; Hayashi, K.; Saito, K.; Nemoto, Y.; Arakawa, M. A Consideration of the Morphology of Electrochemically Deposited Lithium in an Organic Electrolyte. *J. Power Sources* **1998**, *74*, 219–227.
- (120) Steiger, J.; Kramer, D.; Möning, R. Mechanisms of Dendritic Growth Investigated by *in situ* Light Microscopy During Electrodeposition and Dissolution of Lithium. *J. Power Sources* **2014**, *261*, 112–119.
- (121) Sand, H. J. S. III. On the Concentration at the Electrodes in a Solution, with Special Reference to the Liberation of Hydrogen by Electrolysis of a Mixture of Copper Sulphate and Sulphuric Acid. *Philos. Mag.* **1901**, *1*, 45–79.
- (122) Rosso, M.; Brissot, C.; Teyssot, A.; Dollé, M.; Sannier, L.; Tarascon, J.-M.; Bouchet, R.; Lascaud, S. Dendrite Short-Circuit and Fuse Effect on Li/Polymer/Li Cells. *Electrochim. Acta* **2006**, *51*, 5334–5340.
- (123) Brissot, C.; Rosso, M.; Chazalviel, J. N.; Lascaud, S. Dendritic Growth Mechanisms in Lithium/Polymer Cells. *J. Power Sources* **1999**, *81*–*82*, 925–929.
- (124) Park, H. E.; Hong, C. H.; Yoon, W. Y. The Effect of Internal Resistance on Dendritic Growth on Lithium Metal Electrodes in the Lithium Secondary Batteries. *J. Power Sources* **2008**, *178*, 765–768.
- (125) Brissot, C.; Rosso, M.; Chazalviel, J. N.; Baudry, P.; Lascaud, S. *In situ* Study of Dendritic Growth in Lithium/PEO-Salt/Lithium Cells. *Electrochim. Acta* **1998**, *43*, 1569–1574.
- (126) Akolkar, R. Mathematical Model of the Dendritic Growth During Lithium Electrodeposition. *J. Power Sources* **2013**, *232*, 23–28.
- (127) Nishikawa, K.; Mori, T.; Nishida, T.; Fukunaka, Y.; Rosso, M. Li Dendrite Growth and Li⁺ Ionic Mass Transfer Phenomenon. *J. Electroanal. Chem.* **2011**, *661*, 84–89.
- (128) Crowther, O.; West, A. C. Effect of Electrolyte Composition on Lithium Dendrite Growth. *J. Electrochem. Soc.* **2008**, *155*, A806–A811.
- (129) Porthault, H.; Decaux, C. Electrodeposition of Lithium Metal Thin Films and Its Application in All-Solid-State Microbatteries. *Electrochim. Acta* **2016**, *194*, 330–337.
- (130) Stark, J. K.; Ding, Y.; Kohl, P. A. Nucleation of Electrodeposited Lithium Metal: Dendritic Growth and the Effect of Co-Deposited Sodium. *J. Electrochem. Soc.* **2013**, *160*, D337–D342.
- (131) Liu, X. H.; Zhong, L.; Zhang, L. Q.; Kushima, A.; Mao, S. X.; Li, J.; Ye, Z. Z.; Sullivan, J. P.; Huang, J. Y. Lithium Fiber Growth on the Anode in a Nanowire Lithium Ion Battery During Charging. *Appl. Phys. Lett.* **2011**, *98*, 183107.
- (132) Sano, H.; Kitta, M.; Matsumoto, H. Effect of Charge Transfer Resistance on Morphology of Lithium Electrodeposited in Ionic Liquid. *J. Electrochem. Soc.* **2016**, *163*, D3076–D3079.
- (133) Tang, C.-Y.; Dillon, S. J. *In Situ* Scanning Electron Microscopy Characterization of the Mechanism for Li Dendrite Growth. *J. Electrochem. Soc.* **2016**, *163*, A1660–A1665.
- (134) Steiger, J.; Kramer, D.; Moenig, R. Microscopic Observations of the Formation, Growth and Shrinkage of Lithium Moss During Electrodeposition and Dissolution. *Electrochim. Acta* **2014**, *136*, 529–536.
- (135) Park, M. S.; Ma, S. B.; Lee, D. J.; Im, D.; Doo, S.-G.; Yamamoto, O. A Highly Reversible Lithium Metal Anode. *Sci. Rep.* **2015**, *4*, 3815.
- (136) Sun, F.; Moroni, R.; Dong, K.; Markötter, H.; Zhou, D.; Hilger, A.; Zielke, L.; Zengerle, R.; Thiele, S.; Banhart, J.; et al. A Study of the Mechanisms of Internal Short Circuit in a Li/Li Cell by Synchrotron X-Ray Phase Contrast Tomography. *ACS Energy Lett.* **2017**, *2*, 94–104.
- (137) Aryanfar, A.; Brooks, D. J.; Colussi, A. J.; Hoffmann, M. R. Quantifying the Dependence of Dead Lithium Losses on the Cycling Period in Lithium Metal Batteries. *Phys. Chem. Chem. Phys.* **2014**, *16*, 24965–24970.
- (138) Sun, M.; Liao, H.-G.; Niu, K.; Zheng, H. Structural and Morphological Evolution of Lead Dendrites During Electrochemical Migration. *Sci. Rep.* **2013**, *3*, 3227.
- (139) Lin, T.-H.; Lin, C.-W.; Liu, H.-H.; Sheu, J.-T.; Hung, W.-H. Potential-Controlled Electrodeposition of Gold Dendrites in the Presence of Cysteine. *Chem. Commun.* **2011**, *47*, 2044–2046.
- (140) Chen, L.; Zhang, H. W.; Liang, L. Y.; Liu, Z.; Qi, Y.; Lu, P.; Chen, J.; Chen, L. Q. Modulation of Dendritic Patterns During Electrodeposition: A Nonlinear Phase-Field Model. *J. Power Sources* **2015**, *300*, 376–385.
- (141) Bai, P.; Li, J.; Brushett, F. R.; Bazant, M. Z. Transition of Lithium Growth Mechanisms in Liquid Electrolytes. *Energy Environ. Sci.* **2016**, *9*, 3221–3229.
- (142) Orsini, F.; du Pasquier, A.; Beaudouin, B.; Tarascon, J. M.; Trentin, M.; Langenhuijsen, N.; de Beer, E.; Notten, P. In Situ SEM Study of the Interfaces in Plastic Lithium Cells. *J. Power Sources* **1999**, *81*–*82*, 918–921.
- (143) Sano, H.; Sakaebe, H.; Senoh, H.; Matsumoto, H. Effect of Current Density on Morphology of Lithium Electrodeposited in Ionic Liquid-Based Electrolytes. *J. Electrochem. Soc.* **2014**, *161*, A1236–A1240.
- (144) Seong, I. W.; Hong, C. H.; Kim, B. K.; Yoon, W. Y. The Effects of Current Density and Amount of Discharge on Dendrite Formation in the Lithium Powder Anode Electrode. *J. Power Sources* **2008**, *178*, 769–773.
- (145) Zhang, R.; Cheng, X.-B.; Zhao, C.-Z.; Peng, H.-J.; Shi, J.-L.; Huang, J.-Q.; Wang, J.; Wei, F.; Zhang, Q. Conductive Nanostructured Scaffolds Render Low Local Current Density to Inhibit Lithium Dendrite Growth. *Adv. Mater.* **2016**, *28*, 2155–2162.
- (146) Cheng, X.-B.; Peng, H.-J.; Huang, J.-Q.; Wei, F.; Zhang, Q. Dendrite-Free Nanostructured Anode: Entrapment of Lithium in a 3D Fibrous Matrix for Ultra-Stable Lithium–Sulfur Batteries. *Small* **2014**, *10*, 4257–4263.
- (147) Lu, L.-L.; Ge, J.; Yang, J.-N.; Chen, S.-M.; Yao, H.-B.; Zhou, F.; Yu, S.-H. Free-Standing Copper Nanowire Network Current Collector for Improving Lithium Anode Performance. *Nano Lett.* **2016**, *16*, 4431–4437.
- (148) Zhang, R.; Li, N.-W.; Cheng, X.-B.; Yin, Y.-X.; Zhang, Q.; Guo, Y.-G. Advanced Micro/Nanostructures for Lithium Metal Anodes. *Adv. Sci.* **2017**, *4*, 1600445.
- (149) Ota, H.; Shima, K.; Ue, M.; Yamaki, J.-i. Effect of Vinylene Carbonate as Additive to Electrolyte for Lithium Metal Anode. *Electrochim. Acta* **2004**, *49*, 565–572.
- (150) Mogi, R.; Inaba, M.; Iriyama, Y.; Abe, T.; Ogumi, Z. In Situ Atomic Force Microscopy Study on Lithium Deposition on Nickel Substrates at Elevated Temperatures. *J. Electrochem. Soc.* **2002**, *149*, A385–A390.
- (151) Akolkar, R. Modeling Dendrite Growth During Lithium Electrodeposition at Sub-Ambient Temperature. *J. Power Sources* **2014**, *246*, 84–89.
- (152) Love, C. T.; Baturina, O. A.; Swider-Lyons, K. E. Observation of Lithium Dendrites at Ambient Temperature and Below. *ECS Electrochem. Lett.* **2015**, *4*, A24–A27.
- (153) Barai, P.; Higa, K.; Srinivasan, V. Effect of Initial State of Lithium on the Propensity for Dendrite Formation: A Theoretical Study. *J. Electrochem. Soc.* **2017**, *164*, A180–A189.
- (154) Hirai, T.; Yoshimatsu, I.; Yamaki, J. i. Influence of Electrolyte on Lithium Cycling Efficiency with Pressurized Electrode Stack. *J. Electrochem. Soc.* **1994**, *141*, 611–614.
- (155) Aryanfar, A.; Brooks, D.; Merinov, B. V.; Goddard, W. A.; Colussi, A. J.; Hoffmann, M. R. Dynamics of Lithium Dendrite Growth and Inhibition: Pulse Charging Experiments and Monte Carlo Calculations. *J. Phys. Chem. Lett.* **2014**, *5*, 1721–1726.
- (156) Aryanfar, A.; Brooks, D. J.; Colussi, A. J.; Merinov, B. V.; Goddard III, W. A.; Hoffmann, M. R. Thermal Relaxation of Lithium Dendrites. *Phys. Chem. Chem. Phys.* **2015**, *17*, 8000–8005.
- (157) Mayers, M. Z.; Kaminski, J. W.; Miller, T. F. Suppression of Dendrite Formation Via Pulse Charging in Rechargeable Lithium Metal Batteries. *J. Phys. Chem. C* **2012**, *116*, 26214–26221.

- (158) Tan, J. W.; Tartakovsky, A. M.; Ferris, K.; Ryan, E. M. Investigating the Effects of Anisotropic Mass Transport on Dendrite Growth in High Energy Density Lithium Batteries. *J. Electrochem. Soc.* **2016**, *163*, A318–A327.
- (159) Ely, D. R.; Jana, A.; Garcia, R. E. Phase Field Kinetics of Lithium Electrodeposits. *J. Power Sources* **2014**, *272*, 581–594.
- (160) Aryanfar, A.; Cheng, T.; Colussi, A. J.; Merinov, B. V.; Goddard, W. A.; Hoffmann, M. R. Annealing Kinetics of Electro-deposited Lithium Dendrites. *J. Chem. Phys.* **2015**, *143*, 134701.
- (161) Tao, R.; Bi, X.; Li, S.; Yao, Y.; Wu, F.; Wang, Q.; Zhang, C.; Lu, J. Kinetics Tuning the Electrochemistry of Lithium Dendrites Formation in Lithium Batteries through Electrolytes. *ACS Appl. Mater. Interfaces* **2017**, *9*, 7003–7008.
- (162) Wang, J.; Lin, F.; Jia, H.; Yang, J.; Monroe, C. W.; NuLi, Y. Towards a Safe Lithium–Sulfur Battery with a Flame-Inhibiting Electrolyte and a Sulfur-Based Composite Cathode. *Angew. Chem., Int. Ed.* **2014**, *53*, 10099–10104.
- (163) Jia, H.; Wang, J.; Lin, F.; Monroe, C. W.; Yang, J.; NuLi, Y. Tppi as a Flame Retardant for Rechargeable Lithium Batteries with Sulfur Composite Cathodes. *Chem. Commun.* **2014**, *50*, 7011–7013.
- (164) Shiga, T.; Kato, Y.; Kondo, H.; Okuda, C.-a. Self-Extinguishing Electrolyte Using Fluorinated Alkyl Phosphate for Lithium Batteries. *J. Mater. Chem. A* **2017**, *5*, 5156–5162.
- (165) Chen, X.; Hou, T.-Z.; Li, B.; Yan, C.; Zhu, L.; Guan, C.; Cheng, X.-B.; Peng, H.-J.; Huang, J.-Q.; Zhang, Q. Towards Stable Lithium–Sulfur Batteries: Mechanistic Insights into Electrolyte Decomposition on Lithium Metal Anode. *Energy Storage Mater.* **2017**, *8*, 194–201.
- (166) Leung, K.; Qi, Y.; Zavadil, K. R.; Jung, Y. S.; Dillon, A. C.; Cavanagh, A. S.; Lee, S.-H.; George, S. M. Using Atomic Layer Deposition to Hinder Solvent Decomposition in Lithium Ion Batteries: First-Principles Modeling and Experimental Studies. *J. Am. Chem. Soc.* **2011**, *133*, 14741–14754.
- (167) Kuwata, H.; Sonoki, H.; Matsui, M.; Matsuda, Y.; Imanishi, N. Surface Layer and Morphology of Lithium Metal Electrodes. *Electrochemistry* **2016**, *84*, 854–860.
- (168) Heine, J.; Hilbig, P.; Qi, X.; Niehoff, P.; Winter, M.; Bieker, P. Fluoroethylene Carbonate as Electrolyte Additive in Tetraethylene Glycol Dimethyl Ether Based Electrolytes for Application in Lithium Ion and Lithium Metal Batteries. *J. Electrochem. Soc.* **2015**, *162*, A1094–A1101.
- (169) Guo, J.; Wen, Z.; Wu, M.; Jin, J.; Liu, Y. Vinylene Carbonate–LiNO₃: A Hybrid Additive in Carbonic Ester Electrolytes for Sei Modification on Li Metal Anode. *Electrochim. Commun.* **2015**, *51*, 59–63.
- (170) Sano, H.; Sakaue, H.; Matsumoto, H. Observation of Electrodeposited Lithium by Optical Microscope in Room Temperature Ionic Liquid-Based Electrolyte. *J. Power Sources* **2011**, *196*, 6663–6669.
- (171) Markevich, E.; Salitra, G.; Chesneau, F.; Schmidt, M.; Aurbach, D. Very Stable Lithium Metal Stripping–Plating at a High Rate and High Areal Capacity in Fluoroethylene Carbonate-Based Organic Electrolyte Solution. *ACS Energy Lett.* **2017**, *2*, 1321–1326.
- (172) Zhang, X.-Q.; Cheng, X.-B.; Chen, X.; Yan, C.; Zhang, Q. Fluoroethylene Carbonate Additives to Render Uniform Li Deposits in Lithium Metal Batteries. *Adv. Funct. Mater.* **2017**, *27*, 1605989.
- (173) Markevich, E.; Salitra, G.; Aurbach, D. Fluoroethylene Carbonate as an Important Component for the Formation of an Effective Solid Electrolyte Interphase on Anodes and Cathodes for Advanced Li-Ion Batteries. *ACS Energy Lett.* **2017**, *2*, 1337–1345.
- (174) Jung, R.; Metzger, M.; Haering, D.; Solchenbach, S.; Marino, C.; Tsiorvas, N.; Stinner, C.; Gasteiger, H. A. Consumption of Fluoroethylene Carbonate (FEC) on Si-C Composite Electrodes for Li-Ion Batteries. *J. Electrochem. Soc.* **2016**, *163*, A1705–A1716.
- (175) Miao, R.; Yang, J.; Feng, X.; Jia, H.; Wang, J.; Nuli, Y. Novel Dual-Salts Electrolyte Solution for Dendrite-Free Lithium-Metal Based Rechargeable Batteries with High Cycle Reversibility. *J. Power Sources* **2014**, *271*, 291–297.
- (176) Jia, W.; Fan, C.; Wang, L.; Wang, Q.; Zhao, M.; Zhou, A.; Li, J. Extremely Accessible Potassium Nitrate (KNO₃) as the Highly Efficient Electrolyte Additive in Lithium Battery. *ACS Appl. Mater. Interfaces* **2016**, *8*, 15399–15405.
- (177) Han, G.-B.; Lee, J.-N.; Lee, D. J.; Lee, H.; Song, J.; Lee, H.; Ryou, M.-H.; Park, J.-K.; Lee, Y. M. Enhanced Cycling Performance of Lithium Metal Secondary Batteries with Succinic Anhydride as an Electrolyte Additive. *Electrochim. Acta* **2014**, *115*, 525–530.
- (178) Xiang, H.; Shi, P.; Bhattacharya, P.; Chen, X.; Mei, D.; Bowden, M. E.; Zheng, J.; Zhang, J.-G.; Xu, W. Enhanced Charging Capability of Lithium Metal Batteries Based on Lithium Bis-(Trifluoromethanesulfonyl)Imide-Lithium Bis(Oxalato) Borate Dual-Salt Electrolytes. *J. Power Sources* **2016**, *318*, 170–177.
- (179) Wu, F.; Qian, J.; Chen, R.; Lu, J.; Li, L.; Wu, H.; Chen, J.; Zhao, T.; Ye, Y.; Amine, K. An Effective Approach to Protect Lithium Anode and Improve Cycle Performance for Li–S Batteries. *ACS Appl. Mater. Interfaces* **2014**, *6*, 15542–15549.
- (180) Liu, S.; Li, G.-R.; Gao, X.-P. Lanthanum Nitrate as Electrolyte Additive to Stabilize the Surface Morphology of Lithium Anode for Lithium–Sulfur Battery. *ACS Appl. Mater. Interfaces* **2016**, *8*, 7783–7789.
- (181) Jeong, J.; Lee, J.-N.; Park, J.-K.; Ryou, M.-H.; Lee, Y. M. Stabilizing Effect of 2-(Triphenylphosphoranylidene) Succinic Anhydride as Electrolyte Additive on the Lithium Metal of Lithium Metal Secondary Batteries. *Electrochim. Acta* **2015**, *170*, 353–359.
- (182) Li, N.-W.; Yin, Y.-X.; Li, J.-Y.; Zhang, C.-H.; Guo, Y.-G. Passivation of Lithium Metal Anode via Hybrid Ionic Liquid Electrolyte toward Stable Li Plating/Stripping. *Adv. Sci.* **2017**, *3*, 1600400.
- (183) Fang, Z.; Ma, Q.; Liu, P.; Ma, J.; Hu, Y.-S.; Zhou, Z.; Li, H.; Huang, X.; Chen, L. Novel Concentrated Li[(FSO₂)(N-C₄F₉SO₂)N]-Based Ether Electrolyte for Superior Stability of Metallic Lithium Anode. *ACS Appl. Mater. Interfaces* **2017**, *9*, 4282–4289.
- (184) Miao, R.; Yang, J.; Xu, Z.; Wang, J.; Nuli, Y.; Sun, L. A New Ether-Based Electrolyte for Dendrite-Free Lithium–Metal Based Rechargeable Batteries. *Sci. Rep.* **2016**, *6*, 21771.
- (185) Choudhury, S.; Wan, C. T.-C.; Al Sadat, W. I.; Tu, Z.; Lau, S.; Zachman, M. J.; Kourkoutis, L. F.; Archer, L. A. Designer Interphases for the Lithium–Oxygen Electrochemical Cell. *Sci. Adv.* **2017**, *3*, e1602809.
- (186) Wu, H.; Cao, Y.; Geng, L.; Wang, C. In Situ Formation of Stable Interfacial Coating for High Performance Lithium Metal Anodes. *Chem. Mater.* **2017**, *29*, 3572–3579.
- (187) Hu, Z.; Zhang, S.; Dong, S.; Li, W.; Li, H.; Cui, G.; Chen, L. Poly(Ethyl A-Cyanoacrylate)-Based Artificial Solid Electrolyte Interphase Layer for Enhanced Interface Stability of Li Metal Anodes. *Chem. Mater.* **2017**, *29*, 4682–4689.
- (188) Ye, H.; Yin, Y.-X.; Zhang, S.-F.; Shi, Y.; Liu, L.; Zeng, X.-X.; Wen, R.; Guo, Y.-G.; Wan, L.-J. Synergism of Al-Containing Solid Electrolyte Interphase Layer and Al-Based Colloidal Particles for Stable Lithium Anode. *Nano Energy* **2017**, *36*, 411–417.
- (189) Yu, H.; Zhao, J.; Ben, L.; Zhan, Y.; Wu, Y.; Huang, X. Dendrite-Free Lithium Deposition with Self-Aligned Columnar Structure in a Carbonate–Ether Mixed Electrolyte. *ACS Energy Lett.* **2017**, *2*, 1296–1302.
- (190) Zhou, G.; Paek, E.; Hwang, G. S.; Manthiram, A. Long-Life Li/Polysulphide Batteries with High Sulphur Loading Enabled by Lightweight Three-Dimensional Nitrogen/Sulphur-Codoped Graphene Sponge. *Nat. Commun.* **2015**, *6*, 7760.
- (191) Hou, T.-Z.; Chen, X.; Peng, H.-J.; Huang, J.-Q.; Li, B.-Q.; Zhang, Q.; Li, B. Design Principles for Heteroatom-Doped Nano-carbon to Achieve Strong Anchoring of Polysulfides for Lithium–Sulfur Batteries. *Small* **2016**, *12*, 3283–3291.
- (192) Yuan, Z.; Peng, H.-J.; Hou, T.-Z.; Huang, J.-Q.; Chen, C.-M.; Wang, D.-W.; Cheng, X.-B.; Wei, F.; Zhang, Q. Powering Lithium–Sulfur Battery Performance by Propelling Polysulfide Redox at Sulfiphilic Hosts. *Nano Lett.* **2016**, *16*, 519–527.
- (193) Li, W.; Yao, H.; Yan, K.; Zheng, G.; Liang, Z.; Chiang, Y.-M.; Cui, Y. The Synergetic Effect of Lithium Polysulfide and Lithium

- Nitrate to Prevent Lithium Dendrite Growth. *Nat. Commun.* **2015**, *6*, 7436.
- (194) Zhao, C.-Z.; Cheng, X.-B.; Zhang, R.; Peng, H.-J.; Huang, J.-Q.; Ran, R.; Huang, Z.-H.; Wei, F.; Zhang, Q. Li₂S₅-Based Ternary-Salt Electrolyte for Robust Lithium Metal Anode. *Energy Storage Mater.* **2016**, *3*, 77–84.
- (195) Yan, C.; Cheng, X.-B.; Zhao, C.-Z.; Huang, J.-Q.; Yang, S.-T.; Zhang, Q. Lithium Metal Protection through in-situ Formed Solid Electrolyte Interphase in Lithium-Sulfur Batteries: The Role of Polysulfides on Lithium Anode. *J. Power Sources* **2016**, *327*, 212–220.
- (196) Xiong, S.; Xie, K.; Diao, Y.; Hong, X. Characterization of the Solid Electrolyte Interphase on Lithium Anode for Preventing the Shuttle Mechanism in Lithium–Sulfur Batteries. *J. Power Sources* **2014**, *246*, 840–845.
- (197) Rong, G.; Zhang, X.; Zhao, W.; Qiu, Y.; Liu, M.; Ye, F.; Xu, Y.; Chen, J.; Hou, Y.; Li, W.; et al. Liquid-Phase Electrochemical Scanning Electron Microscopy for in situ Investigation of Lithium Dendrite Growth and Dissolution. *Adv. Mater.* **2017**, *29*, 1606187.
- (198) Qian, J.; Xu, W.; Bhattacharya, P.; Engelhard, M.; Henderson, W. A.; Zhang, Y.; Zhang, J.-G. Dendrite-Free Li Deposition Using Trace-Amounts of Water as an Electrolyte Additive. *Nano Energy* **2015**, *15*, 135–144.
- (199) Mehdi, B. L.; Stevens, A.; Qian, J.; Park, C.; Xu, W.; Henderson, W. A.; Zhang, J.-G.; Mueller, K. T.; Browning, N. D. The Impact of Li Grain Size on Coulombic Efficiency in Li Batteries. *Sci. Rep.* **2016**, *6*, 34267.
- (200) Koshikawa, H.; Matsuda, S.; Kamiya, K.; Kubo, Y.; Uosaki, K.; Hashimoto, K.; Nakanishi, S. Effects of Contaminant Water on Coulombic Efficiency of Lithium Deposition/Dissolution Reactions in Tetraglyme-Based Electrolytes. *J. Power Sources* **2017**, *350*, 73–79.
- (201) Zu, C.; Dolocan, A.; Xiao, P.; Stauffer, S.; Henkelman, G.; Manthiram, A. Breaking Down the Crystallinity: The Path for Advanced Lithium Batteries. *Adv. Energy Mater.* **2016**, *6*, 1501933.
- (202) Zu, C.; Manthiram, A. Stabilized Lithium–Metal Surface in a Polysulfide-Rich Environment of Lithium–Sulfur Batteries. *J. Phys. Chem. Lett.* **2014**, *5*, 2522–2527.
- (203) Wood, S. M.; Pham, C. H.; Rodriguez, R.; Nathan, S. S.; Dolocan, A. D.; Celio, H.; de Souza, J. P.; Klavetter, K. C.; Heller, A.; Mullins, C. B. K⁺ Reduces Lithium Dendrite Growth by Forming a Thin, Less-Resistive Solid Electrolyte Interphase. *ACS Energy Lett.* **2016**, *1*, 414–419.
- (204) Ding, F.; Xu, W.; Graff, G. L.; Zhang, J.; Sushko, M. L.; Chen, X.; Shao, Y.; Engelhard, M. H.; Nie, Z.; Xiao, J.; et al. Dendrite-Free Lithium Deposition via Self-Healing Electrostatic Shield Mechanism. *J. Am. Chem. Soc.* **2013**, *135*, 4450–4456.
- (205) Xiao, L.; Chen, X.; Cao, R.; Qian, J.; Xiang, H.; Zheng, J.; Zhang, J.-G.; Xu, W. Enhanced Performance of Li₁LiFePO₄ Cells Using CsPF₆ as an Electrolyte Additive. *J. Power Sources* **2015**, *293*, 1062–1067.
- (206) Zhang, Y.; Qian, J.; Xu, W.; Russell, S. M.; Chen, X.; Nasybulin, E.; Bhattacharya, P.; Engelhard, M. H.; Mei, D.; Cao, R.; et al. Dendrite-Free Lithium Deposition with Self-aligned Nanorod Structure. *Nano Lett.* **2014**, *14*, 6889–6896.
- (207) Ding, F.; Xu, W.; Chen, X.; Zhang, J.; Shao, Y.; Engelhard, M. H.; Zhang, Y.; Blake, T. A.; Graff, G. L.; Liu, X.; et al. Effects of Cesium Cations in Lithium Deposition via Self-Healing Electrostatic Shield Mechanism. *J. Phys. Chem. C* **2014**, *118*, 4043–4049.
- (208) Goodman, J. K. S.; Kohl, P. A. Effect of Alkali and Alkaline Earth Metal Salts on Suppression of Lithium Dendrites. *J. Electrochem. Soc.* **2014**, *161*, D418–D424.
- (209) Wu, B.; Liu, Q.; Mu, D.; Xu, H.; Wang, L.; Shi, L.; Gai, L.; Wu, F. Suppression of Lithium Dendrite Growth by Introducing a Low Reduction Potential Complex Cation in the Electrolyte. *RSC Adv.* **2016**, *6*, 51738–51746.
- (210) Lu, Y.; Tu, Z.; Archer, L. A. Stable Lithium Electrodeposition in Liquid and Nanoporous Solid Electrolytes. *Nat. Mater.* **2014**, *13*, 961–969.
- (211) Lu, Y.; Tu, Z.; Shu, J.; Archer, L. A. Stable Lithium Electrodeposition in Salt-reinforced Electrolytes. *J. Power Sources* **2015**, *279*, 413–418.
- (212) Shi, L.; Xu, A.; Zhao, T. First-Principles Investigations of the Working Mechanism of 2D h-BN as an Interfacial Layer for the Anode of Lithium Metal Batteries. *ACS Appl. Mater. Interfaces* **2017**, *9*, 1987–1994.
- (213) Liu, Q.-C.; Xu, J.-J.; Yuan, S.; Chang, Z.-W.; Xu, D.; Yin, Y.-B.; Li, L.; Zhong, H.-X.; Jiang, Y.-S.; Yan, J.-M.; et al. Artificial Protection Film on Lithium Metal Anode toward Long-Cycle-Life Lithium–Oxygen Batteries. *Adv. Mater.* **2015**, *27*, 5241–5247.
- (214) Ma, L.; Kim, M. S.; Archer, L. A. Stable Artificial Solid Electrolyte Interphases for Lithium Batteries. *Chem. Mater.* **2017**, *29*, 4181–4189.
- (215) Ishikawa, M.; Kawasaki, H.; Yoshimoto, N.; Morita, M. Pretreatment of Li Metal Anode with Electrolyte Additive for Enhancing Li Cycleability. *J. Power Sources* **2005**, *146*, 199–203.
- (216) Wang, H.; Matsui, M.; Kuwata, H.; Sonoki, H.; Matsuda, Y.; Shang, X.; Takeda, Y.; Yamamoto, O.; Imanishi, N. A Reversible Dendrite-Free High-Areal-Capacity Lithium Metal Electrode. *Nat. Commun.* **2017**, *8*, 15106.
- (217) Cheng, X.-B.; Yan, C.; Chen, X.; Guan, C.; Huang, J.-Q.; Peng, H.-J.; Zhang, R.; Yang, S.-T.; Zhang, Q. Implantable Solid Electrolyte Interphase in Lithium-Metal Batteries. *Chem.* **2017**, *2*, 258–270.
- (218) Koch, S. L.; Morgan, B. J.; Passerini, S.; Teobaldi, G. Density Functional Theory Screening of Gas-Treatment Strategies for Stabilization of High Energy-Density Lithium Metal Anodes. *J. Power Sources* **2015**, *296*, 150–161.
- (219) Ma, G.; Wen, Z.; Wu, M.; Shen, C.; Wang, Q.; Jin, J.; Wu, X. A Lithium Anode Protection Guided Highly-Stable Lithium-Sulfur Battery. *Chem. Commun.* **2014**, *50*, 14209–14212.
- (220) Zhang, Y.-J.; Wang, W.; Tang, H.; Bai, W. Q.; Ge, X.; Wang, X. L.; Gu, C. D.; Tu, J. P. An ex-situ Nitridation Route to Synthesize Li₃N-modified Li Anodes for Lithium Secondary Batteries. *J. Power Sources* **2015**, *277*, 304–311.
- (221) Zhu, Y.; He, X.; Mo, Y. Strategies Based on Nitride Materials Chemistry to Stabilize Li Metal Anode. *Adv. Sci.* **2017**, *4*, 1600517.
- (222) Liu, Y.; Lin, D.; Yuen, P. Y.; Liu, K.; Xie, J.; Dauskardt, R. H.; Cui, Y. An Artificial Solid Electrolyte Interphase with High Li-ion Conductivity, Mechanical Strength, and Flexibility for Stable Lithium Metal Anodes. *Adv. Mater.* **2017**, *29*, 1605531.
- (223) Basile, A.; Bhatt, A. I.; O'Mullane, A. P. Stabilizing Lithium Metal Using Ionic Liquids for Long-Lived Batteries. *Nat. Commun.* **2016**, *7*, 11794.
- (224) Jia, W.; Wang, Q.; Yang, J.; Fan, C.; Wang, L.; Li, J. Pretreatment of Lithium Surface by Using Iodic Acid (HIO₃) to Improve Its Anode Performance in Lithium Batteries. *ACS Appl. Mater. Interfaces* **2017**, *9*, 7068–7074.
- (225) Peng, Z.; Wang, S.; Zhou, J.; Jin, Y.; Liu, Y.; Qin, Y.; Shen, C.; Han, W.; Wang, D. Volumetric Variation Confinement: Surface Protective Structure for High Cyclic Stability of Lithium Metal Electrodes. *J. Mater. Chem. A* **2016**, *4*, 2427–2432.
- (226) Jing, H.-K.; Kong, L.-L.; Liu, S.; Li, G.-R.; Gao, X.-P. Protected Lithium Anode with Porous Al₂O₃ Layer for Lithium-Sulfur Battery. *J. Mater. Chem. A* **2015**, *3*, 12213–12219.
- (227) Chen, L.; Connell, J. G.; Nie, A.; Huang, Z.; Zavadil, K. R.; Klavetter, K. C.; Yuan, Y.; Sharifi-Asl, S.; Shahbazian-Yassar, R.; Libera, J. A.; et al. Lithium Metal Protected by Atomic Layer Deposition Metal Oxide for High Performance Anodes. *J. Mater. Chem. A* **2017**, *5*, 12297–12309.
- (228) Kozen, A. C.; Lin, C.-F.; Pearse, A. J.; Schroeder, M. A.; Han, X.; Hu, L.; Lee, S.-B.; Rubloff, G. W.; Noked, M. Next-Generation Lithium Metal Anode Engineering via Atomic Layer Deposition. *ACS Nano* **2015**, *9*, 5884–5892.
- (229) Kazyak, E.; Wood, K. N.; Dasgupta, N. P. Improved Cycle Life and Stability of Lithium Metal Anodes through Ultrathin Atomic Layer Deposition Surface Treatments. *Chem. Mater.* **2015**, *27*, 6457–6462.
- (230) Lee, D. J.; Lee, H.; Kim, Y.-J.; Park, J.-K.; Kim, H.-T. Sustainable Redox Mediation for Lithium–Oxygen Batteries by a

- Composite Protective Layer on the Lithium-Metal Anode. *Adv. Mater.* **2016**, *28*, 857–863.
- (231) Zheng, G.; Lee, S. W.; Liang, Z.; Lee, H.-W.; Yan, K.; Yao, H.; Wang, H.; Li, W.; Chu, S.; Cui, Y. Interconnected Hollow Carbon Nanospheres for Stable Lithium Metal Anodes. *Nat. Nanotechnol.* **2014**, *9*, 618–623.
- (232) Zhang, Y.-J.; Bai, W.-Q.; Wang, X.-L.; Xia, X.-H.; Gu, C.-D.; Tu, J.-P. In Situ Confocal Microscopic Observation on Inhibiting the Dendrite Formation of a-CN_x/Li Electrode. *J. Mater. Chem. A* **2016**, *4*, 15597–15604.
- (233) Zhang, Y. J.; Liu, X. Y.; Bai, W. Q.; Tang, H.; Shi, S. J.; Wang, X. L.; Gu, C. D.; Tu, J. P. Magnetron Sputtering Amorphous Carbon Coatings on Metallic Lithium: Towards Promising Anodes for Lithium Secondary Batteries. *J. Power Sources* **2014**, *266*, 43–50.
- (234) Fan, L.; Zhuang, H.; Gao, L.; Lu, Y.; Archer, L. Regulating Li Deposition at Artificial Solid Electrolyte Interphases. *J. Mater. Chem. A* **2017**, *5*, 3483–3492.
- (235) Wang, L.; Wang, Q.; Jia, W.; Chen, S.; Gao, P.; Li, J. Li Metal Coated with Amorphous Li₃PO₄ via Magnetron Sputtering for Stable and Long-Cycle Life Lithium Metal Batteries. *J. Power Sources* **2017**, *342*, 175–182.
- (236) Choi, S. M.; Kang, I. S.; Sun, Y.-K.; Song, J.-H.; Chung, S.-M.; Kim, D.-W. Cycling Characteristics of Lithium Metal Batteries Assembled with a Surface Modified Lithium Electrode. *J. Power Sources* **2013**, *244*, 363–368.
- (237) Jang, I. C.; Ida, S.; Ishihara, T. Surface Coating Layer on Li Metal for Increased Cycle Stability of Li–O₂ Batteries. *J. Electrochem. Soc.* **2014**, *161*, A821–A826.
- (238) Bucur, C. B.; Lita, A.; Osada, N.; Muldoon, J. A Soft, Multilayered Lithium-Electrolyte Interface. *Energy Environ. Sci.* **2016**, *9*, 112–116.
- (239) Huang, J.-Q.; Zhuang, T.-Z.; Zhang, Q.; Peng, H.-J.; Chen, C.-M.; Wei, F. Permselective Graphene Oxide Membrane for Highly Stable and anti-self-discharge Lithium–Sulfur Batteries. *ACS Nano* **2015**, *9*, 3002–3011.
- (240) Huang, J.-Q.; Zhang, Q.; Peng, H.-J.; Liu, X.-Y.; Qian, W.-Z.; Wei, F. Ionic Shield for Polysulfides Towards Highly-Stable Lithium-Sulfur Batteries. *Energy Environ. Sci.* **2014**, *7*, 347–353.
- (241) Zhuang, T.-Z.; Huang, J.-Q.; Peng, H.-J.; He, L.-Y.; Cheng, X.-B.; Chen, C.-M.; Zhang, Q. Rational Integration of Polypropylene/Graphene Oxide/Nafion as Ternary-Layered Separator to Retard the Shuttle of Polysulfides for Lithium–Sulfur Batteries. *Small* **2016**, *12*, 381–389.
- (242) Song, J.; Lee, H.; Choo, M.-J.; Park, J.-K.; Kim, H.-T. Ionomer-Liquid Electrolyte Hybrid Ionic Conductor for High Cycling Stability of Lithium Metal Electrodes. *Sci. Rep.* **2015**, *5*, 14458.
- (243) Luo, J.; Lee, R.-C.; Jin, J.-T.; Weng, Y.-T.; Fang, C.-C.; Wu, N.-L. A Dual-Functional Polymer Coating on a Lithium Anode for Suppressing Dendrite Growth and Polysulfide Shuttling in Li–S Batteries. *Chem. Commun.* **2017**, *53*, 963–966.
- (244) Zheng, G.; Wang, C.; Pei, A.; Lopez, J.; Shi, F.; Chen, Z.; Sendek, A. D.; Lee, H.-W.; Lu, Z.; Schneider, H.; et al. High-Performance Lithium Metal Negative Electrode with a Soft and Flowable Polymer Coating. *ACS Energy Lett.* **2016**, *1*, 1247–1255.
- (245) Zhu, B.; Jin, Y.; Hu, X.; Zheng, Q.; Zhang, S.; Wang, Q.; Zhu, J. Poly(dimethylsiloxane) Thin Film as a Stable Interfacial Layer for High-Performance Lithium-Metal Battery Anodes. *Adv. Mater.* **2017**, *29*, 1603755.
- (246) Liu, K.; Pei, A.; Lee, H. R.; Kong, B.; Liu, N.; Lin, D.; Liu, Y.; Liu, C.; Hsu, P.-c.; Bao, Z.; et al. Lithium Metal Anodes with an Adaptive “Solid-Liquid” Interfacial Protective Layer. *J. Am. Chem. Soc.* **2017**, *139*, 4815–4820.
- (247) Liu, W.; Lin, D.; Pei, A.; Cui, Y. Stabilizing Lithium Metal Anodes by Uniform Li-ion Flux Distribution in Nanochannel Confinement. *J. Am. Chem. Soc.* **2016**, *138*, 15443–15450.
- (248) Liu, W.; Li, W.; Zhuo, D.; Zheng, G.; Lu, Z.; Liu, K.; Cui, Y. Core–shell Nanoparticle Coating as an Interfacial Layer for Dendrite-Free Lithium Metal Anodes. *ACS Cent. Sci.* **2017**, *3*, 135–140.
- (249) Yamada, Y.; Yamada, A. Review—Superconcentrated Electrolytes for Lithium Batteries. *J. Electrochem. Soc.* **2015**, *162*, A2406–A2423.
- (250) Ma, Q.; Fang, Z.; Liu, P.; Ma, J.; Qi, X. G.; Feng, W. F.; Nie, J.; Hu, Y. S.; Li, H.; Huang, X. J.; et al. Improved Cycling Stability of Lithium-Metal Anode with Concentrated Electrolytes Based on Lithium (fluorosulfonyl)(trifluoromethane-sulfonyl)imide. *ChemElectroChem* **2016**, *3*, 531–536.
- (251) Zheng, J.; Lochala, J. A.; Kwok, A.; Deng, Z. D.; Xiao, J. Research Progress Towards Understanding the Unique Interfaces between Concentrated Electrolytes and Electrodes for Energy Storage Applications. *Adv. Sci.* **2017**, *4*, 1700032.
- (252) Jeong, S.-K.; Seo, H.-Y.; Kim, D.-H.; Han, H.-K.; Kim, J.-G.; Lee, Y. B.; Iriyama, Y.; Abe, T.; Ogumi, Z. Suppression of Dendritic Lithium Formation by Using Concentrated Electrolyte Solutions. *Electrochem. Commun.* **2008**, *10*, 635–638.
- (253) Suo, L.; Hu, Y.-S.; Li, H.; Armand, M.; Chen, L. A New Class of Solvent-in-Salt Electrolyte for High-Energy Rechargeable Metallic Lithium Batteries. *Nat. Commun.* **2013**, *4*, 1481.
- (254) Yamada, Y.; Furukawa, K.; Sodeyama, K.; Kikuchi, K.; Yaegashi, M.; Tateyama, Y.; Yamada, A. Unusual Stability of Acetonitrile-Based Superconcentrated Electrolytes for Fast-Charging Lithium-Ion Batteries. *J. Am. Chem. Soc.* **2014**, *136*, 5039–5046.
- (255) Camacho-Forero, L. E.; Smith, T. W.; Balbuena, P. B. Effects of High and Low Salt Concentration in Electrolytes at Lithium–Metal Anode Surfaces. *J. Phys. Chem. C* **2017**, *121*, 182–194.
- (256) Wan, C.; Xu, S.; Hu, M. Y.; Cao, R.; Qian, J.; Qin, Z.; Liu, J.; Mueller, K. T.; Zhang, J.-G.; Hu, J. Z. Multinuclear Nmr Study of the Solid Electrolyte Interface Formed in Lithium Metal Batteries. *ACS Appl. Mater. Interfaces* **2017**, *9*, 14741–14748.
- (257) Qian, J.; Adams, B. D.; Zheng, J.; Xu, W.; Henderson, W. A.; Wang, J.; Bowden, M. E.; Xu, S.; Hu, J.; Zhang, J.-G. Anode-Free Rechargeable Lithium Metal Batteries. *Adv. Funct. Mater.* **2016**, *26*, 7094–7102.
- (258) Liu, B.; Xu, W.; Yan, P.; Sun, X.; Bowden, M. E.; Read, J.; Qian, J.; Mei, D.; Wang, C.-M.; Zhang, J.-G. Enhanced Cycling Stability of Rechargeable Li–O₂ Batteries using High-Concentration Electrolytes. *Adv. Funct. Mater.* **2016**, *26*, 605–613.
- (259) Yoon, H.; Howlett, P. C.; Best, A. S.; Forsyth, M.; MacFarlane, D. R. Fast Charge/Discharge of Li Metal Batteries using an Ionic Liquid Electrolyte. *J. Electrochem. Soc.* **2013**, *160*, A1629–A1637.
- (260) Togasaki, N.; Momma, T.; Osaka, T. Enhanced Cycling Performance of a Li Metal Anode in a Dimethylsulfoxide-Based Electrolyte Using Highly Concentrated Lithium Salt for a Lithium–Oxygen Battery. *J. Power Sources* **2016**, *307*, 98–104.
- (261) Suo, L.; Borodin, O.; Gao, T.; Olguin, M.; Ho, J.; Fan, X.; Luo, C.; Wang, C.; Xu, K. Water-in-Salt” Electrolyte Enables High-Voltage Aqueous Lithium-Ion Chemistries. *Science* **2015**, *350*, 938–943.
- (262) Tu, Z.; Nath, P.; Lu, Y.; Tikekar, M. D.; Archer, L. A. Nanostructured Electrolytes for Stable Lithium Electrodeposition in Secondary Batteries. *Acc. Chem. Res.* **2015**, *48*, 2947–2956.
- (263) Tikekar, M. D.; Archer, L. A.; Koch, D. L. Stabilizing Electrodeposition in Elastic Solid Electrolytes Containing Immobilized Anions. *Sci. Adv.* **2016**, *2*, e1600320.
- (264) Tikekar, M. D.; Archer, L. A.; Koch, D. L. Stability Analysis of Electrodeposition across a Structured Electrolyte with Immobilized Anions. *J. Electrochem. Soc.* **2014**, *161*, A847–A855.
- (265) Lu, Y.; Das, S. K.; Moganty, S. S.; Archer, L. A. Ionic Liquid-Nanoparticle Hybrid Electrolytes and Their Application in Secondary Lithium-Metal Batteries. *Adv. Mater.* **2012**, *24*, 4430–4435.
- (266) Lu, Y.; Tikekar, M.; Mohanty, R.; Hendrickson, K.; Ma, L.; Archer, L. A. Stable Cycling of Lithium Metal Batteries Using High Transference Number Electrolytes. *Adv. Energy Mater.* **2015**, *5*, 1402073.
- (267) Schaefer, J. L.; Yanga, D. A.; Archer, L. A. High Lithium Transference Number Electrolytes Via Creation of 3-Dimensional, Charged, Nanoporous Networks from Dense Functionalized Nanoparticle Composites. *Chem. Mater.* **2013**, *25*, 834–839.

- (268) Choudhury, S.; Mangal, R.; Agrawal, A.; Archer, L. A. A Highly Reversible Room-Temperature Lithium Metal Battery based on Crosslinked Hairy Nanoparticles. *Nat. Commun.* **2015**, *6*, 10101.
- (269) Li, Y.; Wong, K. W.; Dou, Q.; Ng, K. M. A Single-Ion Conducting and Shear-Thinning Polymer Electrolyte based on Ionic Liquid-Decorated Pmma Nanoparticles for Lithium-Metal Batteries. *J. Mater. Chem. A* **2016**, *4*, 18543–18550.
- (270) Zhou, D.; Liu, R.; He, Y.-B.; Li, F.; Liu, M.; Li, B.; Yang, Q.-H.; Cai, Q.; Kang, F. SiO₂ Hollow Nanosphere-Based Composite Solid Electrolyte for Lithium Metal Batteries to Suppress Lithium Dendrite Growth and Enhance Cycle Life. *Adv. Energy Mater.* **2016**, *6*, 1502214.
- (271) Tu, Z.; Kambe, Y.; Lu, Y.; Archer, L. A. Nanoporous Polymer-Ceramic Composite Electrolytes for Lithium Metal Batteries. *Adv. Energy Mater.* **2014**, *4*, 1300654.
- (272) Tu, Z.; Zachman, M. J.; Choudhury, S.; Wei, S.; Ma, L.; Yang, Y.; Kourkoutis, L. F.; Archer, L. A. Nanoporous Hybrid Electrolytes for High-Energy Batteries Based on Reactive Metal Anodes. *Adv. Energy Mater.* **2017**, *7*, 1602367.
- (273) Chen, W.; Yuan, J.-H.; Xia, X.-H. Characterization and Manipulation of the Electroosmotic Flow in Porous Anodic Alumina Membranes. *Anal. Chem.* **2005**, *77*, 8102–8108.
- (274) Siwy, Z.; Heins, E.; Harrell, C. C.; Kohli, P.; Martin, C. R. Conical-Nanotube Ion-Current Rectifiers: The Role of Surface Charge. *J. Am. Chem. Soc.* **2004**, *126*, 10850–10851.
- (275) Chen, R.; Qu, W.; Guo, X.; Li, L.; Wu, F. The Pursuit of Solid-State Electrolytes for Lithium Batteries: From Comprehensive Insight to Emerging Horizons. *Mater. Horiz.* **2016**, *3*, 487–516.
- (276) Gao, J.; Zhao, Y.-S.; Shi, S.-Q.; Li, H. Lithium-Ion Transport in Inorganic Solid State Electrolyte. *Chin. Phys. B* **2016**, *25*, 018211.
- (277) Thangadurai, V.; Narayanan, S.; Pinzaru, D. Garnet-Type Solid-State Fast Li Ion Conductors for Li Batteries: Critical Review. *Chem. Soc. Rev.* **2014**, *43*, 4714–4727.
- (278) Lin, Z.; Liang, C. Lithium-Sulfur Batteries: From Liquid to Solid Cells. *J. Mater. Chem. A* **2015**, *3*, 936–958.
- (279) Motoyama, M.; Ejiri, M.; Iriyama, Y. Modeling the Nucleation and Growth of Li at Metal Current Collector/Lipon Interfaces. *J. Electrochem. Soc.* **2015**, *162*, A7067–A7071.
- (280) Hu, Y.-S. Batteries: Getting Solid. *Nat. Energy* **2016**, *1*, 16042.
- (281) Manthiram, A.; Yu, X.; Wang, S. Lithium Battery Chemistries Enabled by Solid-State Electrolytes. *Nat. Rev. Mater.* **2017**, *2*, 16103.
- (282) Guo, Q.; Han, Y.; Wang, H.; Hong, X.; Zheng, C.; Liu, S.; Xie, K. Safer Lithium Metal Battery based on Advanced Ionic Liquid Gel Polymer Nonflammable Electrolytes. *RSC Adv.* **2016**, *6*, 101638–101644.
- (283) Bates, J. B.; Dudney, N. J.; Gruzalski, G. R.; Zuhr, R. A.; Choudhury, A.; Luck, C. F.; Robertson, J. D. Fabrication and Characterization of Amorphous Lithium Electrolyte Thin Films and Rechargeable Thin-Film Batteries. *J. Power Sources* **1993**, *43*, 103–110.
- (284) Alpen, U. v.; Rabenau, A.; Talat, G. H. Ionic Conductivity in Li₃n Single Crystals. *Appl. Phys. Lett.* **1977**, *30*, 621–623.
- (285) Boukamp, B. A.; Huggins, R. A. Lithium Ion Conductivity in Lithium Nitride. *Phys. Lett. A* **1976**, *58*, 231–233.
- (286) Murugan, R.; Thangadurai, V.; Weppner, W. Fast Lithium Ion Conduction in Garnet-Type Li₇La₃Zr₂O₁₂. *Angew. Chem., Int. Ed.* **2007**, *46*, 7778–7781.
- (287) Yan, X.; Li, Z.; Wen, Z.; Han, W. Li/Li₇La₃Zr₂O₁₂/LiFePO₄ All-Solid-State Battery with Ultrathin Nanoscale Solid Electrolyte. *J. Phys. Chem. C* **2017**, *121*, 1431–1435.
- (288) Mazza, D. Remarks on a Ternary Phase in the La₂O₃-Me₂O₅-Li₂O System (Me = Nb, Ta). *Mater. Lett.* **1988**, *7*, 205–207.
- (289) Taylor, B. E.; English, A. D.; Berzins, T. New Solid Ionic Conductors. *Mater. Res. Bull.* **1977**, *12*, 171–181.
- (290) Hong, H. Y. P. Crystal Structure and Ionic Conductivity of Li₁₄Zn(GeO₄)₄ and Other New Li⁺ Superionic Conductors. *Mater. Res. Bull.* **1978**, *13*, 117–124.
- (291) Tatsumisago, M.; Takano, R.; Tadanaga, K.; Hayashi, A. Preparation of Li₃BO₃-Li₂SO₄ Glass-Ceramic Electrolytes for All-Oxide Lithium Batteries. *J. Power Sources* **2014**, *270*, 603–607.
- (292) Kamaya, N.; Homma, K.; Yamakawa, Y.; Hirayama, M.; Kanno, R.; Yonemura, M.; Kamiyama, T.; Kato, Y.; Hama, S.; Kawamoto, K.; et al. A Lithium Superionic Conductor. *Nat. Mater.* **2011**, *10*, 682–686.
- (293) Kato, Y.; Hori, S.; Saito, T.; Suzuki, K.; Hirayama, M.; Mitsui, A.; Yonemura, M.; Iba, H.; Kanno, R. High-Power All-Solid-State Batteries Using Sulfide Superionic Conductors. *Nat. Energy* **2016**, *1*, 16030.
- (294) Mercier, R.; Malugani, J.-P.; Fahys, B.; Robert, G. Superionic Conduction in Li₂S - P₂S₅ - LiI - Glasses. *Solid State Ionics* **1981**, *5*, 663–666.
- (295) Kennedy, J. H.; Zhang, Z. Further Characterization of SiS₂-Li₂S Glasses Doped with Lithium Halide. *J. Electrochem. Soc.* **1988**, *135*, 859–862.
- (296) McGrogan, F. P.; Swamy, T.; Bishop, S. R.; Eggleton, E.; Porz, L.; Chen, X.; Chiang, Y.-M.; Van Vliet, K. J. Compliant yet Brittle Mechanical Behavior of Li₂S-P₂S₅ Lithium-Ion-Conducting Solid Electrolyte. *Adv. Energy Mater.* **2017**, *7*, 1602011.
- (297) Zeng, X.-X.; Yin, Y.-X.; Li, N.-W.; Du, W.-C.; Guo, Y.-G.; Wan, L.-J. Reshaping Lithium Plating/Stripping Behavior via Bifunctional Polymer Electrolyte for Room-Temperature Solid Li Metal Batteries. *J. Am. Chem. Soc.* **2016**, *138*, 15825–15828.
- (298) Ma, Q.; Zhang, H.; Zhou, C.; Zheng, L.; Cheng, P.; Nie, J.; Feng, W.; Hu, Y.-S.; Li, H.; Huang, X.; et al. Single Lithium-Ion Conducting Polymer Electrolytes Based on a Super-Delocalized Polyanion. *Angew. Chem., Int. Ed.* **2016**, *55*, 2521–2525.
- (299) Rangasamy, E.; Liu, Z.; Gobet, M.; Pilar, K.; Sahu, G.; Zhou, W.; Wu, H.; Greenbaum, S.; Liang, C. An Iodide-Based Li₇P₂S₈I Superionic Conductor. *J. Am. Chem. Soc.* **2015**, *137*, 1384–1387.
- (300) Liu, X.; Ding, G.; Zhou, X.; Li, S.; He, W.; Chai, J.; Pang, C.; Liu, Z.; Cui, G. An Interpenetrating Network Poly(Diethylene Glycol Carbonate)-Based Polymer Electrolyte for Solid State Lithium Batteries. *J. Mater. Chem. A* **2017**, *5*, 11124–11130.
- (301) Wenzel, S.; Leichtweiss, T.; Krüger, D.; Sann, J.; Janek, J. Interphase Formation on Lithium Solid Electrolytes—an in situ Approach to Study Interfacial Reactions by Photoelectron Spectroscopy. *Solid State Ionics* **2015**, *278*, 98–105.
- (302) Wenzel, S.; Randau, S.; Leichtweiß, T.; Weber, D. A.; Sann, J.; Zeier, W. G.; Janek, J. Direct Observation of the Interfacial Instability of the Fast Ionic Conductor Li₁₀GeP₂S₁₂ at the Lithium Metal Anode. *Chem. Mater.* **2016**, *28*, 2400–2407.
- (303) Richards, W. D.; Miara, L. J.; Wang, Y.; Kim, J. C.; Ceder, G. Interface Stability in Solid-State Batteries. *Chem. Mater.* **2016**, *28*, 266–273.
- (304) Lepley, N. D.; Holzwarth, N. A. W.; Du, Y. A. Structures, Li⁺ Mobilities, and Interfacial Properties of Solid Electrolytes Li₃PS₄ and Li₃PO₄ from First Principles. *Phys. Rev. B: Condens. Matter Mater. Phys.* **2013**, *88*, 104103.
- (305) Li, Y.; Xu, B.; Xu, H.; Duan, H.; Lü, X.; Xin, S.; Zhou, W.; Xue, L.; Fu, G.; Manthiram, A.; et al. Hybrid Polymer/Garnet Electrolyte with a Small Interfacial Resistance for Lithium-Ion Batteries. *Angew. Chem., Int. Ed.* **2017**, *56*, 753–756.
- (306) Zhang, H.; Li, C.; Piszczyk, M.; Coya, E.; Rojo, T.; Rodriguez-Martinez, L. M.; Armand, M.; Zhou, Z. Single Lithium-Ion Conducting Solid Polymer Electrolytes: Advances and Perspectives. *Chem. Soc. Rev.* **2017**, *46*, 797–815.
- (307) Wei, S.; Choudhury, S.; Xu, J.; Nath, P.; Tu, Z.; Archer, L. A. Highly Stable Sodium Batteries Enabled by Functional Ionic Polymer Membranes. *Adv. Mater.* **2017**, *29*, 1605512.
- (308) Lu, Q.; He, Y.-B.; Yu, Q.; Li, B.; Kaneti, Y. V.; Yao, Y.; Kang, F.; Yang, Q.-H. Dendrite-Free, High-Rate, Long-Life Lithium Metal Batteries with a 3D Cross-Linked Network Polymer Electrolyte. *Adv. Mater.* **2017**, *29*, 1604460.
- (309) Sun, C.; Liu, J.; Gong, Y.; Wilkinson, D. P.; Zhang, J. Recent Advances in All-Solid-State Rechargeable Lithium Batteries. *Nano Energy* **2017**, *33*, 363–386.
- (310) Chen, N.; Dai, Y.; Xing, Y.; Wang, L.; Guo, C.; Chen, R.; Guo, S.; Wu, F. Biomimetic Ant-Nest Ionogel Electrolyte Boosts the

- Performance of Dendrite-Free Lithium Batteries. *Energy Environ. Sci.* **2017**, *10*, 1660–1667.
- (311) Shim, J.; Kim, H. J.; Kim, B. G.; Kim, Y. S.; Kim, D.-G.; Lee, J.-C. 2D Boron Nitride Nanoflakes as a Multifunctional Additive in Gel Polymer Electrolyte for Safe, Long Cycle Life and High Rate Lithium Metal Batteries. *Energy Environ. Sci.* **2017**, DOI: 10.1039/C7EE01095H.
- (312) Varzi, A.; Raccichini, R.; Passerini, S.; Scrosati, B. Challenges and Prospects of the Role of Solid Electrolytes in the Revitalization of Lithium Metal Batteries. *J. Mater. Chem. A* **2016**, *4*, 17251–17259.
- (313) Knauth, P. Inorganic Solid Li Ion Conductors: An Overview. *Solid State Ionics* **2009**, *180*, 911–916.
- (314) Zhang, J.; Zhao, N.; Zhang, M.; Li, Y.; Chu, P. K.; Guo, X.; Di, Z.; Wang, X.; Li, H. Flexible and Ion-Conducting Membrane Electrolytes for Solid-State Lithium Batteries: Dispersion of Garnet Nanoparticles in Insulating Polyethylene Oxide. *Nano Energy* **2016**, *28*, 447–454.
- (315) Jung, Y.-C.; Kim, S.-K.; Kim, M.-S.; Lee, J.-H.; Han, M.-S.; Kim, D.-H.; Shin, W.-C.; Ue, M.; Kim, D.-W. Ceramic Separators Based on Li⁺-Conducting Inorganic Electrolyte for High-Performance Lithium-Ion Batteries with Enhanced Safety. *J. Power Sources* **2015**, *293*, 675–683.
- (316) Lin, D.; Liu, W.; Liu, Y.; Lee, H. R.; Hsu, P.-C.; Liu, K.; Cui, Y. High Ionic Conductivity of Composite Solid Polymer Electrolyte via in situ Synthesis of Monodispersed SiO₂ Nanospheres in Poly(Ethylene Oxide). *Nano Lett.* **2016**, *16*, 459–465.
- (317) Liu, Z.; Fu, W.; Payzant, E. A.; Yu, X.; Wu, Z.; Dudney, N. J.; Kiggans, J.; Hong, K.; Rondinone, A. J.; Liang, C. Anomalous High Ionic Conductivity of Nanoporous B-Li₃PS₄. *J. Am. Chem. Soc.* **2013**, *135*, 975–978.
- (318) Yao, X.; Liu, D.; Wang, C.; Long, P.; Peng, G.; Hu, Y.-S.; Li, H.; Chen, L.; Xu, X. High-Energy All-Solid-State Lithium Batteries with Ultralong Cycle Life. *Nano Lett.* **2016**, *16*, 7148–7154.
- (319) Liu, W.; Liu, N.; Sun, J.; Hsu, P.-C.; Li, Y.; Lee, H.-W.; Cui, Y. Ionic Conductivity Enhancement of Polymer Electrolytes with Ceramic Nanowire Fillers. *Nano Lett.* **2015**, *15*, 2740–2745.
- (320) Khurana, R.; Schaefer, J. L.; Archer, L. A.; Coates, G. W. Suppression of Lithium Dendrite Growth Using Cross-Linked Polyethylene/Poly(Ethylene Oxide) Electrolytes: A New Approach for Practical Lithium-Metal Polymer Batteries. *J. Am. Chem. Soc.* **2014**, *136*, 7395–7402.
- (321) Fu, K.; Gong, Y.; Dai, J.; Gong, A.; Han, X.; Yao, Y.; Wang, C.; Wang, Y.; Chen, Y.; Yan, C.; et al. Flexible, Solid-State, Ion-Conducting Membrane with 3D Garnet Nanofiber Networks for Lithium Batteries. *Proc. Natl. Acad. Sci. U. S. A.* **2016**, *113*, 7094–7099.
- (322) Liu, W.; Lee, S. W.; Lin, D.; Shi, F.; Wang, S.; Sendek, A. D.; Cui, Y. Enhancing Ionic Conductivity in Composite Polymer Electrolytes with Well-Aligned Ceramic nanowires. *Nat. Energy* **2017**, *2*, 17035.
- (323) Kalnaus, S.; Tenhaeff, W. E.; Sakamoto, J.; Sabau, A. S.; Daniel, C.; Dudney, N. J. Analysis of Composite Electrolytes with Sintered Reinforcement Structure for Energy Storage Applications. *J. Power Sources* **2013**, *241*, 178–185.
- (324) Lee, S. S.; Lim, Y. J.; Kim, H. W.; Kim, J.-K.; Jung, Y.-G.; Kim, Y. Electrochemical Properties of a Ceramic-Polymer-Composite-Solid Electrolyte for Li-ion Batteries. *Solid State Ionics* **2016**, *284*, 20–24.
- (325) Zheng, J.; Tang, M.; Hu, Y.-Y. Lithium Ion Pathway within Li₇La₃Zr₂O₁₂-Polyethylene Oxide Composite Electrolytes. *Angew. Chem., Int. Ed.* **2016**, *55*, 12538–12542.
- (326) Busche, M. R.; Drossel, T.; Leichtweiss, T.; Weber, D. A.; Falk, M.; Schneider, M.; Reich, M.-L.; Sommer, H.; Adelhelm, P.; Janek, J. Dynamic Formation of a Solid-Liquid Electrolyte Interphase and Its Consequences for Hybrid-Battery Concepts. *Nat. Chem.* **2016**, *8*, 426–434.
- (327) Choi, Y. S.; Lee, Y.-S.; Oh, K. H.; Cho, Y. W. Interface-Enhanced Li ion Conduction in a LiBH₄-SiO₂ Solid Electrolyte. *Phys. Chem. Chem. Phys.* **2016**, *18*, 22540–22547.
- (328) Zhou, W.; Wang, S.; Li, Y.; Xin, S.; Manthiram, A.; Goodenough, J. B. Plating a Dendrite-Free Lithium Anode with a Polymer/Ceramic/Polymer Sandwich Electrolyte. *J. Am. Chem. Soc.* **2016**, *138*, 9385–9388.
- (329) Tian, Y.; Shi, T.; Richards, W. D.; Li, J.; Kim, J. C.; Bo, S.-H.; Ceder, G. Compatibility Issues between Electrodes and Electrolytes in Solid-State Batteries. *Energy Environ. Sci.* **2017**, *10*, 1150–1166.
- (330) Wu, B.; Wang, S.; Evans, W. J., IV; Deng, D. Z.; Yang, J.; Xiao, J. Interfacial Behaviours between Lithium Ion Conductors and Electrode Materials in Various Battery Systems. *J. Mater. Chem. A* **2016**, *4*, 15266–15280.
- (331) Xin, S.; You, Y.; Wang, S.; Gao, H.-C.; Yin, Y.-X.; Guo, Y.-G. Solid-State Lithium Metal Batteries Promoted by Nanotechnology: Progress and Prospects. *ACS Energy Lett.* **2017**, *2*, 1385–1394.
- (332) Chinnam, P. R.; Wunder, S. L. Engineered Interfaces in Hybrid Ceramic–Polymer Electrolytes for Use in All-Solid-State Li Batteries. *ACS Energy Lett.* **2017**, *2*, 134–138.
- (333) Fu, K.; Gong, Y.; Li, Y.; Xu, S.; Wen, Y.; Zhang, L.; Wang, C.; Pastel, G.; Dai, J.; Liu, B. Three-Dimensional Bilayer Garnet Solid Electrolyte Based High Energy Density Lithium Metal-Sulfur Batteries. *Energy Environ. Sci.* **2017**, *10*, 1568–1575.
- (334) Han, X.; Gong, Y.; Fu, K.; He, X.; Hitz, G. T.; Dai, J.; Pearse, A.; Liu, B.; Wang, H.; Rubloff, G.; et al. Negating Interfacial Impedance in Garnet-Based Solid-State Li Metal Batteries. *Nat. Mater.* **2017**, *16*, 572–579.
- (335) Luo, W.; Gong, Y.; Zhu, Y.; Fu, K. K.; Dai, J.; Lacey, S. D.; Wang, C.; Liu, B.; Han, X.; Mo, Y.; et al. Transition from Superlithiophobicity to Superlithiophilicity of Garnet Solid-State Electrolyte. *J. Am. Chem. Soc.* **2016**, *138*, 12258–12262.
- (336) Wang, C.; Gong, Y.; Liu, B.; Fu, K.; Yao, Y.; Hitz, E.; Li, Y.; Dai, J.; Xu, S.; Luo, W.; et al. Conformal, Nanoscale ZnO Surface Modification of Garnet-based Solid-State Electrolyte for Lithium Metal Anodes. *Nano Lett.* **2017**, *17*, 565–571.
- (337) Fu, K.; Gong, Y.; Liu, B.; Zhu, Y.; Xu, S.; Yao, Y.; Luo, W.; Wang, C.; Lacey, S. D.; Dai, J.; et al. Toward Garnet Electrolyte-Based Li Metal Batteries: An Ultrathin, Highly Effective, Artificial Solid-State Electrolyte/Metallic Li Interface. *Sci. Adv.* **2017**, *3*, e1601659.
- (338) Li, Y.; Zhou, W.; Chen, X.; Lü, X.; Cui, Z.; Xin, S.; Xue, L.; Jia, Q.; Goodenough, J. B. Mastering the Interface for Advanced All-Solid-State Lithium Rechargeable Batteries. *Proc. Natl. Acad. Sci. U. S. A.* **2016**, *113*, 13313–13317.
- (339) Ishiguro, K.; Nakata, Y.; Matsui, M.; Uechi, I.; Takeda, Y.; Yamamoto, O.; Imanishi, N. Stability of Nb-doped Cubic Li₇La₃Zr₂O₁₂ with Lithium Metal. *J. Electrochem. Soc.* **2013**, *160*, A1690–A1693.
- (340) Ishiguro, K.; Nemori, H.; Sunahiro, S.; Nakata, Y.; Sudo, R.; Matsui, M.; Takeda, Y.; Yamamoto, O.; Imanishi, N. Ta-Doped Li₇La₃Zr₂O₁₂ for Water-Stable Lithium Electrode of Lithium-Air Batteries. *J. Electrochem. Soc.* **2014**, *161*, A668–A674.
- (341) Sudo, R.; Nakata, Y.; Ishiguro, K.; Matsui, M.; Hirano, A.; Takeda, Y.; Yamamoto, O.; Imanishi, N. Interface Behavior between Garnet-Type Lithium-Conducting Solid Electrolyte and Lithium Metal. *Solid State Ionics* **2014**, *262*, 151–154.
- (342) Tsai, C.-L.; Roddatis, V.; Chandran, C. V.; Ma, Q.; Uhlenbruck, S.; Bram, M.; Heitjans, P.; Guillot, O. Li₇La₃Zr₂O₁₂ Interface Modification for Li Dendrite Prevention. *ACS Appl. Mater. Interfaces* **2016**, *8*, 10617–10626.
- (343) Xu, B.; Li, W.; Duan, H.; Wang, H.; Guo, Y.; Li, H.; Liu, H. Li₃po₄-Added Garnet-Type Li_{6.5}La₃Zr_{1.5}Ta_{0.5}O₁₂ for Li-Dendrite Suppression. *J. Power Sources* **2017**, *354*, 68–73.
- (344) Liu, B.; Gong, Y.; Fu, K.; Han, X.; Yao, Y.; Pastel, G.; Yang, C.; Xie, H.; Wachsman, E. D.; Hu, L. Garnet Solid Electrolyte Protected Li-Metal Batteries. *ACS Appl. Mater. Interfaces* **2017**, *9*, 18809–18815.
- (345) Zhang, X.; Cheng, X.; Zhang, Q. Nanostructured Energy Materials for Electrochemical Energy Conversion and Storage: A Review. *J. Energy Chem.* **2016**, *25*, 967–984.
- (346) Li, Z.; Huang, J.; Yann Liaw, B.; Metzler, V.; Zhang, J. A Review of Lithium Deposition in Lithium-Ion and Lithium Metal Secondary Batteries. *J. Power Sources* **2014**, *254*, 168–182.
- (347) Liang, Z.; Zheng, G.; Liu, C.; Liu, N.; Li, W.; Yan, K.; Yao, H.; Hsu, P.-C.; Chu, S.; Cui, Y. Polymer Nanofiber-Guided Uniform

- Lithium Deposition for Battery Electrodes. *Nano Lett.* **2015**, *15*, 2910–2916.
- (348) Matsuda, S.; Kubo, Y.; Uosaki, K.; Nakanishi, S. Insulative Microfiber 3D Matrix as a Host Material Minimizing Volume Change of the Anode of Li Metal Batteries. *ACS Energy Lett.* **2017**, *2*, 924–929.
- (349) Zhang, Z.; Peng, Z.; Zheng, J.; Wang, S.; Liu, Z.; Bi, Y.; Chen, Y.; Wu, G.; Li, H.; Cui, P.; et al. The Long Life-Span of a Li-Metal Anode Enabled by a Protective Layer Based on the Pyrolyzed N-Doped Binder Network. *J. Mater. Chem. A* **2017**, *5*, 9339–9349.
- (350) Zhang, R.; Chen, X. R.; Chen, X.; Cheng, X. B.; Zhang, X. Q.; Yan, C.; Zhang, Q. Lithiophilic Sites in Doped Graphene Guide Uniform Lithium Nucleation for Dendrite-Free Lithium Metal Anodes. *Angew. Chem., Int. Ed.* **2017**, *56*, 7764–7768.
- (351) Liu, W.; Mi, Y.; Weng, Z.; Zhong, Y.; Wu, Z.; Wang, H. Functional Metal-Organic Framework Boosting Lithium Metal Anode Performance via Chemical Interactions. *Chem. Sci.* **2017**, *8*, 4285–4291.
- (352) Cheng, X.-B.; Hou, T.-Z.; Zhang, R.; Peng, H.-J.; Zhao, C.-Z.; Huang, J.-Q.; Zhang, Q. Dendrite-Free Lithium Deposition Induced by Uniformly Distributed Lithium Ions for Efficient Lithium Metal Batteries. *Adv. Mater.* **2016**, *28*, 2888–2895.
- (353) Chang, C.-H.; Chung, S.-H.; Manthiram, A. Dendrite-Free Lithium Anode via a Homogenous Li-ion Distribution Enabled by a Kimwipe Paper. *Adv. Sust. Syst.* **2017**, *1*, 1600034.
- (354) Zhang, Y.; Luo, W.; Wang, C.; Li, Y.; Chen, C.; Song, J.; Dai, J.; Hitz, E. M.; Xu, S.; Yang, C.; et al. High-Capacity, Low-Tortuosity, and Channel-Guided Lithium Metal Anode. *Proc. Natl. Acad. Sci. U. S. A.* **2017**, *114*, 3584–3589.
- (355) Liu, Y.; Lin, D.; Liang, Z.; Zhao, J.; Yan, K.; Cui, Y. Lithium-Coated Polymeric Matrix as a Minimum Volume-Change and Dendrite-Free Lithium Metal Anode. *Nat. Commun.* **2016**, *7*, 10992.
- (356) Liang, Z.; Lin, D.; Zhao, J.; Lu, Z.; Liu, Y.; Liu, C.; Lu, Y.; Wang, H.; Yan, K.; Tao, X.; et al. Composite Lithium Metal Anode by Melt Infusion of Lithium into a 3D Conducting Scaffold with Lithiophilic Coating. *Proc. Natl. Acad. Sci. U. S. A.* **2016**, *113*, 2862–2867.
- (357) Lin, D.; Liu, Y.; Liang, Z.; Lee, H.-W.; Sun, J.; Wang, H.; Yan, K.; Xie, J.; Cui, Y. Layered Reduced Graphene Oxide with Nanoscale Interlayer Gaps as a Stable Host for Lithium Metal Anodes. *Nat. Nanotechnol.* **2016**, *11*, 626–632.
- (358) Jin, C.; Sheng, O.; Luo, J.; Yuan, H.; Fang, C.; Zhang, W.; Huang, H.; Gan, Y.; Xia, Y.; Liang, C.; et al. 3D Lithium Metal Embedded within Lithiophilic Porous Matrix for Stable Lithium Metal Batteries. *Nano Energy* **2017**, *37*, 177–186.
- (359) Chi, S. S.; Liu, Y.; Song, W. L.; Fan, L. Z.; Zhang, Q. Prestoring Lithium into Stable 3D Nickel Foam Host as Dendrite-Free Lithium Metal Anode. *Adv. Funct. Mater.* **2017**, *27*, 1700348.
- (360) Lin, D.; Zhao, J.; Sun, J.; Yao, H.; Liu, Y.; Yan, K.; Cui, Y. Three-Dimensional Stable Lithium Metal Anode with Nanoscale Lithium Islands Embedded in Ionically Conductive Solid Matrix. *Proc. Natl. Acad. Sci. U. S. A.* **2017**, *114*, 4613–4618.
- (361) Cheng, X.-B.; Peng, H.-J.; Huang, J.-Q.; Zhang, R.; Zhao, C.-Z.; Zhang, Q. Dual-Phase Lithium Metal Anode Containing a Polysulfide-Induced Solid Electrolyte Interphase and Nanostructured Graphene Framework for Lithium–Sulfur Batteries. *ACS Nano* **2015**, *9*, 6373–6382.
- (362) Heine, J.; Rodehorst, U.; Qi, X.; Badillo, J. P.; Hartnig, C.; Wietelmann, U.; Winter, M.; Bieker, P. Using Polyisobutylene as a Non-Fluorinated Binder for Coated Lithium Powder (CLiP) Electrodes. *Electrochim. Acta* **2014**, *138*, 288–293.
- (363) Heine, J.; Krüger, S.; Hartnig, C.; Wietelmann, U.; Winter, M.; Bieker, P. Coated Lithium Powder (CLiP) Electrodes for Lithium-Metal Batteries. *Adv. Energy Mater.* **2014**, *4*, 1300815.
- (364) Kim, J. S.; Yoon, W. Y. Improvement in Lithium Cycling Efficiency by Using Lithium Powder Anode. *Electrochim. Acta* **2004**, *50*, 531–534.
- (365) Ryoo, M.-H.; Lee, Y. M.; Lee, Y.; Winter, M.; Bieker, P. Mechanical Surface Modification of Lithium Metal: Towards Improved Li Metal Anode Performance by Directed Li Plating. *Adv. Funct. Mater.* **2015**, *25*, 834–841.
- (366) Park, J.; Jeong, J.; Lee, Y.; Oh, M.; Ryoo, M.-H.; Lee, Y. M. Micro-Patterned Lithium Metal Anodes with Suppressed Dendrite Formation for Post Lithium-Ion Batteries. *Adv. Mater. Interfaces* **2016**, *3*, 1600140.
- (367) Li, Y.; Jiao, J.; Bi, J.; Wang, X.; Wang, Z.; Chen, L. Controlled Deposition of Li Metal. *Nano Energy* **2017**, *32*, 241–246.
- (368) Yang, C.-P.; Yin, Y.-X.; Zhang, S.-F.; Li, N.-W.; Guo, Y.-G. Accommodating Lithium into 3D Current Collectors with a Submicron Skeleton Towards Long-Life Lithium Metal Anodes. *Nat. Commun.* **2015**, *6*, 8058.
- (369) Zhang, X.; Wang, W.; Wang, A.; Huang, Y.; Yuan, K.; Yu, Z.; Qiu, J.; Yang, Y. Improved Cycle Stability and High Security of Li-B Alloy Anode for Lithium-Sulfur Battery. *J. Mater. Chem. A* **2014**, *2*, 11660–11665.
- (370) Jin, S.; Xin, S.; Wang, L.; Du, Z.; Cao, L.; Chen, J.; Kong, X.; Gong, M.; Lu, J.; Zhu, Y.; et al. Covalently Connected Carbon Nanostructures for Current Collectors in Both the Cathode and Anode of Li–S Batteries. *Adv. Mater.* **2016**, *28*, 9094–9102.
- (371) Zhang, D.; Zhou, Y.; Liu, C.; Fan, S. The Effect of the Carbon Nanotube Buffer Layer on the Performance of a Li Metal Battery. *Nanoscale* **2016**, *8*, 11161–11167.
- (372) Zhang, Y.; Liu, B.; Hitz, E.; Luo, W.; Yao, Y.; Li, Y.; Dai, J.; Chen, C.; Wang, Y.; Yang, C.; et al. A Carbon-Based 3D Current Collector with Surface Protection for Li Metal Anode. *Nano Res.* **2017**, *10*, 1356–1365.
- (373) Matsuda, S.; Kubo, Y.; Uosaki, K.; Nakanishi, S. Lithium-Metal Deposition/Dissolution within Internal Space of CNT 3D Matrix Results in Prolonged Cycle of Lithium-Metal Negative Electrode. *Carbon* **2017**, *119*, 119–123.
- (374) Mukherjee, R.; Thomas, A. V.; Datta, D.; Singh, E.; Li, J.; Eksik, O.; Shenoy, V. B.; Koratkar, N. Defect-Induced Plating of Lithium Metal within Porous Graphene Networks. *Nat. Commun.* **2014**, *5*, 3710.
- (375) Kang, H.-K.; Woo, S.-G.; Kim, J.-H.; Yu, J.-S.; Lee, S.-R.; Kim, Y.-J. Few-Layer Graphene Island Seeding for Dendrite-Free Li Metal Electrodes. *ACS Appl. Mater. Interfaces* **2016**, *8*, 26895–26901.
- (376) Zhang, Y.-j.; Xia, X.-h.; Wang, D.-h.; Wang, X.-l.; Gu, C.-d.; Tu, J.-p. Integrated Reduced Graphene Oxide Multilayer/Li Composite Anode for Rechargeable Lithium Metal Batteries. *RSC Adv.* **2016**, *6*, 11657–11664.
- (377) Zhamu, A.; Chen, G.; Liu, C.; Neff, D.; Fang, Q.; Yu, Z.; Xiong, W.; Wang, Y.; Wang, X.; Jang, B. Z. Reviving Rechargeable Lithium Metal Batteries: Enabling Next-Generation High-Energy and High-Power Cells. *Energy Environ. Sci.* **2012**, *5*, 5701–5707.
- (378) Raji, A.-R. O.; Villegas Salvatierra, R.; Kim, N. D.; Fan, X.; Li, Y.; Silva, G. A. L.; Sha, J.; Tour, J. M. Lithium Batteries with Nearly Maximum Metal Storage. *ACS Nano* **2017**, *11*, 6362–6369.
- (379) Zhang, A.; Fang, X.; Shen, C.; Liu, Y.; Zhou, C. A Carbon Nanofiber Network for Stable Lithium Metal Anodes with High Coulombic Efficiency and Long Cycle Life. *Nano Res.* **2016**, *9*, 3428–3436.
- (380) Ji, X.; Liu, D.-Y.; Prendiville, D. G.; Zhang, Y.; Liu, X.; Stucky, G. D. Spatially Heterogeneous Carbon-Fiber Papers as Surface Dendrite-Free Current Collectors for Lithium Deposition. *Nano Today* **2012**, *7*, 10–20.
- (381) Zuo, T.-T.; Wu, X.-W.; Yang, C.-P.; Yin, Y.-X.; Ye, H.; Li, N.-W.; Guo, Y.-G. Graphitized Carbon Fibers as Multifunctional 3D Current Collectors for High Areal Capacity Li Anodes. *Adv. Mater.* **2017**, *29*, 1700389.
- (382) Kang, H.-K.; Woo, S.-G.; Kim, J.-H.; Lee, S.-R.; Kim, Y.-J. Conductive Porous Carbon Film as a Lithium Metal Storage Medium. *Electrochim. Acta* **2015**, *176*, 172–178.
- (383) Ye, H.; Xin, S.; Yin, Y.-X.; Li, J.-Y.; Guo, Y.-G.; Wan, L.-J. Stable Li Plating/Stripping Electrochemistry Realized by a Hybrid Li Reservoir in Spherical Carbon Granules with 3D Conducting Skeletons. *J. Am. Chem. Soc.* **2017**, *139*, 5916–5922.

- (384) Xie, K.; Wei, W.; Yuan, K.; Lu, W.; Guo, M.; Li, Z.; Song, Q.; Liu, X.; Wang, J.-G.; Shen, C. Toward Dendrite-Free Lithium Deposition via Structural and Interfacial Synergistic Effects of 3D Graphene@Ni Scaffold. *ACS Appl. Mater. Interfaces* **2016**, *8*, 26091–26097.
- (385) Yun, Q.; He, Y.-B.; Lv, W.; Zhao, Y.; Li, B.; Kang, F.; Yang, Q.-H. Chemical Dealloying Derived 3D Porous Current Collector for Li Metal Anodes. *Adv. Mater.* **2016**, *28*, 6932–6939.
- (386) Zhang, Z.; Xu, X.; Wang, S.; Peng, Z.; Liu, M.; Zhou, J.; Shen, C.; Wang, D. Li₂O-Reinforced Cu Nanoclusters as Porous Structure for Dendrite-Free and Long-Lifespan Lithium Metal Anode. *ACS Appl. Mater. Interfaces* **2016**, *8*, 26801–26808.
- (387) Li, Q.; Zhu, S.; Lu, Y. 3D Porous Cu Current Collector/Li-Metal Composite Anode for Stable Lithium-Metal Batteries. *Adv. Funct. Mater.* **2017**, *27*, 1606422.
- (388) Lee, H.; Song, J.; Kim, Y.-J.; Park, J.-K.; Kim, H.-T. Structural Modulation of Lithium Metal-Electrolyte Interface with Three-Dimensional Metallic Interlayer for High-Performance Lithium Metal Batteries. *Sci. Rep.* **2016**, *6*, 30830.
- (389) Pan, Y.; Chou, S.; Liu, H. K.; Dou, S. X. Functional Membrane Separators for Next-Generation High-Energy Rechargeable Batteries. *Natl. Sci. Rev.* **2017**, DOI: 10.1093/nsr/nwx037.
- (390) Liu, Y.; Liu, Q.; Xin, L.; Liu, Y.; Yang, F.; Stach, E. A.; Xie, J. Making Li-Metal Electrodes Rechargeable by Controlling the Dendrite Growth Direction. *Nat. Energy* **2017**, *2*, 17083.
- (391) Shi, C.; Dai, J.; Shen, X.; Peng, L.; Li, C.; Wang, X.; Zhang, P.; Zhao, J. A High-Temperature Stable Ceramic-Coated Separator Prepared with Polyimide Binder/Al₂O₃ Particles for Lithium-Ion Batteries. *J. Membr. Sci.* **2016**, *517*, 91–99.
- (392) Dai, J.; Shi, C.; Li, C.; Shen, X.; Peng, L.; Wu, D.; Sun, D.; Zhang, P.; Zhao, J. A Rational Design of Separator with Substantially Enhanced Thermal Features for Lithium-Ion Batteries by the Polydopamine-Ceramic Composite Modification of Polyolefin Membranes. *Energy Environ. Sci.* **2016**, *9*, 3252–3261.
- (393) Tung, S.-O.; Ho, S.; Yang, M.; Zhang, R.; Kotov, N. A. A Dendrite-Suppressing Composite Ion Conductor from Aramid Nanofibres. *Nat. Commun.* **2015**, *6*, 6152.
- (394) Liu, K.; Bai, P.; Bazant, M. Z.; Wang, C.-A.; Li, J. Soft Non-Porous Separator and Its Effectiveness in Stabilizing Li Metal Anode Cycling at 10 mA/cm² Observed in-situ in a Capillary Cell. *J. Mater. Chem. A* **2017**, *5*, 4300–4307.
- (395) Kim, J.-K.; Kim, D. H.; Joo, S. H.; Choi, B.; Cha, A.; Kim, K. M.; Kwon, T.-H.; Kwak, S. K.; Kang, S. J.; Jin, J. Hierarchical Chitin Fibers with Aligned Nanofibrillar Architectures: A Nonwoven-Mat Separator for Lithium Metal Batteries. *ACS Nano* **2017**, *11*, 6114–6121.
- (396) Hao, X.; Zhu, J.; Jiang, X.; Wu, H.; Qiao, J.; Sun, W.; Wang, Z.; Sun, K. Ultrastrong Polyoxazole Nanofiber Membranes for Dendrite-Proof and Heat-Resistant Battery Separators. *Nano Lett.* **2016**, *16*, 2981–2987.
- (397) Ferrese, A.; Newman, J. Mechanical Deformation of a Lithium-Metal Anode Due to a very Stiff Separator. *J. Electrochem. Soc.* **2014**, *161*, A1350–A1359.
- (398) Shin, W.-K.; Kannan, A. G.; Kim, D.-W. Effective Suppression of Dendritic Lithium Growth Using an Ultrathin Coating of Nitrogen and Sulfur Codoped Graphene Nanosheets on Polymer Separator for Lithium Metal Batteries. *ACS Appl. Mater. Interfaces* **2015**, *7*, 23700–23707.
- (399) Na, W.; Lee, A. S.; Lee, J. H.; Hwang, S. S.; Kim, E.; Hong, S. M.; Koo, C. M. Lithium Dendrite Suppression with UV-Curable Polysilsesquioxane Separator Binders. *ACS Appl. Mater. Interfaces* **2016**, *8*, 12852–12858.
- (400) Luo, W.; Zhou, L.; Fu, K.; Yang, Z.; Wan, J.; Manno, M.; Yao, Y.; Zhu, H.; Yang, B.; Hu, L. A Thermally Conductive Separator for Stable Li Metal Anodes. *Nano Lett.* **2015**, *15*, 6149–6154.
- (401) Ansari, Y.; Guo, B.; Cho, J. H.; Park, K.; Song, J.; Ellison, C. J.; Goodenough, J. B. Low-Cost, Dendrite-Blocking Polymer-Sb₂O₃ Separators for Lithium and Sodium Batteries. *J. Electrochem. Soc.* **2014**, *161*, A1655–A1661.
- (402) Zhu, X.; Jiang, X.; Ai, X.; Yang, H.; Cao, Y. A Highly Thermostable Ceramic-Grafted Microporous Polyethylene Separator for Safer Lithium-Ion Batteries. *ACS Appl. Mater. Interfaces* **2015**, *7*, 24119–24126.
- (403) Chi, M.; Shi, L.; Wang, Z.; Zhu, J.; Mao, X.; Zhao, Y.; Zhang, M.; Sun, L.; Yuan, S. Excellent Rate Capability and Cycle Life of Li Metal Batteries with ZrO₂/Poss Multilayer-Assembled PE Separators. *Nano Energy* **2016**, *28*, 1.
- (404) Zahn, R.; Lagadec, M. F.; Hess, M.; Wood, V. Improving Ionic Conductivity and Lithium-Ion Transference Number in Lithium-Ion Battery Separators. *ACS Appl. Mater. Interfaces* **2016**, *8*, 32637–32642.
- (405) Yang, L.; Zeng, J.; Ding, B.; Xu, C.; Lee, J. Y. Lithium Salt Inclusion as a Strategy for Improving the Li⁺ Conductivity of Nafion Membranes in Aprotic Systems. *Adv. Mater. Interfaces* **2016**, *3*, 1600660.
- (406) Yu, B.-C.; Park, K.; Jang, J.-H.; Goodenough, J. B. Cellulose-Based Porous Membrane for Suppressing Li Dendrite Formation in Lithium–Sulfur Battery. *ACS Energy Lett.* **2016**, *1*, 633–637.
- (407) Mao, X.; Shi, L.; Zhang, H.; Wang, Z.; Zhu, J.; Qiu, Z.; Zhao, Y.; Zhang, M.; Yuan, S. Polyethylene Separator Activated by Hybrid Coating Improving Li⁺ Ion Transference Number and Ionic Conductivity for Li-Metal Battery. *J. Power Sources* **2017**, *342*, 816–824.
- (408) Wu, H.; Zhuo, D.; Kong, D.; Cui, Y. Improving Battery Safety by Early Detection of Internal Shorting with a Bifunctional Separator. *Nat. Commun.* **2014**, *5*, 5193.
- (409) Lin, D.; Zhuo, D.; Liu, Y.; Cui, Y. All-Integrated Bifunctional Separator for Li Dendrite Detection via Novel Solution Synthesis of a Thermostable Polyimide Separator. *J. Am. Chem. Soc.* **2016**, *138*, 11044–11050.
- (410) Liu, K.; Zhuo, D.; Lee, H.-W.; Liu, W.; Lin, D.; Lu, Y.; Cui, Y. Extending the Life of Lithium-Based Rechargeable Batteries by Reaction of Lithium Dendrites with a Novel Silica Nanoparticle Sandwiched Separator. *Adv. Mater.* **2017**, *29*, 1603987.
- (411) Zheng, J.; Yan, P.; Mei, D.; Engelhard, M. H.; Cartmell, S. S.; Polzin, B. J.; Wang, C.; Zhang, J.-G.; Xu, W. Highly Stable Operation of Lithium Metal Batteries Enabled by the Formation of a Transient High-Concentration Electrolyte Layer. *Adv. Energy Mater.* **2016**, *6*, 1502151.
- (412) Yang, H.; Fey, E. O.; Trimm, B. D.; Dimitrov, N.; Whittingham, M. S. Effects of Pulse Plating on Lithium Electrodeposition, Morphology and Cycling Efficiency. *J. Power Sources* **2014**, *272*, 900–908.
- (413) Tan, J.; Ryan, E. M. Computational Study of Electro-Convection Effects on Dendrite Growth in Batteries. *J. Power Sources* **2016**, *323*, 67–77.
- (414) Gonzalez, G.; Marshall, G.; Molina, F. V.; Dengra, S.; Rosso, M. Viscosity Effects in Thin-Layer Electrodeposition. *J. Electrochem. Soc.* **2001**, *148*, C479–C487.
- (415) Huth, J. M.; Swinney, H. L.; McCormick, W. D.; Kuhn, A.; Argoul, F. Role of Convection in Thin-Layer Electrodeposition. *Phys. Rev. E: Stat. Phys., Plasmas, Fluids, Relat. Interdiscip. Top.* **1995**, *51*, 3444–3458.
- (416) Ryu, H.; Kim, T.; Kim, K.; Ahn, J.-H.; Nam, T.; Wang, G.; Ahn, H.-J. Discharge Reaction Mechanism of Room-Temperature Sodium–Sulfur Battery with Tetra Ethylene Glycol Dimethyl Ether Liquid Electrolyte. *J. Power Sources* **2011**, *196*, 5186–5190.
- (417) Xin, S.; Yin, Y.-X.; Guo, Y.-G.; Wan, L.-J. A High-Energy Room-Temperature Sodium-Sulfur Battery. *Adv. Mater.* **2014**, *26*, 1261–1265.
- (418) Xia, C.; Black, R.; Fernandes, R.; Adams, B.; Nazar, L. F. The Critical Role of Phase-Transfer Catalysis in Aprotic Sodium Oxygen Batteries. *Nat. Chem.* **2015**, *7*, 496–501.
- (419) Kim, Y.-J.; Lee, H.; Noh, H.; Lee, J.; Kim, S.; Ryou, M.-H.; Lee, Y. M.; Kim, H.-T. Enhancing the Cycling Stability of Sodium Metal Electrodes by Building an Inorganic–Organic Composite Protective Layer. *ACS Appl. Mater. Interfaces* **2017**, *9*, 6000–6006.
- (420) Bi, X.; Ren, X.; Huang, Z.; Yu, M.; Kreidler, E.; Wu, Y. Investigating Dendrites and Side Reactions in Sodium-Oxygen

- Batteries for Improved Cycle Lives. *Chem. Commun.* **2015**, *51*, 7665–7668.
- (421) Hartmann, P.; Bender, C. L.; Sann, J.; Durr, A. K.; Jansen, M.; Janek, J.; Adelhelm, P. A Comprehensive Study on the Cell Chemistry of the Sodium Superoxide (NaO_2) Battery. *Phys. Chem. Chem. Phys.* **2013**, *15*, 11661–11672.
- (422) Yu, X.; Manthiram, A. Ambient-Temperature Sodium–Sulfur Batteries with a Sodiated Nafion Membrane and a Carbon Nanofiber-Activated Carbon Composite Electrode. *Adv. Energy Mater.* **2015**, *5*, 1500350.
- (423) Slater, M. D.; Kim, D.; Lee, E.; Johnson, C. S. Sodium-ion Batteries. *Adv. Funct. Mater.* **2013**, *23*, 947–958.
- (424) Li, H.; Peng, L.; Zhu, Y.; Chen, D.; Zhang, X.; Yu, G. An Advanced High-Energy Sodium Ion Full Battery Based on Nanostructured $\text{Na}_2\text{Ti}_3\text{O}_7/\text{VPO}_4$ Layered Materials. *Energy Environ. Sci.* **2016**, *9*, 3399–3405.
- (425) Zhang, B.; Rousse, G.; Foix, D.; Dugas, R.; Corte, D. A. D.; Tarascon, J.-M. Microsized Sn as Advanced Anodes in Glyme-Based Electrolyte for Na-Ion Batteries. *Adv. Mater.* **2016**, *28*, 9824–9830.
- (426) Seh, Z. W.; Sun, J.; Sun, Y.; Cui, Y. A Highly Reversible Room-Temperature Sodium Metal Anode. *ACS Cent. Sci.* **2015**, *1*, 449–455.
- (427) Cao, R.; Mishra, K.; Li, X.; Qian, J.; Engelhard, M. H.; Bowden, M. E.; Han, K. S.; Mueller, K. T.; Henderson, W. A.; Zhang, J.-G. Enabling Room Temperature Sodium Metal Batteries. *Nano Energy* **2016**, *30*, 825–830.
- (428) Song, S.; kotobuki, m.; Zheng, F.; Xu, C.; Savilov, S. V.; Hu, N.; Lu, L.; Wang, Y.; Li, W. D. A Hybrid Polymer/Oxide/Ionic-Liquid Solid Electrolyte for Na-Metal Batteries. *J. Mater. Chem. A* **2017**, *5*, 6424–6431.
- (429) Song, J.; Jeong, G.; Lee, A.-J.; Park, J. H.; Kim, H.; Kim, Y.-J. Dendrite-Free Polygonal Sodium Deposition with Excellent Interfacial Stability in a $\text{NaAlCl}_4\text{-}2\text{SO}_4$ Inorganic Electrolyte. *ACS Appl. Mater. Interfaces* **2015**, *7*, 27206–27214.
- (430) Yu, Z.; Shang, S.-L.; Seo, J.-H.; Wang, D.; Luo, X.; Huang, Q.; Chen, S.; Lu, J.; Li, X.; Liu, Z.-K.; et al. Exceptionally High Ionic Conductivity in $\text{Na}_3\text{P}_{0.62}\text{As}_{0.38}\text{S}_4$ with Improved Moisture Stability for Solid-State Sodium-Ion Batteries. *Adv. Mater.* **2017**, *29*, 1605561.
- (431) Ponrouch, A.; Marchante, E.; Courty, M.; Tarascon, J.-M.; Palacin, M. R. In Search of an Optimized Electrolyte for Na-Ion Batteries. *Energy Environ. Sci.* **2012**, *5*, 8572–8583.
- (432) Cohn, A. P.; Muralidharan, N.; Carter, R.; Share, K.; Pint, C. L. Anode-Free Sodium Battery through *in situ* Plating of Sodium Metal. *Nano Lett.* **2017**, *17*, 1296–1301.
- (433) Luo, W.; Zhang, Y.; Xu, S.; Dai, J.; Hitz, E.; Li, Y.; Yang, C.; Chen, C.; Liu, B.; Hu, L. Encapsulation of Metallic Na in an Electrically Conductive Host with Porous Channels as a Highly Stable Na Metal Anode. *Nano Lett.* **2017**, *17*, 3792–3797.
- (434) Hu, X.; Li, Z.; Zhao, Y.; Sun, J.; Zhao, Q.; Wang, J.; Tao, Z.; Chen, J. Quasi-Solid State Rechargeable Na-CO₂ Batteries with Reduced Graphene Oxide Na Anodes. *Sci. Adv.* **2017**, *3*, e1602396.
- (435) Kim, H.; Boysen, D. A.; Newhouse, J. M.; Spatocco, B. L.; Chung, B.; Burke, P. J.; Bradwell, D. J.; Jiang, K.; Tomaszowska, A. A.; Wang, K.; et al. Liquid Metal Batteries: Past, Present, and Future. *Chem. Rev.* **2013**, *113*, 2075–2099.
- (436) Lu, X.; Xia, G.; Lemmon, J. P.; Yang, Z. Advanced Materials for Sodium-Beta Alumina Batteries: Status, Challenges and Perspectives. *J. Power Sources* **2010**, *195*, 2431–2442.
- (437) Xue, L.; Gao, H.; Zhou, W.; Xin, S.; Park, K.; Li, Y.; Goodenough, J. B. Liquid K–Na Alloy Anode Enables Dendrite-Free Potassium Batteries. *Adv. Mater.* **2016**, *28*, 9608–9612.
- (438) Wang, K.; Pei, P.; Ma, Z.; Xu, H.; Li, P.; Wang, X. Morphology Control of Zinc Regeneration for Zinc–Air Fuel Cell and Battery. *J. Power Sources* **2014**, *271*, 65–75.
- (439) Li, Y.; Dai, H. Recent Advances in Zinc-Air Batteries. *Chem. Soc. Rev.* **2014**, *43*, 5257–5275.
- (440) Fu, J.; Cano, Z. P.; Park, M. G.; Yu, A.; Fowler, M.; Chen, Z. Electrically Rechargeable Zinc–Air Batteries: Progress, Challenges, and Perspectives. *Adv. Mater.* **2017**, *29*, 1604685.
- (441) Banik, S. J.; Akolkar, R. Suppressing Dendritic Growth During Alkaline Zinc Electrodeposition Using Polyethylenimine Additive. *Electrochim. Acta* **2015**, *179*, 475–481.
- (442) Arouete, S.; Bl Burton, K. F.; Oswin, H. G. Controlled Current Deposition of Zinc from Alkaline Solution. *J. Electrochem. Soc.* **1969**, *116*, 166–169.
- (443) Despic, A. R.; Popov, K. I. The Effect of Pulsating Potential on the Morphology of Metal Deposits Obtained by Mass-Transport Controlled Electrodeposition. *J. Appl. Electrochem.* **1971**, *1*, 275–278.
- (444) Ibl, N. Some Theoretical Aspects of Pulse Electrolysis. *Surf. Technol.* **1980**, *10*, 81–104.
- (445) Boto, K. Organic Additives in Zinc Electroplating. *Electrodeposition Surf. Treat.* **1975**, *3*, 77–95.
- (446) Aaboubi, O.; Douglade, J.; Abenaqui, X.; Boumedmed, R.; VonHoff, J. Influence of Tartaric Acid on Zinc Electrodeposition from Sulphate Bath. *Electrochim. Acta* **2011**, *56*, 7885–7889.
- (447) Kan, J.; Xue, H.; Mu, S. Effect of Inhibitors on Zn-Dendrite Formation for Zinc-Polyaniline Secondary Battery. *J. Power Sources* **1998**, *74*, 113–116.
- (448) Diggle, J. W.; Despic, A. R.; Bockris, J. O. M. The Mechanism of the Dendritic Electrococrystallization of Zinc. *J. Electrochem. Soc.* **1969**, *116*, 1503–1514.
- (449) Banik, S. J.; Akolkar, R. Suppressing Dendrite Growth During Zinc Electrodeposition by Peg-200 Additive. *J. Electrochem. Soc.* **2013**, *160*, D519–D523.
- (450) Liu, Z.; Cui, T.; Pulletikurthi, G.; Lahiri, A.; Carstens, T.; Olschewski, M.; Endres, F. Dendrite-Free Nanocrystalline Zinc Electrodeposition from an Ionic Liquid Containing Nickel Triflate for Rechargeable Zn-Based Batteries. *Angew. Chem., Int. Ed.* **2016**, *55*, 2889–2893.
- (451) Chamoun, M.; Hertzberg, B. J.; Gupta, T.; Davies, D.; Bhadra, S.; Van Tassell, B.; Erdonmez, C.; Steingart, D. A. Hyper-Dendritic Nanoporous Zinc Foam Anodes. *NPG Asia Mater.* **2015**, *7*, e178.
- (452) Yan, Z.; Wang, E.; Jiang, L.; Sun, G. Superior Cycling Stability and High Rate Capability of Three-Dimensional Zn/Cu Foam Electrodes for Zinc-Based Alkaline Batteries. *RSC Adv.* **2015**, *5*, 83781–83787.
- (453) Parker, J. F.; Chervin, C. N.; Nelson, E. S.; Rolison, D. R.; Long, J. W. Wiring Zinc in Three Dimensions Re-Writes Battery Performance-Dendrite-Free Cycling. *Energy Environ. Sci.* **2014**, *7*, 1117–1124.
- (454) Higashi, S.; Lee, S. W.; Lee, J. S.; Takechi, K.; Cui, Y. Avoiding Short Circuits from Zinc Metal Dendrites in Anode by Backside-Plating Configuration. *Nat. Commun.* **2016**, *7*, 11801.
- (455) Liu, S.; Wang, H.; Imanishi, N.; Zhang, T.; Hirano, A.; Takeda, Y.; Yamamoto, O.; Yang, J. Effect of Co-Doping Nano-Silica Filler and N-Methyl-N-Propylpiperidinium Bis(trifluoromethanesulfonyl)imide into Polymer Electrolyte on Li Dendrite Formation in Li/poly(ethylene oxide)-Li(CF_3SO_2)₂N/Li. *J. Power Sources* **2011**, *196*, 7681–7686.
- (456) Liu, S.; Imanishi, N.; Zhang, T.; Hirano, A.; Takeda, Y.; Yamamoto, O.; Yang, J. Effect of Nano-Silica Filler in Polymer Electrolyte on Li Dendrite Formation in Li/poly(ethylene oxide)-Li(CF_3SO_2)₂N/Li. *J. Power Sources* **2010**, *195*, 6847–6853.
- (457) Liu, S.; Imanishi, N.; Zhang, T.; Hirano, A.; Takeda, Y.; Yamamoto, O.; Yang, J. Lithium Dendrite Formation in Li/Poly(ethylene oxide)-Lithium Bis(trifluoromethanesulfonyl)imide and N-Methyl-N-Propylpiperidinium Bis(trifluoromethanesulfonyl)imide/Li Cells. *J. Electrochem. Soc.* **2010**, *157*, A1092–A1098.
- (458) Li, X.; Zhang, Z.; Yin, K.; Yang, L.; Tachibana, K.; Hirano, S.-i. Mesoporous Silica/Ionic Liquid Quasi-Solid-State Electrolytes and Their Application in Lithium Metal Batteries. *J. Power Sources* **2015**, *278*, 128–132.
- (459) Li, X.; Zhang, Z.; Yang, L.; Tachibana, K.; Hirano, S.-i. TiO₂-Based Ionogel Electrolytes for Lithium Metal Batteries. *J. Power Sources* **2015**, *293*, 831–834.
- (460) Hallinan, D. T.; Mullin, S. A.; Stone, G. M.; Balsara, N. P. Lithium Metal Stability in Batteries with Block Copolymer Electrolytes. *J. Electrochem. Soc.* **2013**, *160*, A464–A470.

- (461) Shim, J.; Lee, J. W.; Bae, K. Y.; Kim, H. J.; Yoon, W. Y.; Lee, J. C. Dendrite Suppression by Synergistic Combination of Solid Polymer Electrolyte Crosslinked with Natural Terpenes and Lithium-Powder Anode for Lithium-Metal Batteries. *ChemSusChem* **2017**, *10*, 2274–2283.
- (462) Safa, M.; Chamaani, A.; Chawla, N.; El-Zahab, B. Polymeric Ionic Liquid Gel Electrolyte for Room Temperature Lithium Battery Applications. *Electrochim. Acta* **2016**, *213*, 587–593.
- (463) Li, Y.; Wong, K.-W.; Ng, K.-M. Ionic Liquid Decorated Mesoporous Silica Nanoparticles: A New High-Performance Hybrid Electrolyte for Lithium Batteries. *Chem. Commun.* **2016**, *52*, 4369–4372.
- (464) Pan, Q.; Smith, D. M.; Qi, H.; Wang, S.; Li, C. Y. Hybrid Electrolytes with Controlled Network Structures for Lithium Metal Batteries. *Adv. Mater.* **2015**, *27*, 5995–6001.
- (465) Hu, J.; Tian, J.; Li, C. Nanostructured Carbon Nitride Polymer-Reinforced Electrolyte to Enable Dendrite-Suppressed Lithium Metal Batteries. *ACS Appl. Mater. Interfaces* **2017**, *9*, 11615–11625.
- (466) Choudhury, S.; Archer, L. A. Lithium Fluoride Additives for Stable Cycling of Lithium Batteries at High Current Densities. *Adv. Electron. Mater.* **2016**, *2*, 1500246.
- (467) Liu, B.; Xu, W.; Yan, P.; Kim, S. T.; Engelhard, M. H.; Sun, X.; Mei, D.; Cho, J.; Wang, C. M.; Zhang, J. G. Stabilization of Li Metal Anode in DMSO-Based Electrolytes Via Optimization of Salt–Solvent Coordination for Li-O₂ Batteries. *Adv. Energy Mater.* **2017**, *7*, 1602605.
- (468) Lang, J.; Song, J.; Qi, L.; Luo, Y.; Luo, X.; Wu, H. Uniform Lithium Deposition Induced by Polyacrylonitrile Submicron Fiber Array for Stable Lithium Metal Anode. *ACS Appl. Mater. Interfaces* **2017**, *9*, 10360–10365.
- (469) Cheng, X.-B.; Yan, C.; Peng, H.-J.; Huang, J.-Q.; Yang, S.-T.; Zhang, Q. Sulfurized Solid Electrolyte Interphase with a Rapid Li Diffusion in Li Metal Batteries. *Energy Storage Mater.* **2017**, DOI: 10.1016/j.ensm.2017.03.008.
- (470) Yan, K.; Lee, H.-W.; Gao, T.; Zheng, G.; Yao, H.; Wang, H.; Lu, Z.; Zhou, Y.; Liang, Z.; Liu, Z.; et al. Ultrathin Two-Dimensional Atomic Crystals as Stable Interfacial Layer for Improvement of Lithium Metal Anode. *Nano Lett.* **2014**, *14*, 6016–6022.
- (471) Liu, P.; Ma, Q.; Fang, Z.; Ma, J.; Hu, Y.-S.; Zhou, Z.-B.; Li, H.; Huang, X.-J.; Chen, L.-Q. Concentrated Dual-Salt Electrolytes for Improving the Cycling Stability of Lithium Metal Anodes. *Chin. Phys. B* **2016**, *25*, 078203.
- (472) Manthiram, A.; Chung, S.-H.; Zu, C. Lithium–Sulfur Batteries: Progress and Prospects. *Adv. Mater.* **2015**, *27*, 1980–2006.
- (473) Huang, J.-Q.; Zhang, Q.; Wei, F. Multi-Functional Separator/Interlayer System for High-Stable Lithium–Sulfur Batteries: Progress and Prospects. *Energy Storage Mater.* **2015**, *1*, 127–145.
- (474) Borchardt, L.; Oschatz, M.; Kaskel, S. Carbon Materials for Lithium Sulfur Batteries—Ten Critical Questions. *Chem. - Eur. J.* **2016**, *22*, 7324–7351.
- (475) Pang, Q.; Liang, X.; Kwok, C. Y.; Nazar, L. F. Advances in Lithium–Sulfur Batteries Based on Multifunctional Cathodes and Electrolytes. *Nat. Energy* **2016**, *1*, 16132.
- (476) Ma, L.; Hendrickson, K. E.; Wei, S.; Archer, L. A. Nanomaterials: Science and Applications in the Lithium–Sulfur Battery. *Nano Today* **2015**, *10*, 315–338.
- (477) Xin, S.; Chang, Z.; Zhang, X.; Guo, Y.-G. Progress of Rechargeable Lithium Metal Batteries Based on Conversion Reactions. *Natl. Sci. Rev.* **2017**, *4*, 54–70.
- (478) Manthiram, A.; Knight, J. C.; Myung, S.-T.; Oh, S.-M.; Sun, Y.-K. Nickel-Rich and Lithium-Rich Layered Oxide Cathodes: Progress and Perspectives. *Adv. Energy Mater.* **2016**, *6*, 1501010.
- (479) Qiu, Y.; Li, W.; Zhao, W.; Li, G.; Hou, Y.; Liu, M.; Zhou, L.; Ye, F.; Li, H.; Wei, Z.; et al. High-Rate, Ultralong Cycle-Life Lithium/Sulfur Batteries Enabled by Nitrogen-Doped Graphene. *Nano Lett.* **2014**, *14*, 4821–4827.
- (480) Liang, X.; Rangom, Y.; Kwok, C. Y.; Pang, Q.; Nazar, L. F. Interwoven Mxene Nanosheet/Carbon-Nanotube Composites as Li–S Cathode Hosts. *Adv. Mater.* **2017**, *29*, 1603040.
- (481) Wu, F.; Yushin, G. Conversion Cathodes for Rechargeable Lithium and Lithium-Ion Batteries. *Energy Environ. Sci.* **2017**, *10*, 435–459.
- (482) Fan, F. Y.; Carter, W. C.; Chiang, Y.-M. Mechanism and Kinetics of Li₂S Precipitation in Lithium–Sulfur Batteries. *Adv. Mater.* **2015**, *27*, 5203–5209.
- (483) Zhou, G.; Tian, H.; Jin, Y.; Tao, X.; Liu, B.; Zhang, R.; Seh, Z. W.; Zhuo, D.; Liu, Y.; Sun, J.; et al. Catalytic Oxidation of Li₂S on the Surface of Metal Sulfides for Li–S Batteries. *Proc. Natl. Acad. Sci. U. S. A.* **2017**, *114*, 840–845.
- (484) Chung, S.-H.; Chang, C.-H.; Manthiram, A. A Core-Shell Electrode for Dynamically and Statically Stable Li–S Battery Chemistry. *Energy Environ. Sci.* **2016**, *9*, 3188–3200.
- (485) Tang, C.; Li, B.-Q.; Zhang, Q.; Zhu, L.; Wang, H.-F.; Shi, J.-L.; Wei, F. CaO-Templated Growth of Hierarchical Porous Graphene for High-Power Lithium–Sulfur Battery Applications. *Adv. Funct. Mater.* **2016**, *26*, 577–585.
- (486) Nandasiri, M. I.; Camacho-Forero, L. E.; Schwarz, A. M.; Shutthanandan, V.; Thevuthasan, S.; Balbuena, P. B.; Mueller, K. T.; Murugesan, V. In Situ Chemical Imaging of Solid-Electrolyte Interphase Layer Evolution in Li–S Batteries. *Chem. Mater.* **2017**, *29*, 4728–4737.
- (487) Peng, H.-J.; Huang, J.-Q.; Cheng, X.-B.; Zhang, Q. Review on High-Loading and High-Energy Lithium–Sulfur Batteries. *Adv. Energy Mater.* **2017**, *7*, 1700260.
- (488) Kim, J.-S.; Hwang, T. H.; Kim, B. G.; Min, J.; Choi, J. W. A Lithium–Sulfur Battery with a High Areal Energy Density. *Adv. Funct. Mater.* **2014**, *24*, 5359–5367.
- (489) Chung, S.-H.; Chang, C.-H.; Manthiram, A. A Carbon-Cotton Cathode with Ultrahigh-Loading Capability for Statically and Dynamically Stable Lithium–Sulfur Batteries. *ACS Nano* **2016**, *10*, 10462–10470.
- (490) Fang, R.; Zhao, S.; Hou, P.; Cheng, M.; Wang, S.; Cheng, H.-M.; Liu, C.; Li, F. 3d Interconnected Electrode Materials with Ultrahigh Areal Sulfur Loading for Li–S Batteries. *Adv. Mater.* **2016**, *28*, 3374–3382.
- (491) Zeng, F.; Wang, A.; Wang, W.; Jin, Z.; Yang, Y. The Strategies of Constructing Stable and High Sulfur Loading Cathodes Based on Blade-Casting Technique. *J. Mater. Chem. A* **2017**, *5*, 12879–12888.
- (492) Fu, Y.; Su, Y.-S.; Manthiram, A. Highly Reversible Lithium/Dissolved Polysulfide Batteries with Carbon Nanotube Electrodes. *Angew. Chem., Int. Ed.* **2013**, *52*, 6930–6935.
- (493) Kang, W.; Deng, N.; Ju, J.; Li, Q.; Wu, D.; Ma, X.; Li, L.; Naebe, M.; Cheng, B. A Review of Recent Developments in Rechargeable Lithium–Sulfur Batteries. *Nanoscale* **2016**, *8*, 16541–16588.
- (494) Zhou, G.; Sun, J.; Jin, Y.; Chen, W.; Zu, C.; Zhang, R.; Qiu, Y.; Zhao, J.; Zhuo, D.; Liu, Y.; et al. Sulfophilic Nickel Phosphosulfide Enabled Li₂S Impregnation in 3D Graphene Cages for Li–S Batteries. *Adv. Mater.* **2017**, *29*, 1603366.
- (495) Hou, T.-Z.; Xu, W.-T.; Chen, X.; Peng, H.-J.; Huang, J.-Q.; Zhang, Q. Lithium Bond Chemistry in Lithium–Sulfur Batteries. *Angew. Chem., Int. Ed.* **2017**, *56*, 8178–8182.
- (496) Seh, Z. W.; Sun, Y.; Zhang, Q.; Cui, Y. Designing High-Energy Lithium–Sulfur Batteries. *Chem. Soc. Rev.* **2016**, *45*, 5605–5634.
- (497) Liu, M.; Ye, F.; Li, W.; Li, H.; Zhang, Y. Chemical Routes toward Long-Lasting Lithium/Sulfur Cells. *Nano Res.* **2016**, *9*, 94–116.
- (498) Cao, R.; Xu, W.; Lv, D.; Xiao, J.; Zhang, J.-G. Anodes for Rechargeable Lithium–Sulfur Batteries. *Adv. Energy Mater.* **2015**, *5*, 1402273.
- (499) Xin, S.; Guo, Y.-G.; Wan, L.-J. Nanocarbon Networks for Advanced Rechargeable Lithium Batteries. *Acc. Chem. Res.* **2012**, *45*, 1759–1769.
- (500) Peng, H.-J.; Zhang, G.; Chen, X.; Zhang, Z.-W.; Xu, W.-T.; Huang, J.-Q.; Zhang, Q. Enhanced Electrochemical Kinetics on Conductive Polar Mediators for Lithium–Sulfur Batteries. *Angew. Chem., Int. Ed.* **2016**, *55*, 12990–12995.

- (501) Peng, H.-J.; Xu, W.-T.; Zhu, L.; Wang, D.-W.; Huang, J.-Q.; Cheng, X.-B.; Yuan, Z.; Wei, F.; Zhang, Q. 3D Carbonaceous Current Collectors: The Origin of Enhanced Cycling Stability for High-Sulfur-Loading Lithium–Sulfur Batteries. *Adv. Funct. Mater.* **2016**, *26*, 6351–6358.
- (502) Liu, M.; Qin, X.; He, Y.; Li, B.; Kang, F. Recent Innovative Configurations in High-Energy Lithium-Sulfur Batteries. *J. Mater. Chem. A* **2017**, *5*, 5222–5234.
- (503) Aurbach, D.; Pollak, E.; Elazari, R.; Salitra, G.; Kelley, C. S.; Affinito, J. On the Surface Chemical Aspects of very High Energy Density, Rechargeable Li–Sulfur Batteries. *J. Electrochem. Soc.* **2009**, *156*, A694–A702.
- (504) Xiong, S.; Xie, K.; Diao, Y.; Hong, X. Properties of Surface Film on Lithium Anode with LiNO_3 as Lithium Salt in Electrolyte Solution for Lithium–Sulfur Batteries. *Electrochim. Acta* **2012**, *83*, 78–86.
- (505) Xu, R.; Li, J. C. M.; Lu, J.; Amine, K.; Belharouak, I. Demonstration of Highly Efficient Lithium-Sulfur Batteries. *J. Mater. Chem. A* **2015**, *3*, 4170–4179.
- (506) Zhang, S. S. Role of LiNO_3 in Rechargeable Lithium/Sulfur Battery. *Electrochim. Acta* **2012**, *70*, 344–348.
- (507) Ding, N.; Zhou, L.; Zhou, C.; Geng, D.; Yang, J.; Chien, S. W.; Liu, Z.; Ng, M.-F.; Yu, A.; Hor, T. S. A.; et al. Building Better Lithium-Sulfur Batteries: From LiNO_3 to Solid Oxide Catalyst. *Sci. Rep.* **2016**, *6*, 33154.
- (508) Lv, D.; Zheng, J.; Li, Q.; Xie, X.; Ferrara, S.; Nie, Z.; Mehdi, L. B.; Browning, N. D.; Zhang, J.-G.; Graff, G. L.; et al. High Energy Density Lithium–Sulfur Batteries: Challenges of Thick Sulfur Cathodes. *Adv. Energy Mater.* **2015**, *5*, 1402290.
- (509) Yuan, Z.; Peng, H.-J.; Huang, J.-Q.; Liu, X.-Y.; Wang, D.-W.; Cheng, X.-B.; Zhang, Q. Hierarchical Free-Standing Carbon-Nanotube Paper Electrodes with Ultrahigh Sulfur-Loading for Lithium–Sulfur Batteries. *Adv. Funct. Mater.* **2014**, *24*, 6105–6112.
- (510) Cao, Y.; Meng, X.; Elam, J. W. Atomic Layer Deposition of Lixalys Solid-State Electrolytes for Stabilizing Lithium-Metal Anodes. *ChemElectroChem* **2016**, *3*, 858–863.
- (511) McCloskey, B. D. Attainable Gravimetric and Volumetric Energy Density of Li–S and Li Ion Battery Cells with Solid Separator-Protected Li Metal Anodes. *J. Phys. Chem. Lett.* **2015**, *6*, 4581–4588.
- (512) Ma, G.; Wen, Z.; Wang, Q.; Shen, C.; Jin, J.; Wu, X. Enhanced Cycle Performance of a Li–S Battery Based on a Protected Lithium Anode. *J. Mater. Chem. A* **2014**, *2*, 19355–19359.
- (513) Wu, M.; Wen, Z.; Jin, J.; Chowdari, B. V. R. Trimethylsilyl Chloride-Modified Li Anode for Enhanced Performance of Li–S Cells. *ACS Appl. Mater. Interfaces* **2016**, *8*, 16386–16395.
- (514) Wu, M.; Jin, J.; Wen, Z. Influence of a Surface Modified Li Anode on the Electrochemical Performance of Li–S Batteries. *RSC Adv.* **2016**, *6*, 40270–40276.
- (515) Lin, D.; Liu, Y.; Chen, W.; Zhou, G.; Liu, K.; Dunn, B.; Cui, Y. Conformal Lithium Fluoride Protection Layer on Three-Dimensional Lithium by Nonhazardous Gaseous Reagent Freon. *Nano Lett.* **2017**, *17*, 3731–3737.
- (516) Lee, J.; Song, J.; Lee, H.; Noh, H.; Kim, Y.-J.; Kwon, S. H.; Lee, S. G.; Kim, H.-T. A Nanophase-Separated, Quasi-Solid-State Polymeric Single-Ion Conductor: Polysulfide Exclusion for Lithium–Sulfur Batteries. *ACS Energy Lett.* **2017**, *2*, 1232–1239.
- (517) Sheng, O.; Jin, C.; Luo, J.; Yuan, H.; Fang, C.; Huang, H.; Gan, Y.; Zhang, J.; Xia, Y.; Liang, C.; et al. Ionic Conductivity Promotion of Polymer Electrolyte with Ionic Liquid Grafted Oxides for All-Solid-State Lithium-Sulfur Batteries. *J. Mater. Chem. A* **2017**, *5*, 12934–12942.
- (518) Tao, X.; Liu, Y.; Liu, W.; Zhou, G.; Zhao, J.; Lin, D.; Zu, C.; Sheng, O.; Zhang, W.; Lee, H.-W.; et al. Solid-State Lithium–Sulfur Batteries Operated at 37 °C with Composites of Nanostructured $\text{Li}_x\text{La}_3\text{Zr}_2\text{O}_{12}$ /Carbon Foam and Polymer. *Nano Lett.* **2017**, *17*, 2967–2972.
- (519) Huang, C.; Xiao, J.; Shao, Y.; Zheng, J.; Bennett, W. D.; Lu, D.; Saraf, L. V.; Engelhard, M.; Ji, L.; Zhang, J.; et al. Manipulating Surface Reactions in Lithium–Sulphur Batteries Using Hybrid Anode Structures. *Nat. Commun.* **2014**, *5*, 3015.
- (520) Kong, L.-L.; Zhang, Z.; Zhang, Y.-Z.; Liu, S.; Li, G.-R.; Gao, X.-P. Porous Carbon Paper as Interlayer to Stabilize the Lithium Anode for Lithium–Sulfur Battery. *ACS Appl. Mater. Interfaces* **2016**, *8*, 31684–31694.
- (521) Cheng, X.-B.; Yan, C.; Huang, J.-Q.; Li, P.; Zhu, L.; Zhao, L.; Zhang, Y.; Zhu, W.; Yang, S.-T.; Zhang, Q. The Gap between Long Lifespan Li–S Coin and Pouch Cells: The Importance of Lithium Metal Anode Protection. *Energy Storage Mater.* **2017**, *6*, 18–25.
- (522) Zhou, G.; Li, L.; Wang, D.-W.; Shan, X.-y.; Pei, S.; Li, F.; Cheng, H.-M. A Flexible Sulfur-Graphene-Polypropylene Separator Integrated Electrode for Advanced Li–S Batteries. *Adv. Mater.* **2015**, *27*, 641–647.
- (523) Hagen, M.; Fanz, P.; Tübke, J. Cell Energy Density and Electrolyte/Sulfur Ratio in Li–S Cells. *J. Power Sources* **2014**, *264*, 30–34.
- (524) Song, R.; Fang, R.; Wen, L.; Shi, Y.; Wang, S.; Li, F. A Trilayer Separator with Dual Function for High Performance Lithium–Sulfur Batteries. *J. Power Sources* **2016**, *301*, 179–186.
- (525) Fang, R.; Zhao, S.; Sun, Z.; Wang, D. W.; Cheng, H. M.; Li, F. More Reliable Lithium-Sulfur Batteries: Status, Solutions and Prospects. *Adv. Mater.* **2017**, *29*, 1606823.
- (526) Wu, S.; Zhu, K.; Tang, J.; Liao, K.; Bai, S.; Yi, J.; Yamauchi, Y.; Ishida, M.; Zhou, H. A Long-Life Lithium Ion Oxygen Battery Based on Commercial Silicon Particles as the Anode. *Energy Environ. Sci.* **2016**, *9*, 3262–3271.
- (527) Girishkumar, G.; McCloskey, B.; Luntz, A. C.; Swanson, S.; Wilcke, W. Lithium–Air Battery: Promise and Challenges. *J. Phys. Chem. Lett.* **2010**, *1*, 2193–2203.
- (528) Freunberger, S. A.; Chen, Y.; Drewett, N. E.; Hardwick, L. J.; Bardé, F.; Bruce, P. G. The Lithium–Oxygen Battery with Ether-Based Electrolytes. *Angew. Chem., Int. Ed.* **2011**, *50*, 8609–8613.
- (529) Chang, Z.-w.; Xu, J.-j.; Liu, Q.-c.; Li, L.; Zhang, X.-b. Recent Progress on Stability Enhancement for Cathode in Rechargeable Non-Aqueous Lithium–Oxygen Battery. *Adv. Energy Mater.* **2015**, *5*, 1500633.
- (530) Luo, W. B.; Gao, X. W.; Chou, S. L.; Kang, Y. M.; Wang, J. Z.; Liu, H. K.; Dou, S. X. Investigation of Promising Air Electrode for Realizing Ultimate Lithium Oxygen Battery. *Adv. Energy Mater.* **2017**, *7*, 1700234.
- (531) Kim, B. G.; Kim, J.-S.; Min, J.; Lee, Y.-H.; Choi, J. H.; Jang, M. C.; Freunberger, S. A.; Choi, J. W. A Moisture- and Oxygen-Impermeable Separator for Aprotic $\text{Li}-\text{O}_2$ Batteries. *Adv. Funct. Mater.* **2016**, *26*, 1747–1756.
- (532) Younesi, R.; Hahlin, M.; Roberts, M.; Edström, K. The Sei Layer Formed on Lithium Metal in the Presence of Oxygen: A Seldom Considered Component in the Development of the $\text{Li}-\text{O}_2$ Battery. *J. Power Sources* **2013**, *225*, 40–45.
- (533) Geng, D.; Ding, N.; Hor, T. S. A.; Chien, S. W.; Liu, Z.; Wuu, D.; Sun, X.; Zong, Y. From Lithium–Oxygen to Lithium–Air Batteries: Challenges and Opportunities. *Adv. Energy Mater.* **2016**, *6*, 1502164.
- (534) Jang, I.-C.; Ida, S.; Ishihara, T. Lithium Depletion and the Rechargeability of $\text{Li}-\text{O}_2$ Batteries in Ether and Carbonate Electrolytes. *ChemElectroChem* **2015**, *2*, 1380–1384.
- (535) Sun, Y. Lithium Ion Conducting Membranes for Lithium–Air Batteries. *Nano Energy* **2013**, *2*, 801–816.
- (536) Yi, J.; Zhou, H. A Unique Hybrid Quasi-Solid-State Electrolyte for $\text{Li}-\text{O}_2$ Batteries with Improved Cycle Life and Safety. *ChemSusChem* **2016**, *9*, 2391–2396.
- (537) Kumar, B.; Kumar, J.; Leese, R.; Fellner, J. P.; Rodrigues, S. J.; Abraham, K. M. A Solid-State, Rechargeable, Long Cycle Life Lithium–Air Battery. *J. Electrochem. Soc.* **2010**, *157*, A50–A54.
- (538) Balaish, M.; Kraytsberg, A.; Ein-Eli, Y. A Critical Review on Lithium–Air Battery Electrolytes. *Phys. Chem. Chem. Phys.* **2014**, *16*, 2801–2822.
- (539) Walker, W.; Giordani, V.; Uddin, J.; Bryantsev, V. S.; Chase, G. V.; Addison, D. A Rechargeable $\text{Li}-\text{O}_2$ Battery Using a Lithium

Nitrate/N,N-Dimethylacetamide Electrolyte. *J. Am. Chem. Soc.* **2013**, *135*, 2076–2079.

(540) Visco, S. J.; Katz, B. D.; Nimon, Y. S.; De Jonghe, L. C. U.S. Patent US 7282295, 2007.

(541) Imanishi, N.; Hasegawa, S.; Zhang, T.; Hirano, A.; Takeda, Y.; Yamamoto, O. Lithium Anode for Lithium-Air Secondary Batteries. *J. Power Sources* **2008**, *185*, 1392–1397.

(542) Zhou, B.; Guo, L.; Zhang, Y.; Wang, J.; Ma, L.; Zhang, W.-H.; Fu, Z.; Peng, Z. A High-Performance Li–O₂ Battery with a Strongly Solvating Hexamethylphosphoramide Electrolyte and a LiPON-Protected Lithium Anode. *Adv. Mater.* **2017**, *29*, 1701568.

(543) Le, H. T. T.; Ngo, D. T.; Ho, V.-C.; Cao, G.; Park, C.-N.; Park, C.-J. Insights into Degradation of Metallic Lithium Electrodes Protected by a Bilayer Solid Electrolyte Based on Aluminium Substituted Lithium Lanthanum Titanate in Lithium-Air Batteries. *J. Mater. Chem. A* **2016**, *4*, 11124–11138.

(544) Wang, D.; Xiao, J.; Xu, W.; Zhang, J.-G. High Capacity Pouch-Type Li–Air Batteries. *J. Electrochem. Soc.* **2010**, *157*, A760–A764.

(545) Fergus, J. W. Recent Developments in Cathode Materials for Lithium Ion Batteries. *J. Power Sources* **2010**, *195*, 939–954.

(546) Zhang, Y.; Li, Y.; Xia, X.; Wang, X.; Gu, C.; Tu, J. High-Energy Cathode Materials for Li-ion Batteries: A Review of Recent Developments. *Sci. China: Technol. Sci.* **2015**, *58*, 1809–1828.

(547) Kim, M. G.; Cho, J. Reversible and High-Capacity Nanostructured Electrode Materials for Li-ion Batteries. *Adv. Funct. Mater.* **2009**, *19*, 1497–1514.

(548) Ellis, B. L.; Lee, K. T.; Nazar, L. F. Positive Electrode Materials for Li-ion and Li-Batteries. *Chem. Mater.* **2010**, *22*, 691–714.

(549) Li, W.; Kim, U.-H.; Dolocan, A.; Sun, Y.-K.; Manthiram, A. Formation and Inhibition of Metallic Lithium Microstructures in Lithium Batteries Driven by Chemical Crossover. *ACS Nano* **2017**, *11*, 5853–5863.

(550) Que, M.; Tong, Y.; Wei, G.; Yuan, K.; Wei, J.; Jiang, Y.; Zhu, H.; Chen, Y. Safe and Flexible ion Gel Based Composite Electrolyte for Lithium Batteries. *J. Mater. Chem. A* **2016**, *4*, 14132–14140.